The seismic stratigraphy, geological evolution and CO_2 storage potential of the offshore Durban Basin, South Africa.

By:
Nigel Hicks

Submitted in fulfilment of the degree Doctor of Philosophy

In the Discipline of Geological Sciences

School of Agricultural, Earth and Environmental Sciences
College of Agriculture, Engineering and Science
University of KwaZulu-Natal,
Durban
South Africa

October
2017

As the candidate's supervisor I have/have not approved this thesis/dissertation for submission.

Signed: _____ Name: _____ Date: ____

Preface

The research described in this thesis was undertaken in the Discipline of Geological Sciences, University of KwaZulu-Natal, Westville, and the Council for Geoscience, Pietermaritzburg, from August 2013 to October 2017, under the supervision of Professor A.N. Green.

These studies represent original work by the author and have not otherwise been submitted in any form for any degree or diploma to any tertiary institution. Where use has been made of the work of others it is duly acknowledged in the text.

Analysis, writing and diagrammatic content of this thesis which appear in peer-reviewed publications are original work of the publications first author as part of this dissertation. Secondary authors are acknowledged solely on the basis of their supervisory roles.

*Signed:*_____ *Name:*_____ *Date:*_____

Declaration 1 – Plagiarism

I, Nigel Hicks, declare that:

1. The research reported in this thesis, except where otherwise indicated, is my original research.

2. This thesis has not been submitted for any degree or examination at any other university.

3. This thesis does not contain other persons' data, graphs or other information, unless specifically acknowledged as being sourced from other persons.

4. This thesis does not contain any other persons writing, unless specifically acknowledged as being sourced from other researchers. Where other written sources have been quoted then:

> *a. Their words have been re-written but the general information attributed to them has been referenced*
>
> *b. Where their exact words have been used, then their writing has been placed in italics and inside quotation marks, and referenced.*

5. This thesis does not contain text, graphics or tables copied from the Internet, unless specifically acknowledged, and the source being detailed in the thesis and in the References section.

*Signed:*_____ *Name:*_____ *Date:*_____

Declaration 2 – Publications

A detailed account of the contributions by the authors of published work is given in section 1.4 Structure and layout of Thesis (page 5). All publications are presented in the Appendices attached at the end of this thesis.

Published, open-source papers comprise the following:

• Article I, Chapters 3 and 4 – (Appendix I):
Hicks, N., Davids, S., Beck, B., Green, A.N. 2014. Investigation of CO_2 storage potential of the Durban basin in South Africa. Energy Procedia, 63, 5200-5210.
https://doi.org/10.1016/j.egypro.2014.11.551

Published, peer-reviewed papers comprise the following:

• Article II, Chapter 6 – (Appendix II):
Hicks, N., Green, A.N. 2016. Sedimentology and depositional architecture of a submarine delta-fan complex in the Durban Basin, South Africa. Marine and Petroleum Geology, 78, 390-404.
https://doi.org/10.1016/j.marpetgeo.2016.09.032

• Article III, Chapter 7 – (Appendix III):
Hicks, N., Green, A.N. 2017. A Mid-Miocene erosional unconformity from the Durban Basin, SE African margin: A combination of global eustatic sea level change, epeirogenic uplift, and ocean current initiation. Marine and Petroleum Geology, 86, 798-811. https://doi.org/10.1016/j.marpetgeo.2017.06.037

• Article IV, Chapters 8 and 9 – (Appendix IV):
Hicks, N., Green, A.N. 2017. A first assessment of potential stratigraphic traps for geological storage of CO_2 in the Durban Basin, South Africa. International Journal of Greenhouse Gas Control, 64, 73–86. https://doi.org/10.1016/j.ijggc.2017.06.015

In each case N. Hicks drafted all manuscripts and figures/tables for submission as the primary and corresponding author based on research carried out for this thesis. The second author (Prof. A.N. Green) provided conceptual advice and editorial responsibility as project supervisor.

*Signed:*_____ *Name:*_____ *Date:*_____

Acknowledgements

The financial assistance of the South African Centre for Carbon Capture and Storage towards this research is hereby acknowledged. Opinions expressed and conclusions arrived at, are those of the author and are not necessarily to be attributed to SACCCS.

This PhD. research was funded by a PhD bursary grant supplied by the South African Centre for Carbon Capture and Storage (SACCCS), a division of the South African National Energy Development Institute (SANEDI) to cover all direct running costs for the project. Furthermore the project was funded as part of the Council for Geoscience (CGS) statutory programme (ST-2013-1183) which covered all staff time for Mr N. Hicks to complete the project. I am therefore sincerely indebted to the Council for Geoscience as well as SANEDI/SACCCS for their financial and technical support towards the project. Without this assistance this research could not have been undertaken.

Special mention needs to go to Mr Brendan Beck, Mr Noel Kamrajh, and Ms. Evelyn Nyandoro from SANEDI for their continued support and faith in the research. Within the Council for Geoscience, Dr Greg Botha needs extensive thanks for putting up with my comings and goings in the KwaZulu-Natal office, and continual questions on various topics of research. Dr Marthinus Cloete is thanked for pioneering CCS research in the CGS, without this base the project may never have been.

I further acknowledge the Petroleum Agency South Africa for supplying all legacy seismic and well data to the University of KwaZulu-Natal as academic licence data. I would also like to acknowledge IHS for the Kingdom Suite academic software grant supplied to the University of KwaZulu-Natal.

I would like to thank my supervisor Professor Andrew Noel Green for providing critical reviews of this dissertation and its associated peer-reviewed manuscripts. Furthermore I would like to thank Prof. Green for organising office space, software, and participating in the many beer-fuelled discussions over the duration of the project.

On a personal note, to my wife Joanne, thank you for putting up with all the trials and tribulations that went along with this research over the last 4 years. It warms my heart and moistens my tear ducts when I think that I am married to such an amazing loving person. I love you with all my heart.

To my parents, mom and dad; I love you guys. Without all your efforts getting me though my studies I would not be where I am today. Words cannot describe the thanks you deserve.

Finally to all the UKZN staff and post-grad students, especially Lauren Hoyer, Lauren Pretorius, Errol Wiles and Carlos Loureiro, thanks for making time at UKZN so pleasurable it was an honour to work beside you all.

Abstract

Within offshore frontier sedimentary basins, legacy data are important tools in basin-scale exploration for potential CO_2 storage. The seismic stratigraphy, evolution, depositional framework and CO_2 storage potential of a frontier basin, the offshore Durban Basin, along a sheared-passive margin in southeast Africa are described. Based on single-channel 2D seismic reflection data and well data, six seismic units (A-F) are revealed, separated by major sequence boundaries. Internal seismic reflector geometries and sedimentology suggest a range of depositional regimes from syn-rift to upper slope and outer shelf. Nearshore and continental facies are not preserved, with episodic shelf and slope sedimentation related to periods of tectonic-induced base level fall. The sedimentary architecture shows a change from a structurally defined shelf (shearing phase), to shallow ramp and then terminal passive margin sedimentary shelf settings. Sedimentation occurred predominantly during normal regressive conditions with the basin dominated by the progradation of a constructional submarine delta (Tugela Cone) during sea-level lowstands (LST).

Erosional unconformity surfaces (sequence boundaries) are key features for oil and gas exploration representing regions of potential effective reservoir accumulation as well as migration pathways. These surfaces further act as indicators for variations in eustatic sea level, ocean dynamics and climatic conditions which significantly affect depositional environments of sedimentary successions. Using available 2D seismic data Mesozoic and Cenozoic sequence boundaries are identified and described, with new evidence of a mid-Miocene age erosional unconformity that can be correlated with analogous horizons around the entire southern African continental margin. Cenozoic submarine unconformity surfaces within the basin are typified by submarine canyon incision. Polycyclic epeirogenic uplift of southern Africa characterised the Mesozoic and Cenozoic, with erosion and sediment bypass offshore concomitant with increases in offshore sedimentation rates and deposition of potential sand-rich reservoir systems. Although epeirogenic uplift appears to be the dominant mechanism affecting formation of the identified sequence boundaries, it is postulated that, for the mid-Miocene boundary in particular, an interplay between global eustatic sea-level fall, expansion of the east Antarctic ice sheets, and changes in deep oceanic current circulation patterns may have substantially contributed to sequence boundary formation during this period.

Single-channel 2D seismic reflection data and well log data are further utilised to provide new evidence of reservoir/seal pairs in saline aquifers that may represent potential storage sites for CO_2 injection. Multiple, previously undefined and regionally pervasive stratigraphic traps have been mapped through a detailed seismo-sedimentary analysis. These include shelf-bound shallow-marine-sheet and deltaic sandstone packages of Turonian and Maastrichtian age respectively. Coeval with these laterally extensive shelf packages, multiple basin floor fan systems have been identified on the palaeo-slope. These systems are correlated with analogous hydrocarbon-bearing sequences throughout a large region of the south-east African continental shelf. Using conservative assumptions, it is proposed that 328 Mt CO_2 could potentially be stored in two laterally extensive shelf sand sequences, with a further potential for 464 Mt CO_2 storage in basin floor fan systems in the distal basin.

Potential undrilled structural traps are identified within the Durban Basin which include compactional anticlinal structures and faulted closures. Compactional anticlines are represented by sediment drapes covering deep-seated basement horst structures whilst faulted closures are represented by rollover anticlinal structures related to gravity faulting. Multiple growth fault structures identified within the southern portion of the Durban Basin are related to gravitational tectonics associated with instability along the edge of the continental rise. The southern portion of the Durban Basin was subject to sediment starvation with the formation of a wide continental rise rather than a shelf and shelf break leading to instability and gravitational tectonism allowing the formation of fault closures within this area.

Potential CO_2 storage capacities for structural closures are calculated to be 46 Mt CO_2 at a P90 probability level (93 Mt - P50; 158 Mt – P10). These values can further be subdivided into two closure types. Faulted rollover anticlinal closures within the basin account for 2 Mt potential CO_2 storage at a P90 probability level (4 Mt -

P50; 7 Mt – P10); whilst compactional anticlinal closures overlying basement structures account for 44 Mt potential CO_2 storage capacity at a P90 level (89 Mt – P50; 152 Mt – P10).

Prospective storage sites within the basin are individually defined through basin-scale assessment and are comparable with sedimentary and structural trap sites around the southern African continental shelf, as well as within CO_2 storage sites defined internationally. This study therefore provides a basin-scale, effective CO_2 storage capacity estimation with site-specific characterisation and capacity estimations for both structural and stratigraphical traps within the Durban Basin, east coast of South Africa.

CONTENTS

CHAPTER 1

INTRODUCTION

1.1 BACKGROUND

Since the 20th century, atmospheric concentrations of anthropogenic greenhouse gases have increased through accelerated population growth, urbanisation and industrialisation. In order to achieve stabilisation of key greenhouse gas concentrations in the atmosphere, the United Nations Framework Convention on Climate Change (UNFCCC, 1992) called for a global initiative to reduce anthropogenic carbon dioxide (CO_2) emissions to prevent "*threats of serious or irreversible damage*," and "*dangerous anthropogenic interference with the climate system*." The IPCC (2005) however, suggest that for stabilization of anthropogenic greenhouse gases to occur effectively, the rate of global emissions must be reduced to a level equal to the rate at which the natural global processes can remove them from the atmosphere. However, recent studies (IPCC, 2014) indicate that, despite a growing number of mitigation policies, global greenhouse gas emissions have accelerated in the last decade. It is therefore suggested that, in order to stabilise temperature increases in the 21st century below 2°C relative to pre-industrial levels, a global departure from business-as-usual (Fig. 1.1) is required in order to stabilise atmospheric CO_2 concentrations around 450 ppm by 2100 (IPCC, 2014).

In order to limit this long-term global temperature increase to 2°C, CO_2 emissions need to be reduced via a number of low carbon energy technologies, including Carbon Capture and Storage (CCS), nuclear energy, renewable energy, fuel switching and fuel efficiency techniques (IEA, 2008; Fig. 1.1). As the global need for energy increases, so do energy-related CO_2 emissions, with the lead energy supply being that of fossil-fuels. By 2050 the IEA estimate that CCS will contribute 14% of total global emissions reduction (Fig. 1.1), with 70% of CCS deployment occurring in non-Organisation for Economic Co-operation and Development (OECD) countries (IEA, 2012). The IPCC (2005) suggest that targets for emission reductions in each technology will depend upon factors such as cost, capacity, environmental impact, the rate at which the technology can be introduced, and social factors such as public acceptance.

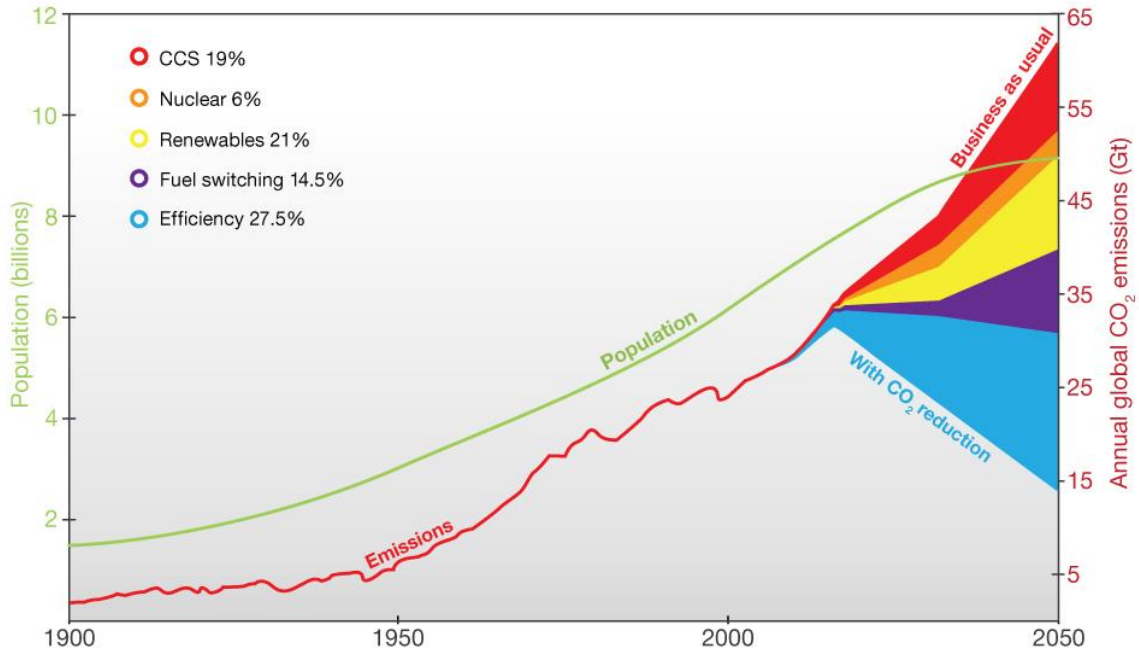

Figure 1.1: Wedge diagram adapted by CO2CRC (Cook, 2012) from the IEA (2012) to indicate potential global CO_2 emission reductions against "business as usual" practices, based upon increased energy technologies and a drive away from fossil-fuel based power.

Results obtained by the IPCC (2014) suggest that, in 2010, energy production through the burning of fossil fuels accounted for 34% of global anthropogenic greenhouse gas emissions in the form of CO_2. South Africa, like many countries worldwide, is heavily reliant on fossil fuels for energy supply, with about 90% of primary energy derived from either coal, oil or gas (Engelbrecht et al., 2004). Coal-fired power generation is the largest contributor to CO_2 emissions worldwide, and currently provides around 40 per cent of total electricity output (IEA, 2014). South Africa is heavily dependent on fossil fuels with 90% of electricity generation coming from coal (Cloete, 2010). This, together with a relatively small population, results in South Africa being a significant contributor (in terms of per capita emissions) to CO_2 emissions on a worldwide scale.

Carbon dioxide Capture and Storage (CCS) has been identified as one of the technical approaches to mitigating global climate change induced by carbon dioxide and other greenhouse gas emissions from fossil fuel based energy production and industry. Geological storage of anthropogenic CO_2 via Carbon Capture and Storage (CCS) technologies represents a crucial component to the mitigation of global climate change. For the geological storage of CO_2 to be optimised, suitable strata and reservoir conditions need to be identified. Whilst a wealth of knowledge exists for CCS projects associated with hydrocarbon provinces (IPCC, 2005; US DOE, 2008; Würdemann et al., 2010; Underschultz et al., 2011; Hutcheon et al., 2016), saline aquifer storage, specifically in under-explored frontier basins, is commonly hampered by a lack of physical data needed to define CO_2 storage reservoirs and their storage efficiency due to limited exploration activities (Wilkinson et al., 2013).

The Global CCS Institute (2015) suggested that, if implemented globally, the capture, transportation and storage of anthropogenic CO_2 in geological formations could account for ~17% of prospected global reduction in CO_2 emissions (Fig. 1.2). Storage of CO_2, either as a condensed phase, or as a gas, has been undertaken since the 1970's to enhance hydrocarbon production (NETL, 2010). The Global CCS Institute (2016) and International Energy Agency (IEA, 2016) identified fifteen (15) large-scale CCS projects operational worldwide with pilot and demonstration-scale projects numbering in the hundreds. Successful storage of CO_2 in a number of geologic mediums such as depleted oil or gas reservoirs, unmineable coal beds, deep saline-water saturated aquifers, and basaltic formations, has been demonstrated over the last two decades in onshore and offshore environments (GCCSI, 2016). Deep saline aquifers occur throughout the world and provide large, potentially accessible storage opportunities for Carbon Capture and Storage (CCS) technologies (IPCC, 2005). It is suggested (GCCSI, 2015) that CCS is the only technology which can reduce emissions on a significant scale from fossil fuel power plants and other industrial processes.

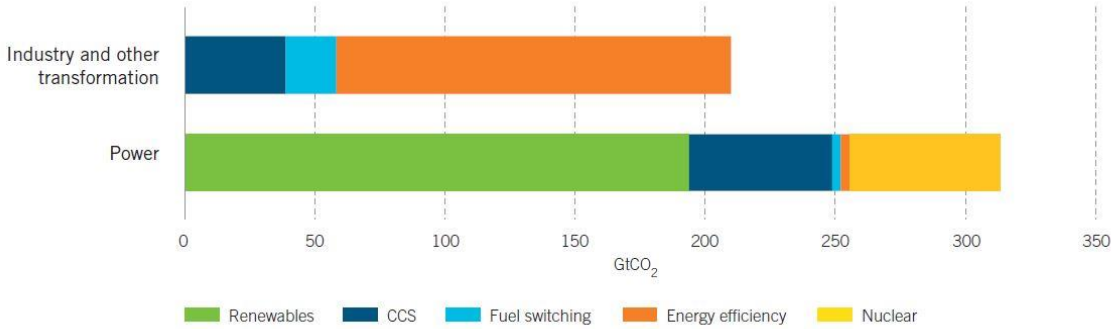

Figure 1.2: Prospected cumulative CO_2 emissions reductions in power and industry, 2012-2050 (after GCCSI, 2015).

A country-scale analysis of the geological storage potential of CO_2 has previously been undertaken, identifying potential storage capacity in multiple onshore and offshore Mesozoic sedimentary basins (Viljoen et al., 2010) (Fig. 1.3). During this national review of geological storage of CO_2 in South Africa, Viljoen et al. (2010) indicated that 98% of South Africa's CO_2 storage potential lay in offshore Mesozoic basins around the

continental shelf. On the eastern seaboard of South Africa, Viljoen et al. (2010) proposed a theoretical storage capacity of 42000 Mt CO_2 for the combined offshore Durban and Zululand Basins (Figs 1.3: 1.4).

The ~10000 km^2 Durban Basin (Broad et al., 2006) that borders the Zululand Basin to the north (Figs 1.3: 1.4) represents a poorly explored frontier basin (Singh and McLachlan, 2003). Hydrocarbon exploration is limited to low resolution single-channel seismic reflection interpretations (du Toit and Leith, 1974; Dingle et al., 1978; Martin, 1984; Goodlad, 1986) and four wildcat wells that focused upon potential structural plays beneath the continental shelf (Fig. 1.4). Within the Durban Basin, no significant coal or organic rich strata have been identified with prospectivity focussing upon saline aquifers within syn-rift and early drift phase deposits identified through seismic mapping and exploration drilling on the continental shelf.

Although the Durban Basin did not rank as the most prospective offshore basin in the national review (Viljoen et al., 2010), it was selected for Basin-Scale Assessment due to the following factors:

- its proximity to potential CO_2 transport pipelines from major CO_2 sources
- its proximity to local CO_2 sources
- its geological storage potential based upon identified structures.

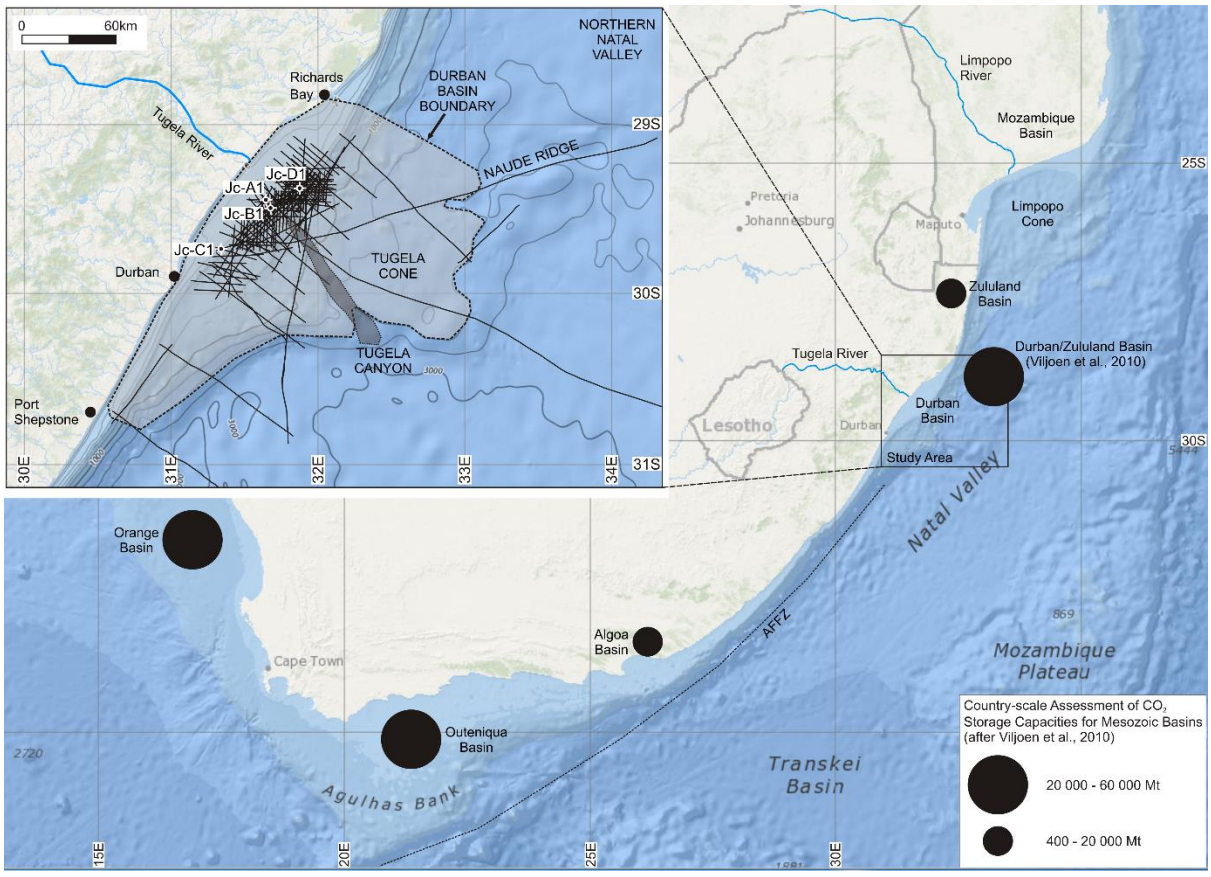

Figure 1.3: Locality map detailing the study area location with National Oceanic and Atmospheric Administration (1 min grid) UTM bathymetric grid. The areal extent of the Durban Basin is depicted within the shaded polygon. Note the relative position of the Jc-series boreholes drilled on the continental shelf to that of the deep water Tugela Cone. The CO_2 storage estimates of Mesozoic basins defined by Viljoen et al. (2010) are shown.

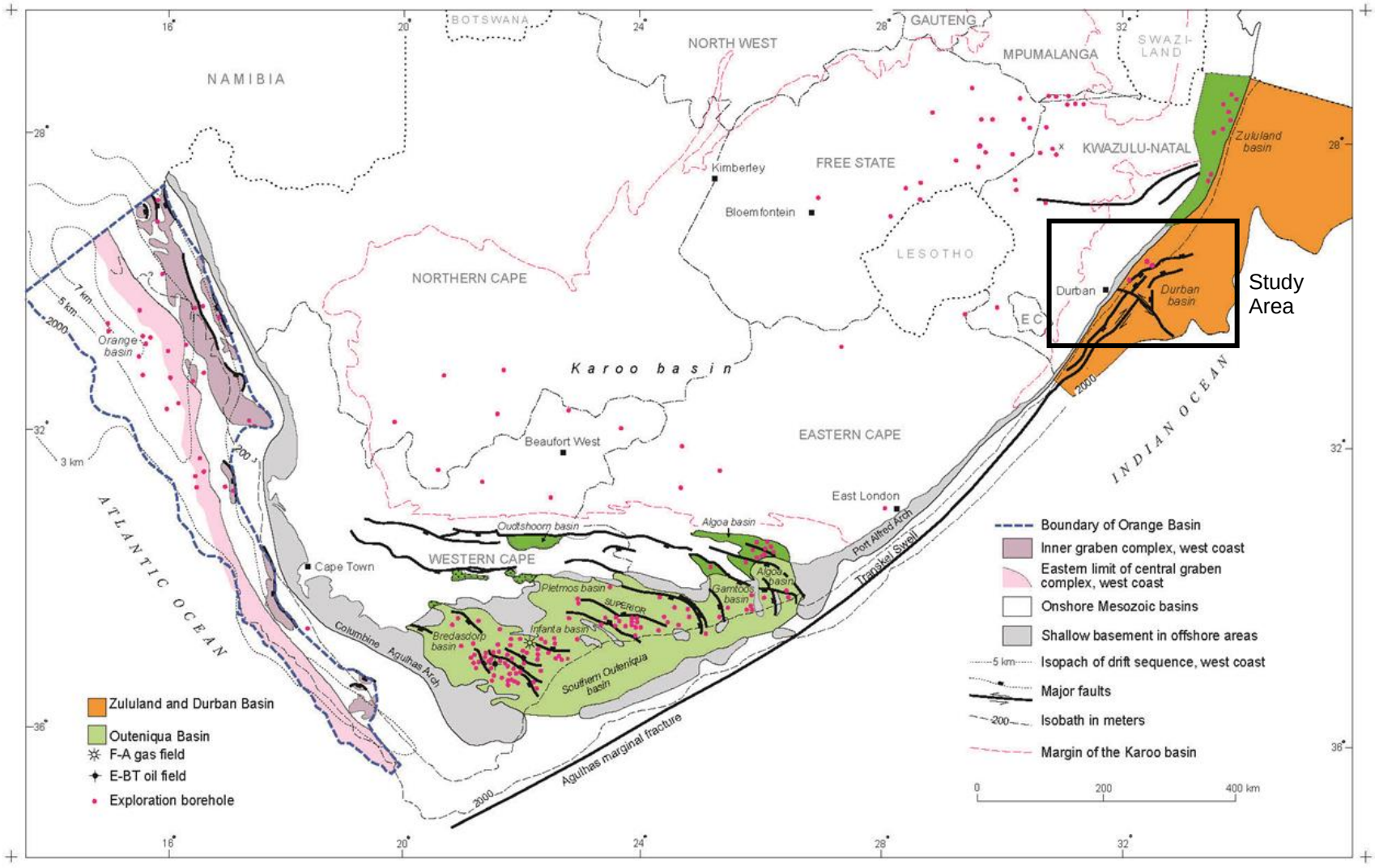

Figure 1.4: Location map of onshore and offshore Mesozoic Basins in South Africa (after Van Vuuren et al., 1998).

1.2 AIMS AND OBJECTIVES

A multidisciplinary scientific programme is underway to identify and assess the possibilities for CCS in South Africa. A component of this research, of which this thesis forms a part, is a detailed geological investigation into the storage potential of sedimentary basins both onshore and on the continental shelf of South Africa. This investigation was preceded by broader assessments of the technical and geological host alternatives for CO_2 storage in South Africa (Viljoen et al., 2010) which identified five Mesozoic sedimentary basins with potential storage, two of which were onshore and the remaining three underlying the submerged continental shelf surrounding South Africa (Fig. 1.4).

The aim of this study is to define and map the areal extent of major unconformity horizons identified in seismic section, as well as to map the extent of potential sand-rich horizons, potential basin floor fans, and sediment drape structures in the offshore Durban Basin through analysis of existing 2D seismic data and well log information (lithology, gamma ray and resistivity). This includes analysis of legacy 2D seismic and exploration borehole data, so as to provide a better understanding of the stratigraphic architecture, and possible CO_2 storage capabilities of this portion of the South African continental shelf. These data will ultimately be combined to define the capacity for the safe storage of CO_2 in the subsurface aquifer rocks.

The objectives of this study are as follows:

- To assess and define the stratigraphy and sedimentology of the Mesozoic Durban Basin, with specific emphasis upon sequence stratigraphy.
- To classify individual sequences and system tracts to create a sequence stratigraphic framework of the Durban Basin, highlighting controls on sedimentation identified through seismic reflection and stratigraphic analysis.
- To assess and map the areal extent of potential sand-rich horizons within target areas identified from seismic and stratigraphic interpretations
- To understand and predict the timing of basin floor fan formation with regards to global and local sea level fluctuations.
- To identify and quantify potential CO_2 storage sites/areas based on the above seismic and stratigraphic interpretation
- To define a capacity estimate for the safe storage of CO_2 in subsurface aquifer rocks in the Durban Basin.

1.3 RATIONALE

Sedimentary successions developed along east Africa's passive continental margins are known to host giant hydrocarbon accumulations (Palermo et al., 2014). The Durban Basin forms part of the Natal Valley (Fig. 1.3), a north-south trending, sediment filled, rift basin on the eastern seaboard of southern Africa (Dingle et al., 1978). Although dominated to the north and south by a narrow shelf (Green and Garlick, 2011; Cawthra, et al., 2012), the Tugela Bank between Durban and Richards Bay, represents a 45 km wide shelf with a late Cretaceous to Tertiary-age (McMillan, 2003) deep-water fan complex, the Tugela Cone, developed beneath and seaward of the present shelf break (Fig. 1.3).

The Mesozoic evolution of the basin is poorly documented (du Toit and Leith, 1974; McMillan, 2003); with work focussed on either low resolution single-channel seismic reflection data (Dingle et al., 1978; Martin, 1984; Goodlad, 1986), or seafloor sediment dynamics, submarine canyon formation and Late Pleistocene/Holocene stratigraphy (Green and Garlick, 2011; Cawthra et al., 2012; Green et al., 2013; Wiles et al., 2013).

The Durban Basin was the focus of a hydrocarbon exploration programme by national oil company SOEKOR between 1974 and 1990, during which time 2761 km of 2D seismic data were acquired (Fig. 1.3), together with

the drilling of three deep offshore boreholes (Jc series, A1; B1; C1). A fourth borehole Jc-D1 was drilled in 2000 by Phillips Petroleum (Fig. 1.3). To date only limited exploration has been undertaken in the Durban Basin, with no substantial oil or gas reserves having been located. Previous exploration focused upon possible structural trap sites beneath the Tugela Cone. A minor gas show in the Jc-B1 well was identified, with the Jc-D1 well providing evidence for an active petroleum system (Petroleum Agency SA, 2012) with Singh and McLachlan (2003) confirming overlooked traces of oil in the well.

1.4 THESIS STRUCTURE

This thesis constitutes a collection of articles published in international peer-reviewed journals collated as individual chapters (Chapters 6, 7, 8 and 9). Chapter 2 outlines the key elements of Carbon Capture and Storage technologies and processes in a global context. Chapter 3 details the criteria needed in defining a sedimentary basin and its associated saline aquifers storage potential as defined by the Carbon Sequestration Leadership Forum (CSLF, 2008).

In chapter 4 the thesis discusses the regional setting of the study area highlighting the formation of the Natal Valley and subsequent sedimentary basin fill successions in terms of tectonic setting and attributes. Chapter 5 is concerned with the methodologies utilised in the study to define the seismo-stratigraphic architecture of the continental shelf and slope in the Durban Basin.

Chapters 6 and 7 represent two published works, with chapter 6 (Hicks and Green, 2016) detailing the seismo-stratigraphy, evolution and depositional framework of the Durban Basin with specific focus on the formation of the Tugela Cone submarine delta-fan complex. Chapter 7 (Hicks and Green 2017a) discusses the development and significance of major sequence boundaries and their associated unconformity surfaces. This chapter further emphasises the link between sequence boundary formation, epeirogenic processes, variations in eustatic sea level, ocean dynamics and climatic conditions.

Chapters 8 and 9 are a combination of one published article (Hicks and Green 2017b) discussing the CO_2 storage potential and capacities of stratigraphic traps within the basin as defined from seismic analysis. Further to these, unpublished data on the storage potential and capacities of structural traps within the basin are discussed.

It should be noted that this thesis makes no attempt to define factors relating to CCS regulation, public perception, or economic viability based upon water depths, drilling depths or other factors.

CHAPTER 2

CONTEXT OF CARBON CAPTURE AND STORAGE

Carbon Capture and Storage (CCS) represents a crucial component of low carbon dioxide emission technologies to assist in the mitigation of climate change. The technology involves the capture and long-term geological storage of anthropogenic CO_2 produced through either the combustion of fossil fuels in power generation or industrial processes such as the production of cement, iron or steel. It is globally accepted that anthropogenic CO_2 emissions are a major contributing factor to the effects of climate change, with CO_2 concentrations in the atmosphere increasing from pre-industrial levels of 280 ppm to just under 400 ppm in 2012 (IPCC, 2005).

2.1 CHARACTER OF CO_2

Carbon Dioxide (CO_2) represents the single most important anthropogenic greenhouse gas, occurring in a gaseous state at standard pressures and temperatures of 1 bar and 20°C respectively (standard pressures adopted from NIST). Although many current conceptions refer to "carbon emissions" as a greenhouse product, this is in fact incorrect as it is the molecule CO_2 comprising a single carbon atom, and two oxygen atoms, rather than the element C, that is the contributing factor. The descriptions of CO_2 as a "poisonous" gas are also misleading as, although CO_2 represents an asphixiant (and is therefore used in fire extinguishers), it is used in numerous day to day products including carbonated soft drinks. Although often represented as an anthropogenic greenhouse gas, naturally occurring CO_2 is an essential component of life, with the global carbon cycle comprising a complex array of geologic, oceanic and biological processes that constantly recycle CO_2 around the globe to keep an atmospheric concentration of approximately 390 parts per million (Cook, 2012).

CO_2 as a gas occurs as a colourless and odourless vapour which is soluble in water and has a density higher than that of air at ~1.98 kg/m^3. If cooled and condensed to above its triple point temperature and pressure (-56.6°C and 5.185 bar), CO_2 condenses to form a white solid commonly known as "dry ice". Below this triple point pressure (Fig. 2.1a), CO_2 will revert directly into a gas above its sublimation (boiling) point of -78.5°C. CO_2 only attains a liquid phase above its triple point, but below its thermodynamic critical point (31.1° and 73.9 bars), this liquid phase is generally immiscible in water. However some soluble CO_2 can form a weak carbonic acid similar to that which forms when gaseous CO_2 dissolves in water. Bachu and Adams (2003) suggest that CO_2 solubility is initially inversely proportional to temperature, with a solubility decrease between standard room temperature (20°C) and ~100°C at 1 bar pressure. Following this initial decrease, solubilities appear to increase with an increase in temperature from ~200°C at 1 bar pressure. At increased pressures, the initial decrease in solubility is short-lived with CO_2 solubility increasing at much lower temperatures. Bachu and Adams, (2003) show that although CO_2 solubility is inversely proportional to salinity, CO_2 solubility increases with increased pressure and temperature.

CO_2 can also be present in a "supercritical" phase (Fig. 2.1a) which occurs under operating conditions above the critical point (73.9 bar and 31.1°C), as a fluid phase that has the density of a liquid, but the viscosity of a gas (Cook, 2012). In this phase, CO_2 can have densities between 150 to 1060 kg/m^3 (Bachu, 2003). It is within geological reservoirs where CO_2 can be stable in this phase that storage is most viable. The International Panel on Climate Change special report (IPCC, 2005) suggests that, under average geothermal gradients and hydrostatic conditions, burial depths in sedimentary basins need to exceed 800 m to achieve conditions suitable for CO_2 storage under supercritical phase conditions (Fig. 2.1b).

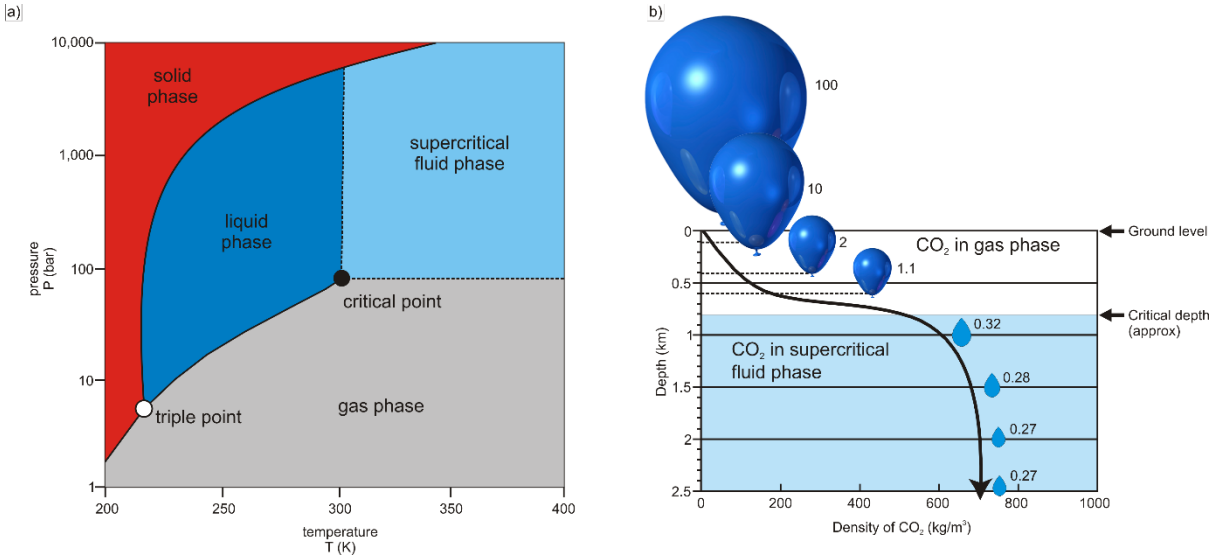

Figure 2.1: a) CO_2 phase diagram. b) Supercritical phase CO_2 graph depicting the density and associated volume of CO_2 as a gaseous phase and then as a supercritical phase. Note the decrease in volume with increase in depth and density (modified after CO2CRC, 2008).

Although safe injection potential is defined by the rock characteristics and not depth, as is seen with CO_2 storage in shallow gas fields, storage within the supercritical phase (below ~800 m) in saline aquifers enhances the volumes of CO_2 that can potentially be stored. CO_2 density increases with pressure (depth beneath surface), and therefore once pressurised the volume of the CO_2 is reduced dramatically (Fig. 2.1b). At standard surface pressures and temperatures CO_2 gas covers an area more than 100 times larger than when CO_2 occurs in a supercritical state (Fig. 2.1a). Storage of CO_2 in its gaseous phase is possible with numerous studies having demonstrated safe storage of CO_2 gas in oil and gas reservoirs above ~800 m depth, however for large-scale, effective storage of CO_2, a supercritical or "dense" phase CO_2 flood is preferred as volumetrically more CO_2 can be stored in the reservoir.

2.2 GEOLOGICAL STORAGE OF CO_2

The injection of CO_2 into the subsurface is not a new scientific field, with oil companies having been injecting CO_2 into ageing fields to enhance recovery (CO_2EOR) since the 1970's (Global CCS Institute, 2016). The Global CCS Institute (2016) estimates that there are currently more than 130 operations which recycle CO_2 by re-injecting it into the producing reservoir, effectively storing the CO_2 permanently in the subsurface. CO_2 storage in geological formations has been a natural process for millions of years, with CO_2 trapped as accessory gases or fluids in oil and natural gas reservoirs. For CCS purposes, the equivalent geological conditions that have trapped oil and gas reserves for millions of years in the subsurface are targeted as potential storage sites.

From a geological perspective, CO_2 can be sequestrated into a number of geological mediums which primarily occur in sedimentary basins. These include deep saline aquifers, depleted oil and natural gas reservoirs, and unmineable coal seams (Fig. 2.2). Other geological strata that could potentially be used for storage include basalts and shales.

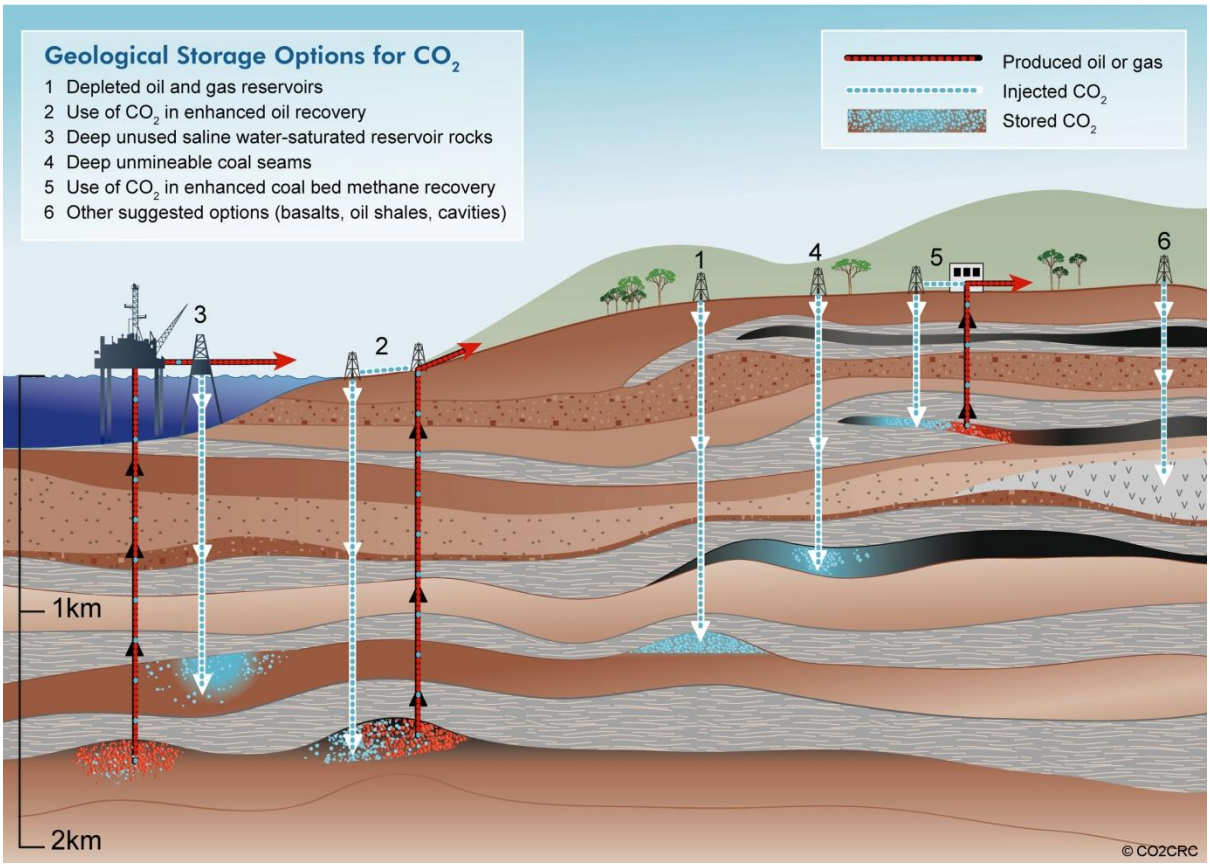

Figure 2.2: Geological storage options for CO_2 (after CO2CRC, 2008).

For injection and containment of CO_2 in a geological reservoir to be feasible, a number of criteria need to be met (IPCC, 2005):
1) The reservoir must have adequate injectivity potential (porosity and permeability) with a storage capacity capable of containing the injected CO_2.
2) The reservoir needs to be in a relatively stable tectonic regime to limit the potential risks of leakage through compromised reservoir integrity.
3) The reservoir needs to have a sealing cap rock, or suitable trapping mechanism that will prevent the migration of CO_2 into surrounding lithologies.

Sedimentary basins commonly consist of stacked successions of sandstone, siltstone and mudstone, in varying proportions, which in many cases, such as major petroleum provinces; consist of adequate reservoir/seal pairs which can act as traps for CO_2. A high-level global CO_2 storage potential classification, based upon the petroleum potential of sedimentary basins (Fig. 2.3), was undertaken by Bradshaw and Dance (2005) who separated the basins into highly prospective, prospective and non-prospective domains.

2.2.1 Saline Aquifer Storage

Many prospective sedimentary basins, although not containing world-class oil or gas provinces contain deep saline aquifers which represent highly prospective reservoirs for CO_2 storage. Saline aquifers occur in deep, porous and permeable formations which are saturated with saline formation water or brines. The salinity of the brines or formation water in these reservoirs makes them unsuitable for human consumption or agricultural use. The vast areas over which these reservoirs extend make them viable targets for potential CO_2 storage, with the injected CO_2 trapped by various mechanisms such as structural/stratigraphic means, residual, solubility, and mineral trapping. Saline aquifer storage is often hampered by a lack of physical data needed to define the reservoirs and their CO_2 storage prospectivity due to limited exploration activities.

2.2.2 Depleted Oil and Gas Reservoir Storage

Depleted oil or gas fields represent prime candidates for CO_2 storage due to the preserved structural and stratigraphic traps that previously contained oil or gas. A large percentage of current CCS projects in operation are based in world class oil or gas provinces. The detailed knowledge of the structures based upon oil and gas exploration is used to define the fields and their suitability for CO_2 storage. In most instances the containment potential of the site is proven by the existence of hydrocarbon reserves. By utilising proven oil and gas exploration and production techniques, the structural and containment integrity of these reservoirs have been extensively studied increasing the safety of such a project (IPCC, 2005). The structures needed to trap natural concentrations of oil or gas can be utilised to store CO_2 once a field has been depleted of hydrocarbons. CO_2 injection is commonly used in conjunction with operation to enhance recovery (EOR) in producing fields whereby CO_2 is injected into a producing oil reservoir to create a CO_2 flood which reduces the oils viscosity, offering potential economic gain via increased flow rate.

2.2.3 Unmineable Coal Seam Storage

Coal seams that are either too thin, or too deep for economically viable mining can be utilised for CO_2 storage through enhanced coalbed methane (ECBM) extraction. Initial recovery utilises dewatering and depressurisation of the coal seams which does not allow for complete methane gas extraction (Viljoen et al., 2010). The injection of CO_2 liberates the remaining methane with three to thirteen molecules of CO_2 being preferentially absorbed on the coal for each molecule of liberated methane, dependant on coal rank (Viljoen et al., 2010). ECBM operations are however complex, requiring multiple injection wells and a firm knowledge of the CO_2-coal-methane-water system, and are therefore at an early stage of research for use in CCS (Van Bergen et al., 2011).

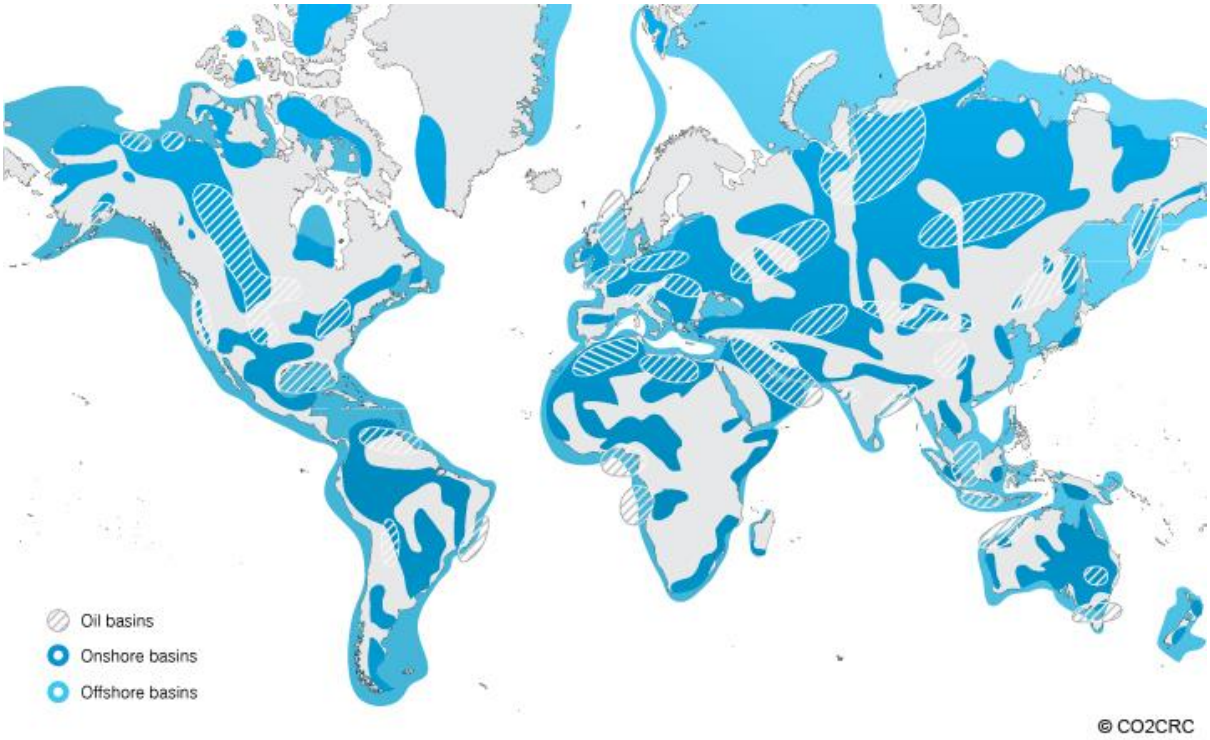

Figure 2.3: Distribution of sedimentary basins worldwide with potential CO_2 storage capacity (after Bradshaw and Dance, 2005).

2.3 CO_2 TRAPPING MECHANISMS

CO_2 injected in deep saline aquifers will partially dissolve in the formation water and migrate with the formation water flow in the reservoir (Cook, 2012). This allows for the CO_2 to be entrained in the formation water and trapped via a combination of trapping mechanisms.

2.3.1 Structural Trapping

The most common short-term trapping mechanism is that of structural trapping, where supercritical phase CO_2 in a saline aquifer is more buoyant than the formation waters, and rises updip where it is trapped below low permeability caprock in a domal structure (Fig. 2.4a). This form of trapping is analogous to many oil or gas reservoirs where the hydrocarbons are retained in anticlinal structures in the subsurface. In reservoirs that have been affected by faulting, the fault plane can potentially form a structural seal if the lithologies produce an impermeable barrier that prevents the flow of CO_2 either up the fault plane, or laterally into adjacent lithologies (Fig. 2.4b).

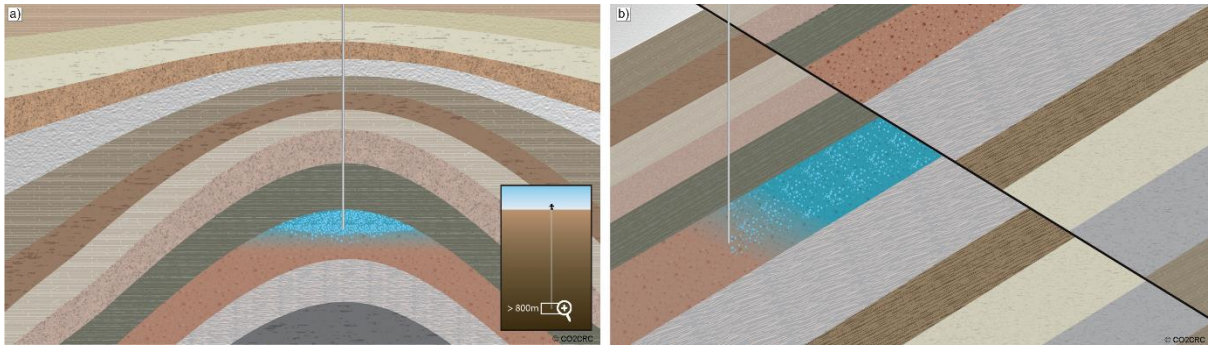

Figure 2.4: Structural trapping mechanisms in saline aquifers: a) CO_2 injected into an anticlinal structure. b) CO_2 injected into a reservoir with a fault seal updip. Note the cap rock bounding the reservoir on the hanging wall of the fault (modified after CO2CRC, 2008).

2.3.2 Stratigraphic Trapping

Stratigraphic trapping is often included with structural trapping as the sealing properties of the overlying impermeable units in an underground structure form a stratigraphic trap. However in the instance where no structures are evident in the subsurface CO_2 injected into reservoirs formed in specific sedimentary environments, such as braided rivers, can be trapped by lateral stratigraphic seals, such as flood plain mud deposits (Fig. 2.5a). This is evident in the Ketzin CO_2 project where injection occurs into braided fluvial channel deposits bounded by impermeable overbank mudstones (Norden and Frykman, 2013). Stratigraphic trapping can also occur when a porous and permeable reservoir unit pinches out against an unconformity with the overlying rock consisting of impermeable cap rock (Fig. 2.5b).

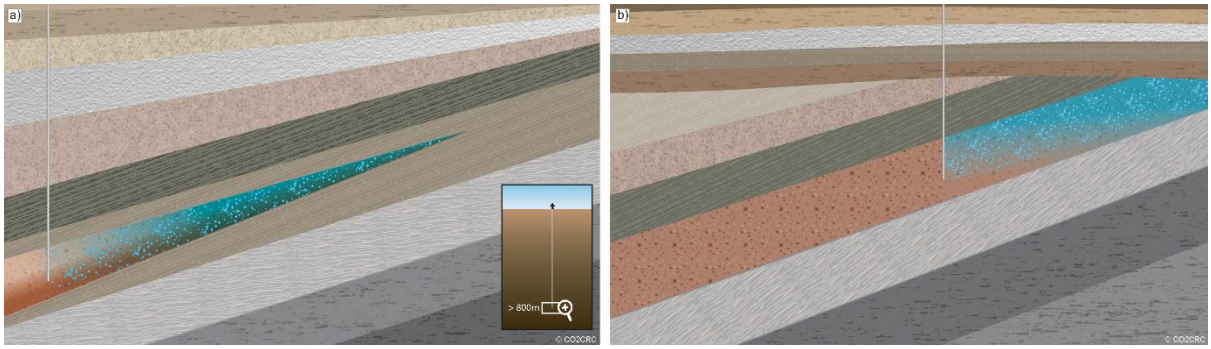

Figure 2.5: Stratigraphic trapping mechanisms in saline aquifers: a) CO_2 injected into a porous unit with facies variation forming a lateral and top seal. b) CO_2 injected into a reservoir overlain unconformably updip by a horizontal caprock (modified after CO2CRC, 2008).

2.3.3 Hydrodynamic Trapping

Hydrodynamic trapping occurs in "open", shallowly dipping saline aquifers (Fig. 2.6) where no lateral or structural traps occur. The formation waters are unconfined and slowly (few meters of lateral movement per year – Cook, 2012) migrate over 10's to 100's of kilometres (Fig. 2.6). The entrained and immiscible CO_2 injected into the reservoir migrates with the formation waters leading to a residence time of thousands to millions of years (Viljoen et al., 2010).

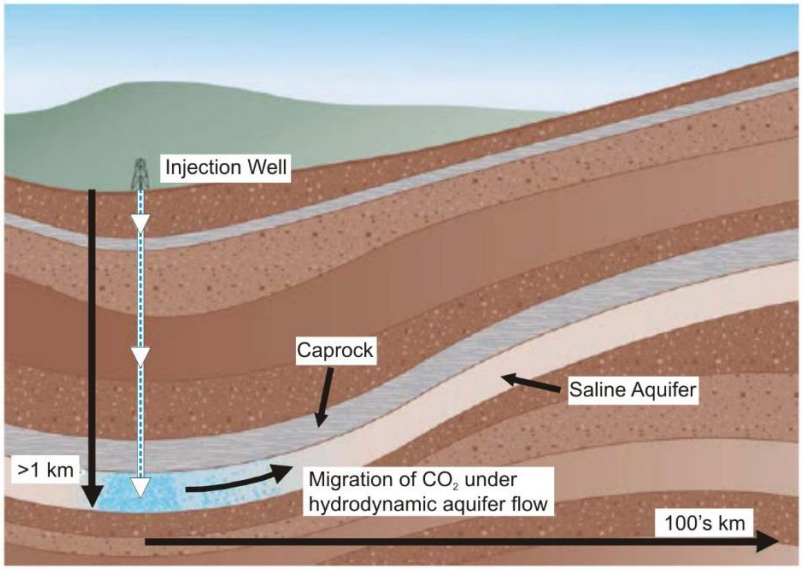

Figure 2.6: Hydrodynamic flow and trapping of CO_2 over 100's of km in a dipping saline aquifer system (modified after CO2CRC, 2008).

2.3.4 Residual Trapping

Residual trapping occurs when immiscible CO_2 is trapped in pore spaces within the reservoir (Fig. 2.7). Capillary action acting on the CO_2 will trap the fluid within pore space when the CO_2 concentration is not large enough to overcome the capillary pressure of the formation fluid in the pore throat. The formation then flows around the CO_2 in the pore space which is permanently trapped (Fig. 2.7). Cook (2012) suggests that estimating the proportion of CO_2 that will be residually trapped is difficult as this is defined by the "connectivity" of the pores based upon the geometry of the grains and associated pore throats. Based upon relative permeability curves, Viljoen et al. (2010) suggest that residual CO_2 saturation can range between 5 and 30%.

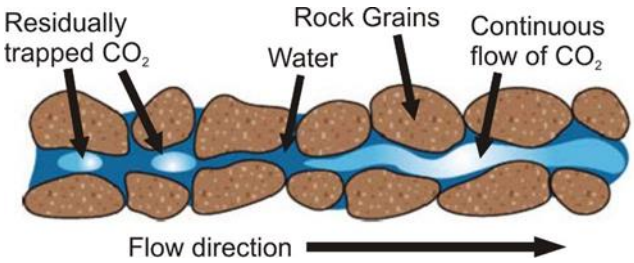

Figure 2.7: Residual trapping of CO_2 within pore spaces between grains in a saline aquifer system. Once trapped in this way Co2 is permanently stored and cannot migrate (modified after CO2CRC, 2008).

2.3.5 Solubility Trapping

During injection into saline aquifers a small proportion of the predominantly immiscible CO_2 is dissolved into the formation waters to form a layer of weak carbonic acid (Fig. 2.8). If reservoir conditions are constant, after time the proportion of storable CO_2 increases, which ultimately increases the density of the formation water over hundreds of years (Cook, 2012). Is has been illustrated by Pau et al. (2010) and Green and Ennis-King (2013), that once the resulting layer of carbonic acid is dense enough (time in thousands of years) it begins to sink (Fig. 2.8a). This creates convection within the underlying brine column (Fig. 2.8b), which increases the CO_2 intake at the top of the column. This suggests that over time, solubility trapping reduces the chance of supercritical CO_2 escape from saline aquifers due to diffusion and convection of dense carbonic acids in the reservoir.

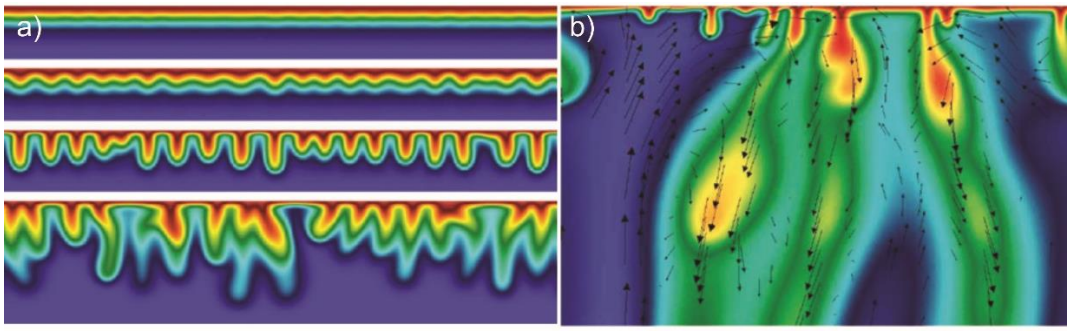

Figure 2.8: a) Evolution of density-driven CO_2 diffusion in brine. Increase in time from top to bottom. Red is concentrated CO_2 and carbonic acid. Blue is brine. b) Convection within the reservoir with arrows indicating flow orientations of brine and carbonic acid solutions. (after Pau et al., 2010).

2.3.6 Mineral Trapping

In some circumstances the mineralogy of the reservoirs host rock (calcium or magnesium silicates) allows for mineral trapping, whereby injected CO_2 reacts with cations of the formation waters or host rock to produce new stable mineral phases, such as calcium or magnesium carbonate (Cook, 2012). This trapping mechanism is thought to take place over thousands of years and is not relevant in human timescales, but once CO_2 is precipitated, the trapping is permanent. Research into mechanisms to speed up the process is underway (Cook, 2012).

2.3.7 Adsorption Trapping

Adsorption trapping is generally not related to deep saline aquifer storage and is mainly utilised in CO_2 storage through Enhanced Coal-Bed Methane recovery techniques, whereby the CO_2 is adsorbed onto coal during methane gas release.

CHAPTER 3

CRITERIA FOR ASSESSING GEOLOGICAL RESERVOIRS FOR STORAGE

3.1 INTRODUCTION

Although the geological storage of CO_2 has been proven viable through Enhanced Oil Recovery (EOR), as well as in industry-scale projects such as Sleipner in Norway and Boundary Dam in the Canada (GCCSI, 2015), new projects need to assess a number of criteria to aid in the evaluation of a potential storage site both economically and geologically. Although the surface geology in countries which host world-class oil or gas provinces is well known, often the lack of subsurface geological data below ~800 m hampers accurate assessment of storage calculations. This is especially true in countries such as South Africa whereby, except in areas such as the Witwatersrand goldfields in Johannesburg where large-scale deep mining occurs, the upper 100 m of the geology is well understood but data below that are exceptionally limited. The identification of prospective basins is defined by a number of characteristics, defined below, that allow for a basin to be ranked based upon its properties.

3.1.1 Basin-scale Selection and Characterisation

The Carbon Sequestration Leadership Forum (CSLF, 2008) compiled a techno-economic resource-reserve pyramid (Fig. 3.1) to depict the progression of a basins storage prospectivity based upon the scale of the investigation (*It must be noted that in this instance, although similar, the term "resource" and "reserve" are based upon the CSLF, [2008] classification and not the South African SAMREC code*[1], *with CO_2 storage capacity being defined as a geological commodity*). This pyramid was adapted by CO2CRC (2008) to define a basin's "Prospective, Potential and Operational" storage capacity. A country-scale screening undertaken by Viljoen et al. (2010), defined the theoretical capacity of South Africa's CO_2 storage potential, identifying basins with CO_2 prospectivity based upon criteria defined by CO2CRC (2008).

The effective (CSLF, 2008) or prospective (CO2CRC, 2008) storage capacity represents a basin-scale assessment (Fig. 3.1) and is obtained by "considering that part of the theoretical storage capacity that can be physically accessed and which meets a range of geological and engineering criteria" (CSLF, 2008). Forthwith it will be defined as prospective storage capacity as per CO2CRC (2008).

CSLF (2008) indicate that the prospective storage capacity of a specific sedimentary basin represents a subset of theoretical capacity, as it is obtained by considering site specific details such as tectonic and geological setting, geographical setting, depth to the top of reservoir, containment, subsurface geological properties, injectivity potential, and existing natural resources (Bradshaw et al., 2002). Prospective storage capacity estimates are therefore obtained through a basin-scale and regional-scale assessment as defined by (CSLF, 2008). Basin-scale assessments focus on evaluation of a sedimentary basin as a whole, to quantify its prospective storage capacity and identify potential suitable regions for CO_2 storage. Regional-scale assessment is then performed at an increasing level of detail in order to quantify the storage potential of selected regions within the basin that have

[1] A 'Mineral Resource' is a concentration or occurrence of material of economic interest in or on the earth's crust in such form, quality and quantity that there are reasonable and realistic prospects for eventual economic extraction. The location, quantity, grade, continuity and other geological characteristics of a Mineral Resource are known, or estimated from specific geological evidence, sampling and knowledge interpreted from an appropriately constrained and portrayed geological model. Mineral Resources are subdivided, and must be so reported, in order of increasing confidence in respect of geoscientific evidence, into Inferred, Indicated or Measured categories. (SAMREC Code 2009).

A 'Mineral Reserve' is the economically mineable material derived from a Measured or Indicated Mineral Resource or both. It includes diluting and contaminating materials and allows for losses that are expected to occur when the material is mined. Appropriate assessments to a minimum of a Pre-Feasibility Study for a project and a Life of Mine Plan for an operation must have been completed, including consideration of, and modification by, realistically assumed mining, metallurgical, economic, marketing, legal, environmental, social and governmental factors (the modifying factors). Such modifying factors must be disclosed.

known large potential for CO_2 storage (CSLF, 2008). Potential regions can then be scored and ranked in order to identify those with the best CO_2 storage prospectivity.

The prospective storage capacity of the basin defined as "*that quantity of pore space into which it is estimated, on a given date, that CO_2 will potentially be technically and economically injectable into an, as yet undiscovered, storage site or sites"* (CO2CRC, 2008). A workflow that details the different scales of assessment is depicted in Fig. 3.2.

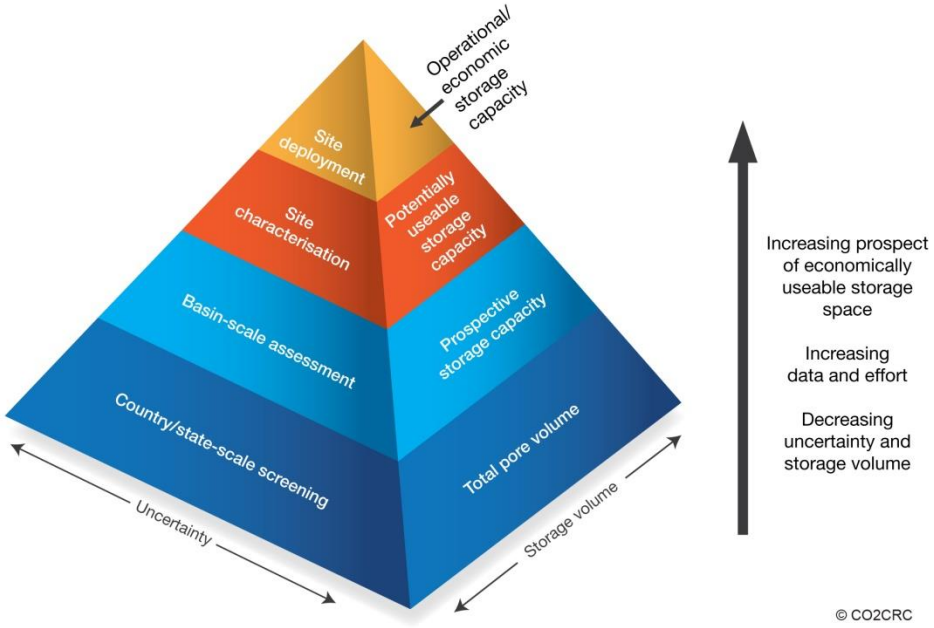

Figure 3.1: Techno-Economic Resource-Reserve Pyramid (after CO2CRC, 2008) showing matched storage volume (capacity) against scale of area/site assessment. The more detailed the assessment, the more accurate the storage capacity estimate.

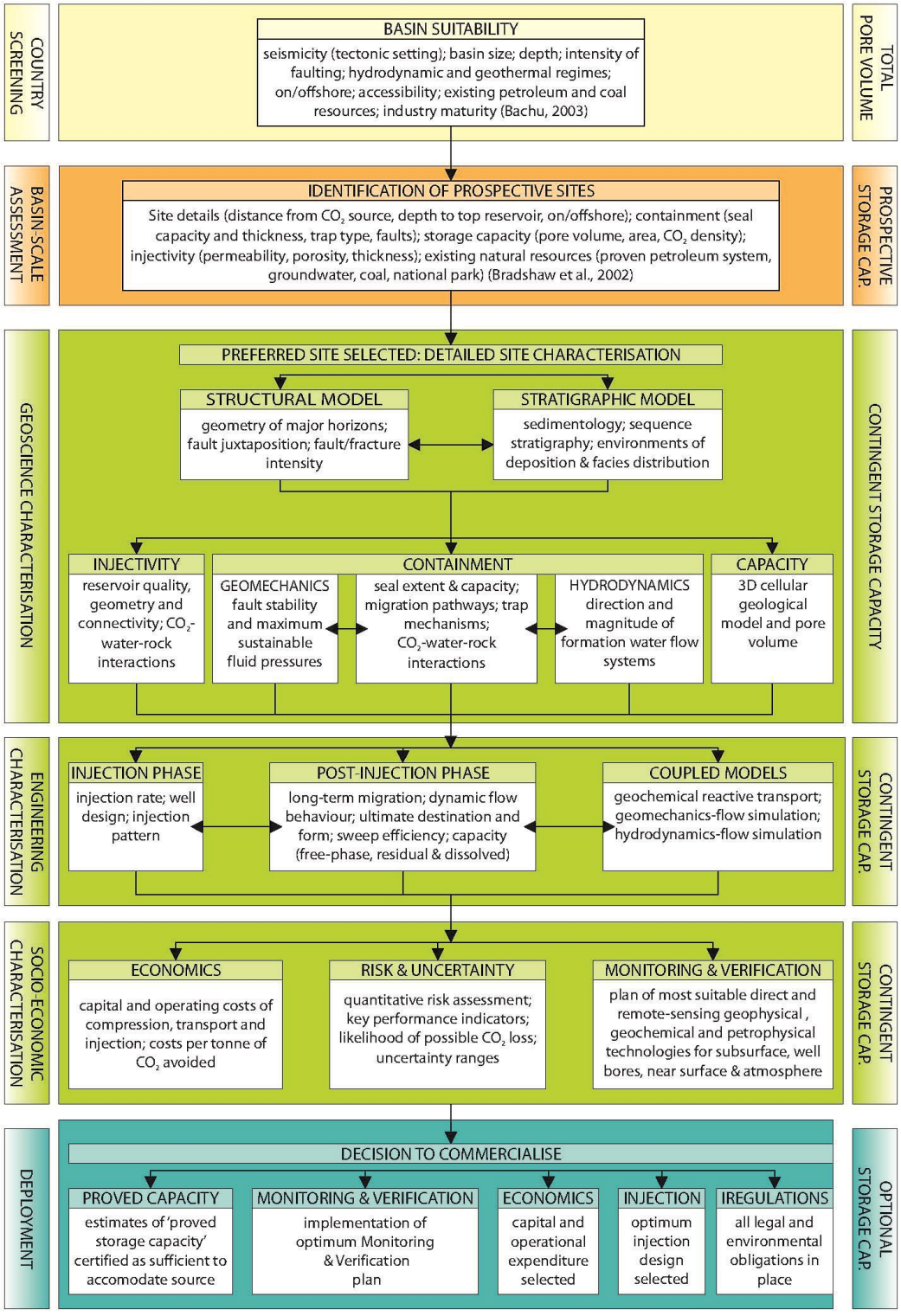

Figure 3.2: Site characterization workflow for geological storage of CO_2 (after CO2CRC, 2008).

A basin-scale assessment of a potential sedimentary basins geology is appraised in three steps (CO2CRC, 2008) to identify potential CO_2 injection and storage areas for further site specific investigation:

1. **Review basin stratigraphy**: The stratigraphy of both the basement and basin fill is reviewed to define basin formation and structure, and to identify sedimentary successions that may host potential units that will form reservoir-seal pairs.
2. **Determine presence, depth and distribution of reservoir-seal pairs**: Once potential sedimentary successions have been identified, the distribution of reservoir-seal pairs within the succession need to be mapped using available data, such as geological and structural maps, seismic sections and borehole data. Of major significance, are the mapping of top and base horizons (minimum and maximum depth) of potential reservoirs and their associated seals. For CO_2 to be in a dense, supercritical (and therefore less voluminous) state, the minimum depth for the top of the target reservoir (or base of overlying seal) must be below ~800 m depth from surface or seafloor (IPCC, 2005; CO2CRC, 2008). Focus should be upon potential reservoir/seal pairs below 800 m depth, however if potential marginal reservoirs (300-800 m depth) do exist these should not be discounted, but reference made to the fact that CO_2 will be subcritical and therefore too shallow for efficient CO_2 storage (CO2CRC, 2008). The maximum depth distribution is generally established from economic constraints such as the maximum cut-off depth for economic drilling of injection boreholes (~3500 m defined by CO2CRC, 2008) or the maximum number of boreholes that will be economically viable. Geological factors also play important roles in defining the depth distribution of potential reservoirs, with porosity and associated permeability reducing with depth due to diagenetic porosity loss (Ehrenberg and Nadeau, 2005). Although the depth window will vary within basins due to varying geological factors such as geothermal gradient, pressure, fluid composition and mineralogy, injectivity potential of a reservoir is generally reduced enough at depths below ~3500 m that it is no longer sufficient to allow for viable injection.
3. **Assess CO_2 migration pathways and possible traps**: The structural integrity and subsurface geometry of potential reservoirs and associated seals must be assessed to identify physical traps, such as structural closures and stratigraphic pinchouts, as well as to identify possible CO_2 migration pathways. CO2CRC (2008) suggest that this can be achieved using structural contour and isopach maps defined by seismic profile mapping, in combination with available borehole data. In the case of an open aquifer with little to no identifiable structural trapping mechanisms, potential reservoir/seal pairs may be applicable if the expected migration pathway is sufficiently long to residually trap or dissolve the injected CO_2 into the formation waters before it reaches subcritical depths or the surface (CO2CRC 2008).

3.1.2 Regional-scale Screening of Prospective Areas within a Basin

Once the basin-scale assessment has been completed and prospective sites/reservoirs have been identified, a regional-scale assessment can take place which ranks the relative merits of one potential reservoir area over another. CO2CRC (2008) proposed five key factors that are fundamental to any potential CO_2 storage site: storage capacity, injectivity potential, containment, site logistics and existing natural resources. The following definitions are taken from CO2CRC (2008).

1. **Storage Capacity**: this evaluates the total pore volume available for CO_2 storage at a particular site, and compares it to the likely CO_2 source volume that the site will need to accommodate (storage capacity). This is controlled by parameters such as size of the injection site area, the thickness of the reservoir, the pore volume available and the density of the CO_2. This is a very simplistic storage volume calculation at this point, as the data available at this semi-regional level of characterisation is unlikely to be sufficient to establish more than Prospective Storage Capacity.
2. **Injectivity Potential**: this considers the reservoir characteristics, such as permeability and porosity, which will impact on how easily the CO_2 can be injected into the reservoir.
3. **Site Logistics**: these are a reflection of the likely economic and technological feasibility, such as how deep an injection well needs to be drilled (depth to reservoir) or how far a pipeline might need to extend (distance from source).
4. **Containment**: this considers the seal and trap characteristics, such as the likely effectiveness of the seal based on its thickness, extent and lithology, or the migration distance (the longer the migration distance the greater the probability for secure trapping by residual, hydrodynamic or mineralisation mechanisms). Faulting size and intensity are also important containment considerations.
5. **Existing Natural Resources**: this assesses the likely presence of another resource that could potentially be compromised by CO_2 storage, such as oil and gas, mineable coal, potable water or proximity to population centres or national parks, which could limit surface operations.

3.2 SUITABILITY OF THE DURBAN BASIN FOR CO_2 STORAGE

Due to limited hydrocarbon exploration (Singh and McLachlan, 2003), Viljoen et al. (2010) indicate that prospectivity for CO_2 storage in South Africa is focussed upon saline aquifers within drift phase marine sedimentary rocks and sediments on the continental shelf. The prospectivity of a basin is defined by thirteen parameters ranging from geological factors such as tectonic setting, to economic constraints such as infrastructure development. The prospectivity of the Durban Basin is modelled in Table 3.1 (modified from Bachu, 2003).

The Durban Basin obtains a ranking of 0.59 based upon the above criteria. Initial rankings for the combined Durban/Zululand Basins by Viljoen et al. (2010) indicated an overall suitability ranking of 0.65 placing the basin 8th out of 13 basins considered. Viljoen et al. (2010) do however indicate that the basin obtains a high ranking (2nd out of 13) based upon geological suitability, but this is reduced due to lack of infrastructure and limited exploration within the basin.

Table 3.1: Criteria and classes used to assess the CO_2 geological storage potential of the Durban Basin (modified after Bachu, 2003; Viljoen et al., 2010). Red or 1 indicates the lowest score for a specific criterion, while dark green or 5 indicates a high suitability for a specific criterion. Final scores are divided by a total potential score of 65.

	Criterion	Classes				
		1	2	3	4	5
1	Tectonic setting	Very unstable	Unstable	Intermediate	Mostly stable	Stable
2	Size of basin	Very small (<1000 km^2)	Small (1000–5000 km^2)	Medium (5000–25000 km^2)	Large (25000–50000 km^2)	Very large (>50000 km^2)
3	Depth of basin	Very shallow (<300 m)	Shallow (300–800 m)		Deep (>3500 m)	Intermediate (800–3500 m)
4	Geology: reservoir/seal pairs	Poor		Intermediate		Excellent
5	Faulting intensity	Extensive		Moderate		Limited
6	Intrusions	Extensive		Moderate		None
7	Geothermal gradient	Warm basin (>30 ºC/km)		Moderate (30–40 ºC/km)		Cold basin (<30 ºC/km)
8	Hydrocarbon potential	None	Small	Medium	Large	Giant
9	Maturity	Unexplored	Exploration	Developing	Mature	Over mature
10	On-/offshore	Deep offshore	Shallow-Deep offshore	Shallow offshore		Onshore
11	Other economic commodities	Large-scale mining	Active mining	Confirmed (no mining)	Potential	None
12	Infrastructure	None	Minor		Moderate	Extensive
13	Major CO_2 sources	>1000 km	500–1000 km		300–500 km	<300 km

3.2.1 Tectonic setting and seismicity

The Durban Basin represents an extensional rift basin formed during the Jurassic and early Cretaceous as a result of extension during the breakup of Gondwana (Leinweber and Jokat, 2011). Initial extension resulted in trans-tensional stress, forming horst and graben basins along the continental shelf (Watkeys and Sokoutis, 1998) with the opening of the western Indian Ocean (Ben-Avraham et al., 1993). This was followed by dextral strike-slip which dominated the southern margin of the Durban Basin at the juncture with the termination of the Agulhas Falkland Fracture Zone (AFFZ). There is no onshore or seismic evidence to suggest that faulting affects strata younger than the Albian (von Veh and Andersen, 1990; Watkeys and Sokoutis, 1998; Watkeys, 2006). The basement beneath the continental shelf and Tugela Cone comprises block-faulted continental crust (du Toit and Leith, 1974; Goodlad 1986), whilst the abyssal plain is floored by either, highly thinned and rifted continental crust (Iliffe et al., 1991, Nairn et al., 1991), or rifted oceanic crust as part of a NE-SW spreading centre (Tikku et al., 2002; Leinweber and Jokat, 2011).

The Durban Basin is currently stable, with the USGS global seismicity database identifying three seismic events that have occurred in the Durban Basin since 1900 (Fig. 3.3a). Two events occurred to the north of the Tugela

Cone along the Naude Ridge (Fig. 3.3b). The first occurred on the 31st December 1932 and registered a magnitude of 6.6, whilst the second occurred on the 24th June 2006 and registered a magnitude of 4.4. The 6.6 magnitude event is recognised as the largest registered event to affect South Africa and its continental shelf. A recent 4.3 magnitude earthquake occurred in June 2015, centred along the KwaZulu-Natal north coast with the epicentre at a depth of 15 km (Fig. 3.3b). Hartnady (1990) suggests that this event is related to East African rifting with known events in the offshore Zululand and Mozambique Basins representing extensions of the Lake Malawi and Davie Ridge axes respectively (Fig. 3.3a). It must be noted however, that the lack of continued seismic activity identified in the USGS database for either the Durban Basin (Fig. 3.3b), or along the Agulhas Falkland Fracture System off the KwaZulu-Natal coastline (Fig. 3.3a), suggests that extension in these regions has ceased.

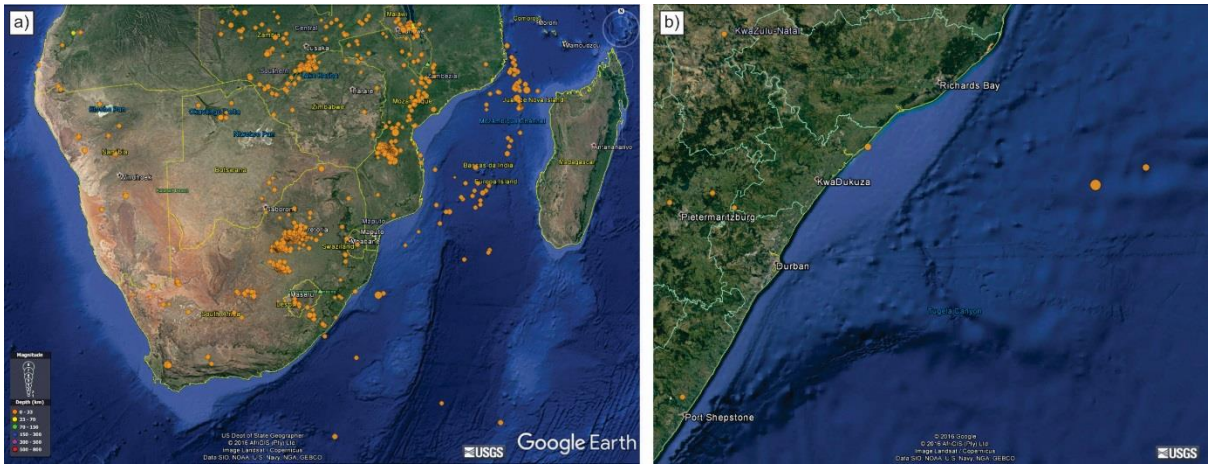

Figure 3.3: USGS seismic database maps illustrating all registered events between 1900-2017, with magnitudes of between 2.5 and 9 illustrated. a) Note the two linear zones of the East African Rift system, with the Lake Malawi zone on the left and the Davie Ridge zone on the right extending into the Mozambique Basin. b) Google Earth™ image of South Africa with associated seismicity based upon the USGS database. Note the clustering of events around gold mining activities in the Gauteng and Free State Provinces.

3.2.2 Size of the basin

The basin covers an area of ~10000 km^2 from offshore Durban to Richards Bay, extending to the east down to the 2500 m isobath (Broad et al., 2006). The Durban Basin is bounded to the north by the Naude Ridge, the east by the Mozambique Ridge, and to the south by the Southern Natal Valley (Fig. 1.3). Kitchin, (1995) and Ben-Avraham et al. (1997) propose that the southern boundary coincides with a major east-west trending fault system that forms the northern limit of the AFFZ.

3.2.3 Depth and thickness of the basin

The Cretaceous succession in the Durban Basin is up to 1000 m thick, overlain by ~2500 m of Cenozoic drift sediments (Broad et al., 2006). Depths to basin floor are highly variable with numerous basement highs located within the deep Natal Valley. The basement comprises multiple horst and graben structures with basal contacts varying between ~3500 m on basement highs (Jc-A1; Leith, 1971) to ~4500 m in graben structures (Jc-B1; GGS, 1983). The sedimentary succession forms a basinward-thickening sediment wedge attaining a potential maximum thickness of ~6000 m off the continental shelf break on the Tugela Cone (Goodlad, 1986).

3.2.4 Geology: Reservoir/Seal pairs

The lithological succession of the Durban Basin, comprises Mesozoic to Cenozoic deposits that can be biostratigraphically correlated with the onshore Zululand and Maputaland Groups north of Richards Bay (McMillan, 2003). The basal syn-rift sediments represent tectonically compartmentalised Late Jurassic to Late Cenomanian sediments consisting primarily of interbedded, claystones, siltstones and sandstones with fine-grained sandstone units defining major unconformities within the succession. Petroleum Agency SA, (2012) indicate that as the boreholes in the Durban Basin were drilled upon basement highs, no sandstones of appreciable thickness were intersected. Singh and McLachlan (2003) suggest that the wells were sited to intersect synrift sediments draped over basement horst structures, but these zones have been reinterpreted as sediment bypass zones, with large sediment thicknesses identified basinward of the drilled area. However, well completion reports for Jc-B1 (GGS, 1983), Jc-C1 (Muntingh, 1983) and Jc-D1 (Phillips Petroleum, 2000) note the development of sandstone packages at multiple depths. Seismic evidence suggests that sandstones are likely to be present as basin floor fans, turbidites, channel systems, and stacked structural closures (Singh and McLachlan, 2003).

Kitchin and McLachlan, (1996) suggest that Cretaceous-age seal units within the Durban Basin are represented by claystones of varying ages. Although it has been considered that within the Jc-series boreholes the Turonian is overlain by deep marine claystones of late Turonian to Campanian age, Kitchin and McLachlan (1996) indicate that further detailed mapping is needed to accurately define the quality of the seals. Unfortunately as limited coring was undertaken in all wells, a lack of data exist to accurately define the quality and capabilities of the seals in the Durban Basin.

3.2.5 Fault intensity

Faulting within the basin is confined predominantly to Jurassic basement lithologies and does not appear to affect units younger than the Albian (von Veh and Andersen, 1990; Watkeys, 2006). Offshore, Ben-Avraham et al. (1997), describe arcuate NE-SW to ENE-WSW trending structural elements similar to those described by Von Veh and Andersen (1990) onshore (Fig. 3.4). Although numerous minor extensional faults exist within the offshore basement, the basement morphology is dominated by four major normal faults, defining a deep rift graben landward of a major basement horst structure (Ben-Avraham et al. 1997). Minor faulting therefore occurs on the 1-5 km scale, whilst major basement faults occur on a ~10 km scale

3.2.6 Intrusions

The synrift and drift sedimentary successions preserved in the Durban Basin accumulated subsequent to the termination of Karoo Igneous Province volcanic activity (Watkeys, 2006). No volcanic or intrusive units affect the drift phase sedimentary succession within the basin.

3.2.7 Geothermal regime

Leith (1971) indicates a geothermal gradient of 2.73°C/100 m within the Jc-A1 borehole with a static temperature of 72.2°C at a depth of 2378.4 m. Geothermal gradients recorded within the Jc-B1 well, although potentially overprinted by intrusive igneous bodies at depth (GGS, 1983), indicate a low geothermal gradient of 2.6 – 3.0°C/100 m (Fig. 3.5). Muntingh (1983) defines a geothermal gradient of 2.67°C/100 m for the Jc-C1 well, with a static temperature of 94°C at 3121 m depth. Geohistory modelling was undertaken by GGS (1983) in an attempt to simulate geothermal variations through igneous intrusions. A maximum high gradient of 4°C/100 m cooling to 2.7°C/100 m at depth was modelled, however these high values are merely speculative.

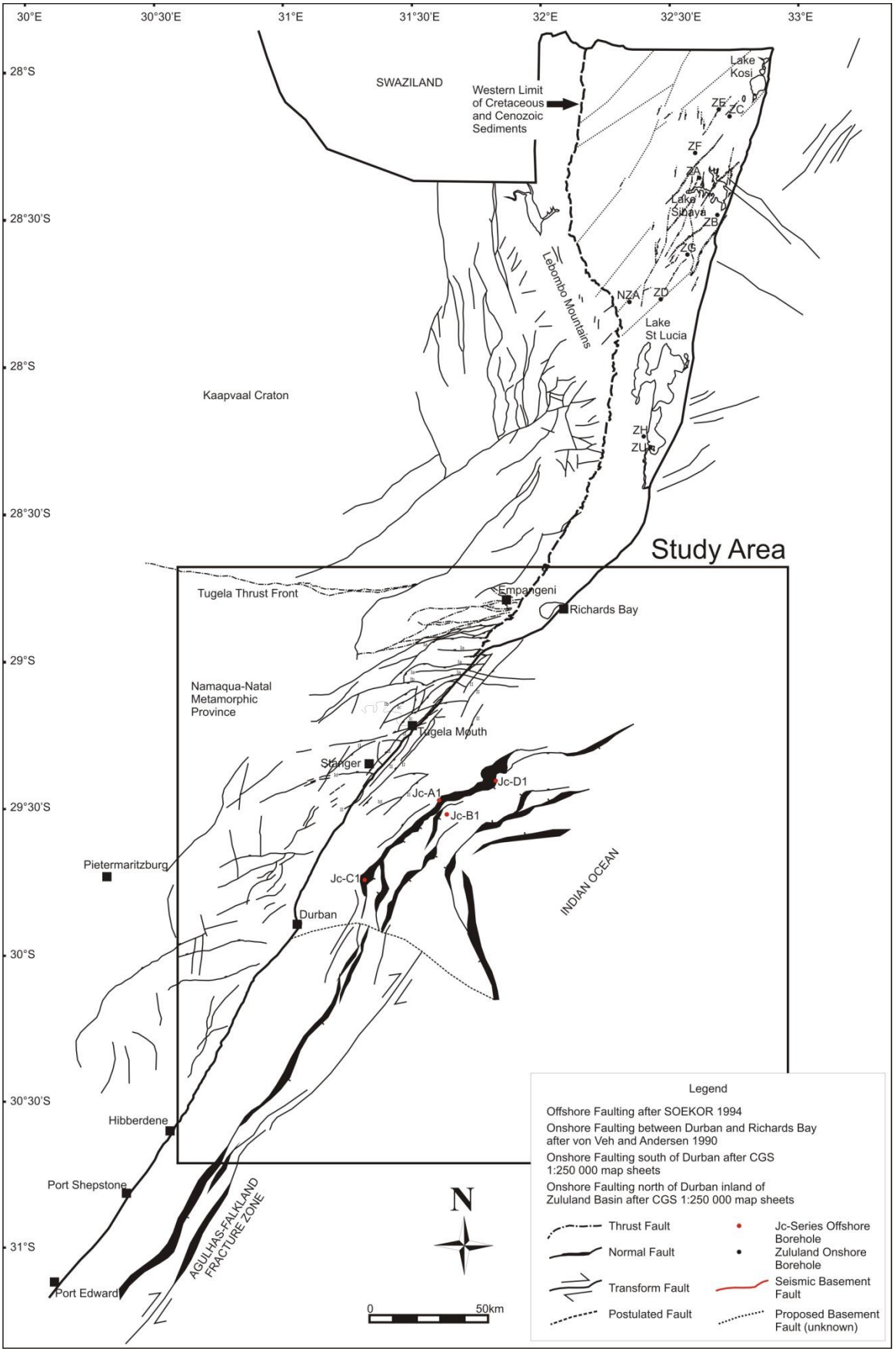

Figure 3.4: Tectonic map of the offshore Durban Basin compiled from Kitchin (1995) and Ben-Avraham et al. (1997). Onshore data compiled from Von Veh and Andersen (1990).

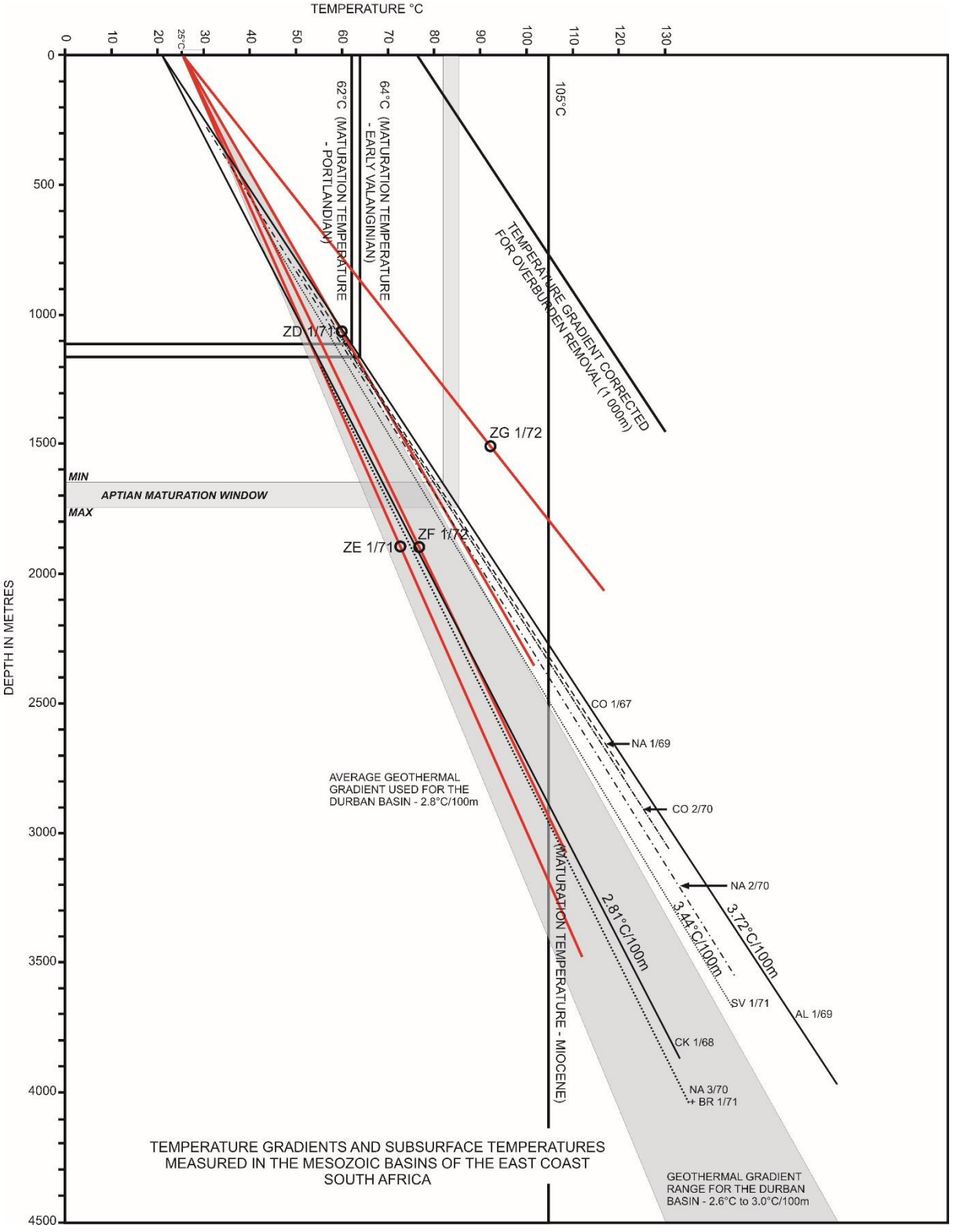

Figure 3.5: Geothermal gradient plot measured for Mesozoic Basins along the east coast of South Africa. Geothermal gradient range for the Durban Basin shown in grey (modified after GSS, 1983). Geothermal gradients (red lines) for wells listed ZD 1/71; ZE 1/71; ZF 1/72; ZG 1/72 are from the onshore Zululand Basin in northern KwaZulu-Natal. Geothermal gradients for wells listed Br 1/71; NA 3/70; CK 1/68; SV 1/71; AL 1/69; NA 2/70; CO2/70; NA 1/69; CO 1/67 (black dashed and solid lines) represent gradients for the onshore Algoa Basin near Port Elizabeth.

3.2.8 Presence or potential, and size of oil/gas deposits

Analyses undertaken by Petroleum Agency SA have identified numerous potential organic-rich shale source rocks within the Durban Basin (Singh and McLachlan, 2003). It is proposed by Singh and McLachlan (2003) that these units are likely to occur within Jurassic grabens, as well as Barremian to Aptian, and Cenomanian to Turonian shales identified in wells. Despite showing good oil and gas reservoir characteristics, limited oil or gas shows have been identified during exploration drilling, with the Jc-B1 well exhibiting a minor gas show within shales with a total organic content between 2.75 and 5% (Petroleum Agency SA, 2012). Fluid inclusion studies of core from the Jc-D1 well identified fluorescence and evidence for light hydrocarbon seeps which yielded slightly biodegraded oil derived from marine claystone of Cretaceous to Jurassic age (Petroleum Agency SA, 2012).

3.2.9 Maturity

Maturation information from the Jc-B1 well is hampered at depth in syn-rift formations by the presence of numerous intrusive igneous bodies within syn-rift sediments below 3434 m (GGS, 1983). However the geothermal gradients suggest that oil generation could only occur at depths below 3 km. Some geohistory modelling was undertaken by GGS (1983) in an attempt to simulate possible geothermal gradient variations caused by intrusions.

3.2.10 Onshore/offshore sites

In comparison with onshore sites, offshore basins are generally much more costly to utilise for storage of CO_2, however the offshore regions in South Africa host the most potential for CO_2 storage (98%). The wealth of offshore exploration data that allows one to define these areas as prospective is attractive, as onshore data are often not available. Although the Durban Basin remains a frontier basin with only four exploration wells compared with ten in the onshore Zululand Basin to the north, the areal extent of the basin, combined with detailed seismic data make this a viable basin for research.

3.2.11 Economic mineral commodities

Other than potentially undiscovered oil or gas plays, no economic mineral commodities are known in the Durban Basin. Petroleum SA (2012) identified numerous potential play types, including four-way dip anticlinal structures, basin floor fan complexes and pinchout plays.

3.2.12 Infrastructure

The offshore Durban Basin has no hydrocarbon extraction infrastructure. Four capped wells exists, but offshore pipelines are limited to the SAPREF Refinery's (a joint venture between Shell SA Refining and BP Southern Africa) offshore pumping pipeline that serves for import of crude oil to the Durban-based refinery. Onshore however, road and rail infrastructure is numerous (Fig. 3.6). Oil and gas pipelines currently operate between Durban, Richards Bay and Secunda in the Mpumalanga Province.

3.2.13 Distance from major CO_2 sources

Although Durban-based industry produces ~20 Mt CO_2/a, Engelbrecht, et al. (2004) suggest that 90% of major CO_2 point sources occur within the Gauteng and Mpumalanga Provinces (< 105 257 Gg/a), with other hubs producing only a fraction of the emissions (Fig. 3.7)

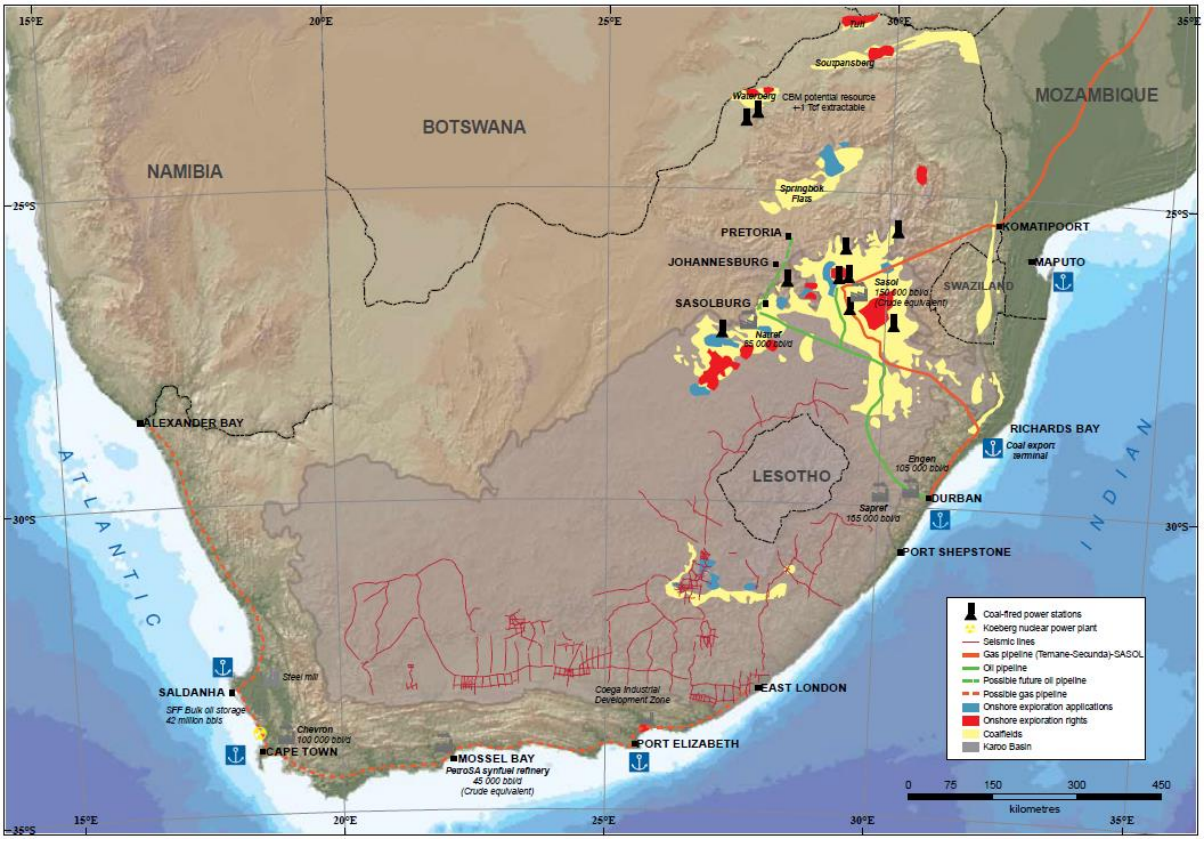

Figure 3.6: Illustrative map of major stationary CO_2 sources (coal-fired power plants), coalfields and onshore seismic and pipeline infrastructure in South Africa (after Petroleum Agency SA, 2008).

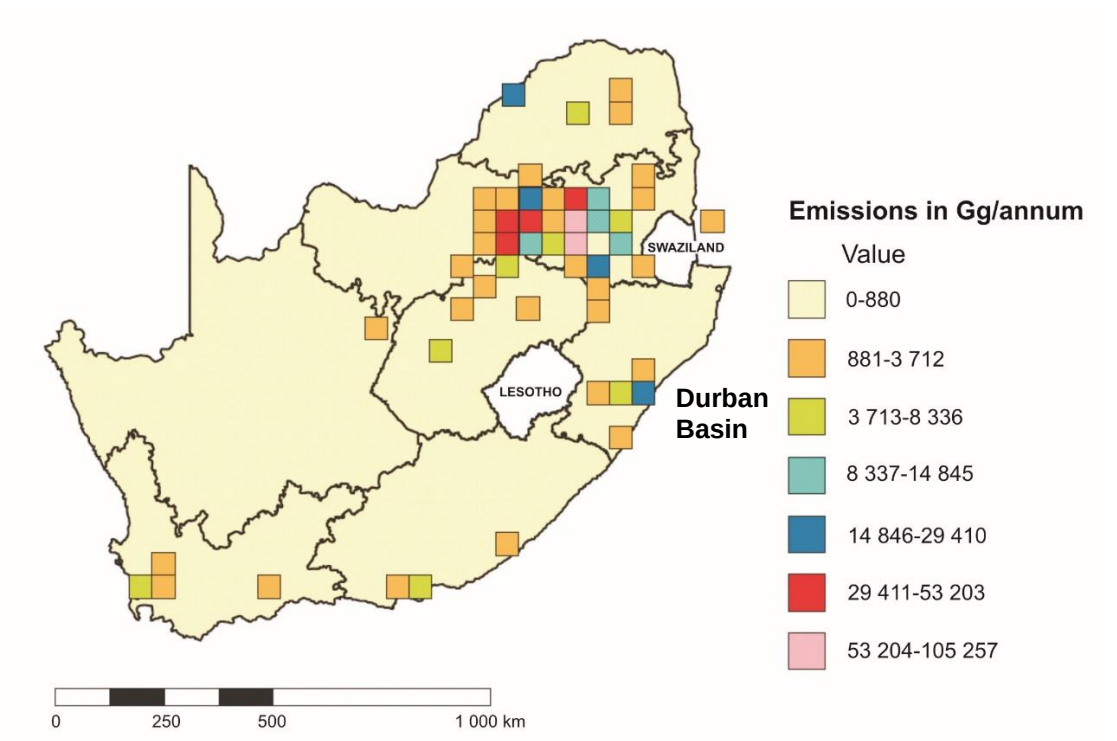

Figure 3.7: Illustrative map of CO_2 emissions point sources and concentrations in South Africa (after Engelbrecht et al., 2004).

CHAPTER 4

REGIONAL SETTING

4.1 LOCALITY

The study area (Fig. 1.3) lies along the eastern continental margin of South Africa, defined by a narrow 10000 km^2 (Broad et al., 2006) sedimentary basin, the offshore Durban Basin. The eastern continental margin of South Africa is unique, having been subject to prolonged periods of sediment starvation, coupled with tectonic-induced periods of abundant sediment supply (Green, 2011a). It is dominated by an extremely narrow (~2-12 km) shelf (Martin, 1984; Martin and Flemming, 1986; Green and Garlick, 2011; Cawthra, et al., 2012), considered a morphologically inherited feature of the initial shearing phase during margin development (Martin, 1984). This study examines the Durban Basin of the SE African margin, a north-south trending, sediment-filled, sheared-rift basin (Dingle et al., 1978). The basin itself is conspicuous by the development of the Tugela Cone, an anomalous deep-water fan complex of late Cretaceous to Tertiary-age (McMillan, 2003), that occurs beneath and seaward of the present shelf break.

Limited research has been undertaken on the geological evolution and depositional history of pre-Cenozoic sediments (du Toit and Leith, 1974; Dingle et al., 1978; Martin, 1984) with the majority of studies on the KwaZulu-Natal continental shelf have dealt only with near surface geomorphological or geological regimes (du Toit and Leith, 1974; Dingle et al., 1978; Martin, 1984; Sydow, 1988; Ramsay, 1994; 1996; Shaw, 1998; Green et al., 2007; Green and Uken, 2008; Green, 2009a; 2009b; 2011a; Green and Garlick, 2011; Cawthra et al., 2012; Green et al., 2013). This area, although having been the target for oil and gas exploration between 1970's to 2000, has not been well studied (du Toit and Leith, 1974; Goodlad, 1986; Visser, 1998), with a sparse seismic coverage across the east coast of southern Africa amounting to ~7000 km of 2D seismic and four wildcat wells (Petroleum Agency SA, 2015). Until now no detailed study concerning the sedimentology, evolution or CO_2 storage potential of this region has been undertaken.

4.2 PHYSIOGRAPHY

Extending between the coastline and the 2000 m isobaths (Fig. 4.1), the ~5000 m thick sedimentary basin-fill succession is derived from high sediment influx via the large Tugela River as well as short, fast flowing river systems which have been in existence from the mid Cretaceous (Dingle et al., 1978; Partridge and Maud, 2000; Green et al., 2013). The KwaZulu-Natal continental margin is bounded by a narrow shelf, except in the region of the Tugela Bank where it broadens to ~45 km due to the progradation of the Tugela Cone, and a change from sheared margin to rifted section (Martin, 1984; Martin and Flemming, 1986).

The Tugela Bank comprises a shallowly dipping, 0.2° (Goodlad, 1986) continental shelf with the shelf-break at -100 m. Seaward of the shelf-break Goodlad (1986) separated the Tugela Cone into seven physiographic units; within the study area however, these can be combined into a poorly developed continental slope and relatively shallow, broad continental rise (Gerrard and Wood, 1978). The upper slope is defined by shallow gradients of 1.7°-2.1°, compared with world averages of 4.28° (Goodlad, 1986). The slope and rise are dissected by the Tugela Canyon which heads in the upper slope, 50 km offshore and obliquely crosscuts the Tugela Cone from NW to SE (Goodlad, 1986; Wiles et al., 2013). To the west of the Tugela Cone, the continental rise is separated from the Mozambique Ridge by a deep abyssal plain which deepens to the south, finally merging with the Southern Natal Valley at 4000 m water depth (Fig. 4.1).

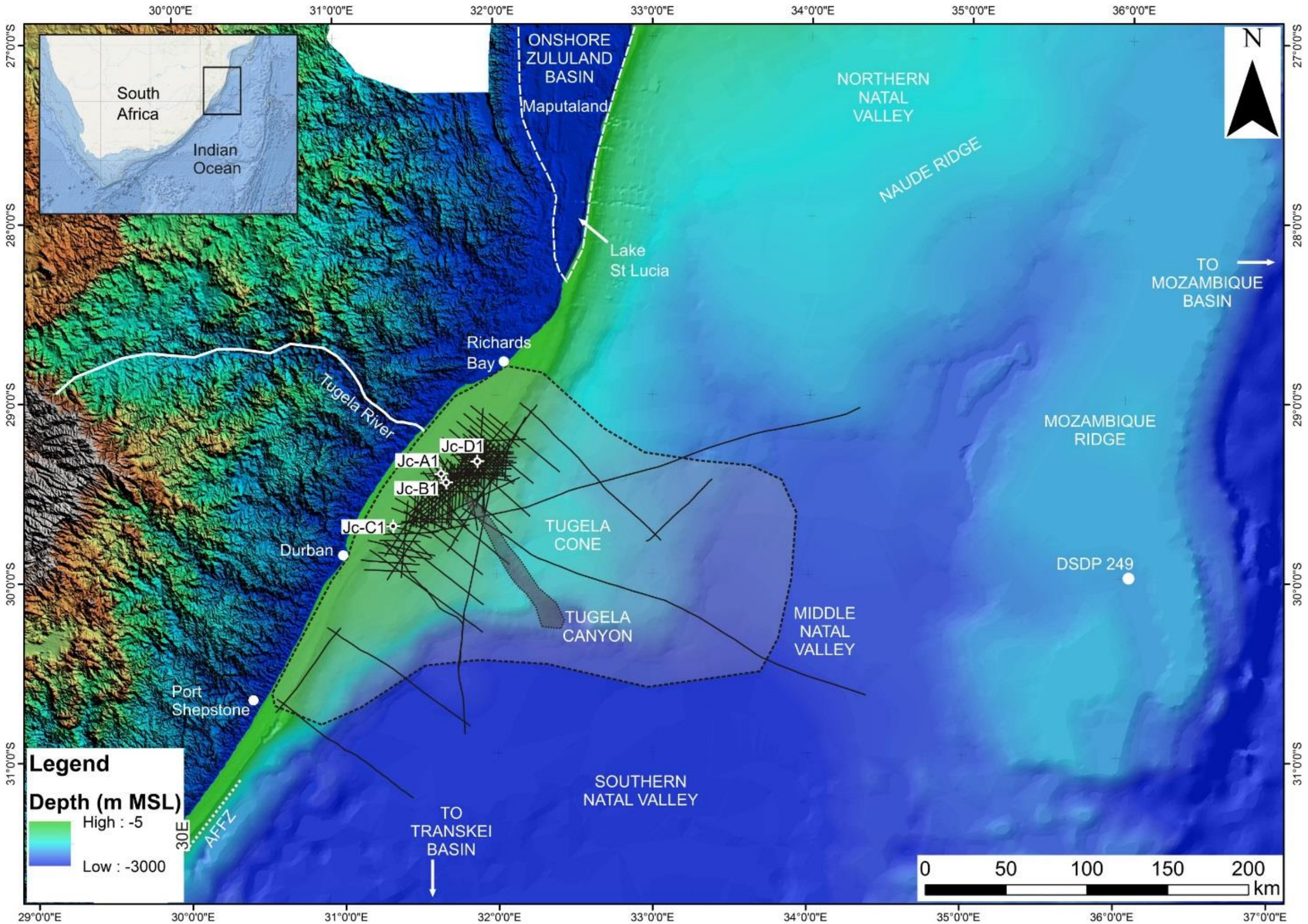

Figure 4.1: Hillshade/bathymetry map detailing study area location. The areal extent of the Durban Basin is shown within the shaded polygon. Note the relative position of the Jc-series boreholes drilled on the continental shelf to that of the deep water Tugela Cone overlying the continental rise, the Natal Valley, and Transkei, Zululand and Mozambique Basins.

4.3 REGIONAL GEOLOGY

The KwaZulu-Natal continental margin is characterised by a multitude of geological units spanning ~3.1Ga (Fig. 4.2a). The basement of the KwaZulu-Natal coastal region south of S 28°45' consists primarily metamorphosed, ~1200-1000 Ma granite-gneiss complexes of the Namaqua-Natal Metamorphic Province (Cornell et al., 2006) which crop out onshore between ~5-30 km inland of the coastline, whilst to the north of S 28°45' the exposed basement comprises Archaean (~3.1Ga) granite and gneiss of the Kaapvaal Craton (Robb et al., 2006) (Figure 3.4; 4.2a). Neither of these units are intersected in offshore boreholes however, with basement comprising sedimentary successions of either Ordovician Natal Group or Carboniferous to early Jurassic Karoo Supergroup (Leith, 1971; Muntingh, 1983). Extension during the late Jurassic resulted in faulting along the eastern margin of the Kaapvaal Craton, forming depocentres which would later constitute Mesozoic basins onshore and offshore of southern Africa from Mozambique to Namibia (Fig. 4.3b).

4.3.1 Basin Development

The Mesozoic evolution of the Durban Basin is poorly documented (du Toit and Leith, 1974; McMillan, 2003); with work focussed on either low resolution single-channel seismic reflection data (Dingle et al., 1978; Martin, 1984; Goodlad, 1986), or seafloor sediment dynamics, submarine canyon formation and Holocene geology (Green and Garlick, 2011; Cawthra et al., 2012; Green et al., 2013; Wiles et al., 2013). The basin is structurally complex with basement comprising rifted Carboniferous-Jurassic sedimentary and volcanic lithologies of the Karoo Supergroup (Johnson et al., 2006).

The basin owes its existence to continental rifting during early Gondwana break-up ~183-159 Ma (Fig. 4.3; Watkeys, 2006; Leinweber and Jokat, 2011), bounded to the north by the Naude Ridge, the east by the Mozambique Ridge, and to the south by the Southern Natal Valley (Figs 1.3; 4.1) (Martin et al., 1981; Goodlad et al., 1982). The southern boundary coincides with a major east-west trending fault system that forms the limit of the Agulhas-Falkland Fracture Zone (AFFZ) (Broad et al., 2006). The final stages of rifting in the basin occurred between 115-90 Ma Watkeys and Sokoutis (1998), with passive margin conditions prevailing since ~90Ma (Ben-Avraham et al., 1993; Watkeys, 2006) (Figs 4.2b; 4.3). It forms a structurally complex, sheared, passive margin basin (Broad et al., 2006), comprising early Cretaceous and Cenozoic sedimentary successions (McMillan, 2003) dominated by a Cenozoic deep-water fan complex, the Tugela Cone, developed beneath and seaward of the present shelf (Broad et al., 2006).

Basement beneath the continental shelf and Tugela Cone comprise block-faulted continental crust (du Toit and Leith, 1974; Goodlad 1986) (Fig. 4.2a), whilst the abyssal plain is floored by either, highly thinned and rifted continental crust (Iliffe et al., 1991, Nairn et al., 1991), or rifted oceanic crust as part of a NE-SW spreading centre (Tikku et al., 2002; Leinweber and Jokat, 2011). The final stages of rifting (Fig. 4.3) in the Natal Valley occurred between 115-90 Ma (Watkeys and Sokoutis, 1998), with passive margin conditions prevailing since ~90Ma (Ben-Avraham et al., 1993; Watkeys, 2006). Although passive continental conditions have prevailed within the study area since the early Cretaceous, the breakup of Gondwana is regarded as a continuous event, commencing in the Jurassic and continuing today (Watkeys, 2006).

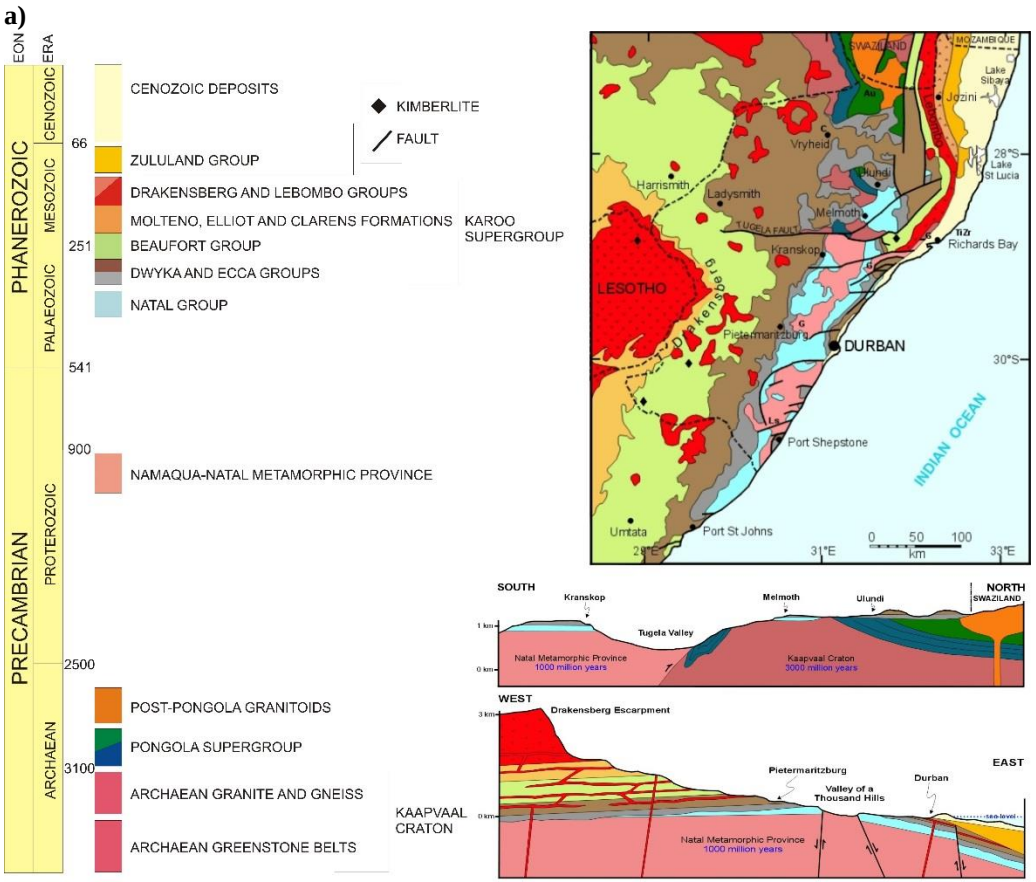

Figure 4.2: a) Stratigraphy, regional geology and geological cross-sections of KwaZulu-Natal (modified after 1:000000 scale geological map sheets, Geological Survey, 1984, Pretoria, Government Printer, NE & SE sheets).

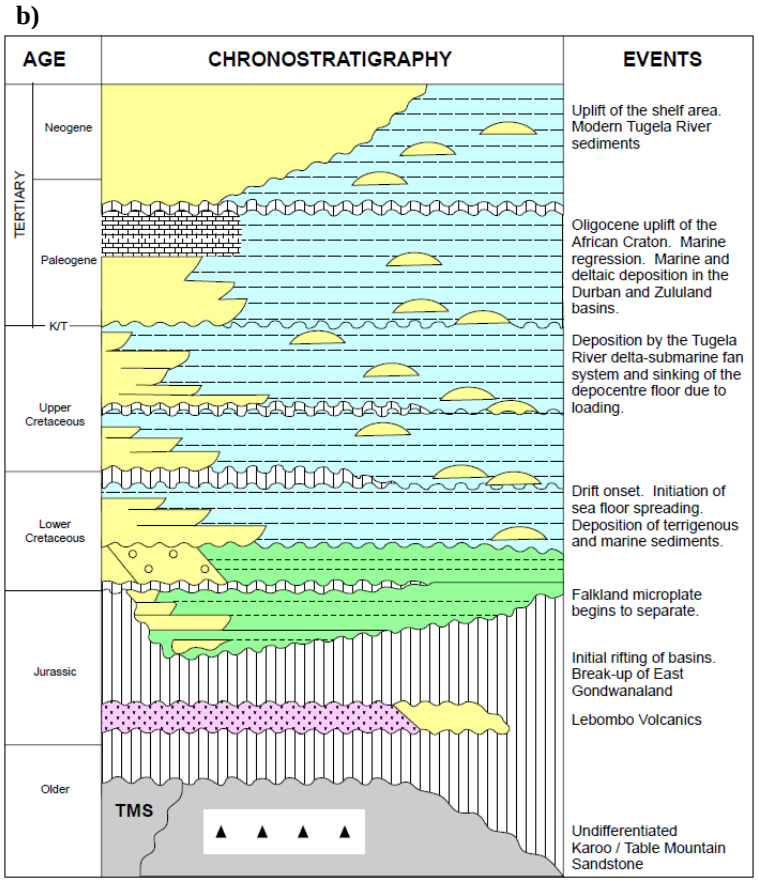

b) Chronostratigraphy and tectonic events within the Durban and Zululand basins, South Africa (after Petroleum Agency SA 2012).

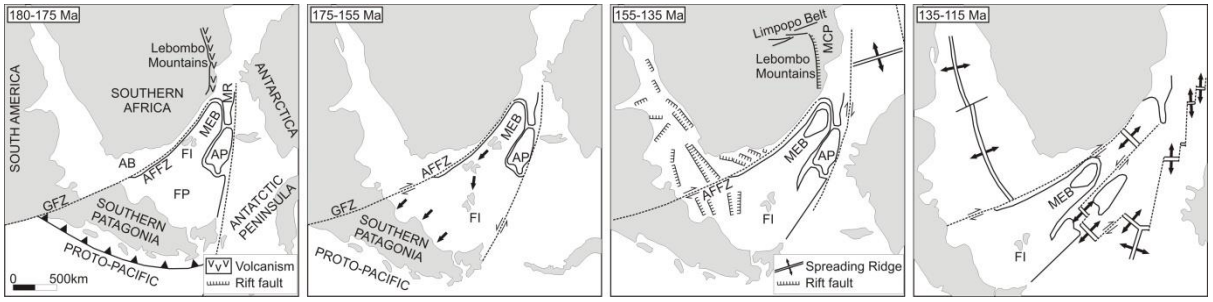

Figure 4.3: Sequence of Gondwana break-up events from 180 Ma to 115 Ma (modified after Watkeys, 2006). The formation of the Agulhas-Falkland Fracture Zone (AFFZ) and extraction of the Maurice Ewing Bank (MEB) and Falkland Islands (FI) to create the Natal Valley (NV) and Mozambique Ridge (MR) is shown.
Key – (GFZ) Gastre Fault Zone, (AB) Agulhas Bank, (FP) Falkland Plateau, (AP) Agulhas Plateau.

4.3.2 Sedimentary Basin-Fill Successions

Work within the offshore basin is limited, with evaluations of the southern- and mid-Natal Valley having been undertaken by Martin (1984) and Goodlad (1986). Regional biostratigraphic and chronostratigraphic analysis has been undertaken by McMillan, (2003), however the most comprehensive sequence stratigraphic work is limited to the Cenozoic deposits located on the narrow continental shelf between Durban and Lake Sibaya (Green, 2009b; Green, 2011a; 2011b; Green and Garlick, 2011; Green, et al., 2013).

During continental separation, high mean surface elevations (2000 to 2500 m amsl) of the hinterland (Fig. 4.1) resulted in rapid erosion along the marginal escarpment, providing much of the sediment budget for the southern African continental shelf during the Cretaceous (Partridge et al., 2006). Barremian to Cenozoic age sediments comprise the basin-fill with the main focus of sedimentation occurring within the Tugela Cone in the Durban Basin (Fig. 4.2b).

Along the coastal margin of the KwaZulu-Natal Province, South Africa, Cretaceous and Cenozoic lithologies are largely absent (Dingle et al., 1983) with lithologies of Santonian to Campanian age limited to small isolated coastal outcrops in southern KwaZulu-Natal. Cretaceous deposits are however well preserved in Maputaland, northern KwaZulu-Natal, where a >2000 m thick succession (Shone, 2006) occurs within the onshore Zululand Basin (Fig. 4.1; 4.2b). The sedimentary basin-fill of the onshore Zululand Basin is defined by the late Barremian to late Maastrichtian Zululand Group which is subdivided into three formations, the lower Makatini, middle Mzinene, and upper St Lucia Formations (Kennedy and Klinger, 1975). Dingle et al. (1983) indicate that the subdivisions are defined by several major unconformities represented by non-sequences across the Upper Aptian / Lower Albian boundary (separating the Makatini and Mzinene Formations), and Upper Cenomanian through Turonian (separating the Mzinene and St Lucia Formations). Although predominantly covered by Cenozoic sands, onshore exposures within the Zululand Basin extend from the lower Mfolozi River valley, along the shorelines of Lake St Lucia through the Mkhuze and Phongola River valleys into Mozambique, a distance of over 250 km (Kennedy and Klinger, 1975).

Palaeocene and Eocene sedimentation is absent throughout the coastal margin, with early Miocene to early Pliocene sediments occurring as a marine regressional package (Uloa and Umkwelane Formations) overlying Cretaceous sediments in northern KwaZulu-Natal (Roberts et al., 2006). The Uloa Formation is represented by an upward shoaling sequence of shallow marine coquina and sandstone overlain by aeolianite, calcarenite and decalcified red soils (Roberts et al., 2006; Porat and Botha, 2008). The lack of preservation of Cenozoic deposits along the KwaZulu-Natal coastline is due to a chain of compounded hiatuses that together span the late Palaeocene to early Pliocene (McLachlan and McMillan, 1979; Dingle et al., 1983). Flores (1973) and Förster (1975) however, indicate substantial Cenozoic deposition to the north in onshore Mozambique, with individual hiatus periods correlated with the early Oligocene, mid-Miocene and early Pliocene (Martin, 1984).

As with the onshore deposits, the inner continental shelf along the KwaZulu-Natal coast is dominated primarily by a major hiatus spanning the late Palaeocene to early Pliocene (Green, 2011a; Green and Garlick, 2011). Green (2011a) proposed that this protracted hiatus occurs through compounded hinterland uplift episodes within south-eastern Africa during the early-Oligocene, mid-Miocene and Pliocene.

Prior to the hydrocarbon exploration of the mid 1980's to 2000's, detailed descriptions of the seismic and well data within the basin were lacking. The work of Martin et al. (1982) and Goodlad (1986) used limited biostratigraphical data (du Toit and Leith, 1974) and regional seismic profiles to define three regional reflecting horizons within the mid-Cretaceous (McDuff), Oligocene (Angus), and Pliocene (Jimmy). These were correlated with major hiatuses in the northern Natal Valley. Reflector McDuff is correlated with a Cenomanian/Turonian hiatus present in all Cretaceous basins around southern Africa (McMillan, 2003). Reflector Angus correlates with an early Oligocene hiatus identified by du Toit and Leith (1974) in Jc-A1 whilst reflector Jimmy, correlates with an early Pliocene hiatus in the offshore Durban Basin (Dingle et al., 1983; Goodlad, 1986).

Based on regional unconformities identified from the biostratigraphy of the Jc-series boreholes and 2D seismic reflection data, Dingle et al. (1978) and McMillan (2003) subdivided the units into syn-rift and drift sequences broadly correlated with the coeval Zululand Group in the onshore Zululand Basin to the north of the study area (Fig. 1.3) (Broad et al., 2006). Here the sediments are subdivided into three unconformity-bound formations, the Makatini, Mzinene and St Lucia Formations (Broad et al., 2006). Since the late Cretaceous, drift phase deposition along the continental shelf is marked by several hiatuses which have resulted in incomplete stratigraphic preservation (Green, 2011a).

McMillan (2003) suggests that the early sedimentary history of the basin is erratic, with sedimentation occurring as graben fill successions loosely correlated with the Makatini and lower Mzinene Formations. A major unconformity spanning mid Cenomanian to upper Turonian times is represented by a regional seismic reflector McDuff (Dingle et al., 1978), which marks the boundary between the Mzinene and overlying St Lucia Formations. This reflector is overlain by a wedge of late Cretaceous strata which pinches out upslope from the deep basin. Although not obvious in legacy, wide-spaced regional seismic data (Dingle et al., 1978; Goodlad, 1986), the Cretaceous/Cenozoic boundary is represented by a prominent reflector (McMillan, 2003) which marks the top of the St Lucia Formation.

Cenozoic deposits characterise the near-shore with large dune cordons developed along the coastline. In the offshore, the Durban and Zululand basins are dominated by Cenozoic basin-fill, with Cretaceous lithologies confined to syn-rift infills. Early Cenozoic deposition within the Durban Basin has no lateral correlation with onshore deposits within South Africa, but can be correlated with offshore successions in Mozambique (Coster et al., 1989). This period of sedimentation is strictly associated with the construction of the Tugela Cone, an asymmetric submarine delta-fan complex developed seaward of the Tugela River (Goodlad, 1986). Dingle et al., (1978) and Goodlad, (1986) correlated a regional seismic reflector "Angus" with either a Miocene or Oligocene hiatus. Dingle et al. (1978) identified a similar period of non-deposition in the abyssal plain between the Maastrichtian and early Miocene (Dingle et al., 1978). A regional seismic reflector Jimmy (Goodlad, 1986) represents a late Pliocene/early Pleistocene unconformity which is traceable throughout the Natal Valley (Green, 2011a) but not in the Jc-Series boreholes. Post-Jimmy deposits reflect sediment starvation of the upper margin, with late Pleistocene deposits occurring as remnant palaeo-dune cordons and coast-parallel reef systems (Ramsay, 1994; Green, 2011b), and Holocene sedimentation occurring as ~20 m thick unconsolidated sediment wedges (Green and Garlick, 2011; Cawthra et al., 2012).

CHAPTER 5

METHODOLOGY

5.1 DATA COLLECTION AND PROCESSING

5.1.1 Introduction

In order to undertake a basin- and regional-scale assessment of a specific basin, CO2CRC (2008) indicate that a range of data are needed with the confidence of the assessment based upon the availability (or lack thereof), and quality of the data. Data confidence levels are therefore initially defined for a basin-scale assessment and are indicated in Table 5.1.

5.1.2 Seismic Data

The Durban Basin is traversed by 2761 km of legacy, reprocessed, migrated stack 2D seismic profiles obtained over a period spanning the 1970's to 1990's. Two thousand kilometres of single-channel 2D seismic were obtained from the Petroleum Agency of South Africa (PASA) in SEGY format which span an area of 175000 km^2, covering the continental shelf, slope and abyssal plain between the KwaZulu-Natal coastline and the Mozambique Ridge (Table 5.2). The seismic data cover eleven seismic exploration projects with 186 SEGY format profiles which form a 32000 km^2 grid at ~4 km^2 grid spacing on the continental shelf. Seismic grids vary from detailed, gridded seismic line programmes, to broadly spaced regional seismic traverses.

The current data utilised for this project are focussed in a gridded pattern over the Tugela Cone and continental shelf offshore Mandini covering an area of 14349 km^2. A tight grid spacing of >2 km is obtainable across the shelf and shelf break but large data gaps occur on the lower slope where only coast perpendicular profiles are available at circa 15 km spacing (Fig. 5.1).

This study's seismic profile analyses utilised IHS Kingdom Suite 2015 software with the individual seismic lines imported into the programme utilising navigation parameters based upon on a WGS84 / UTM zone 35S projection.

Table 5.1: Summary of the main data needs (required and desirable) for all levels of characterization (modified after CO2CRC, 2008). Data confidence levels for data available for the Durban Basin prior to this study are indicated.

Data Needs		Country/State-Scale Screening; Total Pore Volume	Basin-Scale Assessment; Prospective Storage Capacity	Site Characterization; Contingent Storage Capacity	Site Deployment; Operational Storage Capacity
Maps	Regional geology	xx	xx	x	
	Detailed/local geology		x	xx	xx
	Structural contour		x	xx	xx
	Reservoir geometry		x	xx	xx
	Reservoir quality		x	xx	xx
	Fault	x	x	xx	xx
	Seismicity	x	x	xx	xx
	Hydrologic	x	x	xx	xx
	Surface infrastructure	x	x	xx	xx
	Topographic	x	x	xx	xx
Seismic	2D	x	xx	xx	xx
	3D		x	xx	xx
Well logs	Gamma ray		x	xx	xx
	Porosity		x	xx	xx
	Permeability		x	xx	xx
	Sonic			xx	xx
	Density			xx	xx
	Image			xx	xx
Core	Porosity	x	xx	xx	xx
	Permeability	x	xx	xx	xx
	Langmuir volume (coal)	n.a.			
Special core analysis	Ratio vertical/ horizontal permeability			xx	xx
	Relative permeability			xx	xx
Special core analysis	Mercury injection capillary pressure		x	xx	xx
	Mineralogy		x	xx	xx
	Rock strength		x	xx	xx
Subsurface history	Oil/gas production		x	xx	xx
	CSM reservoir conditions	n.a.			
	Water chemistry			xx	xx
Pore pressure	Repeat formation tests; drill stem tests		x	xx	xx
	Subsurface fluid properties		x	xx	xx
	Leak-off tests; formation integrity tests		x	xx	xx
Reservoir characterization	Sequence stratigraphy	x	x	xx	xx
	Regional tectonic history/model	xx	xx	x	
	Regional stress analyses	x	xx	x	
	Biostratigraphy	x	x	xx	xx
	Analogues		x	xx	xx
	Static models			xx	xx
	Dynamic models			xx	xx
Economics				xx	xx
Regulatory framework				xx	xx

x = desirable; xx = required; n.a. = not applicable

No data	Little reliable data	Some Data	Reliable data	Extensive data

Table 5.2: Seismic data available for the project from Petroleum Agency SA.

Seismic Programme	Operator	Year Shot	Year Formatted	Within Basin	Number of SEGY Lines	Number of Tiff Lines
EC 2007	GEMS Survey Ltd / PASA	2007	-	No	11	0
Q74	Geophysical Services International / SOEKOR	1975	1990	No	1	22
R74	Geophysical Services International / SOEKOR	1975	-	Yes	0	13
S69	Kewanee Overseas Oil Company	1969	1996	Yes	0	115
S74	Phillips Petroleum	1974	1996	Yes	30	18
S76	Phillips Petroleum	1976	1996	Yes	53	42
S78	Phillips Petroleum	1978	1996	Yes	13	13
S90	Phillips Petroleum	1990	1996	Yes	11	11
S97	Phillips Petroleum	1997	1997	Yes	51	52
SA76	Phillips Petroleum	1976	1976	Yes	12	12
T72	Shell International Petroleum	1972	-	Yes	4	31

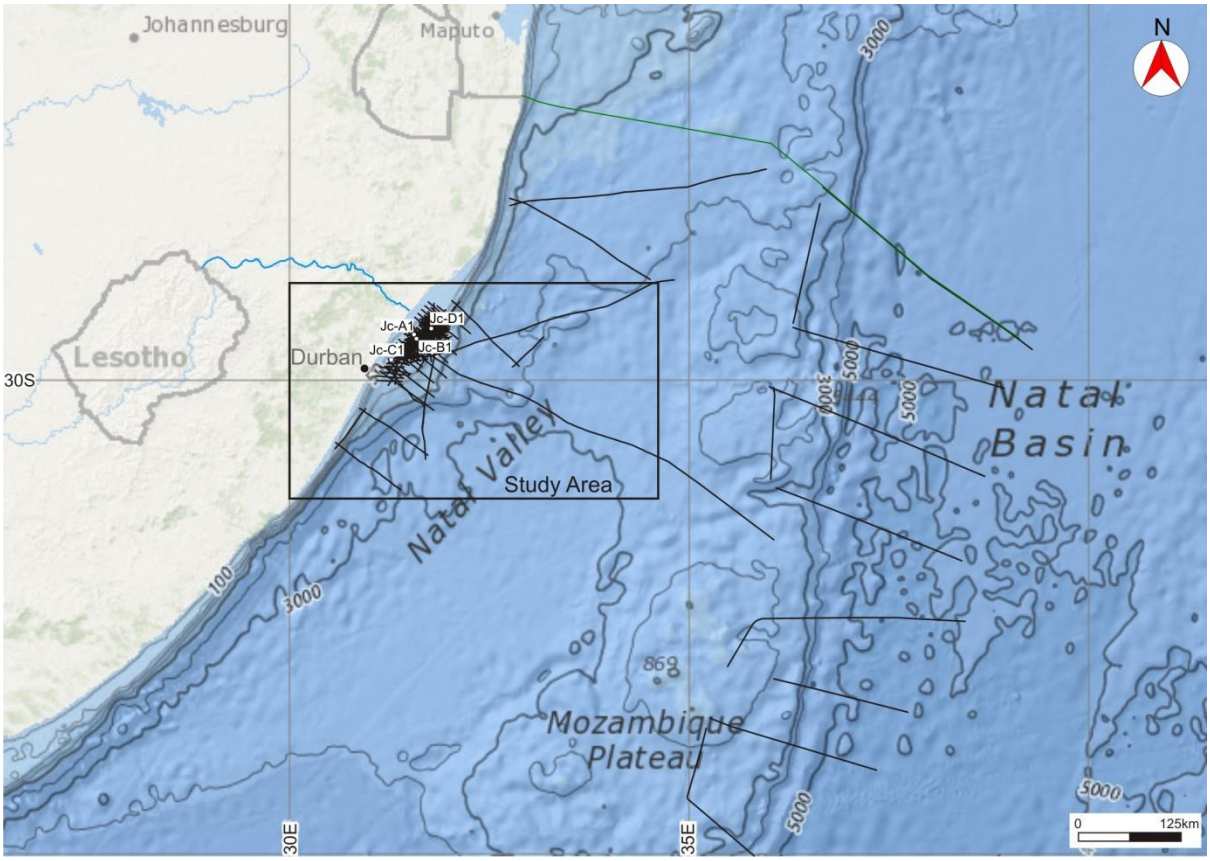

Figure 5.1: Locality map detailing study area location with National Oceanic and Atmospheric Administration (1 min grid) UTM showing study area and Indian Ocean bathymetry. Available seismic line coverage and exploration well positions are shown.

5.1.3 Well Data

Well log and downhole geophysical data were obtained for the four Jc-series exploration wells drilled on the continental shelf offshore between 1970 and 2000 (Fig. 5.1). The wells intersected approximately 2000 m of Cretaceous and late Jurassic sediments representing drift and syn-rift sediments. Well completion reports, engineering reports, lithology logs and log analysis reports, as well as digital well log and downhole geophysical data in LAS format were obtained for the four Jc-Series exploration wells from the Council for Geoscience and PASA. Available logs are indicated in Table 5.3.

Table 5.3: Digital LAS well data available from Petroleum Agency SA.

	Jc-A1	Jc-B1	Jc-C1	Jc-D1
Total Depth (m)	2400	3957	3169	2903
Digital Logs	DT, GR, RHOB, SP, Velocity	CALI, DT, GT, NPHI, RHOB	CAL, GR, NPHI, RHOB, Velocity	CALI, DT, Gas, GR, NPHI, RHOB, RT, SP , Velocity

Digital well logs were imported into IHS Kingdom Suite 2015 and the time-depths matched to seismic profiles utilising existing well shoot / velocity data (time-depth data) for the Jc-D1 borehole supplied by PASA (Table 5.4).

Table 5.4: Wells shoot/ velocity data from offshore Jc-D1 well Durban Basin.

Measured Depth (m)	Two-Way Time (TWT) milliseconds
315.800	0333
415.800	0421
980.500	0834
2230.500	1737
2330.500	1803
2380.500	1834
2430.500	1865
2480.200	1902
2530.000	1936
2629.600	2000
2729.200	2065
2828.800	2112
2878.600	2136
2888.500	2141
2898.500	2147
2902.325	2150

5.2 DATA INTERPRETATION

SEGY data and LAS log data were interpreted utilising IHS Global Inc., Kingdom Advanced V2015.0. Digital well shoot/velocity data from the Jc-D1 well were utilised by PASA to define two-way time vs measured depth (m) in order to tie well bore data to the seismic data. Davids (2009) indicates however, that caution needs to be taken when observing the vintage seismic data as there is no consistency in polarity between different data vintages.

Digital well logs were created in IHS Kingdom based on detailed well logs and well completion reports. All formation tops were defined and inputted to correlative depth intersections (Fig. 5.2). Seismic reflection horizons were then digitised in IHS Kingdom Suite to create horizons, contours (Fig. 5.3) and grids (Fig. 5.4)

across the study area for individual boundaries identified in well logs. Faulting within the basement and syn-rift sediments was defined through fault identification and mapping in IHS Kingdom Suite.

Grids of each mapped horizon were inputted into Vu-Pak® 3D Geology module in IHS Kingdom Suite to create a three dimensional static model and fence diagrams of each mapped reflector. Grids could then be added or removed to define specific items of interest such as closure patterns overlying basement horst structures or sandstone horizons defined and mapped from well log data tied to seismic data (Fig. 5.5).

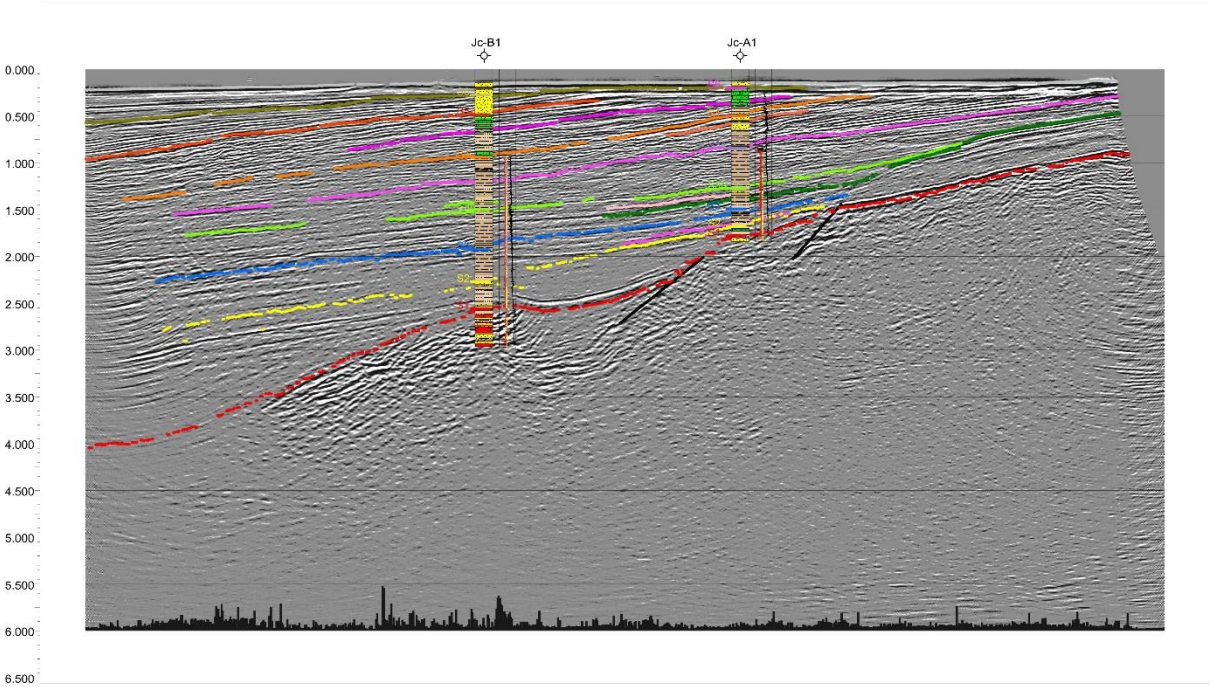

Figure 5.2: Seismic profile S76-020 showing digitised seismic reflection horizons. Reflections are correlated with known unconformities and potential seismic stratigraphic surfaces identified in the Jc-A1 and Jc-B1 wells. The lithology log, gamma ray log (Red) and density log (Black) are shown for both wells.

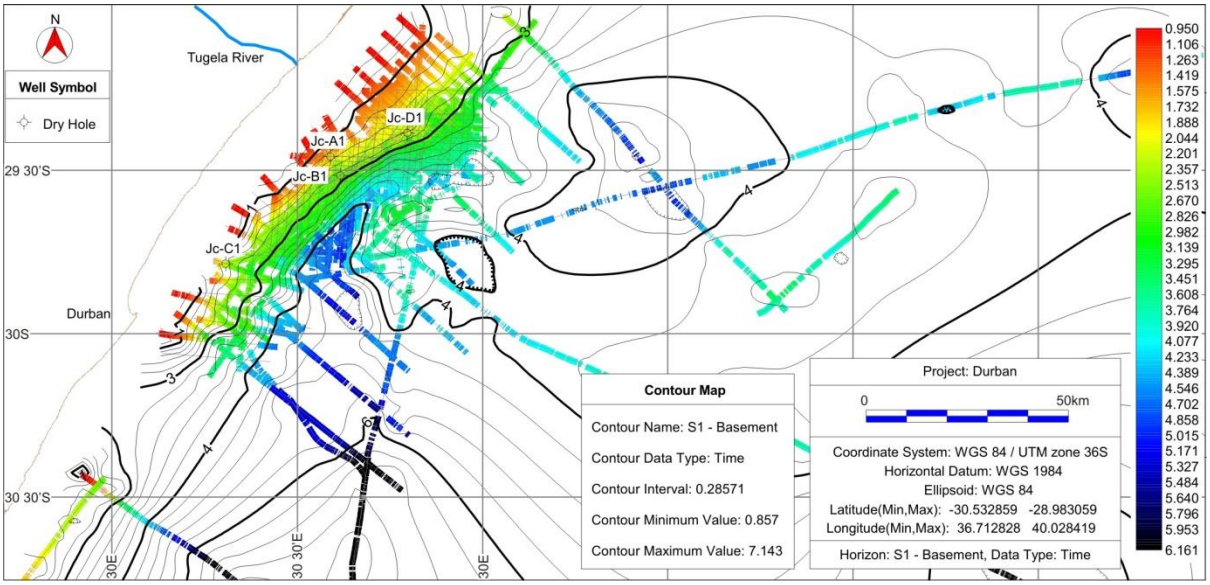

Figure 5.3: Two-way time detail (colour) with contour plot associated with a digitised basement seismic reflection in the offshore Durban Basin.

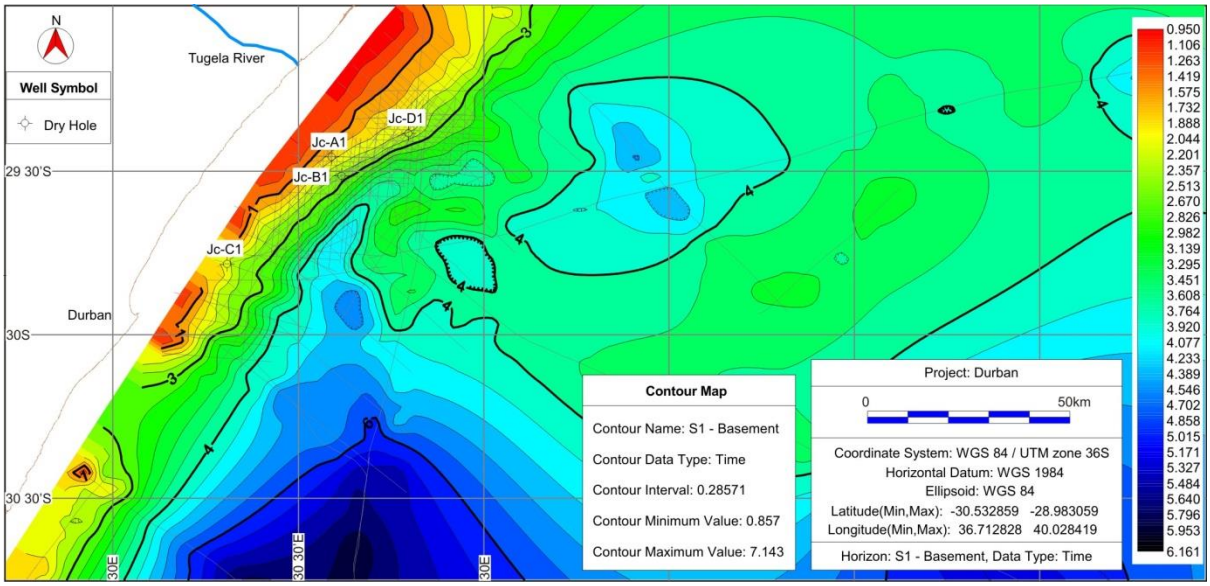

Figure 5.4: Two-way time colour-filled contour plot of digitised seismic basement reflection.

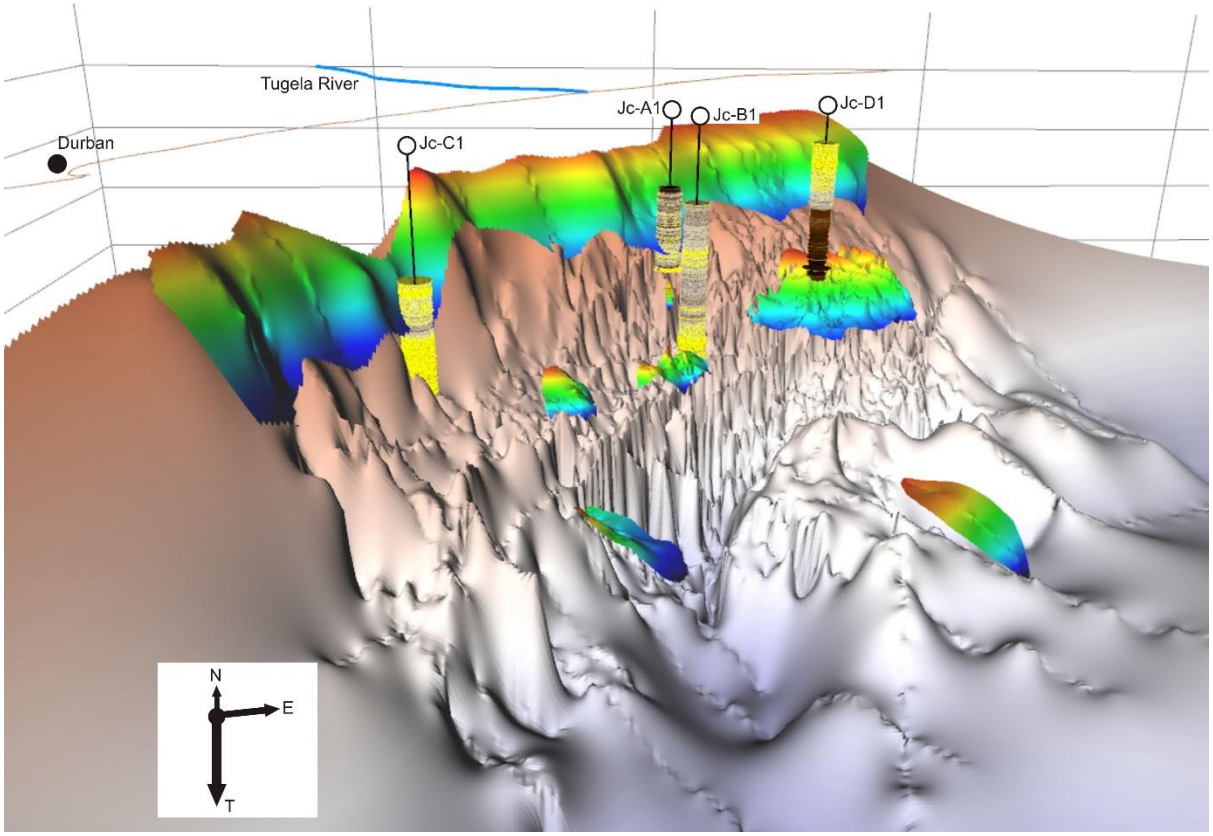

Figure 5.5: Oblique three-dimensional image of seismic basement horizon with mapped sandstone bodies identified at different stratigraphic levels in the four Jc-series wells drilled on the continental shelf. Image orientated north.

5.3 SEQUENCE STRATIGRAPHY

Sequence stratigraphic concepts are the founding methodologies for modern sedimentology with applications ranging from hydrocarbon exploration, to understanding shifts in local and global sea level and sediment supply through the geological record (Vail et al., 1977). Sequence stratigraphy represents an interdisciplinary method, combining autogenic (i.e., from within the system) and allogenic (i.e., from outside the system) processes into a unified model to aid in the determination of the stratigraphic architecture and evolution of sedimentary basins (Catuneanu, 2006). Although initial work focussed primarily upon global climate change (Haq et al., 1987) emphasis has shifted to the determination of sediment accommodation space within a sedimentary basin (Posamentier and Allen, 1999). Posamentier and Allen (1999) define sequence stratigraphy as: "*the analysis of cyclic sedimentation patterns that are present in stratigraphic successions, as they develop in response to variations in sediment supply and space available for sediment to accumulate*." Posamentier and Allen (1999) further propose that primary factors controlling sediment accommodation space include numerous factors such as eustasy, tectonism, basin physiography, sediment flux, and sediment compaction.

Variations in facies, geometric character, and the identification of bounding surfaces are key aspects in defining the development of a basin-fill succession (Catuneanu et al., 2009). The geometry of stratal stacking patterns are defined by variations in sedimentation rate and base level fluctuations with depositional successions reflecting trends that include progradation, retrogradation, aggradation and erosion. Catuneanu et al. (2009) propose that each stratal stacking pattern defines a particular genetic type sequence i.e., 'transgressive', 'normal regressive' and 'forced regressive'; (Hunt and Tucker, 1992; Posamentier and Morris, 2000), with distinct geometries and facies preservation styles.

Posamentier and Allen (1999) summarise sequence stratigraphic interpretation into four steps:

1. Establishing the palaeogeographic setting;
2. Interpreting depositional systems and facies using all available data;
3. Subdividing the stratigraphic succession through the identification of maximum flooding surfaces and sequence boundaries;
4. Analysing facies stacking patterns and identifying systems tracts.

For this study the palaeogeographic setting of the Durban Basin was defined through interpretation of available legacy, reprocessed, migrated stack 2D seismic profiles and well data. Biostratigraphic as well as petrophysical data were, where available, integrated with lithostratigraphic data to assist with determinations of depositional environments and facies variations. Depositional systems and individual sequence tracts were interpreted through integration of well data with 2D seismic profiles to assist in mapping of stratigraphic surfaces.

5.3.1 Seismic Stratigraphic Interpretation

Seismic interpretation within this study is based primarily upon the classification of stratigraphic surfaces identified in seismic profile. Catuneanu (2006) defines stratigraphic surfaces as environment-dependant surfaces which "*mark shifts through time in depositional regimes (i.e., changes in depositional environments, sediment load and/or environmental energy flux), and are created by the interplay of base level changes and sedimentation*". The identification and classification of individual stratigraphic surfaces is fundamental to the interpretation of the sedimentary succession, allowing for delineation of individual systems tracts with definitive internal clinoform architectures.

Depositional sequences that form between sequence stratigraphic surfaces are interpreted through the architecture of their stratal terminations (Catuneanu et al., 2009). The geometry of these within-trend contacts (Embry and Catuneanu, 2001; 2002) helps to define associated depositional trends and shoreline trajectories within a basin. Stratal terminations are utilised primarily during 2D seismic interpretations to define the

geometric relationships between the seismic reflector and the surface against which it terminates. Catuneanu (2006) defines the main types of stratal terminations as: truncation, toplap, onlap, downlap, and offlap (Fig. 5.6).

The concept of stratal terminations have been incorporated into sequence stratigraphic methodologies in order to describe the stacking patterns of depositional units within a basin and to aid in the recognition of the various surfaces and systems tracts.

The types of stratal terminations (Fig. 5.6) are defined from (Mitchum, 1977; Galloway, 1989; Emery and Myers, 1996; Catuneanu, 2006):

- **Truncation**: termination of strata against an overlying erosional surface. *Toplap* may develop into truncation, but truncation is more extreme than toplap and implies either the development of erosional relief or the development of an angular unconformity.

- **Toplap**: termination of inclined strata (clinoforms) against an overlying lower angle surface, mainly as a result of non-deposition (sediment bypass), ± minor erosion. Strata lap out in a landward direction at the top of the unit, but the successive terminations lie progressively seaward. The toplap surface represents the proximal depositional limit of the sedimentary unit. In seismic stratigraphy, the *topset* of a deltaic system (delta plain deposits) may be too thin to be "seen" on the seismic profiles as a separate unit (thickness below the seismic resolution). In this case, the topset may be confused with toplap (i.e., *apparent toplap*).

- **Onlap**: termination of low-angle strata against a steeper stratigraphic surface. Onlap may also be referred to as *lapout*, and marks the lateral termination of a sedimentary unit at its depositional limit. Onlap type of stratal terminations may develop in marine, coastal, and non-marine settings:
    - marine onlap: develops on continental slopes during transgressions (*slope aprons*, Galloway, 1989; *healing-phase deposits*, Posamentier and Allen, 1999), when deepwater transgressive strata onlap onto the maximum regressive surface.
    - coastal onlap: refers to transgressive coastal to shallow-water strata onlapping onto the transgressive (tidal, wave) ravinement surfaces.
    - fluvial onlap: refers to the landward shift of the upstream end of the aggradation area within a fluvial system during base-level rise (normal regressions and transgression), when fluvial strata onlap onto the subaerial unconformity.

- **Downlap**: termination of inclined strata against a lower-angle surface. Downlap may also be referred to as *baselap*, and marks the base of a sedimentary unit at its depositional limit. Downlap is commonly seen at the base of prograding clinoforms, either in shallow-marine or deep-marine environments. It is uncommon to generate downlap in non-marine settings, excepting for lacustrine environments. Downlap therefore represents a change from marine (or lacustrine) slope deposition to marine (or lacustrine) condensation or non-deposition.

- **Offlap**: the progressive offshore shift of the updip terminations of the sedimentary units within a conformable sequence of rocks in which each successively younger unit leaves a portion of the older unit on which it lies exposed. Offlap is the product of base-level fall, so it is diagnostic for forced regressions.

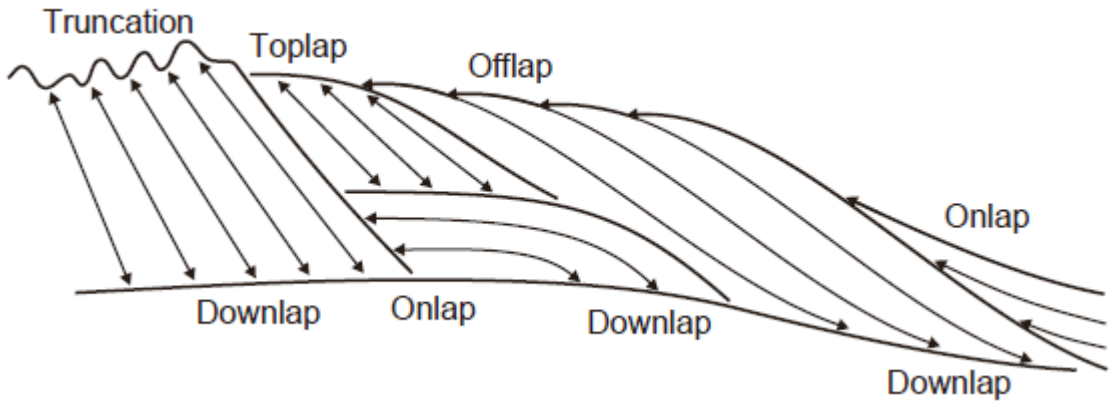

Figure 5.6: Types of stratal terminations (modified from Mitchum, 1977; Galloway, 1989; Emery and Myers, 1996; Catuneanu, 2006).

5.3.2 Well Log Interpretation

Wireline geophysical logging represents a versatile down-hole tool to aid sequence stratigraphic interpretations within a basin. The most common logs are utilised for facies analysis (lithology, porosity, fluid evaluation) and stratigraphic correlations (Catuneanu, 2006). The Schlumberger Oilfield Glossary (www.slb.com/glossary.aspx) defines wireline logging as "*a continuous measurement of formation properties with electrically powered instruments to infer properties and make decisions about drilling and production operations*".

Although valuable as tools to define subsurface rock properties, geophysical data provide only indirect information on the solid and fluid phases in the subsurface (Catuneanu, 2006), and therefore in the absence of cores is deemed somewhat speculative (Posamentier and Allen, 1999). Therefore there is a need for geophysical logs to be complimented by sedimentological data (including sedimentologic, petrographic, biostratigraphic, ichnologic, and geochemical analyses) to help define the potential depositional systems and systems tracts (Posamentier and Allen, 1999).

Although speculative, geophysical logs can aid in the definition of sequence stratigraphic boundaries such as maximum flooding surfaces, and sequence boundaries. Geophysical logs such as the gamma ray and sonic density logs are utilised here to define potential sequence stratigraphic surfaces defined by systematic variations in the well log motifs. These horizons are then correlated with lithological log data obtained during drilling, and biostratigraphical data to help delineate sequence stratigraphic boundaries in the seismic profiles.

Once the key sequence stratigraphic surfaces have been identified from the well logs, these are correlated through seismic profile interpretation in order to identify individual systems tracts based upon their depositional environments and vertical stacking patterns (Posamentier and Allen, 1999).

5.3.4 Systems Tract Interpretation

Systems tract interpretations aid in the definition of links between contemporaneous depositional systems which form the subdivisions of a sequence (Brown and Fisher, 1977; Catuneanu, 2006). Individual sequence tracts are interpreted based on internal stratal stacking patterns, associated bounding surfaces, and position within the sequence (Catuneanu, 2006; Fig. 5.7).

For the purpose of this study, sequence stratigraphic nomenclature and interpretation are based upon current sequence stratigraphic procedures defined by Catuneanu et al. (2009); Catuneanu and Zecchin (2013) and

Zecchin and Catuneanu (2013; 2015). The systems tract nomenclature adopted by Catuneanu et al. (2009) conforms to the scheme proposed by Hunt and Tucker (1992), whereby stratal architecture allow for the subdivision of a sequence into four systems tracts (Fig. 5.7), namely: Highstand Systems Tract (HST); Falling Stage Systems Tract (FSST); Lowstand Systems Tract (LST); and Transgressive Systems Tract (TST).

Catuneanu (2006) defines each systems tract as follows:
Highstand Systems Tract – "*forms during the late stage of base-level rise, when the rates of rise drop below the sedimentation rates, generating a normal regression of the shoreline. Consequently, depositional trends and stacking patterns are dominated by a combination of aggradation and progradation processes. The highstand systems tract is bounded by the maximum flooding surface at the base, and by a composite surface at the top that includes a portion of the subaerial unconformity, the basal surface of forced regression, and the oldest portion of the regressive surface of marine erosion."*

Falling Stage Systems Tract – "*The falling-stage systems tract includes all strata that accumulate in a sedimentary basin during the forced regression of the shoreline. According to standard sequence stratigraphic models, the forced regressive deposits consist primarily of shallow- and deep-water facies, which accumulate at the same time with the formation of the subaerial unconformity in the non-marine portion of the basin. The falling-stage systems tract is bounded at the top by a composite surface that includes the subaerial unconformity, its correlative conformity (sensu Hunt and Tucker, 1992), and the youngest portion of the regressive surface of marine erosion. At the base, the falling-stage systems tract is bounded by the basal surface of forced regression (= correlative conformity of Posamentier and Allen, 1999), and by the oldest portion of the regressive surface of marine erosion*."

Lowstand Systems Tract – *"The lowstand systems tract, when defined as restricted to all sedimentary deposits accumulated during the stage of early-rise normal regression (sensu Hunt and Tucker, 1992), is bounded by the subaerial unconformity and its marine correlative conformity at the base, and by the maximum regressive surface at the top. Where the continental shelf is still partly submerged at the onset of base-level rise, following forced regression, the basal composite boundary of the lowstand systems tract may also include the youngest portion of the regressive surface of marine erosion. The lowstand systems tract forms during the early stage of base-level rise when the rate of rise is outpaced by the sedimentation rate (case of normal regression). Consequently, depositional processes and stacking patterns are dominated by low-rate aggradation and progradation across the entire sedimentary basin."*

Transgressive Systems Tract – *"is bounded by the maximum regressive surface at the base, and by the maximum flooding surface at the top. This systems tract forms during the stage of base-level rise when the rates of rise outpace the sedimentation rates at the shoreline. It can be recognized from the diagnostic retrogradational stacking patterns, which result in overall fining-upward profiles within both marine and non-marine successions. As the rates of creation of accommodation are highest during shoreline transgression, the transgressive systems tract is commonly expected to include the entire range of depositional systems along the dip of a sedimentary basin, from fluvial to coastal, shallow-marine and deep-marine."*

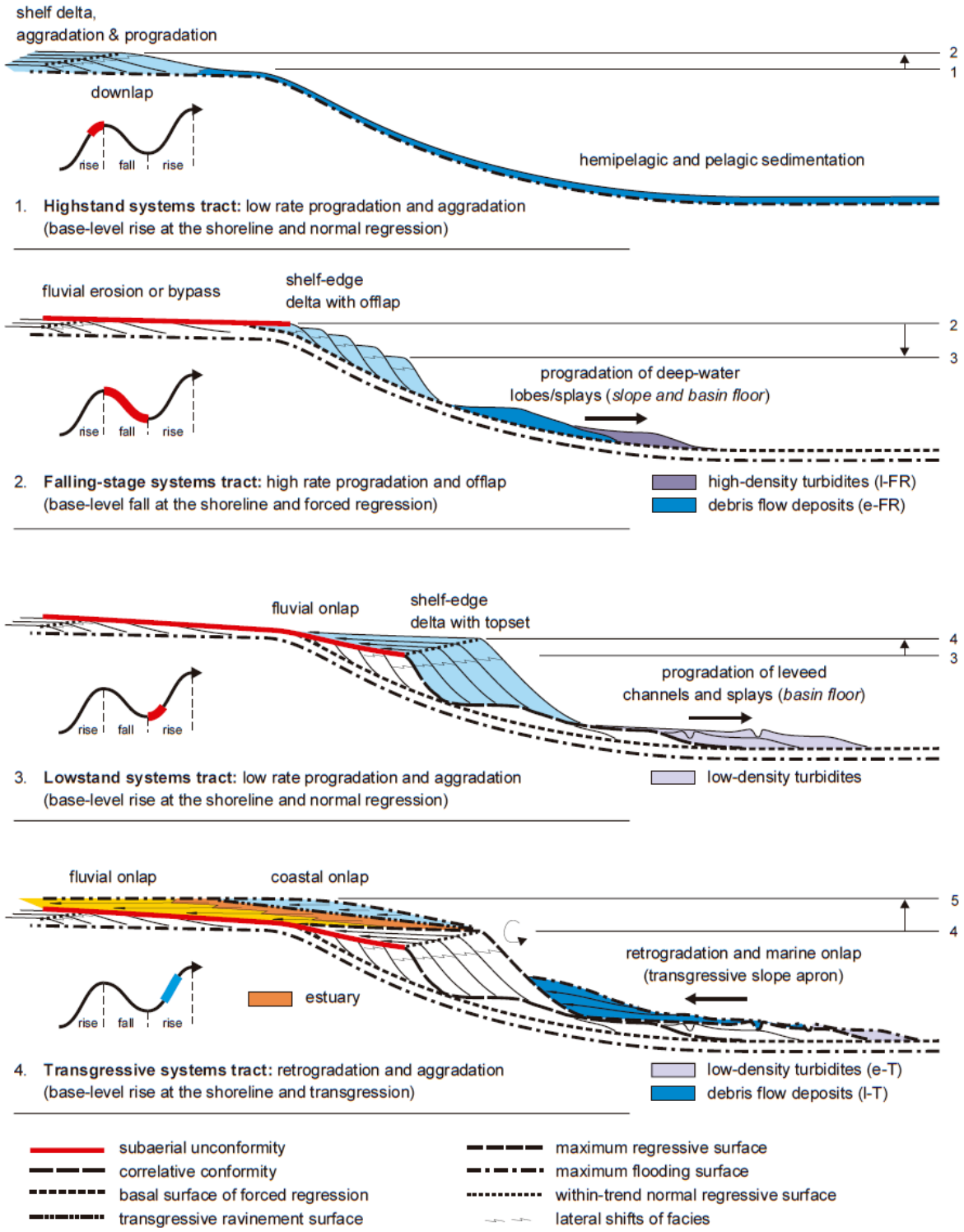

Figure 5.7: A generalised regional architecture for systems tracts, and stratigraphic surfaces defined by Catuneanu (2006), based upon systems tract nomenclature of Hunt and Tucker (1992). Individual systems tracts are separated by seismic bounding surfaces with each systems tract defined by specific stratal stacking patterns. The inferred timing relative to the base-level curve at the shoreline is shown. Abbreviations: e-FR—early forced regression; l-FR—late forced regression; e-T—early transgression; l-T—late transgression (from Catuneanu, 2006).

5.4 SEDIMENTATION RATE CALCULATIONS

The rates of sedimentation are deduced for the Mesozoic succession based upon mean sediment package thicknesses derived from well data, and overall areal extents derived from seismic interpretations. A similar approach to that defined by Walford et al. (2005) and Said et al. (2015) is used. Absolute age constraints for the bounding surfaces of individual units are defined by biostratigraphic ages obtained from the Jc-series wells (du Toit and Leith, 1974; Unstead et al., 1983; Muntingh, 1983; Lester, 2000). Ages are correlated with the currently accepted International Commission on Stratigraphy Time Chart (v2017/02).

5.5 VOLUMETRIC CALCULATIONS

5.5.1 Estimation of processing parameters

No core, porosity or permeability data are available for any wells within the basin, therefore values from analogous formations within the southern African east and west coasts are utilised for volumetric calculations. Data from analogous successions in Ghana (Dailly et al., 2013) are utilised for basin floor fan reservoir systems, whilst data from the onshore Zululand Basin (Gerrard, 1972a; 1972b) and Mozambique coastal plain (Coster et al., 1989; Solomon et al., 2014) are utilised for the shelf sand reservoirs. As limited data are available for the basin, 50% net thicknesses of reservoirs are utilised for this study. CO_2 density values are calculated based upon individual formation tops defined in seismic profiles, as well as a pore fluid pressure of 8.6 ppg and a geothermal gradient of 2.67°C/100 m as defined in borehole Jc-C1 (Muntingh, 1983). The online calculator (www.energy.psu.edu/tools/CO2-EOS), based upon equation of state calculations of Span and Wagner (1996), is used to derive the CO_2 density calculations.

5.5.2 Effective storage capacity estimations

The effective storage capacity of individual reservoir units are assessed using calculations based upon currently accepted storage capacity estimations defined by numerous authors (IPCC, 2005; Bachu et al., 2007; Bachu, 2008; USDOE, 2008; Goodman et al., 2011; Bachu, 2015). Here the United States Department of Energy (US DOE) methodology (Goodman et al., 2011) is utilised, whereby the effective storage capacity in a saline formation, M_{CO2}, is given by:

$$M_{CO2} = A \times h \times \text{ø} \times \rho_{CO2} \times E$$

Where A is the area (m^2), h is the net thickness of the reservoir (m), ø is the average porosity (%), ρ_{CO2} is the average CO_2 density, evaluated at pressures and temperatures that represent storage conditions anticipated for individual deep saline aquifers. E is a storage efficiency factor that reflects the total pore volume filled with CO_2. Efficiency factors at a formation scale have been defined by the IEAGHG (2009) and by Goodman et al. (2011) for different lithologies over P10, P50 and P90 probabilities. For this work the formation-scale values defined by Goodman et al. (2011) are used. All calculations are based upon an upper depth cut-off of 800 m below the seafloor. This centres on the criteria for supercritical CO_2 storage as defined by the IPCC (2005).

Although the Efficiency factor (E) adjusts total gross thickness to net gross thickness, total area to net area, and total porosity to effective porosity (cf. Cook, 2012), "net" thicknesses shown are based on 50% of the maximum thickness measured for an individual reservoir. This was done in order to account for 1) lateral thickness variations and wedge-out up- and down-dip in the case of basin floor fan deposits, and 2) variation in thickness of the shelf sediment wedges due to erosional surfaces and package thinning/pinching into the deep basin.

CHAPTER 6

SEISMIC STRATIGRAPHY

6.1 INTRODUCTION

Globally, passive continental margins are defined by broad (~50 km - Shepard, 1963; ~80 km - Helland-Hansen et al., 2012) gently sloping (0.05°; Kennett, 1982) shallow water regions comprising thick sedimentary successions derived from onshore erosion. These have been the object of intense sequence stratigraphic analyses, namely due to their potential for hydrocarbon reserves. The sequence stratigraphic analyses of sheared, or structurally controlled passive margins are less conspicuous in the literature (cf. de Lépinay et al., 2016). As de Lépinay et al. (2016) point out, a number of questions arise regarding their evolution in the context of gradient and geodynamic and/or sedimentary setting. It is in this context that the Durban Basin, a portion of the sheared-passive KwaZulu-Natal margin of SE Africa is investigated.

This chapter aims to assess the sedimentology and sequence stratigraphic history of the Durban Basin, highlighting controls on sedimentation as the margin evolved from a sheared-rift to drift sequence. A basin model is proposed and compared and contrasted with current models for structurally controlled (Martins-Neto and Catuneanu, 2010; Helland-Hansen et al., 2012) and passive margin (Catuneanu et al., 2011) basins.

6.2 SEDIMENTOLOGY OF THE JC-SERIES WELLS

6.2.1 Jc-A1

The Jc-A1 borehole was drilled as a wildcat exploration well drilled in 71.6 m water depth on the continental shelf 24 km east of Stanger (29°27’41.3”S 031°35’39.7”E). A total of 1390 m of marine Tertiary sediments with a further 735 m of marine upper Cretaceous sediment were intersected before the well was abandoned at 2378.4 m depth (Fig. 6.1). The basement to the well comprises quartzitic sandstone of the Natal Group which underlies 48 m of Dwyka Group tillite of the Karoo Supergroup.

The upper 158 m was drilled into semi-consolidated calcareous sands, below which a succession of coquina and calcareous sandstone was intersected to a depth of 536 m. Below this unit lithologies comprise variable quantities of mudstone and siltstone with subordinate sandstone (Fig. 6.1). Similarly, sequence stratigraphic interpretation of the gamma ray log (Fig. 6.2) suggests that the sedimentary succession comprises an alternating succession of mudstone and siltstone deposited as lowstand and transgressive systems tract deposits.

Three sandstone packages however occur as interbedded sandstone-siltstone successions. The upper sandstones were intersected between 536-585 m and is represented by a sandy limestone that grades into calcareous sandstone. The sandstone is tight to porous, fine-grained with quartz and shell fragments (Leith, 1971). A second sandstone unit is intersected between 650-725 m is similar to the overlying sandstone in composition, but is defined by a number of thin sandstones intercalated with claystone. Although not well defined in the lithology logs, a third sandstone is identified between 1640-1655 m is identified in the gamma ray log underlying seismic reflector 3B. The spike in the gamma ray log (Figs 6.1; 6.2) although not exceptionally well defined, correlates with a high amplitude, bright reflector in seismic lines S76-20 and S97-15B.

6.2.2 Jc-B1

The Jc-B1 borehole was drilled as a wildcat exploration well on the continental shelf ~80 km northeast of Durban, offshore of Stanger (29° 30’ 25.3”S 031° 37’ 28.4”E). The borehole was drilled in 80.4 m of water, to a total depth of 3945 m, intersecting ~1948 m of Tertiary marine sediments followed by ~1374 m of Cretaceous

marine sediments. Below 3429 m a number of dolerite intrusions were intersected, intruding metamorphosed, non-glauconitic sandstone and siltstone. For this study this seismic reflector is taken as the contact with basement within Jc-B1.

Three sandstones have been identified in Jc-B1. The upper sandstone is intersected between 1800-1820 m where a sandstone horizon is noted within the gamma ray log (Figs 6.1; 6.2) which corresponds to a spike within the resistivity logs. The sandstone is defined as fine-grained, tight, and slightly calcareous (Unstead et al., 1983). The unit fines downward passing into siltstone. A second sandstone package is intersected between 3060-3095 m (2.30sec TWT) and represents the most prominent sandstone in the borehole. It is defined as a 28 m thick, upward-coarsening, fine-grained to pebbly sandstone that is calcareous and slightly glauconitic. Within the lithology log, the sandstone is defined as white to light grey in colour, comprising medium-grained, well sorted, angular to rounded quartz grains (Unstead et al., 1983). Below this unit, the succession becomes slightly sandier than the overlying intervals, with thin, ~10 m thick, regressive, coarsening-upward packages noted in the lithology and gamma ray logs at 3105 m (2.31sec TWT) where a third coarse, pebbly sandstone is intersected (Fig. 6.1).

At 3420 m depth a marked variation is noted in the lithology logs and the geophysical logs as an 8 m thick, white to medium grey, very well sorted, fine-grained sandstone was intersected (Unstead et al., 1983). At 3428 m however the sandstone is intruded by a 17 m thick amygdaloidal igneous rock which has caused contact metamorphism of the surrounding sandstones. The intrusion is subsequently underlain by 55 m of interbedded sandstone and siltstone. A ~36 m thick intrusion is intersected at 3504 m, comprising green to grey, crystalline, fine to coarse igneous lithologies. The formation is hard, slightly magnetic, and has locally developed pyrite. The sandstones and igneous intrusions produce a high amplitude, bright reflector wavelength in the seismic profiles, but can be distinguished from the overlying Cretaceous succession due to variation in the reflector pattern.

From 3540 m, a 138 m thick succession of interbedded sandstone and siltstone is dominant; however it is intruded by at least five igneous bodies, ranging in thickness from 3 m to 20 m. Sandstone is white to light grey, fine- to medium-grained with a calcareous cement and varying quantities of argillaceous matrix. The sandstones, siltstones and claystones are hard and tight. A 24 m thick coal-rich layer is present between 3578 m and 3602 m with intrusions above and below it. Below 3678 m to the end of hole at 3943 m, the succession is similar to that above, with interbedded sandstone, siltstone and shales intruded by igneous bodies of varying thickness. The sandstones are tight, fine- to medium-grained, and slightly glauconitic. The siltstones and claystones tend to be calcareous and carbonaceous. From 3859 m to 3900 m the sandstones become quartzitic in nature with coarse-grained angular fragments identified in the cuttings. The hole was stopped in igneous rock at 3943 m.

6.2.3 Jc-C1

The Jc-C1 borehole was drilled 28 km northeast of Durban (29° 44’ 08.1”S 031° 18’ 35.3”E) on the western flank of the Durban Basin. The borehole was drilled in water depth of 97.7 m to a depth of 3169 m, intersecting 1616.3 m of Tertiary marine sediments, underlain by 1364 m of Cretaceous sediments. The borehole was stopped in basaltic volcanics of likely Karoo Supergroup affinity.

The initial 311m was drilled with the marine riser with bit and sample basket samples taken. The interval comprises unconsolidated sand, coquina and minor conglomerate. From 311 to 520m, unconsolidated quartz sands overlies a 138m thick coquina interval with fossils of foraminifera, bryozoa, echinoid spines and shell fragments. Glauconite in the section suggests a shallow marine depositional environment for the section (GGS, 1983). From 520 m depth the deposits comprise an interbedded succession of claystone and sandstone with subordinate siltstone. The claystones are greenish grey in colour becoming progressively darker and more carbonaceous with depth (GGS, 1983). The claystones are commonly silty and constitute the base of two

coarsening upwards packages of claystone-siltstone-sandstone between 590-620 m and 650-740 m. The sandstones in these packages are tight, off-white to light grey, calcareous and frequently argillaceous (GGS, 1983).

A 230 m thick succession of interbedded siltstone and sandstone is intersected between 1290 m and 1520 m. Although small subordinate shales are present, this succession is dominated by sandstone and siltstone with sandstone becoming more prevalent between 1370 m to 1490 m where two ~40 m thick coarsening-upwards siltstone-sandstone packages (1370-1410 m) (1440-1480 m) are identified, each capped with a 20 m thick sandstone unit. This succession comprises tight, fine-grained, and very well sorted sandstones with angular to rounded quartz grains present (GGS, 1983). The upper sandstones in each unit are overlain by siltstone or silty sandstone that forms the base of the following package.

Although defined in the lithology logs as primarily siltstones, the gamma ray logs show a number of small spikes suggesting the possibility of sandy units between 1880-2205 m (Fig. 6.1). The thickest sandstone occurs between 1965 m and 1984 m and although there is no deviation within the SP log, variation within the rate of penetration log as well as positive anomalies within the resistivity and density logs could indicate several coarsening-upward cycles. A 3 m thick sandstone caps an upward coarsening succession identified in the gamma ray logs, marked by a positive shift in the resistivity and density logs at 2113 m. The underlying succession is dominated by argillaceous siltstones, although two 5 m thick sandstones are identified with sandstone tops at 2140 and 2150 m respectively. The sandstones are tight, very fine grained, and well sorted (GGS, 1983).

6.2.4 Jc-D1

The Jc-D1 well was drilled in 2000 along the continental shelf 50 km east of Stanger (29° 23' 22.812" S 31° 48' 29.884"E). The borehole was drilled to a total depth of 2900 m intersecting ~1820 m of Tertiary marine sediment underlain by ~1000 m of Cretaceous and late Jurassic sediments. The borehole was stopped in amygdaloidal volcanics of possible Karoo Supergroup affinity.

From 771 m to 1062 m, the lithology and geophysical logs indicate a more sandy succession of interbedded silty, calcareous sandstone, limestone and subordinate claystone. Sandstone beds range in thickness from 2 m to 15 m, occurring as semi- to unconsolidated, fine- to medium-grained sands that are moderate to well sorted, containing lithic fragments, fossil debris, glauconite and rare nodular pyrite (Phillips Petroleum, 2000). Semi-consolidated sands are generally friable and brittle, owing to weak calcite cement and a calcareous claystone matrix. Limestones in this succession are commonly off-white to grey coloured cryptocrystalline to fine crystalline wackstone and packstone that is firm to hard. A second sandstone occurs at 1392 m – 1404 m where two ~5 m thick sandstone horizons are interbedded with a 2 m thick shale (Phillips Petroleum, 2000).

A major lithology change is noted in the lithology logs at 2720 m where sandstone and conglomerate are intersected. This zone is marked by a major negative shift in the gamma ray log (Figs 6.1; 6.2) which is then constant to the end of hole. The sandstone is dark grey, fine- to medium-grained, soft to firm, and very poorly sorted, grading into pebbly to conglomeratic facies (Phillips Petroleum, 2000). Numerous angular lithic fragments are present with quartzite pebbles forming the major constituent. Conglomerate facies commonly comprise pebbles of quartzite and basalt up to 2 mm in diameter with fragments of larger pebbles up to 10 mm in diameter noted. Pebbles are set in a fine- to coarse-grained angular matrix which appears to have poor porosity. The coarse-grained succession attains a thickness of 179 m after which volcanics are intersected at 2899 m depth through to end of hole at 2900 m. The volcanics are medium to dark grey to dusky purple, very hard, brittle, vitreous, vesicular, and amygdaloidal.

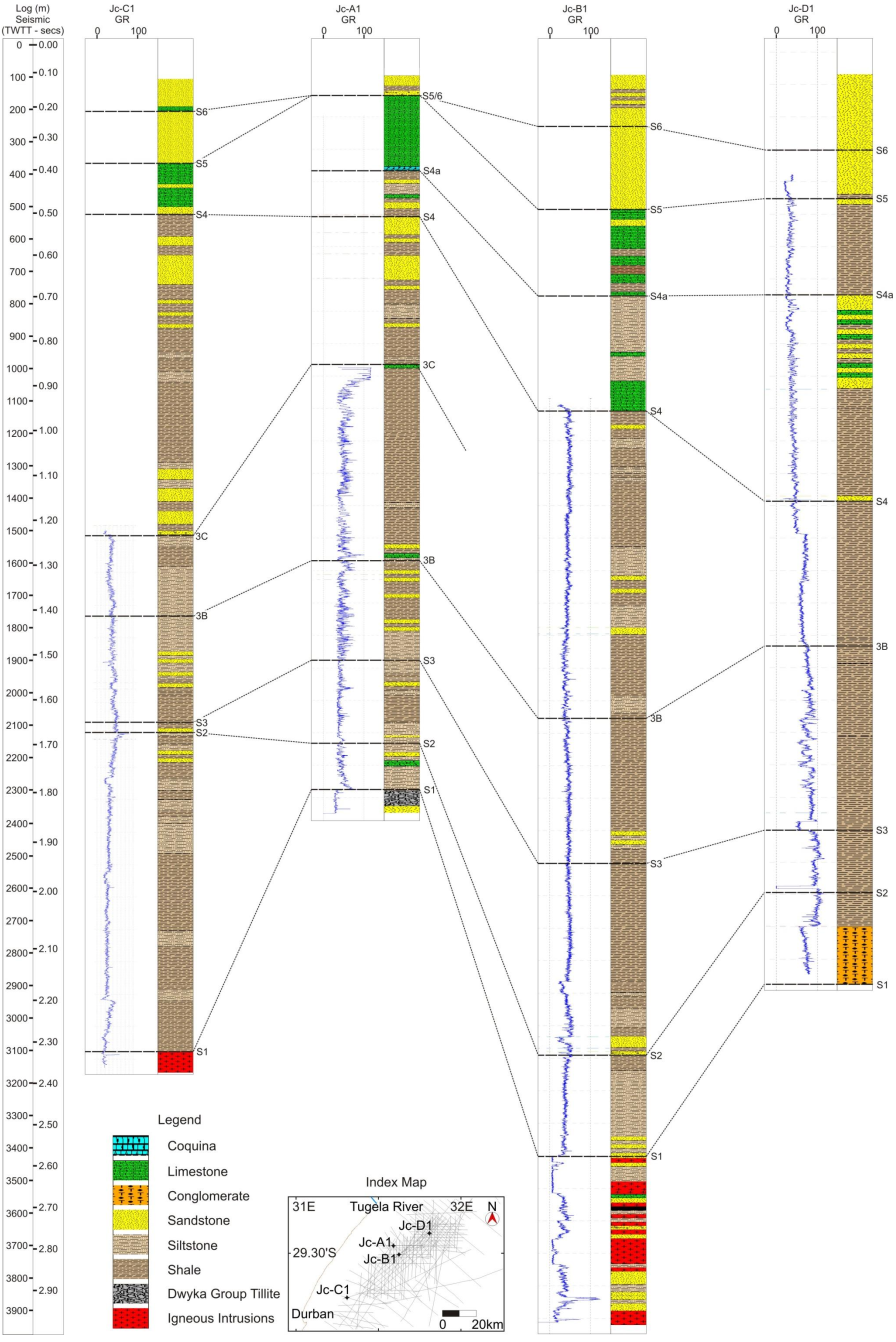

Figure 6.1: Detailed lithologic and gamma ray well logs of the Jc-Series wells. Correlation between major unconformity surfaces based upon biostratigraphical data of du Toit and Leith (1974), Unstead et al., (1983), Muntingh, (1983), McMillan and Dale (2000) and current study analyses are shown with dashed lines.

6.3 SEISMIC INTERPRETATION

Six seismic units are delineated within the Durban Basin based upon seismic bounding features, acoustic impedance, and internal-reflection characteristics (Table 6.1). The units characterised represent sedimentation within the basin that occurred after the formation of the post-Karoo Supergroup basement unconformity. Each unit is separated into facies and associated systems tracts as defined by Catuneanu et al. (2011). Systems tracts are defined by seismic architecture as well as geophysical log signatures as shown in Figure 6.2 and are utilised to interpret a depositional environment for each facies (Table 6.1).

Table 6.1: Simplified sequence stratigraphic framework for the continental margin within the Durban Basin, describing seismic units, facies, bounding surfaces, interpreted depositional environment and the age of each unit (ages based upon McMillan and Dale, 2000; McMillan, 2003; Green et al., 2008).

Unit	Facies	Surface	Modern Description	Stratal Relationship	Thickness (two-way time)	Interpreted depositional environment	Systems Tract	Age
F	F4			Transparent reflector package	0.2s	na	na	Holocene?
	F3		Chaotic Reflector Package	Wavy to chaotic moderate to low amp reflectors	0 to 0.2s	na	na	Pleistocene to Pliocene?
	F2		Progradational wedge	High impedance, sub-parallel, progradational reflectors	0 to 0.2s	Lowstand shelf edge delta	LST	Pliocene
	F1		Channel Fill	Onlapping and lateral accretion fills, chaotic, high amplitude reflectors	0 to 0.2s	Incised Valley Fill	LST	Pliocene
		S6	Shelf-confined erosional reflector					Mid Pliocene
E	E3		Aggradational package	Low impedance, sub-parallel, aggradational reflectors	0 to 0.2s	Inner to Mid Shelf	TST	L- Pliocene? / U-Miocene?
	E2		Progradational wedge	High impedance, sigmoid, progradational reflectors	0 to 0.3s	Lowstand shelf edge delta	LST	Upper Miocene
	E1		Channel Fill	Onlapping and lateral accretion fills, chaotic, moderate amplitude reflectors	0 to 0.2s	Incised Valley Fill	LST	Upper Miocene
		S5	Shelf-confined erosional reflector					Serravallian
D	D3		Progradational wedge	Moderate impedance, steeply dipping, progradational reflectors	1s	Lowstand shelf edge delta	LST	Lower Miocene?
		S4a	Confined northern shelf reflector within unit D					Aquitanian
	D2		Progradational wedge	Moderate impedance, steeply dipping, progradational reflectors	1s	Lowstand shelf edge delta	LST	Miocene? to Upper Oligocene
	D1		Channel Fill	Onlapping and lateral accretion fills, chaotic, moderate amplitude reflectors	0 to 0.2s	Incised Valley Fill	LST	Mid Oligocene
		S4	Basin-wide Erosional Reflector					Mid Oligocene
C	C5		Progradational wedge	Moderate impedance, steeply dipping, progradational reflectors	0 to 0.3s	Highstand wedge	HST	Upper Eocene
		3C	Maximum Flooding Surface					Upper Eocene
	C4		Aggradational to Retrogradational package	Low impedance aggrading reflectors, backstep and onlap 3B landward	0.1 to 0.3s	Healing Phase wedge	TST	Palaeocene
		3B	Maximum Regressive Surface					Danian

	C3		Aggradational to Progradational Wedge	Low to moderate impedance, sub parallel, aggradational reflectors, onlap S3	0 to 0.5s	Delta Margin	LST	Maastrichtian to Campanian
	C2		Progradational wedge	Moderate impedance, steeply dipping, progradational reflectors	0 to 0.5s	Falling stage wedge	FSST	Campanian?
	C1		Slope Fan	Moderate impedance, progradational reflectors, downlap and onlap S3	0 to 0.3s	Falling stage slope fan apron	FSST	Campanian?
		S3	Shelf-confined erosional reflector					Santonian?
	B2		Aggradational ramp	Low to moderate amp, sub parallel reflectors, onlap S2 updip.	0 to 0.5s	Lowstand ramp	LST	Conacian? Turonian
B	B1		Retrogradational Basin-floor Fan	High impedance progradational reflectors that downlap and onlap S2, individual mounds show internal progradation but retrograde as packages.	0 to 0.3s	Falling stage basin floor fan	FSST	Turonian
		S2	Basin-wide Erosional Reflector					Turonian
	A2		Syn-rift valley fill	Aggradational to Progradational packages that onlap S1 against basement highs	0 to 1s	Syn-rift valley fill	Syn-rift TST/HST	Cenomanian to Albian
A		S1a	Graben-confined Erosional Reflector					Late Aptian?
	A1		Syn-rift valley fill	Aggradational to Progradational packages that onlap S1 against basement highs	0 to 1s	Syn-rift valley fill	Syn-rift TST/HST	Aptian to Barremian
		S1	Basin-wide Erosional Reflector					Jurassic
BASEMENT			Acoustic Basement					Jurassic

6.3.1. Unit A

The deepest resolved unit within the basin, unit A, occurs as a discontinuous succession unconformably overlying acoustic basement along a high amplitude reflector S1. The unit terminates updip against faulted pre-breakup basement (Fig. 6.3a-b) but thickens substantially downdip, increasing from 0 to 1sec two-way time in thickness (Fig. 6.3b). In the north of the basin, unit A thins substantially, occurring as a ~0.2sec thick succession defined by high impedance reflectors in small graben-fill successions (Fig. 6.3c). Unit thickness is dependent upon palaeo-topography, with the unit onlapping against basement horst structures (Fig. 6.4) and is best developed in Jc-C1 (Fig. 6.3) where ~900 m of siltstone and claystone with subordinate sandstone is intersected. An upward increase in reflector impedance is noted in the succession (Fig. 6.4), and this can be correlated with sandy to conglomeratic units intersected in Jc-B1 and Jc-D1 (Fig. 6.3c – Jc-D1 Inset i) with the gamma ray logs in Jc-B1 showing an upward coarsening of facies at the top of the unit (Fig. 6.3b – Jc-B1 Inset i).

Within unit A, two seismic facies occur beneath the Tugela Cone, best defined from coast-parallel seismic reflection profiles (Fig. 6.5). Facies A1 is an aggradational succession of low impedance reflectors which increase in impedance strength with stratigraphic height (Fig. 6.5). Reflector architecture is dominated by parallel to sub-parallel internal reflectors which parallel the basement-cover interface. Facies A2 overlies A1, separated by a discontinuous high amplitude surface S1a, identified in coast-parallel profiles (Fig. 6.5). The surface hosts numerous incisions (arrows in Fig. 6.5) which are commonly U-shaped and range from 800 to 1100 m wide and 20 to 30 m (0.30 to 0.4 s TWTT) deep. Although the internal architecture of the facies is the same as facies A1, the base of facies A2 is defined by low impedance reflectors which appear to onlap the incision surface (Fig. 6.5).

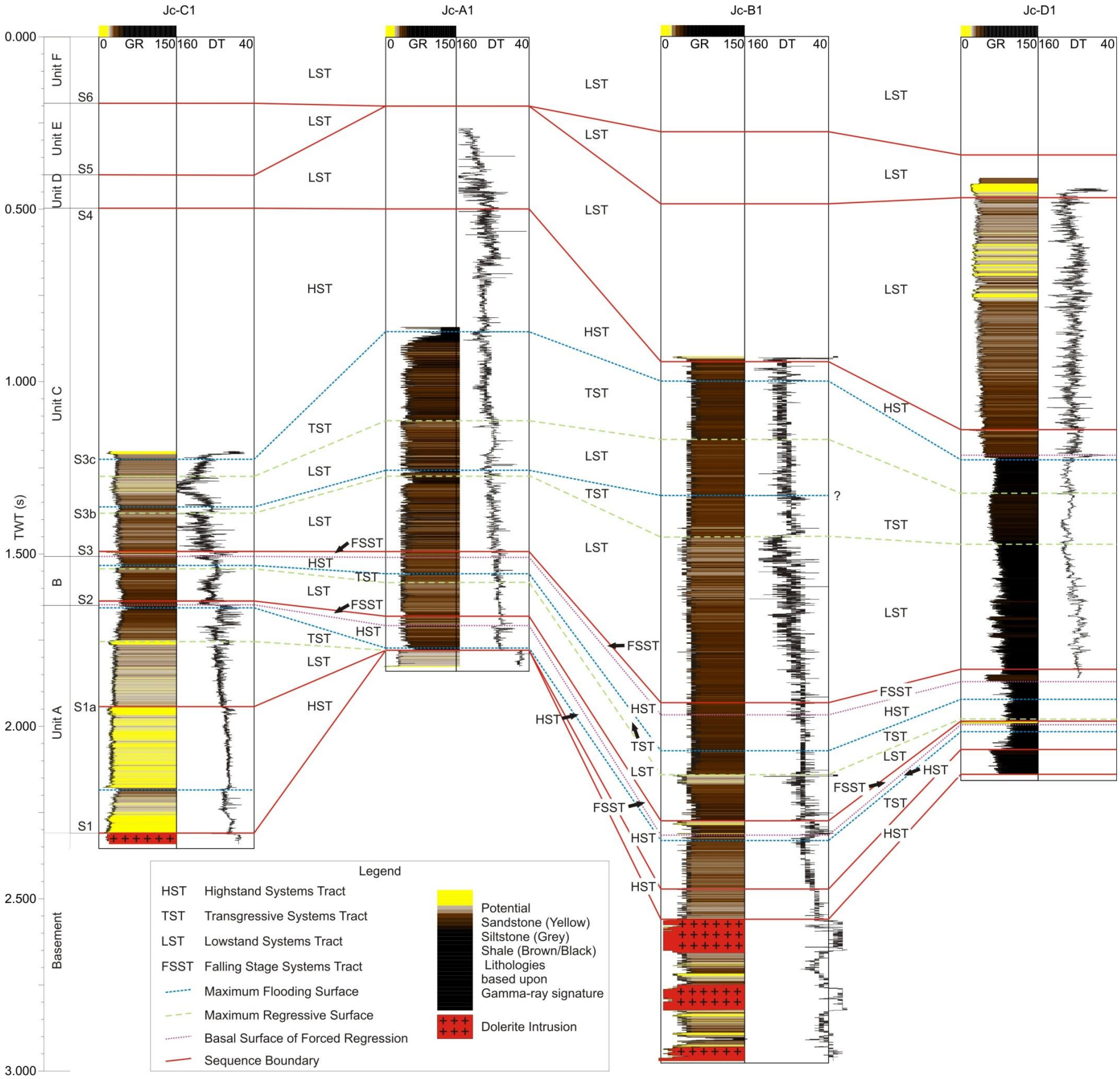

Figure 6.2: Interpretation of potential stratigraphic boundaries within the Durban Basin based upon well log correlation of available gamma ray (GR) and sonic density (DT) logs. Potential systems tracts are detailed. Gamma ray log values shown in API. Sonic density log details shown in millisec. Colour schemes based upon IHS Kingdom Suite 2015 colour bars. Red zones in gamma ray log indicate zones of intrusions in basement lithologies. Contacts of sequence stratigraphic surfaces (S4; S5; S6) where no well logs are available are defined by two-way time depth correlations from lithology logs.

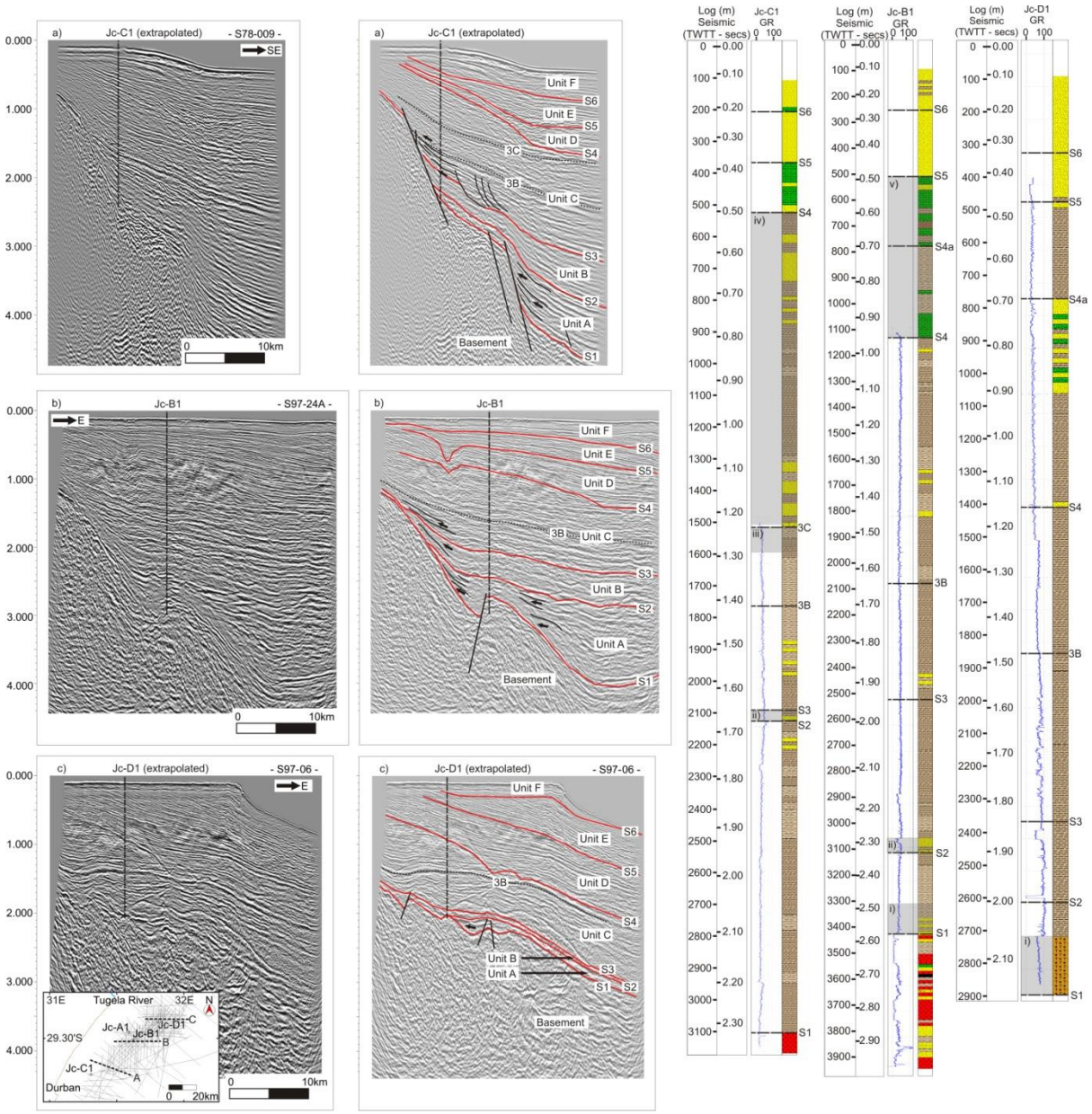

Figure 6.3: Seismic profiles and associated well logs showing sediment architecture and lithological and geophysical properties (gamma-ray log) of units beneath the present continental shelf within the Durban Basin. a) Seismic profile through the southern basin. Arrows show onlap of seismic reflectors against antecedent basement structures. The extrapolated position of Jc-C1 is shown. b) Profile through the central basin. Arrows show onlap of seismic reflectors against antecedent basement structures. The position of Jc-B1 is shown. c) Profile through the northern basin. The extrapolated position of Jc-D1 is shown.

Zones of discussion within the well logs are highlighted by greyed insets numbered i-v.
i) Sandy to conglomeratic facies of Unit A. Note coarsening upward signature in gamma ray log of Jc-B1 and Jc-D1. ii) Coarsening upward sandy packages overlying S2 surface. Note the marked variation in the gamma ray logs in Jc-B1 and Jc-D1. iii) Marine claystone interval between horizon 3B and 3C. Note the moderate to high gamma ray values in Jc-C1 beneath the 3C surface. iv) Facies C5 restricted to the inner shelf and intersected in Jc-C1. v) Mixed siliciclastic-carbonate succession of Unit D.

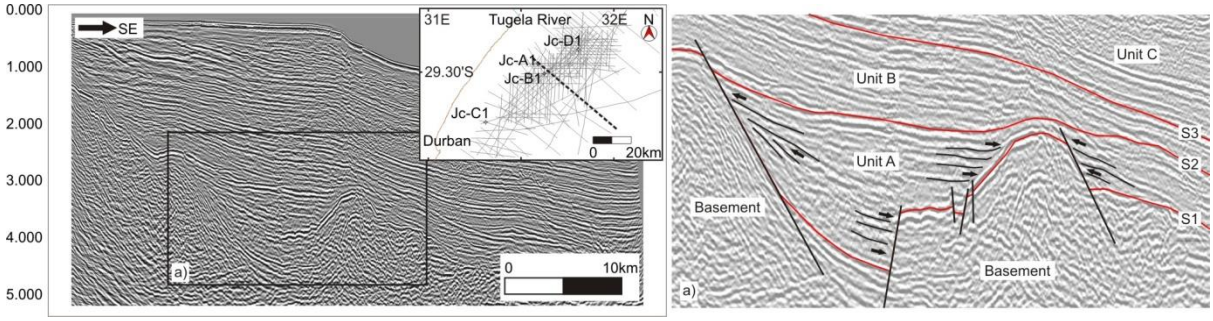

Figure 6.4: Syn-rift infill within a graben system in the central Durban Basin. Note the onlap and truncation of reflectors against basement structures in both directions.

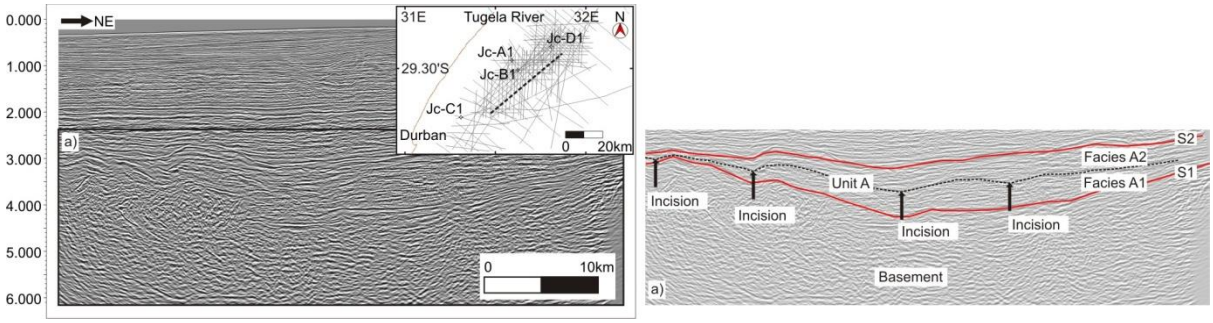

Figure 6.5: Coast-parallel seismic profile of Unit A showing possible incisions into seismic surface S1a separating facies A1 from A2.

6.3.2 Unit B

Unit B overlies unit A along an erosional, high amplitude seismic reflector S2, which can be traced through much of the distal portions of the basin. Proximally, the reflector truncates against faulted basement, with unit B unconformably overlying seismic basement in the updip profile (Fig. 6.3a-b). Two facies are defined (B1-2) with facies B1 represented by a series of laterally discontinuous, high impedance reflectors that occur as mounded zones onlapping and downlapping onto the underlying unit (Figs 6.6; 6.7). The positions of the mounds relative to the contemporary shoreline are shown as polygons on the seismic grid map insets in Figures 6.6 and 6.7. Two dominant architecture styles, *single* and *retrograde*, are identified. Single mounds have a basal progradational structure with seaward-dipping reflectors downlapping the underlying reflector S2 whilst landward dipping reflectors are seen to migrate updip and onlap surface S2 (Fig. 6.6). Where multiple mounds are developed (Fig. 6.7 mounds a-b), an overall retrogradational architecture is recognised as younger features onlap successively landwards onto the underlying feature.

Where facies B1 does not occur, reflectors of facies B2 onlap S2 progressively landward, with downdip reflectors occurring in an aggradational stacking arrangement (Fig. 6.3a). This comprises a succession of high impedance reflectors aggradationally stacked above either facies B1 or unit A (Fig. 6.3a). Facies B2 is represented by a succession of siltstones and claystones of variable thickness within the Jc-Series wells (Fig. 6.3 – Jc-C1 Inset ii). Within Jc-B1 and Jc-C1 (Fig. 6.3), gamma ray logs indicate coarsening upwards sequences capped by thin sandstone packages.

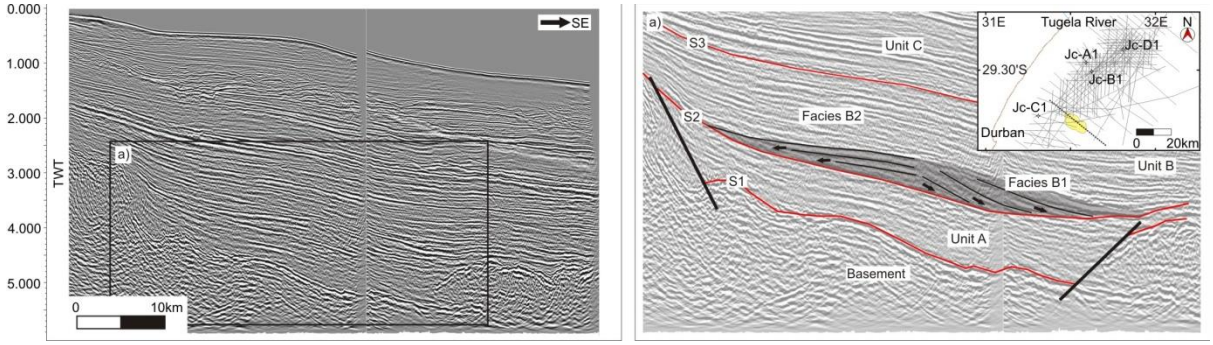

Figure 6.6: Singular, mounded structure constituting facies B1, overlying seismic surface S2 in the southern basin. Note the pronounced onlap updip and downlap of reflectors (arrows) onto the underlying surface.

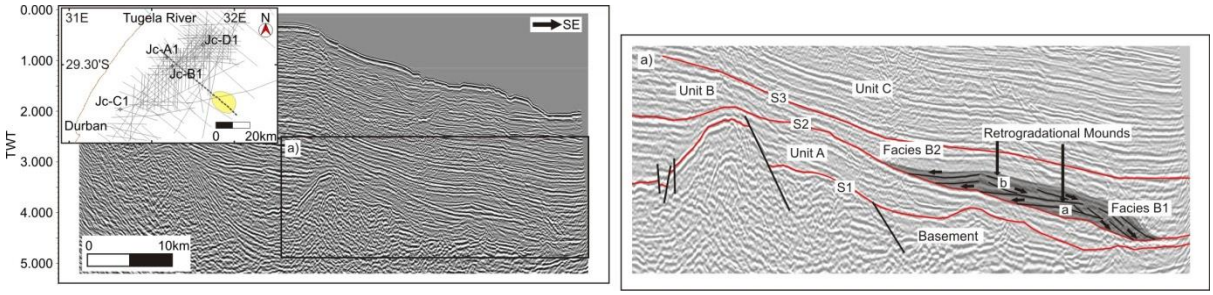

Figure 6.7: Multiple, retrogradational mounded structures overlying seismic surface S2, constituting facies B1 in the central basin. Note the pronounced onlap and downlap of reflectors onto the underlying surface. Note the retrogradational stacking pattern of mound a) vs mound b), with mound b) reflectors downlapping upper surfaces in mound a).

6.3.3 Unit C

Unit C occurs as a prograding package with an offlapping reflector configuration, separated from the underlying unit by an erosional, moderate amplitude reflector S3. Under the Tugela Cone (Fig. 6.8) five facies (C1-5) are resolved. Facies C1 is represented by mounded reflectors that prograde internally, downlapping the underlying reflector S3 (Fig. 6.3c). This facies is laterally discontinuous, developed along the lower slope in the north of the basin where it is capped by a moderate amplitude reflector surface 3A (Fig. 6.3c). Where facies C1 is not developed, reflector S3 is overlain by either facies C2 in the proximal basin, or C3 in the distal basin (Fig. 6.8). Internal reflector architecture for facies C2 is dominantly progradational, with pronounced downlap on surface S3 (Fig. 6.8). Facies C3 shows aggradational to progradational internal reflectors (Fig. 6.8). Facies C3 is not well developed in the southern basin, where unit C is dominated by aggradational reflector architectures (Fig. 6.3a-b). Gamma ray and lithological logs (Figs 6.1; 6.2) indicate that facies C3 is composed of siltstones and claystones with subordinate sandstone stringers which cap upward-coarsening cycles.

Facies C4 is observed throughout the study area, overlying facies C2 and C3 along a high amplitude reflector surface 3B that marks the base of the most prominent onlap. The facies comprises low impedance, sub-parallel to parallel aggradational to weakly retrogradational reflectors that distinctly onlap the underlying facies C2 updip (Fig. 6.8). Within the wells, the facies is dominated by claystones and siltstones, capped by a moderate to high gamma ray signature claystone in Jc-C1 (Fig. 6.3 – Jc-C1 Inset iii) and by a 6 m thick limestone in Jc-A1.

Facies C5 is confined to the proximal basin and occurs as a prograding wedge which oversteps facies C2 and C4 seaward along a downlap surface 3C (Fig. 6.8). The facies is intersected only in Jc-C1 where the package is dominated by coarse- to medium-grained sandstones and subordinate claystones (Fig. 6.3 Jc-C1 Inset iv). No geophysical logs are available for this facies. Thicknesses of facies C5 are variable, with the sequence truncated by a major erosional reflector S4.

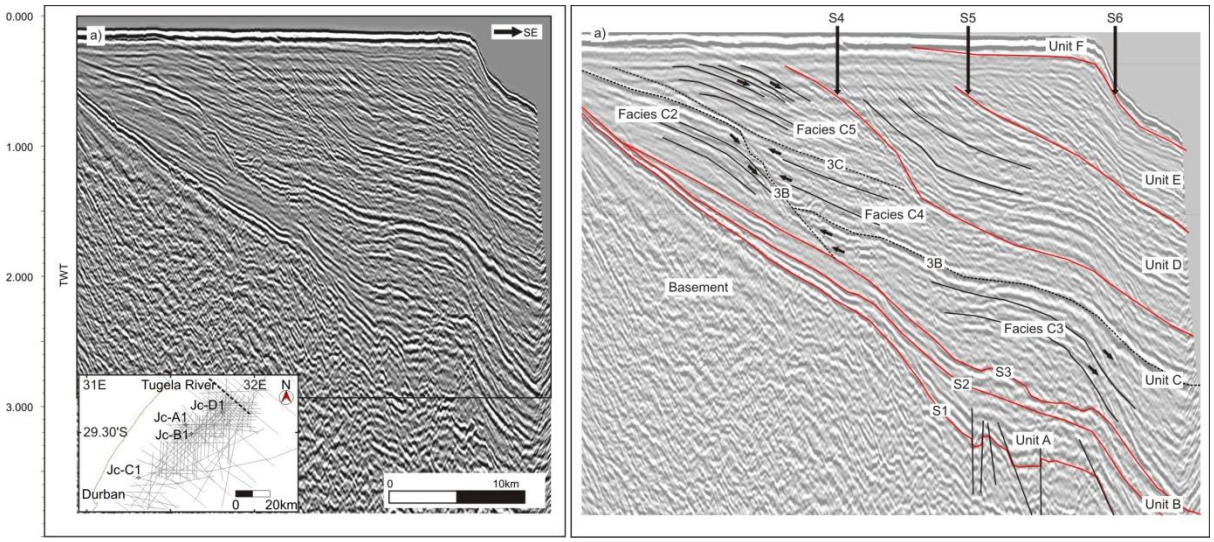

Figure 6.8: Seismic architecture of unit C in the northern basin. Note the downlapping progradational reflector package of facies C2 in the inner shelf with progradational reflectors of facies C3 preserved in the deeper portion of the basin. Note the aggradational to retrogradational "healing phase" deposits of facies C4 that progressively onlap facies C2 updip. Note the final progradational reflector package C5 which caps the sequence.

6.3.4 Unit D

Along coastal strike, unit D overlies a pronounced erosional surface S4 that delineates a series of U and V-shaped incisions up to 70 m (0.9 s TWTT) deep. Unit D can be separated into two facies which together represent a seaward thickening succession in the northern portion of the study area, but a relatively thin succession in the southern portion of the basin. Facies D1 is an infilling facies with onlapping high amplitude reflectors restricted to coast-perpendicular incisions (Fig. 6.9). Facies D1 is overlain by facies D2, a seaward dipping, aggradational to progradational set of high impedance, low amplitude reflectors. This facies is laterally continuous along strike (Fig. 6.3b-c) and comprises calcarenite and coquina interbedded with sandstone and siltstones in all wells (Fig. 6.3 – Jc-B1 Inset v). In the northern portion of the basin facies D2 can be subdivided into D2 and D3, which constitute the main components of a sediment wedge, separated by a local reflector S4a.

6.3.5 Unit E

Although unit E is similar in its internal reflector architecture to unit D, the two are separated by an erosional surface S5 that is identifiable in coast-parallel section and delimits a series of U and V-shaped incisions up to 50 m (0.6 s TWTT) deep (Fig. 6.10). In the northern portion of the Tugela Cone, unit E occurs as a seaward prograding reflector package with pronounced downlap on the underlying S5 surface (Fig. 6.11). Three facies are identified within unit E, with facies E1 having a similar architecture to that of facies D1, represented by incision fill with high amplitude reflectors onlapping the incision flanks. Incisions and associated fills are identified along both the palaeo-shelf and slope, with both drape fill and flank-attached deposits (Fig. 6.10). Facies E2 overlies either facies E1 or unit D if E1 is not preserved. Facies E2 consists of high impedance reflectors that in downdip section occur as a seaward prograding set of high impedance reflectors which exhibit pronounced downlap on the underlying S5 surface. Facies E3 forms the uppermost facies, represented by low impedance parallel reflectors that show aggradational stacking patterns. Facies E3 is separated from the underlying facies by a moderate amplitude reflector.

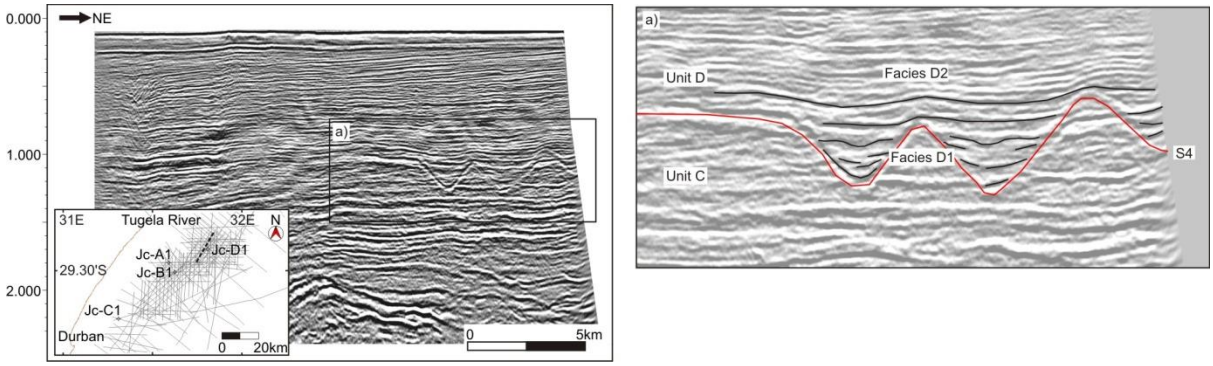

Figure 6.9: Coast-parallel seismic profile indicating multiple incisions and associated incision-fill along seismic surface S4 in the northern basin.

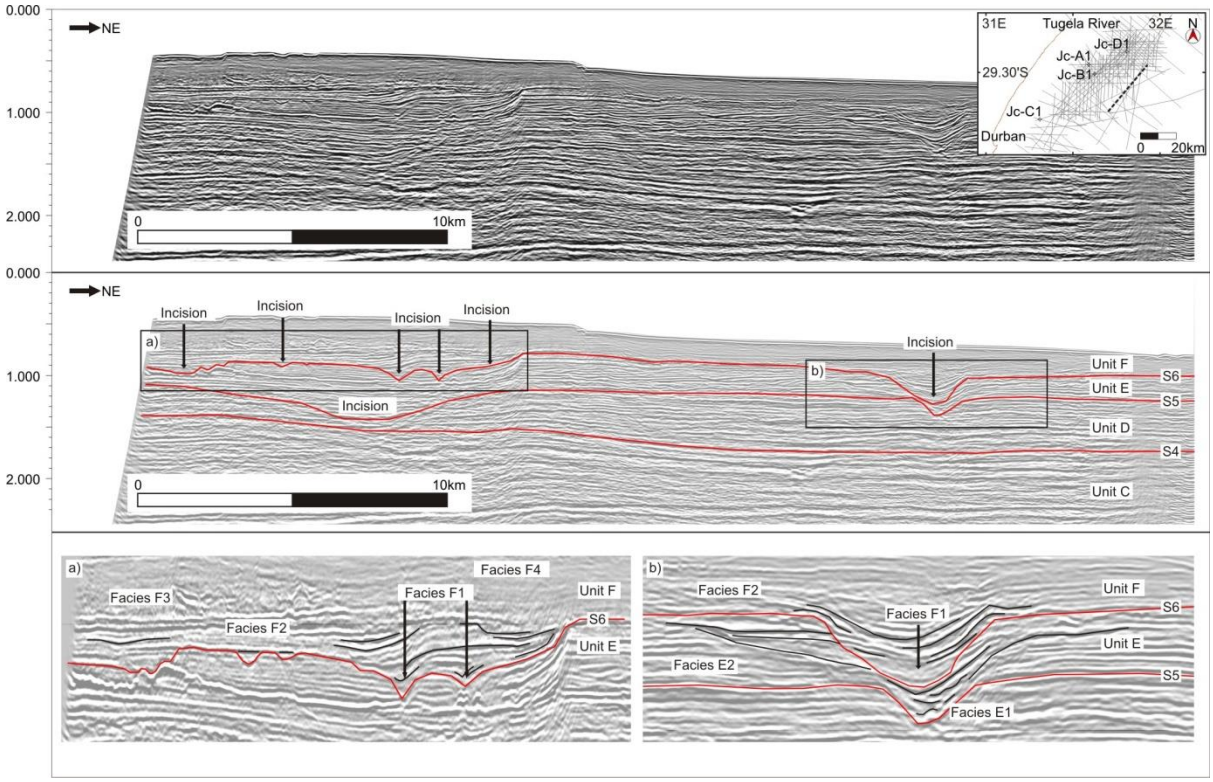

Figure 6.10: Coast-parallel seismic profile indicating multiple incisions and associated incision-fill along multiple seismic surfaces S5 and S6 in the southern basin. Note the multiple incision episodes in singular incisions as shown in inset b).

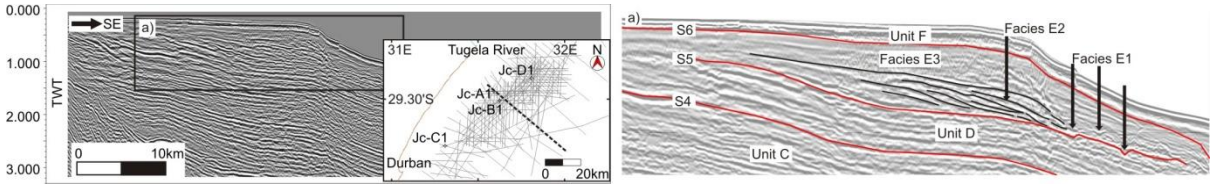

Figure 6.11: Progradational reflector package comprising facies E2 overlying seismic surface S5.

6.3.6 Unit F

Unit F corresponds to a prograding sediment wedge that occurs on the continental shelf and at the shelf break. The unit is bounded at the base by an erosional high amplitude reflector, S6, with incisions into the underlying unit. In many instances the internal architecture of the unit is obscured by seafloor multiples, but in coast-parallel section (Fig. 6.10) the succession can be delineated and comprises four facies (F1-F4). Facies F1 represents incision fill where onlapping high amplitude reflectors are restricted to incisions on the palaeo-shelf and slope (Fig. 6.10a-b). Facies F2 represents high impedance sub-parallel to parallel reflectors. In coast perpendicular section, this facies occurs as a prograding wedge of seaward dipping reflectors, with facies F2 occurring as a distal succession of aggradational reflectors underlying the seafloor (Fig. 6.10b). Facies F3 is only evident in coast-parallel section, occurring as chaotic low impedance reflectors (Fig. 6.10a). Unit F is capped by facies F4 which occurs as low impedance sub-parallel to parallel reflectors.

6.4 DISCUSSION

Sedimentation within the Durban Basin is represented by both syn-rift and drift phase sequences. Although conventional sequence stratigraphic analysis (cf. Catuneanu et al., 2011; Zecchin and Catuneanu, 2013) is generally focussed on drift phase sediments in passive margin basins, for rifted sequences separate models need to be utilised with typical rift sequences comprising transgressive and highstand system tracts (cf. Martins-Neto and Catuneanu, 2010). In order to identify major sequence boundaries within the basin, biostratigraphic sediment distribution (McMillan and Dale, 2000; McMillan, 2003), and known local and global fluctuations in sea level (Siesser and Dingle, 1981; Haq et al., 1987; Miller et al., 2005) are correlated in Figure 6.12 to aid sequence stratigraphic analyses.

6.4.1 Early syn-rift infillings

The spatial distribution of unit A is irregular (Fig. 6.13a), and represents syn-rift, graben fill of likely lacustrine to fluvial origin (Stojcic, 1979; McMillan, 2003). Seismic reflector architecture in individual grabens shows onlap of chaotic reflectors against fault scarps similar to that defined by Prosser (1993) for “rift initiation” fluvial sedimentation. The identification of continental syn-rift sediments (Fig. 6.3c – Jc-D1 Inset i) in facies A1 (Stojcic, 1979; McMillan, 2003), overlain by lacustrine facies A2 sediments in the Jc-B1 and Jc-D1 wells (McMillan, 2003) supports Kitchin and McLachlan’s (1996) proposal that the interval represents a major marine transgression which can be correlated with global sea level rise in the early Albian (Haq et al., 1987) (Fig. 6.12). Facies A2 likely correlates with “rift climax” sedimentation of subaerial alluvial fans and shoal-type deltas as defined by Prosser (1993).

The increase in reflector impedance upwards in the facies (Fig. 6.4) suggests a succession of coarsening upward packages bounded by flooding surfaces similar to that defined by Martins-Neto and Catuneanu (2010) for active rift basins. Here a thin transgressive systems tract (TST) of retrogradational reflectors is overlain by aggradational to progradational facies of the highstand systems tract (HST) (Martins-Neto and Catuneanu, 2010). This fits well with the syn-rift deposits identified below 3100m in Jc-B1 (Figs 6.3b; 6.12 – Inset a), which comprise ~40 m thick upward coarsening, regressive cycles of claystone, siltstone and sandstone (Kitchin and McLachlan, 1996). This facies is likely the equivalent of the Makatini and Mzinene Formations from the adjoining Zululand Basin (Broad et al., 2006) which span the late Barremian to middle Cenomanian.

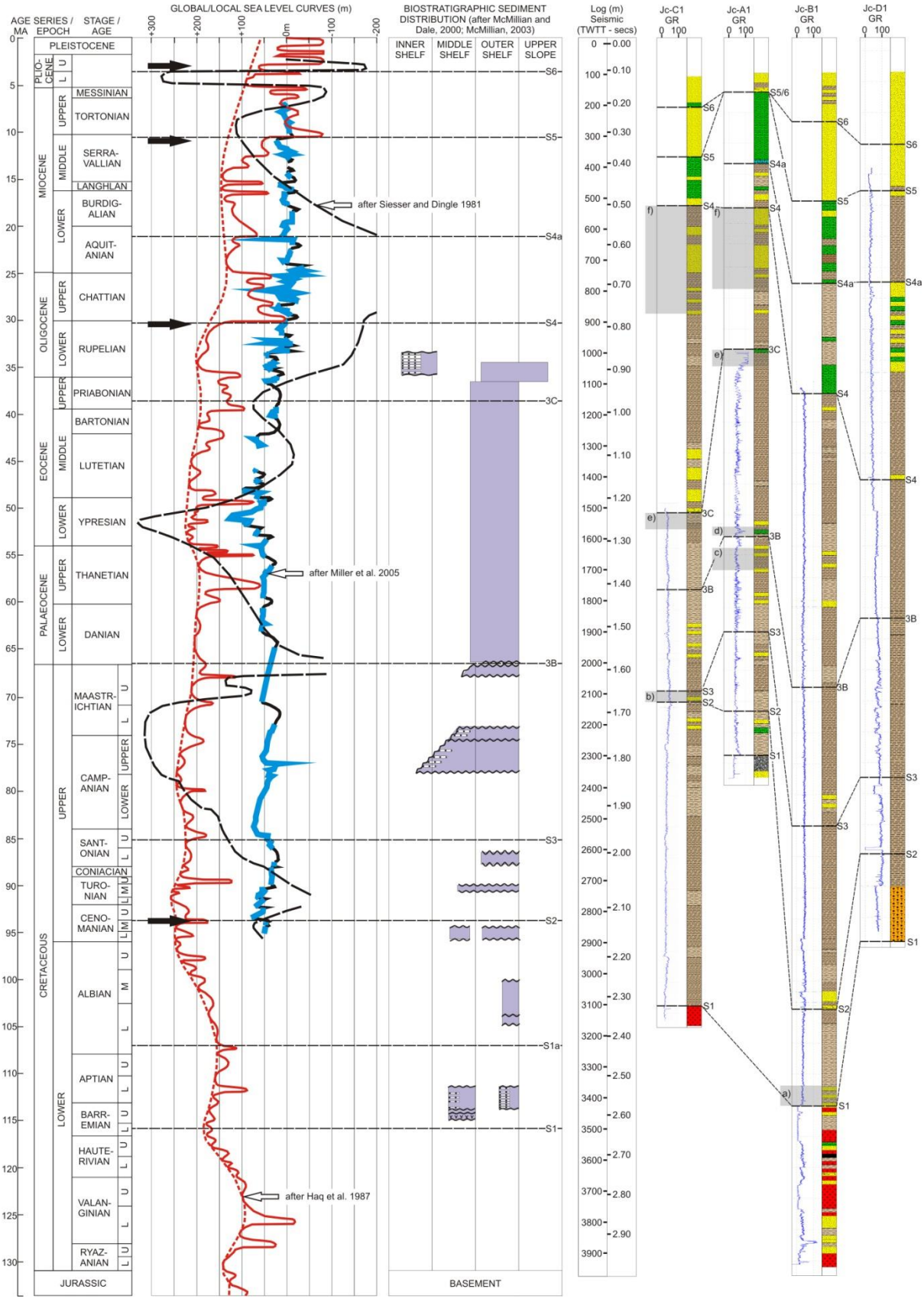

Figure 6.12: Biostratigraphy of the Durban Basin (after McMillan and Dale, 2000; McMillan, 2003) compared with Jurassic to Pliocene sea-level curves in southern Africa (modified after Siesser and Dingle, 1981) and global eustatic sea-level curves (modified after Haq et al., 1987; Miller et al., 2005). Filled black arrows on sea-level curves denote uplift episodes (after Siesser and Dingle, 1981; Dingle et al., 1983;

Partridge and Maud, 2000). Geological and gamma ray logs for all Jc-series boreholes are presented with depths in m and TWTT (sec). Logs are correlated with sea level curve graphs via mapped seismic surfaces (S2; S3 etc.).
Areas of interest discussed in log data are shown in greyed areas.
a) Syn-rift continental sediments in Jc-B1. b) Limited sediment deposition/preservation in Jc-C1 between S2 and S3 surfaces. c) Lowstand wedge coarsening upwards parasequences in Jc-A1. d) High gamma ray signature carbonate in Jc-B1. e) Condensed section (maximum flooding surface) in Jc-A1. f) Sandstone packages associated with progradation of HST and early FSST.

6.4.2 Ramp margin deposition

The syn-rift succession (Fig. 6.13a) is overlain by deposits of unit B, which are bounded at their base by regional seismic reflector S2. This surface marks a major regional hiatus [McDuff – (Goodlad, 1986); 15At1 – (McMillan, 2003)] that, through biostratigraphical data (McMillan and Dale, 2000; McMillan, 2003), is shown to span the late Cenomanian to early Turonian (Fig. 6.12). This period coincides with marked forced regression and sea level fall around southern Africa as defined by Dingle et al. (1983) (Fig. 6.12). In the proximal basin, S2 represents a subaerial unconformity (Fig. 6.13b) with erosion of the underlying units and sediment bypass into the deep basin. Within the deeper basin, facies B1 sediments show progradation and downlap on reflector S2 with mounded, prograding structures (Figs 6.6; 6.7) representative of deep water, basin floor fans formed by off-shelf sediment forcing and the deposition of high density turbidites (cf. Catuneanu et al., 2011). Figure 6.13b shows a zone of proximal bypass and the deposition of isolated fans of facies B1. It is thus postulated that these fans were deposited during forced regression of the falling stage systems tract (FSST) along the palaeo-shelf (sensu Catuneanu et al., 2009; 2011). Due to the downlap evident in reflectors overlying surface S2, it is proposed that, in the deep basin, S2 represents a basal surface of forced regression "BSFR" (sensu Posamentier and Allen, 1999) with facies B1 separated from facies B2 by a correlative conformity (Hunt and Tucker, 1992) separating FSST and lowstand systems tracts (LST) deposits on the basin floor.

Facies B2 is dominated by aggradational reflectors, and as such represents deposition during a phase of normal regression during the ensuing LST (Catuneanu et al., 2011) with the corresponding sedimentology from Jc-B1 (Fig. 6.3b) suggesting deposition of deep marine shales in a slope environment (Kitchin and McLachlan, 1996) (Fig. 6.12). The architecture of facies B2 is dominated by gently dipping, parallel reflector patterns suggestive of deep water deposition within a narrow, 10 km wide, ramp margin (Fig. 6.13b), similar to that defined by Seyedmehdi et al. (2016) in the Canning Basin, Australia. Antecedent topography defines the mid ramp depositional characteristics with units pinching out laterally updip against surface S2 (Figs 6.3; 6.8; 6.13b), whilst the landward section of the basin is dominated by a rugged erosional unconformity which is interpreted as a subaerial unconformity based upon a biostratigraphical hiatus (Muntingh, 1983) and limited sedimentation in Jc-C1 (Figs 6.3a; 6.12 – Inset b).

6.4.3 Proximal erosional hiatuses and distally focussed deposition

Although outer shelf deposits of Early Santonian age are identified onshore (Anderson, 1906; McMillan, 2003) and beneath the inner continental shelf (Green and Garlick, 2011), representing remnants of the TST and HST correlated with a period of sea-level high within the Durban Basin (Dingle, et al., 1983), post-unit B TST and HST successions are not preserved distally offshore. It is considered that this period marked non-deposition in the distal basin between the late Turonian and early Campanian (Fig. 6.12) as identified in the biostratigraphy (McMillan, 2003), with a laterally extensive bounding surface S3 separating unit B from the overlying unit C.

Based upon biostratigraphical ages defined by McMillan and Dale (2000) and McMillan (2003) (Fig. 6.12) unit C represents a period of almost continuous distal basin deposition from the Upper Campanian to Eocene. Five facies are resolved, with mounded structures of facies C1 downlapping the underlying surface S3 with progradational internal reflectors similar to retrogressive turbidite lobes identified by Shanmugam (2016); it is

thus considered that these structures represent deposition as slope and basin floor fans within the late FSST (Fig. 6.13c). These were focussed offshore of the position of the contemporary Tugela River (Fig. 6.13c). Furthermore, in the northern portion of the basin, reflector architecture of facies C2 shows marked progradation with pronounced offlap and limited topset development (Fig. 6.8) and is truncated above by a subaerial unconformity, a reflector architecture synonymous with forced regressive conditions in the proximal FSST (Zecchin and Catuneanu, 2013). The C2 facies package has been identified along much of the KwaZulu-Natal margin (Fig. 6.13c) (Green, 2011b; Green and Garlick, 2011) and has been correlated with the relative sea level fall of the late Campanian and early Maastrichtian (Dingle et al., 1983), with sedimentation a product of deltaic deposition from large river systems (Dingle et al., 1983; Goodlad, 1986). In this regard, facies C2 is interpreted as a truncated shelf-edge delta (Fig. 6.13c) within the FSST as defined by Hunt and Tucker (1992) with facies C1 representing coeval forced regressive submarine fans. This marks the early stages in construction of the nascent shelf edge.

Facies C3 is resolved seaward of the facies C2 FSST (Fig. 6.13d) and occurs as a seaward thickening wedge of aggradational to progradational reflectors (Fig. 6.8). The wedge tapers landward, onlapping the underlying S3 surface in the mid-shelf (Fig. 6.8). The forestepping nature of the reflectors is similar to that of wedges produced during the late LST (cf. Posamentier and Allen, 1999), suggesting stable accommodation space change relative to sediment supply. The C3 lowstand wedge is intersected in Jc-A1, where numerous coarsening-upwards parasequences of claystone and sandstone are identified (Fig. 6.12 – Inset c). Deposition in a prograding delta margin setting similar to that discussed by Porebski and Steel (2003) is thus envisioned, with LST sedimentation overlying the FSST slope component. Truncated clinoforms within the FSST shelf-edge delta suggest that this facies has been prone to erosion through current activity, shelf-edge slumping and/or sediment bypass during early lowstand (Fig. 6.8).

The seismic reflector 3B which overlies facies C2 and C3 (Fig. 6.8) is coincident with the Cretaceous-Tertiary boundary and forms the base of a distinct retrograding parasequence set in the slope environment. Although difficult to identify in the borehole logs which show limited sedimentological variation due to their location in the deeper shelf settings (Fig. 6.3; 6.12), in Jc-A1, the surface is overlain by a ~6 m thick carbonate that exhibits a marked high gamma ray signal (Fig. 6.12 – Inset d). The reflector is often not well defined in seismic section, and is not mapped by previous studies (Dingle et al., 1978; Martin, 1984; Goodlad, 1986). Although a limited biostratigraphical hiatus is defined by McMillan (2003), biostratigraphy within the Jc-D1 well (Lester, 2000) suggests continued deposition across the boundary, with a change from more proximal LST deposits to distal TST Tertiary sedimentation. This is corroborated by the sea level curves of Siesser and Dingle (1981), which show a change from regressive to transgressive conditions across the boundary (Fig. 6.12). Due to the seismic architecture of the parasequences above and below this surface (Fig. 6.8) combined with sedimentological and biostratigraphical well log data, it is proposed that surface 3B represents the maximum regressive surface marking the change from lowstand normal regression to transgression (cf. Catuneanu et al., 2009).

Overlying surface 3B, facies C4 is recognised from borehole studies (du Toit and Leith, 1974) as a ~440 m thick Palaeocene and Eocene-age (Lester, 2000) succession of marine claystones. This occurs throughout the study area (Fig. 6.13e). The seismic architecture of facies C4 is best represented in the northern Tugela Cone (Fig. 6.8) where reflectors show consistent retrogradation landward over the underlying FSST (Facies C2), with prominent onlap against the 3B surface. The succession thins to the south, identified in Jc-C1 as a ~200 m thick succession of claystone which coarsens upwards to siltstone (Fig. 6.12). The stratal architecture bears similarity to the architecture of "healing phase" TST wedges as defined by other authors (sensu Catuneanu, 2006). The limited occurrence of Palaeocene and Eocene sediments on the inner shelf is discussed by Siesser and Dingle (1981), Green and Garlick (2011), and Green (2011a), who consider it a function of non-preservation due to intervening episodes of sediment bypass and later erosion.

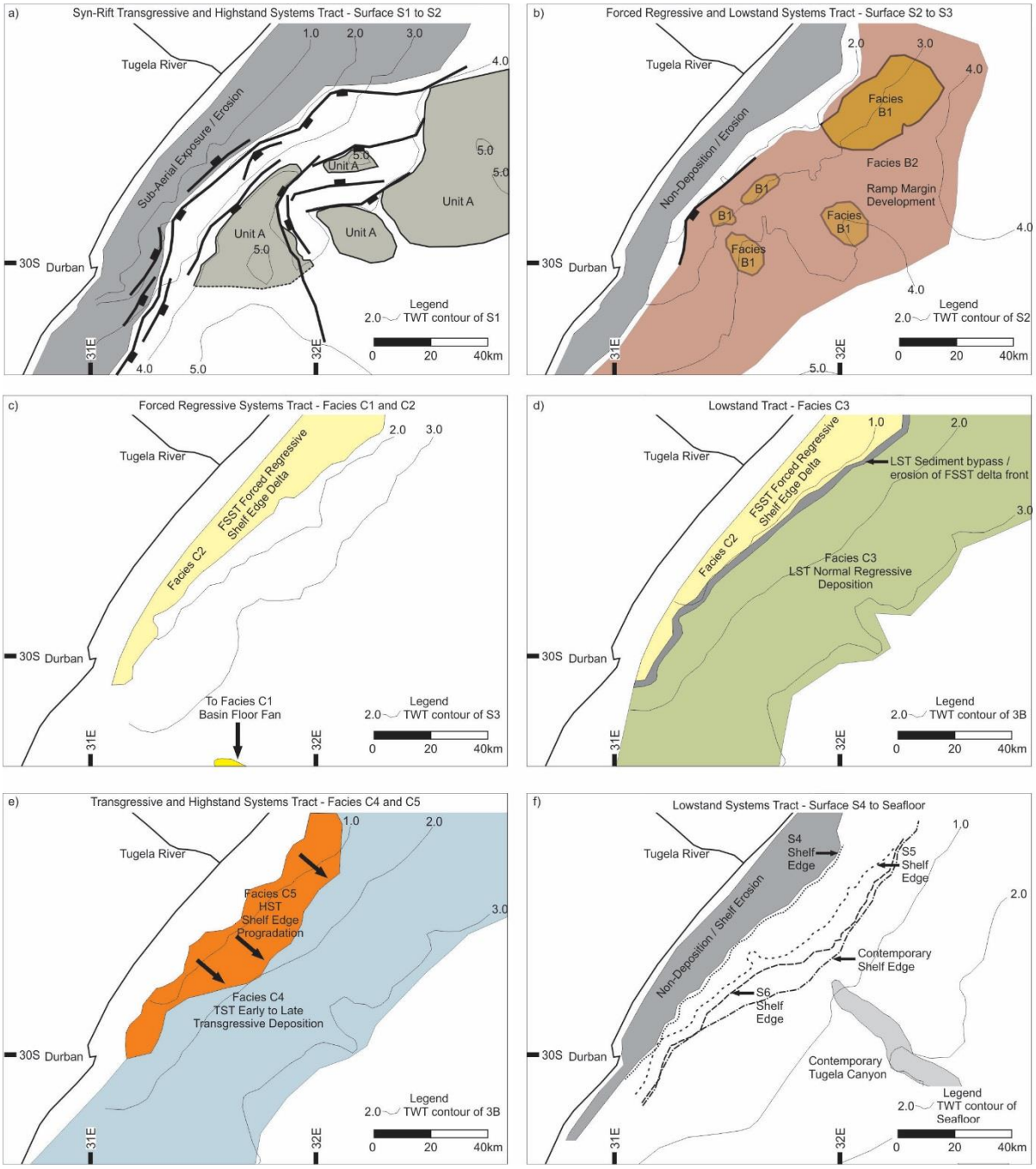

Figure 6.13: Spatial distribution for each unit within the Durban Basin. a) Syn-rift, transgressive to highstand systems tract sedimentation of unit A in restricted structurally-defined depocentres. b) Position of falling stage and lowstand basin floor fans (Facies B1) overlain by ramp margin sedimentation of facies B2. c) Position of basin floor fan relative to facies C2 shelf edge delta. d) Deposition of facies C3 basinward of the palaeo-shelf edge. e) Transgressive systems tract deposition of facies C4 overlain by progradational (arrows) shelf edge delta facies C5. f) Lowstand shelf edge progradation of units D-F defined by relative positions of the palaeo-shelf edge associated with horizons S4, S5 and S6 relative to the contemporary shelf break.

Facies C4 is capped by surface 3C (Fig. 6.8) which correlates with a 5 m thick limestone horizon (Fig. 6.12 - Inset e) evident at 975 m depth in Jc-A1 (du Toit and Leith, 1974). The overlying facies C5 (Fig. 6.8) is intersected by borehole Jc-A1 where three Palaeocene age coarsening upward packages of shale to sandstone are identified (du Toit and Leith, 1974). Sandstones vary in thickness from 5 to 40 m (Fig. 6.12 – Inset f) and the progradational nature of the seismic reflections suggests that these are likely representative of shallow marine shoreface sands (Catuneanu, 2006). Siesser and Dingle (1981) suggest that the Palaeogene was a period of protracted sea level rise along the east coast (Fig. 6.12) with TST deposits identified along the northern KZN shelf (Green, 2009b). Although a minor regressive phase in the early Eocene is postulated by Siesser and Dingle (1981), this study shows continued marine transgression throughout the Palaeogene with highstand conditions prevailing in the late Eocene consistent with sea level curves of Siesser and Dingle (1981).

As surface 3C caps the TST in Jc-A1, with the corresponding limestone in Jc-A1 having a high gamma ray signature typical of condensed sections (Fig. 6.12 – Inset e), it is proposed that the surface is representative of a maximum flooding surface that caps the healing phase wedge (Fig. 6.8). The progradational facies C5, which overlies this surface is correlated with inner shelf sands and thus considered the subsequent HST wedge (Fig. 6.13e) (Catuneanu et al., 2011). This mantles the underlying C4 and spans almost the entire study area along-strike (Fig. 6.13e).

6.4.4 Large scale sediment influx, cone development and shelf construction

Unit C is truncated by a regional unconformity surface S4 (Angus – Goodlad, 1986), which correlates with a basin-wide early Oligocene hiatus identified in the Jc-A1 well (du Toit and Leith, 1974). The Oligocene hiatus correlates with hinterland uplift (Partridge and Maud, 1987), as well as a global sea level lowstand during the middle Oligocene (Fig. 6.12) (Haq et al., 1987; Miller et al., 2005; Miller, 2009). Siesser and Dingle (1981) suggest sea level fall around southern Africa of -500 m during the early to middle Oligocene (Fig. 6.12), whilst Dingle et al. (1983) propose -100 to -200 m sea level fall along the east coast. Within the Durban Basin, the Oligocene sequence boundary S4 is marked by numerous channel incisions on the palaeo-shelf (Fig. 6.9). This boundary thus represents the subaerial unconformity and its seaward extension (correlative conformity cf. Posamentier and Allen, 1999), with lower shelf and slope incisions formed by off-shelf sediment forcing and turbidity current incision. At this time, deepwater slope fans would have been deposited (Catuneanu, 2006), however Wiles et al. (2013) suggest that these deposits have been subsequently reworked or completely eroded by bottom currents active in the adjoining Natal Valley.

The overlying unit D represents periodic, but voluminous deposition by short, fast-flowing and entrenched river systems that drained the nearby coastal escarpment during the late Oligocene to early Miocene. Periods of hinterland uplift and denudation are notable during this time period (Partridge and Maud, 1987; Walford et al., 2005; Green, 2011b; Said et al., 2015), producing a zone of erosion/sediment bypass in the shelf and deposition near the contemporary shelf edge (Fig. 6.13f). The dominantly progradational reflectors of unit D depict the associated basinward advance of a large, normal regressive, constructional, submarine delta (Tugela Cone) during sea-level lowstand. Facies D1 represents the LST fill of submarine canyons preserved in the underlying erosional unconformity. The higher amplitude seismic reflections relative to the adjacent incised units, suggest coarser-grained sedimentary infill along the lines of canyons described by Di Celma (2011). Posamentier and Walker, (2006) suggest that, in active continental margin settings, coarse-grained canyon fill is common with deepwater canyon systems linked directly to short and steep fluvial systems similar to that identified in the Durban Basin. Although no canyon/channel systems are intersected by the boreholes offshore, the increase in sediment supply during this period is identified in Jc-C1 and Jc-D1 and best shown in Jc-A1. Fossil assemblages within the sandstone packages of Jc-A1 (Leith, 1971) suggest a similar middle shelf environment to that outlined by Zecchin et al. (2011) for the early stages of submarine canyon fills in the Crotone Basin, Italy. Although not recognised in the northern portion of the basin (Green, 2011b), an architecturally similar, though undated, canyon fill is identified by Wiles et al. (2013) within the adjoining Tugela Canyon. Current data from this study corroborates this and thus it is proposed that initial canyon incision corresponded with the mid

Oligocene hiatus, with subsequent canyon quiescence and infilling related to late Oligocene to Miocene transgression (Fig. 6.9). Facies D2, the overlying moderate amplitude, aggradational-progradational offlapping seismic reflections, constitute a LST shelf-edge wedge deposit (sensu Santra et al., 2013). This marks the development of the shelf-break system which characterises the area to date. In the northern basin, Facies D2 can be sub-divided into 2 facies (D2 and D3) by a shelf-confined northern shelf reflector, S4a. The overlying Facies D3 is identical to facies D2, depicting further progradation of the shelf edge wedge in the northern region.

Truncating unit D is a second highly erosional surface S5, which shows large-scale channel incision along the shelf (Fig. 6.10), correlated with subaerial erosion and sediment bypass. The complete lack of TST or HST post-unit D, has been discussed by Green (2011a; 2011b) who suggests that the continental shelf was subject to alternating periods of sediment influx (FSST and LST) and sediment starvation with ensuing erosion/non deposition (TST and HST). This is corroborated by Green and Garlick (2011) and Green et al. (2013) who identify a prolonged hiatus on the inner shelf spanning the late Eocene to Pliocene; and further suggests the deposition of deep water slope fans and turbidites during this period. The lack of preserved FSST deposits within unit E is however due to reworking by bottom currents as described by Wiles et al. (2013) within the Natal Valley since the Oligocene.

Unit E is architecturally similar to unit D, characterised by progradational to aggradational reflections which form an offlapping LST wedge on the shelf-edge (Fig. 6.13f). Within the progradational shelf-edge wedge, facies E1 occurs as high amplitude channel/valley fill deposits (Fig. 6.10b) similar to that of the early LST facies D1. Facies E2 consists of progradational offlapping seismic reflections forming a seaward dipping LST shelf-edge wedge similar to that of facies D2. Updip these reflectors pass into the diffusely reflective facies E3 in the proximal portion of the wedge. Due to the wedging out updip of the unit, no boreholes intersect these deposits. However, the transparent nature of facies E3 is likely associated with uniform mud-rich lithologies as discussed by Santra et al. (2013) for the New Jersey continental shelf wedge.

6.4.5 Sediment starvation

Unit F represents the uppermost resolvable seismic unit. The base of the unit is a highly erosional surface S6, which can be correlated with the early Pliocene seismic reflector "Jimmy" (Martin, 1984; Goodlad, 1986). Green (2011b) suggests that, along the northern KwaZulu-Natal continental shelf, an extended hiatus correlated with this reflector spans the late Palaeocene to early Pliocene, having occurred through a combination of sediment starvation, non-deposition, and sediment bypass. Channel incision has occurred both on the continental shelf through erosion and sediment bypass during forced regression, as well as on the upper slope where canyon formation is identified beneath the present Tugela Canyon. Like the repeating units beneath, unit F comprises an early LST channel fill facies F1 with high impedance reflections which onlap against the channel/canyon flanks (Fig. 6.10). Green et al. (2008) dated the wedge, which is continuous along-strike, at the late Pliocene. These deposits thus coincide with local sea-level rise following rapid sea-level fall in the early Pliocene (Dingle et al., 1983). The progradational nature of the overlying facies F2 suggests normal regressive deposition during early sea level rise as part of a lowstand shelf-edge delta (e.g. Fig. 6.13f). Green (2011b) showed that this final phase of shelf-edge wedge aggradation formed the contemporary shelf break of the Zululand Basin. A similar situation can be defined for the Durban Basin with subsequent sediment starvation (e.g. Green, 2011b) having left this feature preserved as a moribund shelf break.

6.4.6 Shelf evolution– a combination of structural and sedimentary shelf dominance

The Durban Basin and its associated sediments have a complex depositional history with sedimentation interrupted by protracted periods of erosion or non-deposition. In all cases however, sedimentation can be related to both local and global sea-level fluctuations (Haq et al., 1987; 1988; Siesser and Dingle, 1981; Dingle

et al., 1983) with sedimentation following closely (albeit not completely) with currently accepted sequence stratigraphic principles (Posamentier and Allen, 1999; Catuneanu, 2006; Catuneanu et al., 2011). Unlike the continental margin to the north and south, the area investigated in this study is represented by major sediment input from the Tugela and Umgeni Rivers with bypass of the shelf and proximal ramp areas and deposition initially dominant on the upper slope as the construction of the shelf ensued.

The formation of the shelf is however unlike that described for other passive margin settings (Carvajal et al., 2009; Catuneanu et al., 2011; Santra et al., 2013), as early sedimentation was controlled by fluvial deposition in a narrow, sheared, structurally bounded basin (Figs 6.13a; 6.14a) similar to sedimentation styles in rifted margins (Martins-Neto and Catuneanu, 2010). The result is a combined structural–sedimentary shelf (Fig. 6.12a) similar to that defined by Helland-Hansen et al. (2012).

Sedimentation styles within the basin changed dramatically during the mid-Cretaceous, with deep water deposition of basin floor fans in the Turonian (Fig. 6.14b) followed by the formation of a shallow, planar ramp during lowstand conditions (Fig. 6.14c). Although ramp margins are commonly related to carbonate geology (Helland-Hansen et al., 2012), the Durban Basin represents a siliciclastic ramp margin similar to those discussed by Varban and Plint (2008).

Tectonism and active spreading had ceased by the Cenomanian (Ben-Avraham et al., 1993; Watkeys, 2006), however the formation of the proto-shelf on the Turonian ramp was still nucleated close to the original structural shelf break (Fig. 6.14c) similar to that seen in active structural shelves (Helland-Hansen et al., 2012). Increased sediment supply and base-level fall during the Campanian saw the initial formation of a shelf break (Facies C2) in the basin defined by a narrow, forced regressive shelf-edge wedge (Fig. 6.14d) marking a change from ramp-dominated to shelf-edge sedimentation. The change in depositional style from structural-sedimentary shelf to progradational sedimentary shelf (Helland-Hansen et al., 2012) coincides with McMillan's (2003) suggestion that basin began acting as a single depo-centre during this period. Continuous deposition through lowstand, transgressive (Fig. 6.14e) and highstand (Fig. 6.14f) conditions dominated the Maastrichtian to Eocene, with the Eocene highstand wedge prograding from the incipient shelf break, initially defined by facies C2. This highstand shelf-edge wedge later controlled the positioning of the future shelf breaks by providing an anchor point from which successive episodes of protracted lowstand sediment delivery could build succeeding aggrading and prograding shelf-edge wedges (Unit D-F). This transformed the shelf edge into the sharp feature that currently marks the contemporary shelf break (Fig. 6.14g-h). The progradational units D and E are similar in architecture to moderately deep water margins defined by Carvajal et al. (2009) and progradational to aggradational shelf margins defined by Gong et al. (2015) in the South China Sea. Clinoform architecture and the absence of large sediment aprons at the base of the slope suggests modest sediment input regimes during this period when compared with similar margins defined by Carvajal et al. (2009).

Subsequent to the final stages of sediment influx during the late Miocene, the basin has experienced renewed sediment starvation, with a thin veneer of Pleistocene to Holocene sediment preserved on the shelf and shelf edge (McMillan, 2003; Green, 2011b), suggesting that the major phases of hinterland uplift and attendant sediment supply drove the construction of main basin almost in its entirety. Unlike other authors suggestions (e.g. Martin, 1984, Martin and Flemming, 1986), the overall narrowness of the adjoining shelf in the basin is not a product of the initial rifting of the margin, but rather a fortuitous alternation between an overabundance of uplift-driven sediment delivery and normal regression, followed by generally quiescent conditions until today.

Although combined structural-sedimentary shelves generally form in young seascapes related to active extensional regimes (Helland-Hansen et al., 2012), the Durban Basin represents a unique case where structurally controlled deposition and later sedimentary shelf progradation is related to base level fluctuations and sediment supply regimes rather than tectonically induced accommodation space creation.

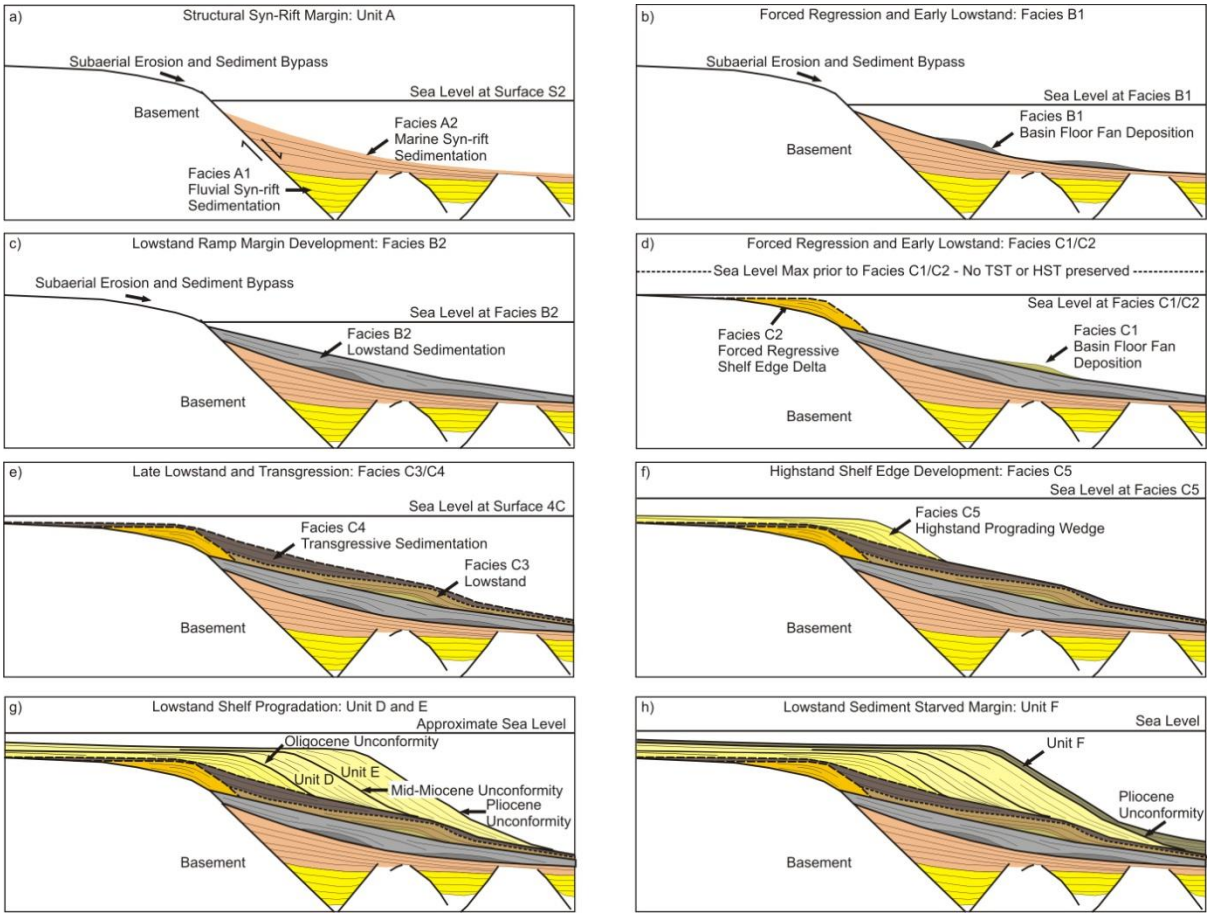

Figure 6.14: Schematic model of the evolution of the Durban Basin defining syn-rift structural-sedimentary deposition followed by ramp margin development and finally sedimentary shelf progradation (modified after Helland-Hansen et al., 2012).

CHAPTER 7

SEDIMENT SUPPLY AND UNCONFORMITY SURFACE EVOLUTION

7.1 INTRODUCTION

Continental shelves in passive margin settings commonly comprise thick sedimentary successions, allowing for documentation of variations in sediment supply regimes, eustatic sea level, ocean dynamics and climatic conditions (Mountain et al., 2007; Nittrouer et al., 2007; Zecchin et al., 2015). The recognition of palaeo-geomorphic features including progradational clinoform architecture (Liu et al., 2011), submarine canyon incision (Fulthorpe et al., 2000; Jobe et al., 2011; de Almeida et al., 2015), and basin-scale erosional surfaces (sequence boundaries) (Fulthorpe et al., 2000; Zecchin et al., 2015) have been utilised to define relative sea-level changes (Vail et al., 1977; Haq et al., 1987; 1988) or variations in oceanic and global climatic conditions (Zachos et al., 1997; 2001).

The Durban Basin, developed along the eastern continental margin of South Africa, has been subject to protracted hiatus events since the late Jurassic. Previous studies of the inner continental shelf (Dingle et al., 1983; Green 2011a; 2011b; Green and Garlick, 2011; Green et al., 2013) suggest that erosional/non-depositional regimes were dominant between the Maastrichtian and latest Pliocene. Work within this study (Chapter 6) has however, identified prolonged Cenozoic depositional periods beneath the outer continental shelf and slope, separated by regional unconformities (sequence boundaries) related to eustatic sea level fall. The most prominent is a previously undefined mid-Miocene erosional unconformity preserved beneath the outer shelf and slope offshore Durban. This chapter represents the first detailed examination of these erosional events within the Durban Basin. Specific focus is given to the mid-Miocene erosional event, with correlation between analogous mid-Miocene sequence boundaries around the southern African continental shelf, as well as in the global context.

The southeast African continental margin currently represents a major frontier basin region for hydrocarbon exploration, with the Durban Basin located south of the gas-rich Mozambique Basin and coastal plain (Singh and McLachlan, 2003). Although the Durban Basin margin is under-explored, recent 3D seismic acquisition within the deepwater Natal Valley (Pisaniec et al., 2017) suggests the potential for additional work in this region. The hydrocarbon potential of the east African margin is further highlighted by the super-giant (80 TCF) discoveries made offshore northern Mozambique within the Mamba Field, a Lower Eocene fan complex affected by strong, deep water bottom currents that influenced gravity-flow deposition (Palermo et al., 2014). This chapter focuses on the identification and interpretation of previously unrecognised unconformities that span these basins, an outcome that may prove valuable to the future hydrocarbon exploration in the region.

7.2 RESULTS

7.2.1 Seismic Reflection Geometry

As discussed in Chapter 6, syn-rift and early drift phase sedimentary infill (Units A-B; Table 7.1) define a low-angle marine ramp margin in the Durban Basin. Unit A occurs as a discontinuous graben fill succession unconformably overlying acoustic basement. As the unit is confined to isolated depocentres, thickness is highly variable with sedimentation terminating updip against faulted pre-breakup basement structures. Seismic geometry of unit A is defined by a predominantly aggradational succession separated by an internal seismic surface S1a which is identified through gamma ray log signatures (Fig. 6.2) as well as variations in seismic amplitude. This surface exhibits U-shaped incisions (Fig. 6.5) ranging from 800 to 1100 m wide and 20 to 30 m (0.30 to 0.4 s TWTT) deep. These incisions however are not resolvable over large regions as they are limited to single seismic line intersections and therefore the extent and orientation is currently unknown.

Erosional seismic reflector S2 separates unit A from unit B (Table 7.1), but truncates proximally against faulted basement, with unit B unconformably overlying seismic basement in the updip profile (Fig. 6.3a-b). This erosional seismic reflector however, does not exhibit large incisions into the underlying unit A, rather forming a shallow ramp structure as discussed in Chapter 6. Although unit B is separated into two facies (Table 7.1), the distal facies B1 and proximal facies B2, only facies B2 is laterally extensive in the proximal shelf and slope regions. Seismic reflector architecture of facies B2 is predominantly aggradational, but exhibits a slight onlap on surface S2 (Fig. 6.3a).

Unit C occurs as a prograding package with an offlapping reflector configuration, separated from the underlying unit by an erosional, moderate amplitude reflector S3. Under the Tugela Cone (Fig. 6.8) five facies (C1-5) are resolved (Table 7.1) and discussed in detail in Chapter 6. Internal reflector architecture is dominantly progradational to aggradational for facies C1-3, with facies C4 exhibiting aggradational to weakly retrogradational reflectors that distinctly onlap the underlying facies (Fig. 6.8). The proximal facies C5 occurs as a prograding wedge which oversteps facies C4 seaward along a downlap surface“3C” (Fig. 6.8).

Unit C into which erosional surface S4 incises (Fig. 7.1), forms the incipient shelf, shelf edge and slope within the basin (Fig. 7.2). The palaeo-shelf edge at S4 time is defined by the offlap break of the most-seaward reflector of unit C (Fig. 7.2). Although largely removed by later erosional episodes, where preserved, the palaeo-shelf break forms a linear feature orientated northeast-southwest approximately 20 km offshore of the contemporary coastline (Fig. 7.3).

Unit D immediately overlying erosional surface S4, is defined by a north-eastward thickening sediment wedge, most prominent between Jc-B1 and Jc-D1 (Fig. 7.1). The inflection point of the most-seaward clinoforms of unit D occurs at ~0.4s TWT (Fig. 7.2), and outlines the seaward progradation of an approximately 10 km wide and 30 km long mixed carbonate/siliciclastic wedge between boreholes Jc-B1 and Jc-D1 (Figs 7.1; 7.2). The intercalated succession of carbonate and siliciclastic sediments (Figs 7.1; 7.2) can be subdivided into three seismic facies D1-3. Facies D1 occurs as a discontinuous infilling basal facies confined to incisions along the S4 surface (Figs 7.1; 7.2).

Facies D2 and D3, which constitute the main components of the sediment wedge, are separated by a local reflector S4a (Figs 7.1; 7.2). Facies D2 attains a maximum thickness of ~600 m and comprises high amplitude, wavy reflectors. These constitute interbedded siltstones and calcarenites in Jc-B1 and a coarsening upward succession of siltstones and interbedded sandstone and limestone in Jc-D1 (Fig. 7.1). Facies D3 attains a maximum thickness of ~350 m in the vicinity of Jc-D1 (Fig. 7.1) but is truncated to the south of Jc-B1 by an overlying erosional surface S5. Diffuse low amplitude reflectors in the southern portion of the wedge are defined by calcarenites in Jc-B1 (Fig. 7.1). Northward, in the vicinity of Jc-D1, facies D3 is defined by medium to high amplitude north-easterly dipping reflectors (Fig. 7.2) that comprise a succession of siltstone with limited carbonates (Fig. 7.1).

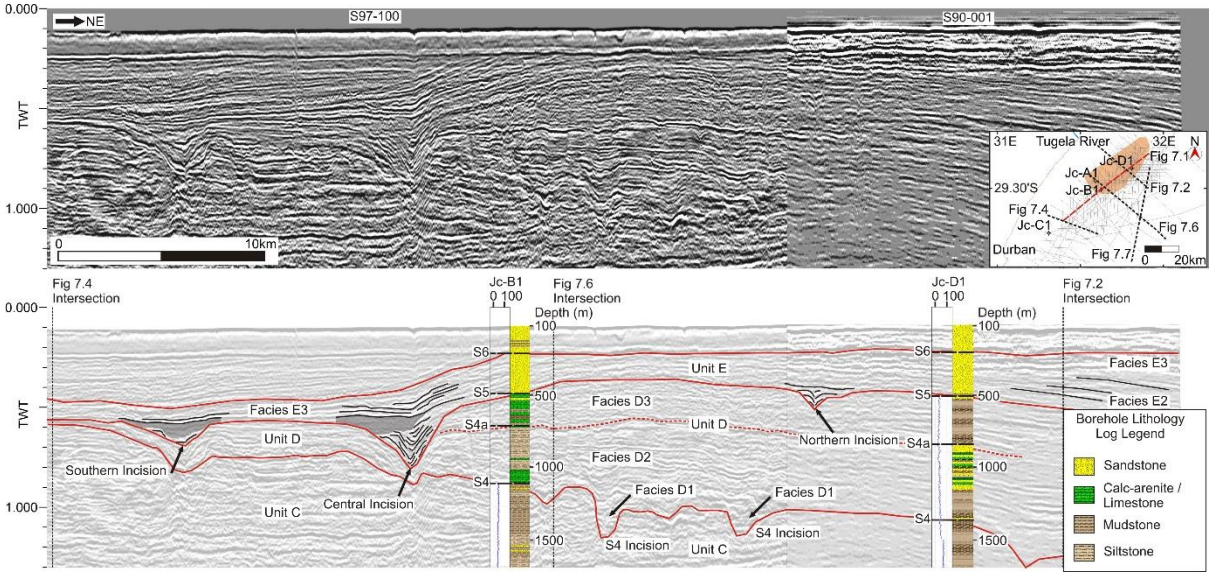

Figure 7.1: Coast-parallel, composite seismic profile of seismic lines S97-100 (South) and S90-001 (North) indicating multiple incisions and associated incision-fill along multiple seismic surfaces (S4, S5, S6). Stratigraphic control is given by borehole intersections with Jc-B1 and Jc-D1. Lithological and gamma ray logs are displayed. The spatial position and extent of unit D's siliciclastic-carbonate wedge is defined by the shaded polygon in the spatial inset box on the un-interpreted figure.

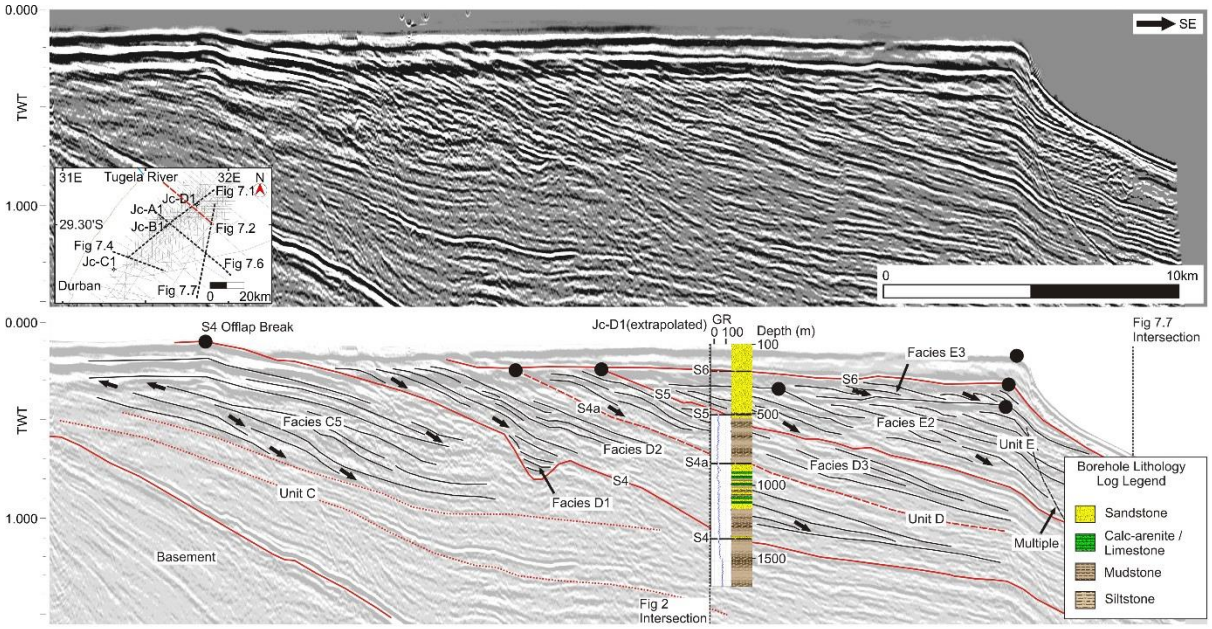

Figure 7.2: Dip-orientated profile of seismic line S76-009 intersecting Unit D's siliciclastic-carbonate wedge. Note the well-defined palaeo-shelf edge of the underlying unit C. Incision within the S4 unconformity surface can be identified. Stratigraphic control is given by extrapolated borehole intersection with Jc-D1. Note the progradational nature of the clinoforms within units D-E.

Table 7.1: Simplified sequence stratigraphic framework for the study area. Seismic units, facies, bounding surfaces, interpreted depositional environments, sediment accumulation rates and units ages are described. Ages are based on previous work (McMillan and Dale, 2000; McMillan, 2003; Green et al., 2008).

Unit	Facies	Surface	Interpreted depositional environment	Thickness (two-way time)	Average Shelf Sediment Thickness (m)	Sedimentology	Systems Tract	Age	Time Period (myr)	Sediment Accumulation Rate (m/myr)	Areal Extent of Sedimentation (km^2)	Sediment Flux ($x10^3 km^3/myr$)
F	F4		na	0.2s	80	Glauconitic sandstones subordinate claystone	na	Holocene?	5.3	15.1	2000	5.7
	F3		na	0 to 0.2s			na	Pleistocene to Pliocene?				
	F2		Lowstand shelf edge delta	0 to 0.2s			LST	Pliocene				
	F1		Incised valley fill	0 to 0.2s			LST	Pliocene				
		S6	Shelf-confined erosional reflector					Mid Pliocene				
E	E3		Inner to mid shelf	0 to 0.2s	200	Glauconitic sandstones subordinate claystone	TST	L-Pliocene? / U-Miocene?	8.5	23.5	2000	5.5
	E2		Lowstand shelf edge delta	0 to 0.3s			LST	Upper Miocene				
	E1		Incised valley fill	0 to 0.2s		Sandstone, subordinate claystone	LST	Upper Miocene				
		S5	Shelf and slope-confined, regionally developed erosional reflector					Serravallian				
D	D3		Lowstand shelf edge delta	0.5	200	Carbonate-rich calcarenite and limestone	LST	Lower Miocene?	10.1	19.8	2000	3.9
		S4a	Confined northern shelf reflector within unit D					Aquitanian				
	D2		Lowstand shelf edge delta	0.5	350	Carbonate-rich calcarenite and limestone	LST	Miocene? to U-Oligocene	10	35.0	2000	7.0
	D1		Incised valley fill	0 to 0.2s		Sandstone, calcarenite and limestone	LST	Mid Oligocene				
		S4	Basin-wide erosional reflector					Mid Oligocene				
C	C5		Highstand wedge	0 to 0.3s	250	Interbedded sandstone and siltstone	HST	Upper Eocene	22.1	11.3	3000	1.5
		3C	Maximum flooding surface					Upper Eocene				

	C4		Healing phase wedge	0.1 to 0.3s	250	Deep marine claystone	TST	Palaeocene				
		3B	Maximum regressive surface					Danian				
	C3		Delta margin	0 to 0.5s	350	Siltstone, claystone and subordinate sandstone	LST	Maastrichtian to Campanian	17.6	19.9	3000	3.4
	C2		Falling stage wedge	0 to 0.5s	200	Siltstone, claystone and subordinate coarse- to fined-grained sandstone	FSST	Campanian?	10	20.0	2000	4.0
	C1		Falling stage slope fan apron	0 to 0.3s	200	Unknown but likely sandstone and claystone	FSST	Campanian ?				
		S3	Shelf-confined erosional reflector					Santonian?				
B	B2		Lowstand ramp	0 to 0.5s	200	Siltstone, claystone and subordinate coarse- to fined-grained sandstone	LST	Conacian? Turonian	7.6	26.3	2000	6.9
	B1		Falling stage basin floor fan	0 to 0.3s		Unknown but likely sandstone and claystone	FSST	Turonian				
		S2	Basin-wide Erosional Reflector					Turonian				
A	A2		Syn-rift valley fill	0 to 1s	200	Interbedded claystone, siltstone and sandstone.	Syn-rift TST/HST	Cenomanian to Albian	19.1	10.5	3000	1.6
		S1a	Graben-confined Erosional Reflector					Late Aptian?				
	A1		Syn-rift valley fill	0 to 1s	100	Interbedded claystone, siltstone and sandstone. Conglomeritic facies in Jc-D1	Syn-rift TST/HST	Aptian to Barremian	16.4	6.1	3000	1.1
		S1	Basin-wide Erosional Reflector					Jurassic				
BASEMENT			Acoustic Basement					Jurassic				

In contrast to the central and northern parts of the basin, facies D2 and D3 are not resolved in the southern basin (Fig. 7.1). Instead, an amalgamated succession of "unit D" is preserved. In this region aggradation, as opposed to progradation, is dominant on the shelf and slope (Fig. 7.4). The distal southern basin is dominated by the development of a ~20 km wide continental rise which is not identified in the northern basin (Fig. 7.5).

The upper reflectors of unit D are incised by a number of dip-orientated lows associated with a high amplitude reflector corresponding to an erosional surface S5. From time-depth reconstructions this surface is resolved across an area of 5000 km^2 (Fig. 7.5). The surface is however confined to the mid- and outer shelf, truncated updip by a younger erosional surface S6. The S5 surface has an undulatory geometry forming three V and U-shaped incisions (southern, central and northern) best observed in the coast-parallel sections (Fig. 7.1). In proximal areas, these incisions have a relief of 150-300 m, with a maximum width of 2.8 km (Fig. 7.1), but broaden and increase in relief downslope up to 500-600 m deep and ~7 km wide (Figs 7.5; 7.6; 7.7). The geometry of the southern and central incisions exhibit multiple erosional episodes within these regions, affecting the S4, S5 and S6 surfaces (Figs 7.1; 7.7). Multiple incision episodes are defined by vertically stacked U- and V-shaped incisions as shown in Figures 7.6 and 7.7, with little to no lateral migration evident. The northern incision however, has no stacked pattern (Figs 7.1; 7.7) representing only a single incision episode.

The variable nature of these incisions is evident from the time-depth reconstruction of surface S5 (Fig. 7.5). The U-shaped southern incision, confined to the upper and middle slope, is a sinuous feature with a total length of ~25 km. It incises into an area characterised by a subdued slope gradient profile (Fig. 7.4), terminating on the continental rise in the southern part of the basin (Figs 7.5; 7.7). The V-shaped, linear, central incision is the most prominent, with a total length of ~45 km, incising along the southern margin of the unit D wedge (Fig. 7.5). This incision underlies the contemporary Tugela Canyon in the distal basin (Figs 7.6; 7.7). The V-shaped northern incision is particularly linear, attaining a total length of ~30 km and incising the steep slope associated with the underlying unit D sediment wedge (Fig. 7.5). Only the central and northern incisions indent the palaeo-shelf edge (Fig. 7.5), defined by the inflection point of the most-seaward clinoforms of unit D.

Unit E, comprising predominantly fine-grained, glauconitic sandstone and minor siltstone overlies reflector S5 throughout the study area. Three seismic facies (E1-3) are resolved. Facies E1 consists of incision infill, with an internal reflector architecture that varies from south to north. The southern incision infill is defined by basal, diffuse, wavy reflectors, overlain by laterally continuous, high amplitude, draped reflectors (Fig. 7.1). The central incision's fill comprises basal, high amplitude, onlapping, wavy reflectors, overlain by diffuse wavy reflectors (Fig. 7.1). This is capped by a series of draped, laterally continuous, high amplitude reflectors (Fig. 7.1). The northern incision has only flank-attached, onlapping, high amplitude reflectors (Fig. 7.1).

In the northern portion of the basin, northward of Jc-B1, seaward dipping, aggradational to progradational reflectors of high impedance, and low amplitude (Facies E2) overlie S5 adjacent to, and updip of, the central and northern incisions (Figs 7.2; 7.6). This facies is laterally continuous along strike to the north, with a basinward-prograding clinoform architecture that defines successive migration of the dip inflection point and the clinoform toe of the clinoform front (Figs 7.2; 7.6).

In the southern portion of the basin however, unit E, as with the underlying unit D, is poorly developed, with sediment fill defined by aggradational reflectors of facies E3 (Fig. 7.4). In all areas, unit E reflectors are erosionally truncated by regional reflector S6, which marks the third phase of erosion within the study area (Figs 7.1; 7.4; 7.6; 7.7).

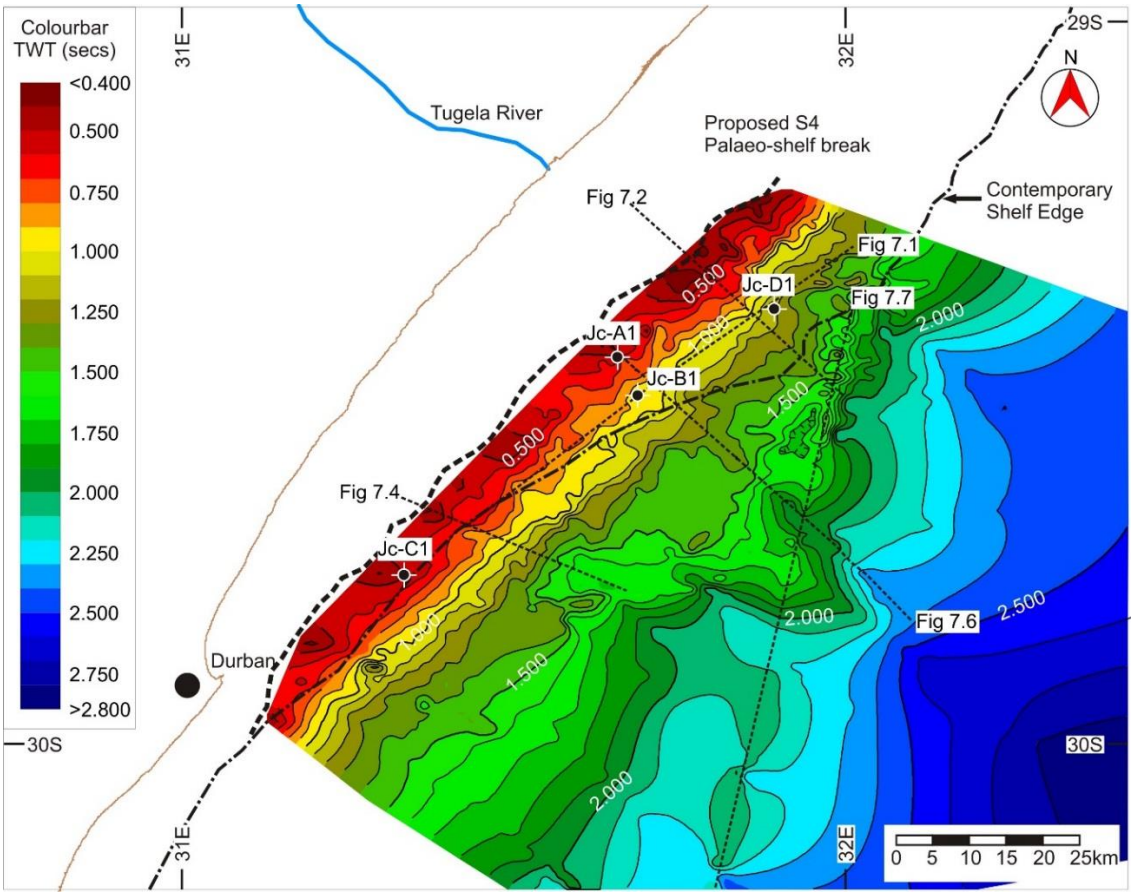

Figure 7.3: Two-way time contour map of the S4 (Mid-Oligocene) erosional surface. Note the proposed linear shelf break (thick dashed line) as shown in Fig. 7.2.

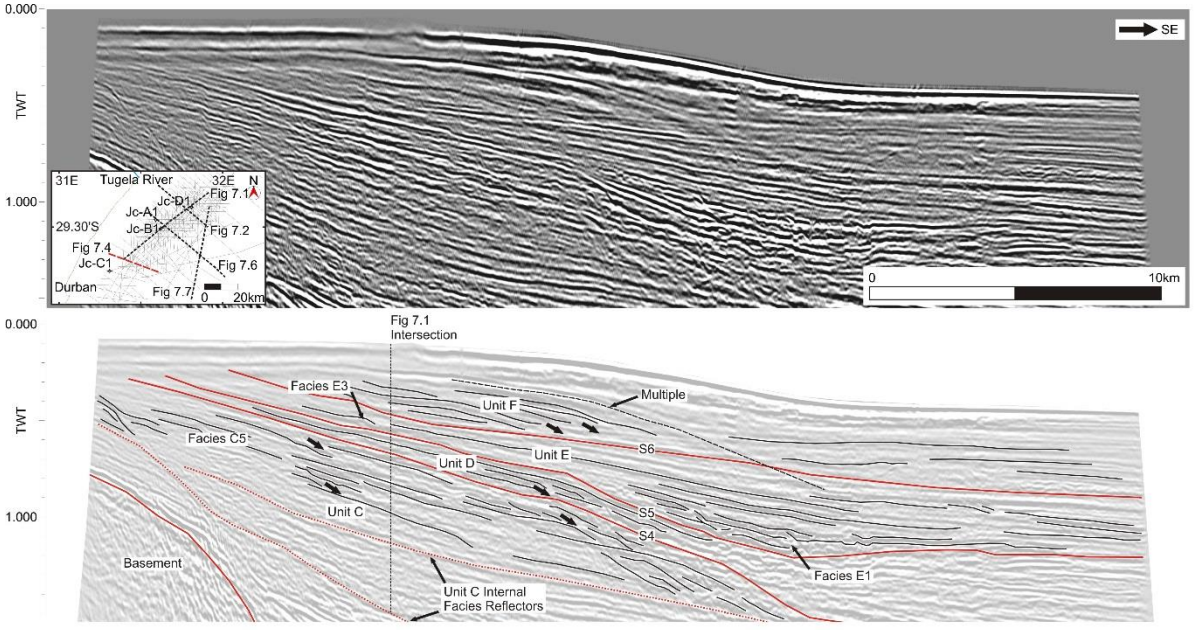

Figure 7.4: Dip-orientated profile of seismic line S78-009 intersecting the southern region of the Durban Basin. Note the limited thickness of units D and E, suggesting sediment starvation in this portion of the basin. Note the lack of a well-defined palaeo-shelf edge, suggesting a ramp, as opposed to shelf-break, type margin.

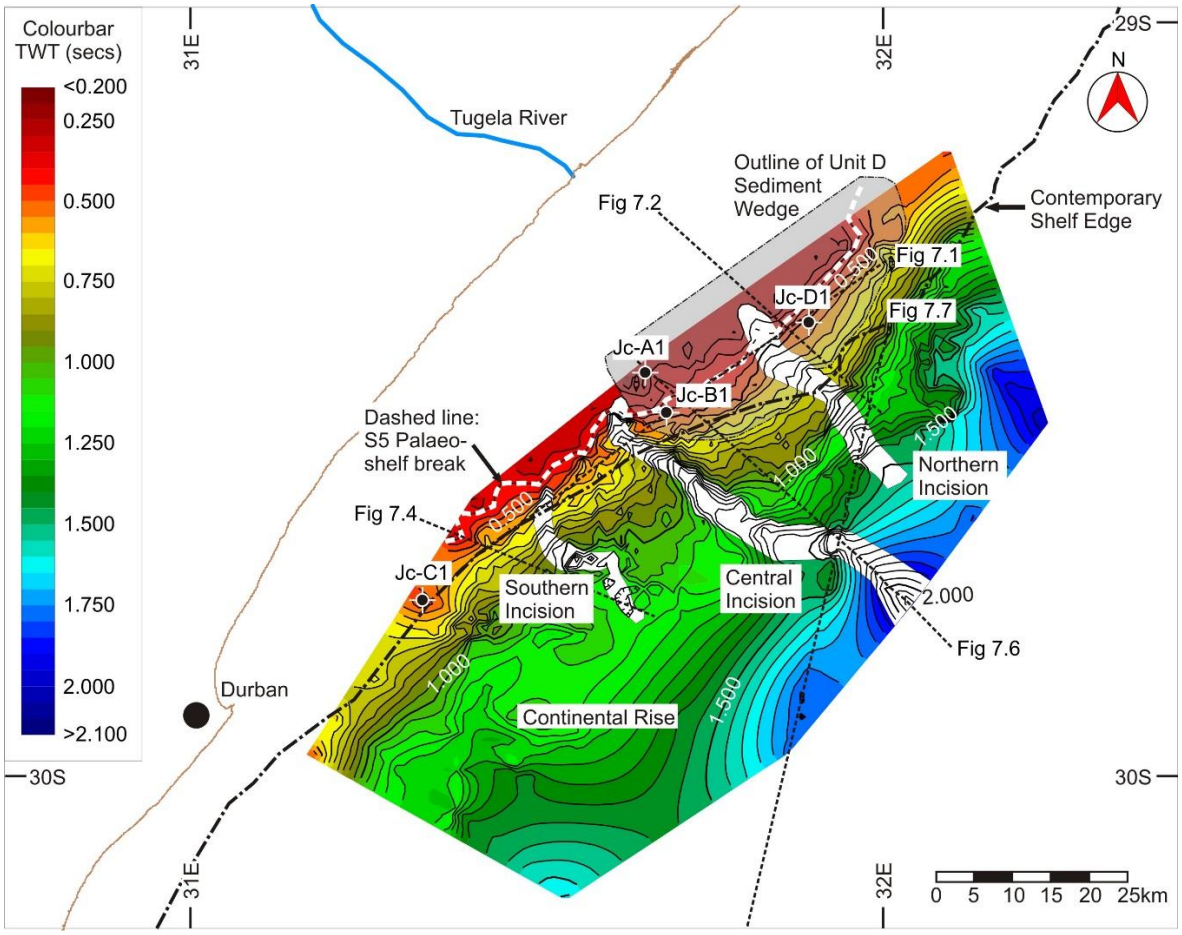

Figure 7.5: Two-way time contour map of the S5 (mid-Miocene) erosional surface. Note the prograded shelf edge north of Jc-B1, related to the deposition of unit D. White polygons denote position and orientation of canyon systems incised into surface S5. Note the sinuous nature of the slope-confined southern canyon, compared with the linear palaeo-shelf indenting central and northern canyons, and the relatively shallow slope gradient between 1.0 and 1.5s TWT across the southern basin compared with the steep gradients north of Jc-B1.

7.2.2 Sedimentation Rates

Although well data within the basin are limited, and distances between data are large, all wells intersect the entire succession. Average sediment thicknesses of individual units with average sedimentation rates in m/myr are outlined in Table 7.1.

Due to its limited areal extent, sedimentation rates of unit A are potentially erroneous as the succession thickens downdip of borehole intersections. Sedimentation rates during deposition of unit A between the Barremian and Cenomanian indicate a slight increase in sedimentation rate from 6.1 m/myr for facies A1 to 10.5 m/myr for facies A2.

A marked sedimentation rate increase of 15.8 m/myr is noted across the S2 erosional surface in the basin. Although no sedimentation rate data exist for facies B1 as it has not been intersected, the marked increase in sedimentation is noted in facies B2 with a rate of 26.3 m/myr and a flux of 6.9 $x10^3 km^3$/myr (Table 7.1).

Although a slight decrease in sedimentation rate is noted in Unit C across the S3 erosional surface, rates remain high throughout the late Cretaceous (Table 7.1). Sedimentation rates during this period are exceptionally

consistent showing a rate of 20.0 m/Myr for facies C2 and 19.9 m/myr for facies C3. A lowering of sedimentation rates are suggested for facies C5 prior to the development of the Oligocene S4 erosional surface.

The Oligocene is represented by an increase in sedimentation within the basin from 11.3 m/myr to 35 m/myr across the S4 erosional boundary. Sedimentation rates diminished slightly in the late Oligocene and early Miocene (Table 7.1). Sedimentation rates defined for Jc-B1 and Jc-C1 in Table 7.2 suggest that, during the Oligocene and early Miocene, the southern basin was subject to sediment starvation with a sedimentation rate of 5 m/myr, compared to 38 m/myr and 23.8 m/myr for facies D2 and D3 respectively. Renewed sedimentation throughout the basin is noted across the S5 erosional boundary with the late Miocene defined by elevated rates of 23.5 m/myr (Table 7.1).

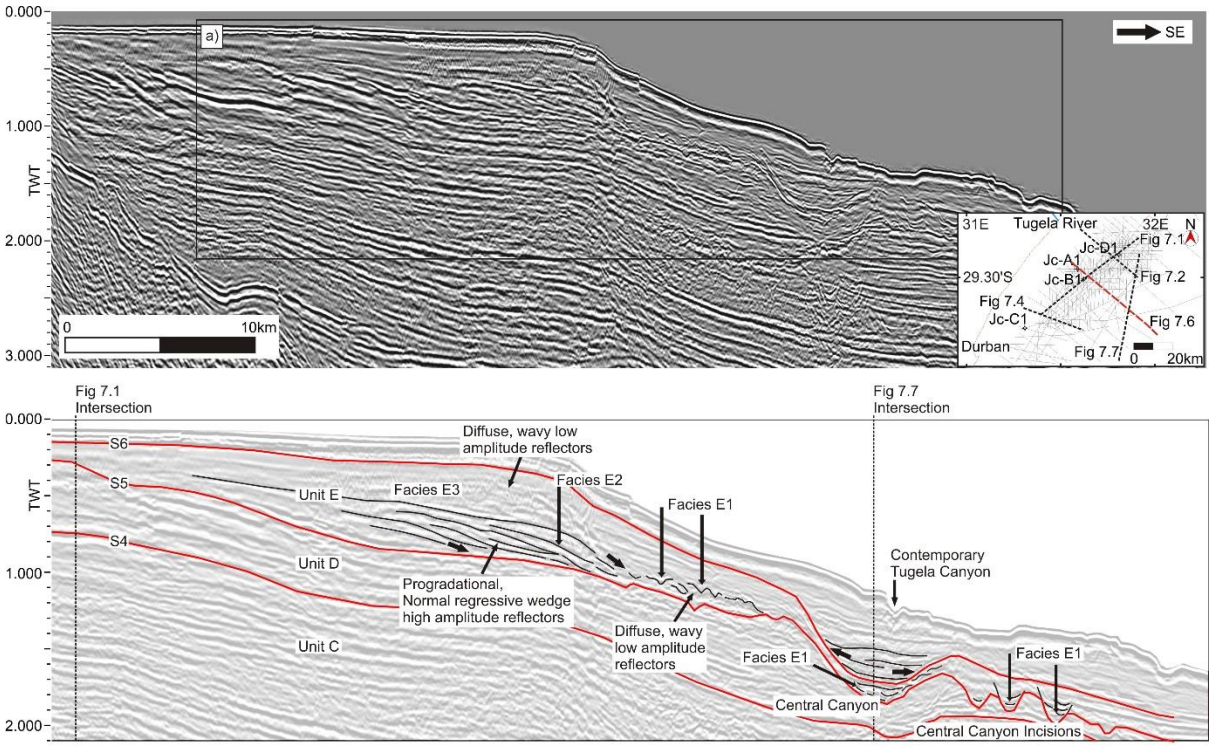

Figure 7.6: Dip-orientated seismic profile S74-007 indicating progradational reflector package facies E2 overlying seismic surface S5. Note the slope confined canyon incisions of the central canyon, and associated canyon fill, downdip of the progradational shelf-edge wedge.

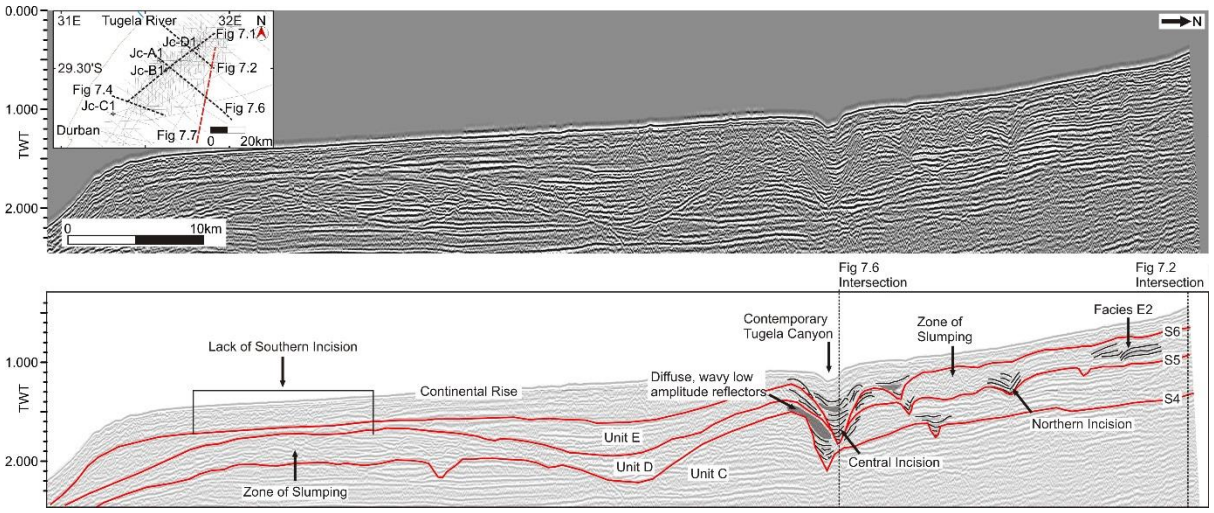

Figure 7.7: Dip-orientated seismic profile SA76-159 indicating multiple canyon incision episodes within the central and northern canyon systems. Note the absence of multiple canyons beneath the southern canyon of the shallower gradient, lower slope area.

7.3 DISCUSSION

7.3.1 Sediment supply regimes

Since the initiation of Gondwana breakup in the mid-Jurassic (Watkeys and Sokoutis, 1998) several hundred thousand cubic kilometres of material have been eroded from the southern African continent (Said et al., 2015). Voluminous denudation in southern Africa lead to the formation of the Great Escarpment (Partridge and Maud, 1987; Partridge, 1997; 1998; Moore, 1999; Partridge and Maud, 2000; Guillocheau et al., 2012) which separates a high altitude (1000-1500 m) interior plateau from deeply incised coastal regions (Figs 4.1; 7.8).

Two fundamentally different hypothesis for the timing of uplift in southern Africa have been proposed. A Mesozoic period of uplift is proposed by Brown et al. (2002), de Wit (2007) and Tinker et al. (2008), whilst a mid- to late Tertiary origin of the modern topography is proposed by Partridge and Maud (1987); Partridge (1997), Moore (1999) and Burke and Gunnell (2008). Flowers and Schone (2010) suggest that these two hypotheses reflect fundamentally different causes of elevation gain with Mesozoic uplift potentially related to deep mantle processes (cf. de Wit, 2007), whilst Cenozoic uplift could be a result of shallow convection and thermal modification of the upper mantle (cf. Burke and Gunnell, 2008).

Flowers and Schone (2010) suggest that the southern African plateau was subject to major unroofing in the Mesozoic, coincident with kimberlite magmatism in the interior of South Africa between 143-145 Ma, and continental rifting within and along the plate margins. Within the Durban Basin however, early Cretaceous sediment supply is limited, with sedimentation confined to individual graben depocentres. This localised deposition is also noted by Walford et al. (2005) and Said et al. (2015) in Mozambique, with McMillan (2003) suggesting that the Durban Basin only came into being as a single major depocentre in the mid-Campanian.

Increased sedimentation within the basin does however occur subsequent to the major S2 sequence boundary which formed during the Cenomanian-Turonian (~90 Ma). This period is coincident with large scale erosion around southern Africa associated with forced regression on the continental shelves (McMillan, 2003). Flowers and Schone (2010) identified apatite thermochronometry dates for southern Africa clustering around ~100 Ma, and therefore suggested that the Cenomanian represents a change from Mesozoic mantle heating to mid- to late Cretaceous cooling in the subcontinent. It is further suggested that plateau elevation gain and subsequent

denudation in the mid- to late Cretaceous was due to mantle buoyancy related to deep mantle processes which drove the breakup of Gondwana (Flowers and Schone, 2010).

Said et al. (2015) propose a major shift in drainage which affected south-eastern Africa during the Late Cretaceous–earliest Palaeocene. This shift, defined by numerous authors (Moore and Larkin, 2001; Haddon and McCarthy, 2005; Goudie, 2005), is suggested to have been accompanied by intracratonic subsidence as well as flexural uplift along the Indian Ocean margin (Said et al., 2015). Said et al. (2015) suggest that during this event, the size of the drainage basin supplying sediment to the east African margin was decreased significantly, reducing sediment supply rates to the northern Natal Valley. This however is not the case in the Durban Basin, whereby high sedimentation rates in unit C suggest off-shelf sediment-forcing during sea level lowstands with sedimentation of facies C2 a product of deltaic deposition from large river systems (Dingle et al., 1983; Goodlad, 1986). Brown et al. (2002) suggest that the KwaZulu-Natal coastal margin underwent rapid post-breakup river incision seaward of a pre-existing drainage divide located east of the present escarpment. This period of polycyclic erosion is defined by Partridge and Maud (1987) as the "African Cycle of Erosion" which resulted in advanced planation of the subcontinent interior and multiple pulses of epeirogenic sedimentation in the newly formed Mesozoic basins. Partridge and Maud (1987) suggest that these sedimentation pulses are exemplified by the late Cretaceous St Lucia Formation in the onshore Zululand Basin, coeval with lowstand systems tract deposition of facies C2 and C3 in the Durban Basin.

During the Cenozoic, south-eastern Africa was subject to multiple phases of epeirogenic uplift (Partridge and Maud, 1987; Partridge 1998; Moore, 1999; Walford et al., 2005), leading to the development of the African planation surface, fluvial incision and increased sediment supply to the offshore areas (McCormick et al., 1992; Burke and Gunnell, 2008). Although the most prominent period of uplift is defined for the Oligocene, Walford et al. (2005) propose two periods of Neogene uplift, the smaller of which is thought to have begun in Early Miocene times, whilst a second greater magnitude event occurred in the Pliocene.

Within South Africa, Partridge and Maud (1987) propose that moderate uplift and westward tilting of the sub-continent during the early Miocene was accompanied by minor coastal monoclinal warping with maximum uplift occurring along the Ciskei-Swaziland Axis in KwaZulu-Natal (Fig. 7.8). This episode accounts for the development of the Post-African I erosion surface, with renewed sedimentation to the coastal zone via short, fast flowing minor river systems allowing for the deposition of the Uloa Formation (Partridge and Maud, 1987). Only the palaeo-Tugela River (Fig. 4.1) represented a major point of sediment flux. However, as defined by the geometry of the seismic reflectors associated with units D and E, sediment supply appears to have been imbalanced, with abundant supply to the north (Figs 7.1; 7.2) and sediment starvation of the shelf in the southern portions of the basin (Figs 7.1; 7.4).

Partridge and Maud (1987) and Burke and Gunnell (2008) suggest that Miocene uplift during the post African Surface I cycle caused erosional rejuvenation with active deltaic and deep marine fan sedimentation along the east African margin through the lower to mid-Miocene. Seismic reflection analysis from the current study, suggests that mid-Miocene sedimentation occurred predominantly on the slope, with zones of sediment bypass and erosion dominant within the shelfal region of the basin (Fig. 7.2). Although Burke and Gunnell (2008) suggest that deep water slope fans would have been deposited during this lowstand event, Goodlad (1986) and Wiles et al. (2013) propose that flow initiation, winnowing and reworking by North Atlantic Deep Water (NADW) since the early Miocene may have led to removal of such features in the deep basin (Figs 7.6; 7.8). These sedimentation patterns appear similar to systems defined by Palermo et al. (2014) for the Eocene deep water fan system of the Coral Sequence in Mozambique.

Table 7.2: Sediment accumulation rates within the Jc-B1 and Jc-C1 wells offshore Durban.

Unit	Facies	Surface	Time Period (myr)	Jc-B1 Average Sediment Thickness (m)	Jc-B1 - Sediment Accumulation Rate (m/myr)	Jc-C1 Average Sediment Thickness (m)	Jc-C1 - Sediment Accumulation Rate (m/myr)
F	F4		5.3	50	9.4	60	11.3
	F3						
	F2						
	F1						
		S6					
E	E3		8.5	230	27.1	180	21.2
	E2						
	E1						
		S5					
D	D3		10.1	240	23.8	50	5.0
		S4a					
	D2		10	380	38.0	50	5.0
	D1						
		S4					
C	C5		22.1	1000	45.2	700	31.7
		3C					
	C4		10	210	21.0	250	25.0
		3B					
	C3		17.6		0.0		0.0
	C2		10	300	30.0	450	45.0
	C1		10		0.0		0.0
		S3					
B	B2		7.6	50	6.6	550	72.4
	B1						
		S2					
A	A2		19.1	400	20.9	150	7.9
	A1		16.4	450	27.4	200	12.2
		S1					
BASEMENT							

7.3.2 Sedimentation Rates

Detailed analyses of sedimentation rates for various regions of the southeast African continental margin have been undertaken (Martin, 1987; McCormick et al., 1992; Walford et al., 2005; Said et al., 2015; Uenzelmann-Neben and Clift, 2015). Although many studies deal primarily with recent sedimentation, Walford et al. (2005) and Said et al. (2015) depict sedimentation in Mozambique from the early Cretaceous (Fig. 7.8). Results from these studies are largely similar to results obtained here, with peak sedimentation rates (Fig. 7.8; Tables 7.1; 7.2) coinciding with periods of epeirogenic uplift in southeast Africa (Partridge and Maud, 1987).

Sedimentation flux rates identified for the early Cretaceous depocentres within the Durban Basin (Table 7.1) indicate limited sedimentation of ~6–10 m/myr (Table 7.1). These are similar to results obtained by Walford et al. (2005) and Said et al. (2015) in Mozambique suggesting limited sedimentation along the east African shelf during this period. The variability in early Cretaceous sedimentation rates dependent on depocentre focus and depth can be noted in Table 7.2 where marked differences are identified for facies A2 in Jc-B1 (20.9 m/myr) and Jc-C1 (7.9 m/myr).

De Wit (2007) and Tinker et al. (2008) identified pronounced increases in denudation and denudation rates in the interior of southern Africa in the mid Cretaceous (~100 to ~80 Ma), with coincident increases in sediment accumulation rates at ~95 to ~70 Ma in the Outeniqua Basin on the south coast. This event coincides with the Cenomanian-Turonian unconformity identified around southern African (McMillan, 2003) with similar increases in sediment supply noted in the Turonian-age facies B2 in the Durban Basin (Table 7.1). It must be noted that as this period coincided with rapid sea-level fall and shelf bypass, sedimentation was restricted primarily to the shelf and slope, as indicated in Jc-B1 and Jc-C1 sedimentation rates for this period (Table 7.2).

Sediment flux within the Durban Basin shows a marked increase from 1.6 to 6.9 $x10^3 km^3$/myr across the S2 sequence boundary. Similar increases in sedimentation in the Mozambique Basin and northern Natal Valley are documented by Walford et al (2005) and Said et al. (2015) respectively (Fig. 7.8). Walford et al. (2005) suggest a period of increased sediment flux (4 $x10^3 km^3$/myr) in late Cretaceous (90-65 Ma) times, which they propose was synchronous with rapid denudation in the Zambezi River catchment of central southern Africa. Said et al. (2015) show similar sediment flux within the northern Natal Valley, whereby sediment input increases dramatically at ~110 Ma (Fig. 7.8). Said et al. (2015) propose that the northern Natal Valley underwent an extended period of high sediment flux (~5 $x10^3 km^3$/myr) throughout the late Cretaceous suggesting that increased uplift and denudation was associated with mid- to late Cretaceous kimberlite volcanism across the southern African hinterland. In accordance with Partridge and Maud (1987), it is proposed that, by the mid-Cretaceous southern Africa attained high absolute elevations which led to the initiation of the Great Escarpment during initial denudation during the African cycle of Erosion in the mid- to late Cretaceous. These high interior elevations led to increased denudation especially along the KwaZulu-Natal coast (cf. Brown et al., 2002) with increased offshore sediment flux limited to the slope and basin floor.

A marked decrease in early Cenozoic sedimentation rate is identified in both Jc-B1 and Jc-C1 (Table 7.2). This reduction in sedimentation is likely related to limited sedimentation due to associated marine transgression and highstand during this period. This is identified in facies C4 representative of a transgressive systems tract healing phase wedge comprising deep marine claystone. Although not pronounced in overall sediment flux rates (Fig. 7.8), a marked increase in sedimentation is noted across the 3C surface (Table 7.2), with sedimentation of facies C5 correlated with progradation of the proto-Tugela Cone during sea level highstand in the Eocene (cf. Haq et al., 1987). Similarly in Mozambique, Walford et al. (2005) and Said et al. (2015), indicated reduced sediment flux during this period compared with the mid- to late Cretaceous (Fig. 7.8).

Similar to the rates defined by Said et al. (2015) for the southern Mozambique coastal plain, sedimentation within the Durban Basin reflects a ~20 m/Myr increase across the S4 erosional reflector (Fig. 7.8). Sedimentation rates, although high, declined marginally through the late Oligocene and early Miocene. An increase of ~4 m/myr occurred across the mid-Miocene S5 erosional surface (Table 7.1), suggests increased

denudation within the southeast African hinterland during this period (cf. Partridge and Maud, 1987; Burke and Gunnell, 2008). It is therefore proposed that, within the Durban Basin, increased sedimentation rates within the Neogene occur following erosional episodes in the early-Oligocene, and mid-Miocene.

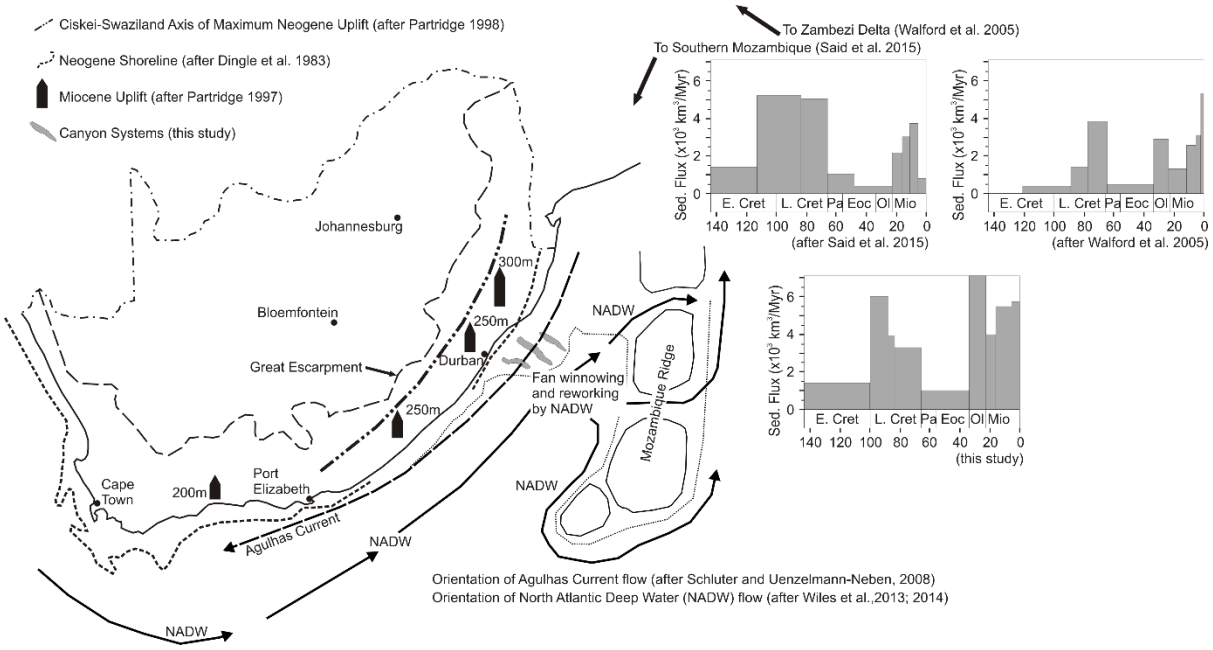

Figure 7.8: Schematic map depicting changes in sedimentation rates, submarine canyon systems, tectonic events, and oceanographic activities that occurred during the mid-Miocene. Amplitudes of epeirogenic uplift along the southeast African margin after Partridge (1997). Axis of maximum Neogene uplift after Partridge (1998). Regional oceanographic currents are adapted from Schlüter and Uenzelmann-Neben (2008) and Wiles et al. (2013, 2014). Sedimentation rates for southern Mozambique and the Zambezi Delta after Said et al. (2015) and Walford et al. (2005) respectively.

7.3.3 Incipient Shelf Development

Neogene sedimentation within the Durban Basin is dominated by the basinward advance of the Tugela Cone delta during normal-regressive sea level lowstands (Chapter 6). The moderate amplitude, aggradational to progradational offlapping seismic reflectors of facies C5 (Unit C) in the northern basin (Fig. 7.2), represent initial progradation of the Tugela Cone delta (sensu Santra et al., 2013). An initial Eocene pulse of lowstand sedimentation (McMillan and Dale, 2000) led to the formation of the incipient shelf edge, from which the contemporary shelf has prograded. This sedimentation pattern is analogous to the lower-Eocene Coral Sequence of the Mamba gas field, Mozambique, which is interpreted as a lowstand deepwater fan deposit overlying a channelized basal erosive unconformity (Palermo et al., 2014).

Deposition of unit D, subsequent to the early Oligocene (McMillan and Dale, 2000) S4 hiatus event, is correlated with a late Oligocene to early Miocene, asymmetrical, mixed siliciclastic-carbonate sediment wedge. Intercalated carbonate (low terrigenous sediment input) and siliciclastic (high terrigenous sediment input) sediments (Figs 7.1; 7.2; 7.5) were possibly fed by occasional discharge from the palaeo-Tugela River (siliciclastic input). The southern basin however, is defined by a shallow ramp margin and wide continental rise, the succession of which is carbonate-dominated (e.g. Jc-C1 borehole), with a ~100 m thick succession of coquina observed (Muntingh, 1983; Chapter 6 this study). It is proposed that this variability in sedimentation is related to oceanic current circulation controlled sedimentation patterns within the Durban Basin as defined by Green (2009a) and Wiles et al. (2014).

In northern KwaZulu-Natal and Mozambique, lower Miocene lagoonal to shallow marine coquina and sandy limestone of the Uloa (Roberts et al., 2006) and Temane Formations (Flores, 1973) crop out as isolated outliers. Cooper et al. (2013) suggest that, within the vicinity of Lake St Lucia, the Uloa Formation represents a multiple stack of normal regressive shoreline deposits. du Toit and Leith (1974) correlated the Uloa Formation with a ~140 m thick coquina identified in the Jc-A1 borehole, and with the identification of early Miocene coquina in all wells within the Durban Basin, it is further proposed that unit D represents the lateral equivalent of the Temane Formation and the offshore equivalent of the Uloa Formation. The unit likely represents a mixed siliciclastic-carbonate wedge deposited during normal regressive, late highstand to lowstand conditions similar to that described by Catuneanu et al. (2011).

In both northern KwaZulu-Natal (King, 1969) and Mozambique (Flores, 1973; Förster, 1975), the early Miocene succession is truncated by a mid-Miocene erosional surface, overlain by glauconitic sandstones or calcarenites of late Miocene to early Pliocene age (King, 1953; 1969; Frankel 1966; 1969). It is therefore proposed that the erosional episode (Surface S5) which incises unit D within the Durban Basin (Figs 7.1; 7.2) is correlative with this erosional surface. This surface marks the termination of the calcarenite succession in borehole Jc-B1, overlain by late Miocene to early Pliocene glauconitic sandstones (Unstead et al., 1983). A similar succession has been identified on the west coast of South Africa (Wigley and Compton, 2006) where a transition from carbonate-dominant to glauconitic sandstone assemblages is identified across a mid-Miocene erosional surface (Weigelt and Uenzelmann-Neben, 2004; Kuhlmann et al., 2010). The identification and correlation of such erosional surfaces around southern Africa suggests that sediment bypass and submarine erosion was dominant throughout the continental shelves during this period.

7.3.4 Development and architecture of submarine canyon systems

The stratigraphy of the Durban Basin is interspersed by regional unconformity surfaces representative of sequence boundaries (Martin, 1984; Goodlad, 1986; Chapter 6 this study). Wiles et al. (2013) identified three erosional surfaces (S4-S6 of this study) related to episodes of uplift and associated marine regression, manifested as a series of incision events within the palaeo-Tugela Canyon (central incision: Figs 7.6; 7.7). Wiles et al. (2013) were however unable to correlate these regionally across the palaeo-shelf and slope. Like Wiles et al. (2013), it is here proposed the incisions of surface S5 in this dataset represent a series of palaeo-canyons that have incised the upper slope and outer shelf of the Durban Basin. It is further proposed that the S5 erosional surface identified in this study correlates with the Miocene sequence boundary and incision episode proposed by Wiles et al. (2013).

New shelf-wide analyses of seismic and well data presented in this study clearly define three canyon systems that are morphologically similar to systems that incise continental margins elsewhere (e.g. Pratson et al., 1994; Wigley and Compton, 2006; Covault et al., 2011; Harris and Whiteway, 2011; Jobe et al., 2011). Cross-slope incision relief profiles of the S5 erosional surface are comparable with a series of buried, U and V shaped, Miocene palaeo-canyon systems on the New Jersey continental shelf (Miller et al., 1987; Fulthorpe et al., 2000). Two canyon morphologies are evident within the Durban Basin; the classically-described Type I canyons (Shepard, 1981; Pratson et al., 1994; Green and Uken, 2008; Lastras et al., 2009; 2011; Pattier et al., 2015) with erosional morphologies and a coarse-grained fill; and Type II canyons (Hagen et al., 1994; Zhu et al., 2009; Jobe et al., 2011; Soulet et al., 2016), defined by aggradation and mud-dominated fills.

It is suggested that the northern and central incisions represent “Type I” canyons which indent the shelf edge (Fig. 7.5) similar to canyons defined by Pratson et al. (1994) and Fulthorpe et al. (2000). These systems have linear trajectories with concave longitudinal profiles comparable with systems along erosional or immature continental margins (Covault et al., 2011). Covault et al. (2011) associate these profiles with steep continental slopes, narrow shelves and short hinterland river systems analogous with the east coast of South Africa. Although no boreholes intersect the canyon systems within the Durban Basin, high amplitude, wavy, onlapping

seismic reflection architecture (shown as annotated reflectors in Figs 7.1; 7.6; 7.7) suggests deposition of coarse-grained canyon fill through either debris flow (Shanmugam, 2000), high energy erosive turbidity currents (Jobe et al., 2011) or mass wasting (Harris and Whiteway, 2011). Gerber et al. (2009) demonstrated that similar linear canyon systems within the narrow Catalan margin formed through erosion by coarse-grained sediment gravity flows on steep slopes terminating in basin floor fan system lobes. The Durban Basin however, is unique as although basin floor fan systems would likely have developed, Wiles et al. (2013) suggest that bottom current winnowing and reworking led to removal/non-deposition of these features.

The southern incision is considered representative of a "Type II" canyon (Fig. 7.5), exhibiting a sinuous to meandering path, similar to the canyon systems defined by Hagan et al. (1994). The aggradational, smooth, U-shaped seismic reflection architecture and diffuse reflector zones (Fig. 7.1) are considered to be related to the low energy deposition of (possibly) mud-dominant channel-fill lithologies (Figs 7.1; 7.7 – grey shade). Jobe et al. (2011) infer similar processes at play in canyons they identified. The southward thinning of the "high-supply" units D and E into the southern basin suggest the formation of a sinuous Type II canyon in a sediment-starved portion of the margin.

The southern canyon system exhibits a slightly concave longitudinal profile, similar to profiles defined by Covault et al. (2011) for mud-rich systems. Although these systems are commonly associated with supply-dominated passive margins (Covault, et al., 2011), it is proposed that the southern canyon in this study is associated with sediment starvation and limited shelf development with incision likely a response to slumping and slope failure (e.g. Harris and Whiteway, 2011). Hagan et al. (1994) propose that the sinuosity of submarine canyons is a function of slope gradient, with Harris and Whiteway (2011) and O'Grady et al. (2000) suggesting that higher sinuosity canyons occur on gentle, subdued continental margins. Here it appears that the southern canyon fed sediment to a low-gradient continental rise (Fig. 7.5), similar to mud-rich canyon systems (e.g. McGregor and Bennett, 1979).

For the Durban Basin, it is suggested that erosional processes caused instability of the shelf-edge wedge, providing the driving force for canyon inception similar to that defined by Green (2011b) for the northern KwaZulu-Natal continental shelf. Green (2009a) however indicates that contemporary and palaeo-shelf development along the KwaZulu-Natal continental margin is a result of a complex interaction between and submarine canyon topography and strong geostrophic ocean current systems (Fig. 7.8).

7.3.5 Ocean current control on sedimentation and hiatus development

Heezen et al. (1966) were the first to propose that geostrophic bottom currents are principal processes that shape continental margins worldwide. Palermo et al. (2014) suggest that, within the deepwater Mamba gas field Mozambique, deposition and sediment winnowing of channelized sand bodies was largely affected by bottom current flow perpendicular to channelized, high volume, sand-rich turbidites. Bottom flow processes are likely related to the equatorward flowing North Atlantic Deep Water (cf. van Aken et al., 2004), which prompted the dispersion of the turbulent fine-grained suspension cloud in asymmetric drift successions with mud-free facies preserved in the channel system. Similarly within the Natal Valley circulation is dominated by bottom current circulation of the equatorward flowing North Atlantic Deep Water (Wiles et al., 2014), whilst upper ocean flow is controlled by the polewards flowing Agulhas Current (Fig. 7.8) (Preu et al., 2011; Wiles et al., 2013).

South of the study area in the Transkei Basin (Fig. 1.3), Niemi et al. (2000) and Schlüter and Uenzelmann-Neben (2007; 2008) proposed that mid-Miocene sequence boundary initiation was the result of a shift in Antarctic Bottom Water (AABW) (Fig. 7.8) which coincided with global cooling (Zachos et al., 2001). Deep water cooling, an increase in global oceanic $\delta^{18}O$ concentrations and ice-growth events within the east Antarctic ice sheet during the mid-Miocene climatic transition (Shackleton and Kennett, 1975; Flower and Kennett, 1994; Miller et al., 2005) was associated with eustatic sea level change in the Southern Ocean (Shevenell et al., 2004).

It is therefore proposed that changes in global oceanic conditions across the mid-Miocene climatic transition account, in part, to S5 sequence boundary development in the Durban Basin.

Sequence boundary development during the mid-Miocene climatic transition is not restricted to southeast Africa. Weigelt and Uenzelmann-Neben (2004) identified a mid-Miocene erosional surface that they correlated with the onset of modern deep oceanic current circulation patterns on the west coast of southern Africa. Liu et al. (2011) identified age correlative surfaces along the western Australian margin. Further evidence for global shifts in eustatic sea levels are identified by John et al. (2011) on the east Australian margin, where a marked shift in foraminifera concentrations, as well as a positive shift in oceanic $\delta^{18}O$ concentrations correspond with a major sequence boundary at ~13.9Ma. It is therefore postulated that, as the timing of this global oceanic event is coincident with epeirogenic uplift in southern Africa, variations in oceanic circulation across the mid-Miocene climate transition may account for a Miocene unconformity identified in the Durban Basin.

In accordance with Siesser and Dingle (1981) and Kuhlmann et al. (2010), it is thus suggested that Cenozoic epeirogenesis (Partridge and Maud, 1987) combined with global changes in eustatic sea level (Haq et al., 1987; 1988; Miller et al., 2005; Miller, 2009 and John et al., 2011) and changes in global oceanic conditions (Shevenell et al., 2004; Holbourn et al., 2007) have had a profound effect on local sea level around southern Africa. These processes have shaped the stratigraphic architecture of the continental shelves through episodes of erosion and sediment bypass or marine deposition. It is therefore proposed that these events lead to submarine canyon incision and the formation of a pronounced offshore erosional surface S5.

CHAPTER 8

POTENTIAL PLAYS / RESERVOIR ZONES WITHIN THE BASIN

8.1 INTRODUCTION

For the geological storage of CO_2 to be optimised, suitable strata and reservoir conditions need to be identified. Whilst a wealth of knowledge exists for CCS projects associated with hydrocarbon provinces (IPCC, 2005; US DOE, 2008; Würdemann et al., 2010; Underschultz et al., 2011; Hutcheon et al., 2016), saline aquifer storage, specifically in under-explored frontier basins, is commonly hampered by a lack of physical data needed to define CO_2 storage reservoirs and their storage capacity due to limited exploration activities (Wilkinson et al., 2013).

This chapter aims to provide the first effective assessment of the CO_2 storage potential (CSLF, 2005; Bradshaw et al., 2007; Bachu, 2015) of sandstone packages within the Durban Basin, through analysis of regional seismic and well log data. Interpretations of the sedimentary architecture of potential stratigraphic traps are discussed.

South Africa, like many countries worldwide, is heavily reliant on fossil fuels for energy supply, with about 90% of primary energy derived from either coal, oil or gas (Engelbrecht et al., 2004). During their technical review, Viljoen et al. (2010) identified a theoretical storage capacity of 42000 Mt CO_2 within the combined offshore Durban and Zululand Basins (Fig. 1.4). Although a low confidence ranking of "1" was given to the Durban Basin based upon data density and sub-surface heterogeneities (Cloete, 2010), it was selected for study due to the following factors:

1. Its proximity to potential CO_2 transport pipelines from major CO_2 sources
2. Large storage potential as defined by Viljoen et al. (2010)
3. Geological storage potential within stratigraphic and structural settings.

The Durban Basin represents a poorly explored frontier basin (Singh and McLachlan, 2003). Hydrocarbon exploration is limited to low resolution single-channel seismic reflection data sets (du Toit and Leith, 1974; Dingle et al., 1978; Martin, 1984; Goodlad, 1986) and four wildcat wells that focused upon potential structural plays beneath the continental shelf. Due to lack of folding and salt diapirism within the basin, structural traps predominantly overlie basement horst structures. Faulting within the basin has however allowed for the formation of roll-over structures through fault drag which are identified as potential trap sites.

Singh and McLachlan (2003) suggest that undrilled plays and leads are developed during two time periods:

- Upper Cretaceous
    - Four way dip closures overlying Palaeozoic basement
    - Distal turbidite slope fans
    - Turbidite sands overlying basement features
- Cenomanian-Turonian
    - Distal turbidite slope fans
    - Basin floor fan complexes
    - Channel sands

The current study however has identified both structural and stratigraphic traps that represent potential sites for CO_2 storage. As the large majority of these features remain undrilled further exploration is needed prior to them being confirmed as a potential CO_2 storage site.

Although Singh and McLachlan (2003) suggest that all four wells were not optimally positioned, located in zones of sediment bypass, which did not allow for the formation of substantially thick sandstone packages, two

laterally extensive sand bodies have been identified. These sand bodies delineate shallow marine shelf sand and deltaic deposits preserved on the palaeo-ramp margin. Additionally, multiple 4-way closure structures, as well as basin floor fan complexes at varying stratigraphic levels have been identified. Seismic profiles were selected to define both the constructional architecture of the continental shelf, as well as delineate potential stratigraphic and structural traps within potential sand-rich zones as defined by either borehole logs from existing wells, or sequence stratigraphy.

8.2 STRATIGRAPHIC TRAP RESERVOIR SYSTEMS

Within the Durban Basin, six seismic units (A–F) are delineated. These are defined by seismic bounding surfaces, reflector and unit impedance, and internal-reflector characteristics (Fig. 8.1; Table 8.1). As discussed in Chapter 6, unit A represents a syn-rift sedimentary succession whilst the overlying units (B–F) were deposited during passive margin construction. Individual units are separated by regionally pervasive, high amplitude, erosional seismic reflectors (Fig. 8.1). Units are commonly characterised by multiple seismic facies defined by specific seismic characteristics and architectures (Fig. 8.1).

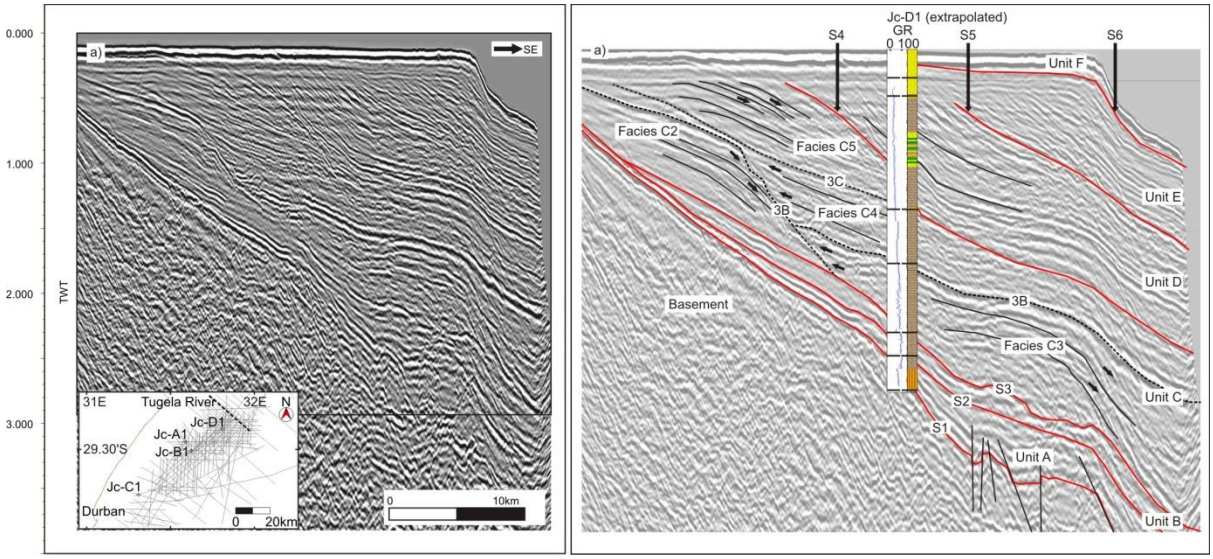

Figure 8.1: General overview of seismic stratigraphy of the Durban Basin.

On the basis of depth below seafloor, sedimentology, seismic architecture and reservoir properties, sedimentary units within four facies are identified as having CO_2 storage potential with well-defined reservoir-seal pairs. These include facies B1 and the basal zone of facies B2 (of unit B), and facies C1 and C2 within unit C (Table 8.1). Table 8.1 defines the reservoir-seal potential for all units within the Durban Basin. The positions of the mounds (Reservoirs A-E; G-H) relative to the contemporary shoreline are shown in insets in Figure 8.2. The spatial position of the shelf-confined ramp and deltaic sediments of Reservoirs F and I are displayed in insets Figure 8.2.

Table 8.1: Simplified sequence stratigraphic framework for the continental margin within the Durban Basin, describing seismic units, facies, bounding surfaces, interpreted depositional environment and reservoir/seal potential of each unit.

Unit	Facies	Surface	Modern Description	Stratal Relationship	Borehole Lithology Summary	Net Thickness	Reservoir and Seal Potential
F	F2		Progradational wedge	Moderate impedance, sub-parallel, progradational reflectors	Unconsolidated sands		None - Too Shallow
		S6	Shelf-confined erosional reflector				
E	E2/3		Progradational wedge	Moderate impedance, sigmoid, progradational reflectors overlain by aggradational reflectors	Sandstone and coquina	200 m	None - No seal
		S5	Shelf-confined erosional reflector				
D	D2/3		Progradational wedge	Moderate impedance, steeply dipping, progradational reflectors	Calcarenite, siltstone and claystone	900 m	None - No seal
		S4	Basin-wide Erosional Reflector				
C	C5		Progradational wedge	Moderate impedance, steeply dipping, progradational reflectors	Inner shelf sandstones and siltstones	950 m	None - seal unknown
		3C	Maximum Flooding Surface				
	C4		Retrogradational package	Low impedance aggrading reflectors, backstep and onlap 3B landward	Deep water mudstones	600 m	Seal
		3B	Maximum Regressive Surface				
	C3		Aggradational to Retrogradational Wedge	Low to moderate impedance, sub parallel, aggradational reflectors, onlap S3	Deep water mudstones and sandy turbidites	500 m	Seal
	C2		Progradational wedge	Moderate impedance, steeply dipping, progradational reflectors	Mudstone and interbedded well-sorted shelf sandstones	300 m	Good - Possible Reservoir
	C1		Slope Fan	Moderate impedance, progradational reflectors, downlap and onlap S3	Unknown - possibly sandy turbidites	250 m	Good - Possible Reservoir
		S3	Shelf-confined erosional reflector				
B	B2		Aggradational ramp	Low to moderate amp, sub parallel reflectors, onlap S2 updip.	Mudstone dominated top Sandstone dominated base	250 m	Seal - Upper facies Good - Basal facies - Possible Reservoir
	B1		Basin-floor Fan	High impedance progradational reflectors that downlap and onlap S2, individual mounds show internal progradation but retrograde as packages.	Unknown - possibly sandy turbidites	250 m	Good - Possible Reservoir
		S2	Basin-wide Erosional Reflector				
A	A1/2		Syn-rift valley fill	Aggradational to Progradational packages that onlap S1 against basement highs	Clay-rich sandstone and conglomerate	950 m	Good – Possible Structural Closure Reservoirs
		S1	Basin-wide Erosional Reflector				
BASEMENT			Acoustic Basement		Diamictite, sandstone and/or volcanics	Unknown	None - Basement

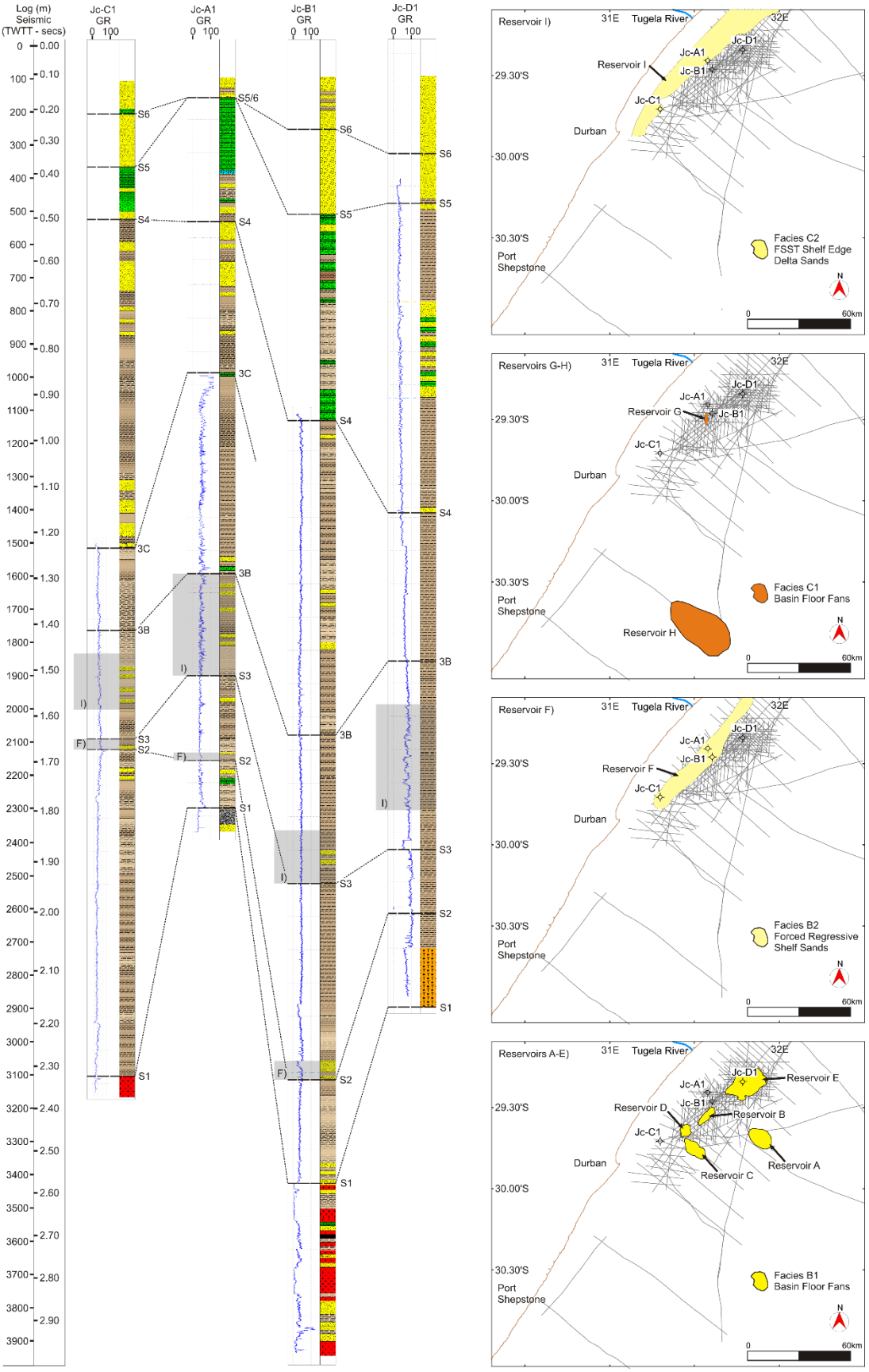

Figure 8.2: Lithographic logs and associated correlations of the Jc-series wells drilled within the Durban Basin. Spatial positions of all identified reservoirs are shown in insets.

8.2.1 Reservoir A - Turonian

Reservoir A is resolved in seismic line S74-007, where a mounded structure is preserved overlying seismic reflector surface S2 basinward of a large horst structure (Closure C). The reflectors form part of facies C1 in unit C, and onlap updip against the underlying reflector. The fan attains a maximum thickness of 283 millisec TWT (~226 m), but thins up and downdip to zero over a length of 15 km along S74-007. The areal extent of the fan complex is unfortunately poorly constrained due to limited intersecting seismic profiles, however a ~125 km^2 extent is postulated.

8.2.2 Reservoir B - Turonian

Reservoir B is intersected in numerous seismic lines, but is most well defined in line S97-19. The basin floor fan complex overlies reflector surface S2, with multiple retrogressive mounded reflector package pinching out updip against the underlying reflector surface. The fan complex attains a potential thickness at its crest of 176 millisec TWT (~140 m) which thins updip to zero over a distance of ~10 km. The areal extent of the fan complex is approximately 300 km^2 defined by bright, high amplitude reflectors.

8.2.3 Reservoir C – Turonian

Reservoir C is intersected by seismic line S74-005, where a ~344 millisec TWT (275 m) thick mounded reflector package is resolved. Internally the reflectors exhibit a progradational architecture, but thin up and downdip, onlapping and downlapping the underlying S2 reflector surface. Seismic control on areal extent is limited to one seismic line, but the fan complex is postulated to cover an area of ~130 km^2.

8.2.4 Reservoir D – Turonian

Reservoir D occurs as a mounded reflector package best resolved in seismic line S97-05. Internal architecture is not well defined, but the fan complex thins up and down dip over a distance of ~10 km. The fan complex attains a maximum thickness of 250 millisec TWT (~200 m) with an areal extent of ~50 km^2.

8.2.5 Reservoir E – Turonian

Reservoir E is preserved seaward of Jc-D1 whereby mounded reflectors are identified in S97-10B. The complex is defined by bright, high amplitude reflectors which overlie reflector surface S2. At its crest the mounded structure attains a thickness of ~600 millisec TWT (480 m) which thins up and down dip with internal reflectors onlapping against the underlying surface. Mapping of the structure suggests an areal extent of ~300 km^2 for the fan complex.

8.2.6 Reservoir F - Turonian

Reservoir F is intersected in Jc-B1, represented by a 28 m thick, coarsening upward, medium- to coarse-grained sandstone unit. The reservoir directly overlies either the S2 erosional surface or basement in the proximal zone. In both Jc-A1 and Jc-D1 the reservoir zone is marked by a pronounced high to low gamma frequency variation upwards through the succession. The unit can be intermittently traced for ~70 km along a coast-parallel orientation covering an area of approximately 700 km^2.

8.2.7 Reservoir G – Campanian

Reservoir G is identified in seismic line S97-15B where a mounded seismic reflector package overlies seismic reflector surface S3. The lateral extent of the fan complex is not well defined but at its thickest the package is represented by a 188 millisec TWT (150 m) succession of high amplitude, bright reflectors. Internally, reflectors onlap the underlying surface updip over a length of ~8 km. As the complex is not well resolved outside of line S97-15B, an overall extent of ~13 km^2 is postulated.

8.2.8 Reservoir H – Campanian

Reservoir H is resolved along seismic line SA76-8 where a mounded structure overlies seismic reflection surface S3. Unfortunately no lateral seismic control is available for this structure and therefore an areal extent of ~700 km^2 is postulated. The fan complex attains a maximum thickness of ~260 millisec TWT (200 m) with internal reflector geometries suggesting onlap updip and downlap downdip against the underlying surface.

8.2.9 Reservoir I - Campanian

Reservoir I forms a ~120 km long, coast parallel, progradational unit within the inner shelf of the basin. The reservoir unit can be resolved over an area of ~1000 km^2 in the proximal basin, intersected in no less than 20 seismic profiles and three wells (Jc-A1, Jc-B1 and Jc-C1). The succession comprises interbedded sandstone and claystone, attaining a thickness of ~87 m in Jc-C1. Sandstones are fine to coarse-grained, and well sorted with individual sandstone thicknesses varying from 5 to 20 m.

8.3 SEDIMENTOLOGY OF STRATIGRAPHIC TRAP RESERVOIR-SEAL PAIRS

8.3.1 Unit B

Unit B overlies unit A along an erosional, high amplitude seismic reflector S2 (Figs 8.1 and 8.3). Unit B, comprises two facies, B1 and B2 (Fig. 8.3), and is developed on a shallowly dipping proto-margin (Fig. 8.1). Facies B1 is laterally discontinuous, characterised by mounded, high amplitude seismic reflectors (Fig. 8.3). The positions of the mounds (Reservoirs A–E) relative to the contemporary shoreline are shown in Figure 8.2. The seismic architecture of facies B1 is defined by progradational, seaward-dipping reflectors which downlap the underlying reflector S2 (Fig. 8.4). The mound architecture varies between sheet mounds as in Reservoir C, (Fig. 8.4) and stacked mounds such as in Reservoir A (Fig. 8.5). Stacked mounds exhibit a progradational internal clinoform architecture separated by sheet-like High Amplitude Reflection Packages (HARPs) (Figs 8.5 and 8.6). In coast-perpendicular section, the upper mound retrogrades over the lower fan with successive updip migration of the internal clinoforms (Fig. 8.5). These clinoforms onlap successively landwards onto the underlying surface S2 (Fig. 8.5). Along strike, the mounds exhibit erosional internal architectures separating bright, high amplitude reflectors from diffuse, low amplitude zones (Fig. 8.6).

Although mounded structures of facies B1 are not intersected by the boreholes, a 28 m thick, coarsening upward, medium- to coarse-grained sandstone unit is intersected in Jc-B1, 3.8 km updip of a mounded feature (Figs 8.2; 8.3). This unit (Reservoir F) represents a basal package of facies B2, identified in all but the Jc-D1 borehole. A low gamma signature is however noted at this zone in the corresponding petrophysical log of Jc-D1 (Fig. 8.2). The material is a fine- to coarse-grained, very well-sorted sandstone with thicknesses that vary from 5 to 28 m. Overlying the basal package, the seismic reflectors of facies B2 comprise a stacked succession of aggradational, high impedance reflectors best represented in Jc-B1 and Jc-C1 where it is associated with a succession of claystone and subordinate siltstone (Fig. 8.3).

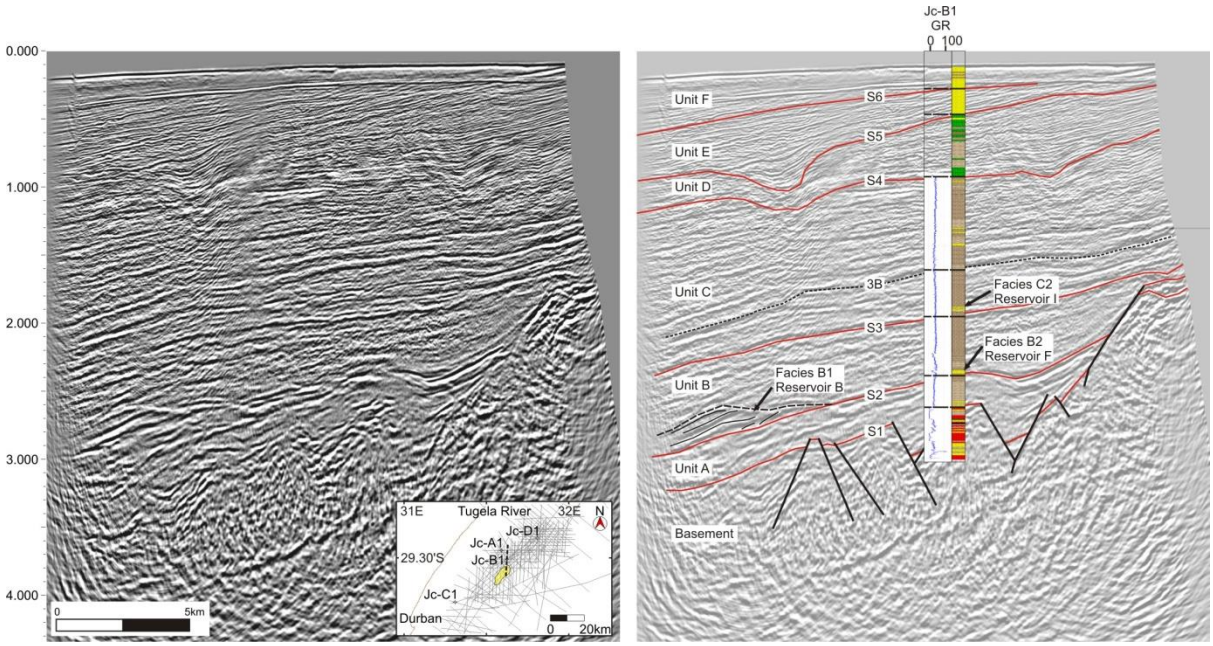

Figure 8.3: Seismic stratigraphy of Reservoirs B, F and I with intersections within Jc-B1 shown. Position of Reservoir B shown as polygon in inset.

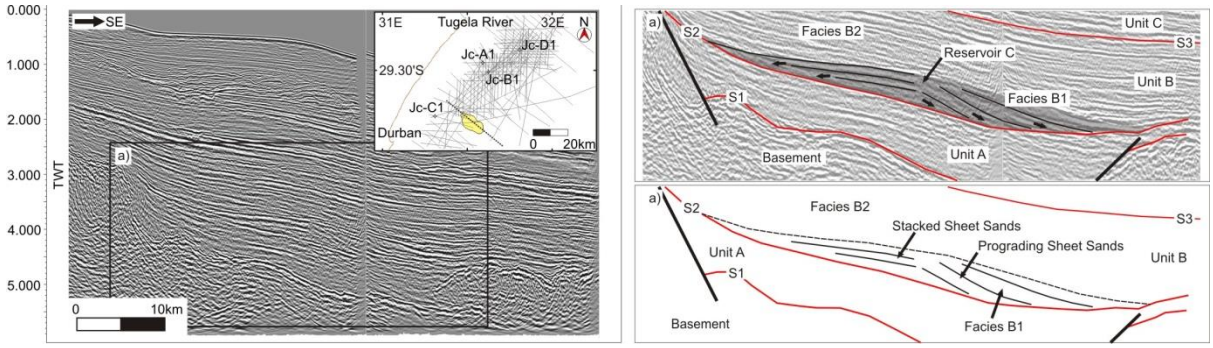

Figure 8.4: Seismic architecture of progradational sheet mound basin floor fan, Reservoir C.

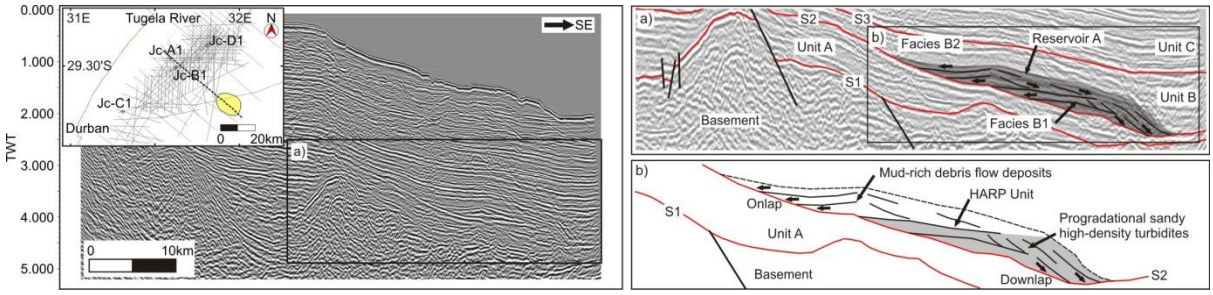

Figure 8.5: Seismic architecture of Reservoir A. Note the progradational internal reflector structure with individual fan structures separated by laterally extensive HARP's.

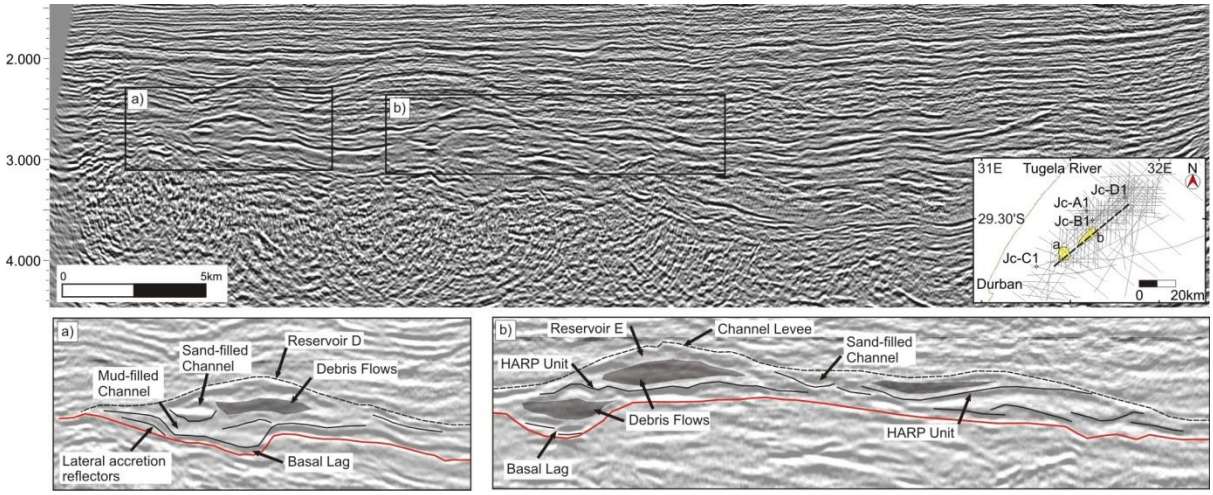

Figure 8.6: Coast-parallel seismic architecture of Reservoirs D and E. Note the channel and levee structures within individual fans.

8.3.2 Unit C

Unit C, erosionally separated from the underlying successions by reflector S3, is defined by moderate amplitude, offlapping, progradational reflectors that downlap the underlying units seaward. Five facies (C1-5) (Fig. 8.1) are resolved beneath the contemporary shelf and slope, separated by diffuse to pronounced reflectors.

Facies C1 is laterally discontinuous, comprising mounded reflectors with prograding internal architectures which downlap the underlying reflector S3 (Fig. 8.7). Along the lower slope, in the south of the basin, a pronounced mounded feature (Reservoir H) that exhibits variable internal reflectors including incision fills, HARPs, and inter-leveed bright to diffuse wavy reflectors is developed (Fig. 8.7).

Facies C2 is confined to the proximal basin where it is defined by a wedge of predominantly progradational seismic reflectors that downlap the underlying surface S3 (Fig. 8.1). Facies C2 is intersected in three wells (Jc-A1, Jc-B1 and Jc-C1) where it comprises an interbedded succession of sandstone and claystone defined as Reservoir I (Figs 8.2; 8.3). This facies attains a thickness of ~87 m in Jc-C1 (Fig. 8.2). Sandstones are fine- to coarse-grained, and well sorted with individual sandstone thicknesses varying from 5 to 20 m.

Facies C3 is resolved seaward of facies C2, in the distal basin, where it overlies either facies C1 or reflector S3 (Fig. 8.1). The facies is defined by aggradational to progradational internal reflectors. The gamma ray and lithological logs suggest siltstone and claystone deposits, with subordinate sandstones lenses capping upward-coarsening cycles (Fig. 8.2).

Facies C4 comprises low impedance, sub-parallel to parallel, aggradational to weakly retrogradational reflectors which overlie facies C2 and C3 along a marked high amplitude reflector surface 3B that defines the base of the most prominent onlap (Fig. 8.1). In this facies, the corresponding lithostratigraphy is dominated by marine claystone and siltstone with the facies capped by a moderate to high gamma ray signature claystone in Jc-C1 (Fig. 8.2).

Facies C5 is confined to the proximal basin, only intersected by the Jc-C1 borehole, where it caps unit C as a prograding wedge. This wedge oversteps facies C4 seaward along a downlap surface 3C (Fig. 8.6). This facies comprises an overall coarsening upward succession of claystone to medium-grained sandstones (Figs 8.1 and 8.2). The succession is truncated by a major regional erosional reflector S4 that incises facies C5 in the proximal basin and facies C4 in the distal basin.

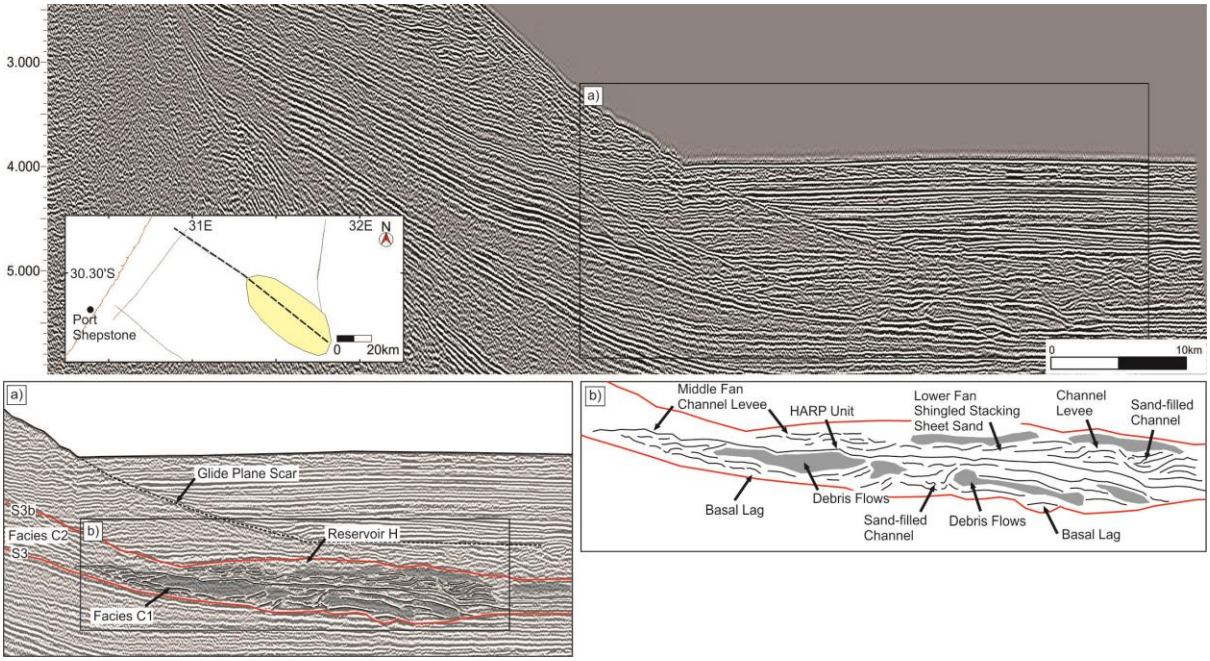

Figure 8.7: Seismic architecture of Reservoir H showing the complex internal reflector structure comprising channel-levee units in the middle fan and stacked sheet sands in the lower fan. Note how individual fan structures are separated by laterally extensive HARP's.

8.4 DISCUSSION - Stratigraphic Trap Reservoirs

Although CO_2 storage is commonly focused on laterally extensive saline aquifers formed by either shallow marine sand-rich shelf systems (Galloway, 2002) or fluvial braid-plain sandstone deposition (Noy et al., 2012; Leetaru and Freiburg, 2014), deep-water hydrocarbon bearing reservoir systems are commonly associated with stacked basin floor fan systems similar to those described by Carman and Young (1981) in the North Sea, and Dailly et al. (2013) offshore Ghana. Such systems have become targets for potential CO_2 storage, as outlined by Gibson-Poole (2009) and Borissova et al. (2013) for basin floor fan systems in Australia. Reservoir packages within the Durban Basin are confined to units B and C with multiple targets identified in basin floor fan systems as well as laterally extensive shallow marine shelf, and deltaic sands.

8.4.1 Cenomanian-Turonian Reservoirs – Domo Formation Equivalents

8.4.1.1 Distal Basin Reservoir Systems

Reservoir systems A–E within facies B1 occur as a series of progradational, mounded features (Figs 8.2-8.6) similar in geometry to the basin floor fan systems defined by Bouma (2000) and Shanmugam (2016). Internal clinoform orientations suggest interaction between progradational sheet sand (Fig. 8.4) and erosional channel and channel-levee structures (Figs 8.5; 8.6) as discussed by Shanmugam et al. (1995), Mayall et al. (2006), and Shanmugam (2016). It is likely these deposits formed by off-shelf sediment forcing of high-density turbidite currents (Lowe, 1982; Heller and Dickinson, 1985; Catuneanu et al., 2011) or sandy debris flows (Shanmugam, 2016). It is therefore proposed that Reservoirs A-E comprise basin floor fan systems deposited during late forced regression and early normal regression, related to global and local sea-level fall during the late Cenomanian and early Turonian (Dingle et al., 1983; Haq et al., 1987, 1988; Miller et al., 2005; Miller, 2009).

Unlike classic submarine canyon-associated fan systems (e.g. Normark, 1970; Bouma et al., 1985; Posamentier and Allen, 1999; Shanmugam, 2016), the Durban Basin at first comprised a ramp margin with no associated single-point canyon feeder system. Heller and Dickinson (1985), Stow and Mayall (2000) and Porebski and

Steel (2003) suggest that, in ramp margin settings where multiple shelf sediment sources are available, proximal fan systems develop with no defined canyon feeder systems. In direct comparison with the fan systems identified in this study, Castelino et al. (2015) indicate a similar lack of shelf indenting, feeder canyons for submarine fan systems of the distal Domo Formation within the Turonian-age Zambezi Delta offshore of the Zambezi River in the Mozambique Basin (Fig. 8.8). It is therefore proposed that similar depositional regimes must have been active and spanned the sum of the Durban and Mozambique Basins during this period.

8.4.1.2 Proximal Basin Reservoir Systems

In the proximal Durban Basin, a laterally extensive sandstone package (Reservoir F) of Turonian age (Leith, 1971; Unstead et al., 1983; McMillan, 2003) is identified in Jc-A1, Jc-B1 and Jc-C1 (Figs 8.2 and 8.3). McMillan (2003) suggests that a comparable unit from onshore, in the adjacent Zululand Basin, represents a Cenomanian-Turonian forced regressive shoreline deposit equivalent to the proximal Domo Formation sandstones in southern Mozambique (Fig. 8.8). Coster et al. (1989) and Salman and Abdula (1995) postulated that the Domo Formation developed as a proximal inner shelf, sheet sandstone with coeval distal submarine fan deposition on the upper palaeo-slope (Fig. 8.8). Coster et al. (1989) further propose that the widespread Domo Formation represents a major target for hydrocarbon exploration within the basin. It is therefore considered that, within the Durban Basin, unit B represents the coeval deposition of proximal, forced regressive, shelf sheet sands (Reservoir F), with distal accumulation of deep water, slope and basin floor fan systems (Reservoirs A–E) in a ramp margin setting. These conditions are identical to age-equivalent depositional environments described by Coster et al. (1989) and Castelino et al. (2015) in Mozambique. This suggests a regional connectivity in response to local sea-level variability around this region of south-eastern Africa; along-strike deposition of a series of coeval deep-water sandy turbidite fan systems, offshore of the major river systems, was active during this period.

8.4.2 Campanian Reservoir Systems – Lower Grudja Formation Equivalents

8.4.2.1 Distal Basin Reservoir Systems

The reservoirs (G-H and I) of unit C were deposited during forced regressive and lowstand conditions in the late Cretaceous (McMillan, 2003; Chapter 6). Facies C1 and C2 were deposited on the palaeo-slope and shelf edge respectively, and are considered coeval (cf. Chapter 6). Reservoirs G and H formed as submarine slope and basin floor fans, with Reservoir H in the southern basin (Figs 8.2; 8.7) the largest of these. Within Reservoir H, the internal architecture of the middle fan along the slope edge, comprises two channel-levee systems with coarse-grained debris flows deposits (Fig. 8.7) (sensu Shanmugam et al., 1995) and high density turbidite flows similar to those discussed by Bouma (2000). These are separated by an unchannelised HARP unit. The lower fan (Fig. 8.7) exhibits shingled stacking of sheet sand lobes in keeping with those described by Bouma (2000). Intervening distributary turbidite channels and associated levees (e.g. Mayall et al., 2006) occur within the lower fan. Similar submarine fan lobes of late Cretaceous age have been identified in the distal slope offshore Mozambique (Castelino et al., 2015).

8.4.2.2 Proximal Basin Reservoir Systems

In the inner shelf, Reservoir I of facies C2 represents a truncated, forced regressive shelf-edge delta (e.g. Hunt and Tucker, 1992). A similar depositional model for sand-rich, multiple source, ramp margins (c.f. Reading and Richards, 1994) is envisaged, whereby the delta front progrades to the shelf edge supplying sediment directly to the upper slope from multiple point sources. These margins commonly exhibit, aggradational, to progradational sequences derived from multiple channel switching (Stow et al., 1996). Coster et al. (1989) and Walford et al. (2005) propose a similar depositional environment for the age-equivalent, hydrocarbon-bearing (Mashaba and Altermann, 2015), lower Grudja Formation in Mozambique, which comprises proximal deltaic and distal basin floor fan sediments (Fig. 8.9). Coster et al. (1989) suggest that the lower Grudja Formation represents excellent reservoirs, having been deposited as beach and chenier barrier sands. Here depositional cycles occur as a stack of upward coarsening packages with net reservoir thicknesses of 16 m and porosities between 15 and 30% (Coster et al., 1989).

Following observations of Green (2011b), it is proposed in Chapter 6 that facies C2 is identified along much of the KwaZulu-Natal margin northwards towards Mozambique. It is therefore suggested that the reservoir systems (G-I) within the Durban Basin are coeval with the lower Grudja Formation in Mozambique (Coster et al., 1989) and were deposited through proximal deltaic, and distal submarine fan deposition during relative sea-level fall during the late Campanian and early Maastrichtian.

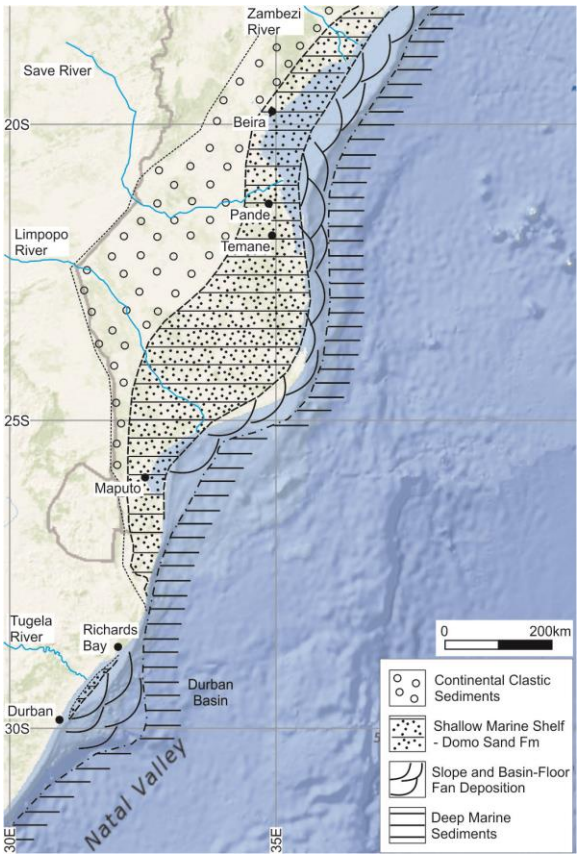

Figure 8.8: Turonian (Domo Formation) reservoir development and depositional environment for the Durban and Zululand basins and Mozambique coastal plain. (modified after Coster et al., 1989).

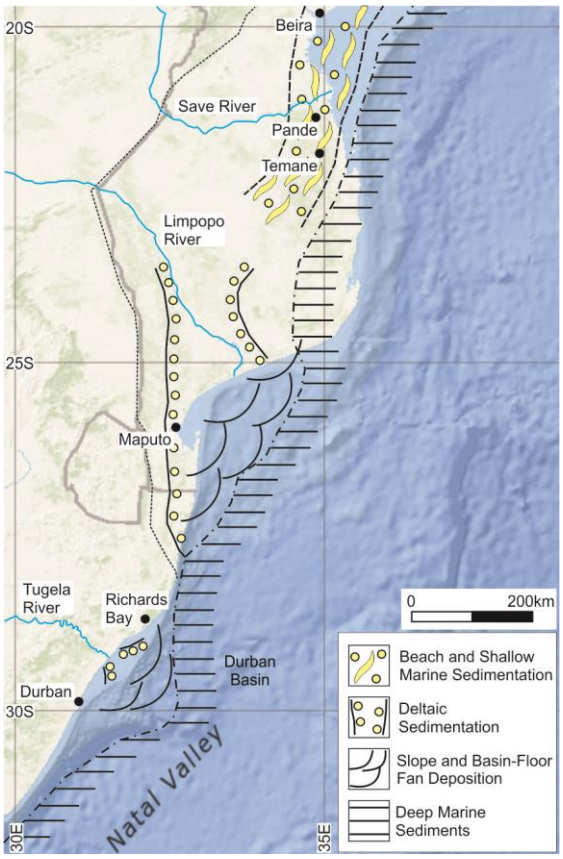

Figure 8.9: Maastrichtian (Lower Grudja Formation) reservoir development and depositional environment for the Durban and Zululand basins and Mozambique coastal plain. (modified after Coster et al., 1989).

8.5 STRUCTURAL TRAP SYSTEMS

The architecture of structural traps is discussed in detail by Selley and Sonnenberg (2015) who indicate that, with reference to an anticlinal trap, the highest point of the trap is the crest with the lowest point at which hydrocarbons may be contained known as the spill point. The vertical distance from crest to spill point defines the closure of the trap. Within the Durban Basin two varieties of structural trap are recognised, namely compactional anticlines and rollover fault traps. The spatial positions of the individual closures (Closures A-E) relative to the contemporary shoreline are shown in Figure 8.10.

Fault and fault related traps were targeted during previous exploration by SOEKOR with the drilling of the Jc-A1, Jc-B1 and Jc-C1 wells. A faulted rollover trap of Campanian-age is identified in this study as Closure E.

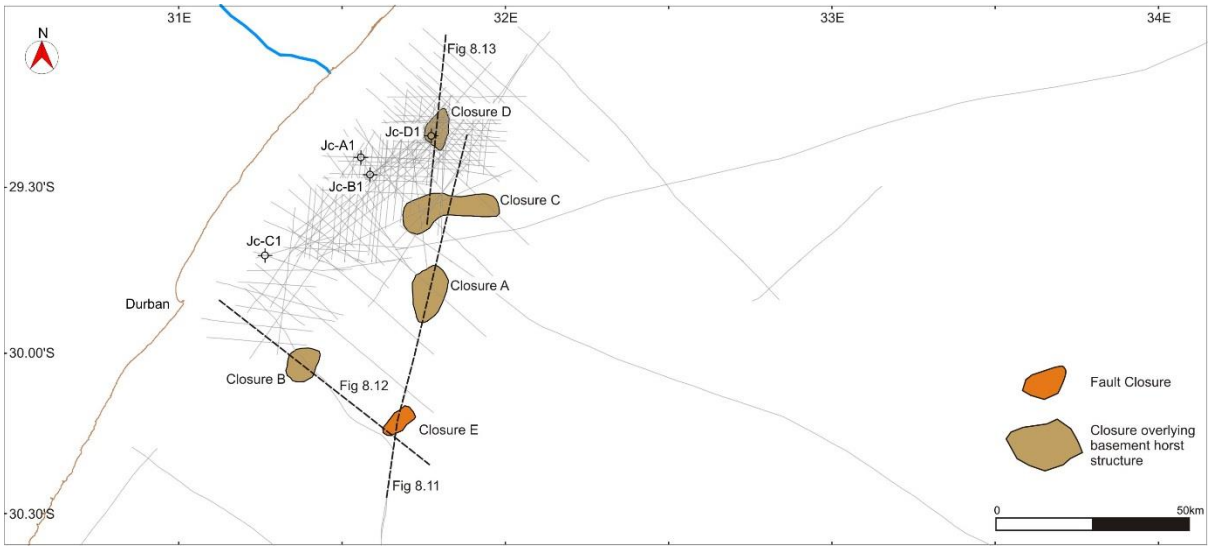

Figure 8.10: Spatial positions of all identified closures within the Durban Basin.

8.5.1 Closure A

Closure A (Fig. 8.11) is identified through two 2D seismic lines, SA74-006 (3118 millisec TWT, SP 218), and SA76-159 (3290 millisec TWT, SP 636). The target interval overlies a large basement horst structure which strikes north-northeast and attains a width of 11 km. The sediment drape covers an area of 133 km^2 with a total closure thickness (crest to updip spill point) of 100 millisec TWT (~80 m).

8.5.2 Closure B

A compactional anticline overlying a basement horst structure (Fig. 8.12) is identified in seismic lines SA76-10 and S74-003 where a normal fault has caused seaward downthrow of basement by 500 millisec TWT. Seismic reflections suggest sediment draping overlying the crest of the structure. The anticlinal structure produced by the draped sediments is ~10 km in coast-perpendicular width, however no seismic lines are available to define the strike of the structure. The sediment drape covers a postulated area of ~80 km^2 with a closure thickness of ~100 millisec TWT (~80 m) from crest to updip spill point.

8.5.3 Closure C

Closure C (Fig. 8.11) occurs as a large ~300 km^2, east-west trending basement horst complex with associated sediment drapes attaining a maximum closure area of ~315 km^2. The structure is evident in multiple seismic lines, but is most well defined in SA76-159 (3100-3400 millisec TWT, SP 290) and S74-007 (2900-3250 millisec TWT, SP 1000). Three individual sediment drapes are identified in three separate seismic lines intersecting the horst. Individual drapes have closure areas of (S74-007) 70 km^2 by ~200 millisec TWT (~160 m); (SA-159) 40 km^2 by ~120 millisec TWT (~96 m); and (S74-008 drape) 140 km^2 by ~200 millisec TWT (~160 m) respectively.

8.5.4 Closure D

Closure D (Fig. 8.13) is intersected by seismic line S97-41 (2168 millisec TWT, SP 1530) and has been prospected by the Jc-D1 borehole. The closure occurs as a horst structure bounded by east-west striking normal faulting on the northern and southern flanks. The closure attains a maximum thickness of ~120 millisec TWT (~96 m) with an overall closure area of ~60 km^2.

8.5.5 Closure E

Closure E (Fig. 8.11) is identified in seismic line SA76-159 (3600 millisec TWT, SP 1250), ~30 km south of Closure A, and consists of a stacked roll-over against a normal fault. The closure has poor seismic control, only being intersected by line SA-159. High amplitude reflectors are identified at the crest of the closure in SA-159 (Fig. 8.11). The area of closure appears to be in the order of 100 km^2 however, without intersecting seismic lines the true 4-way closure area cannot be accurately defined. The reservoir thickness, based upon the thickness of the high amplitude reflectors within the closure, is in the order of 100 millisec TWT (~80 m).

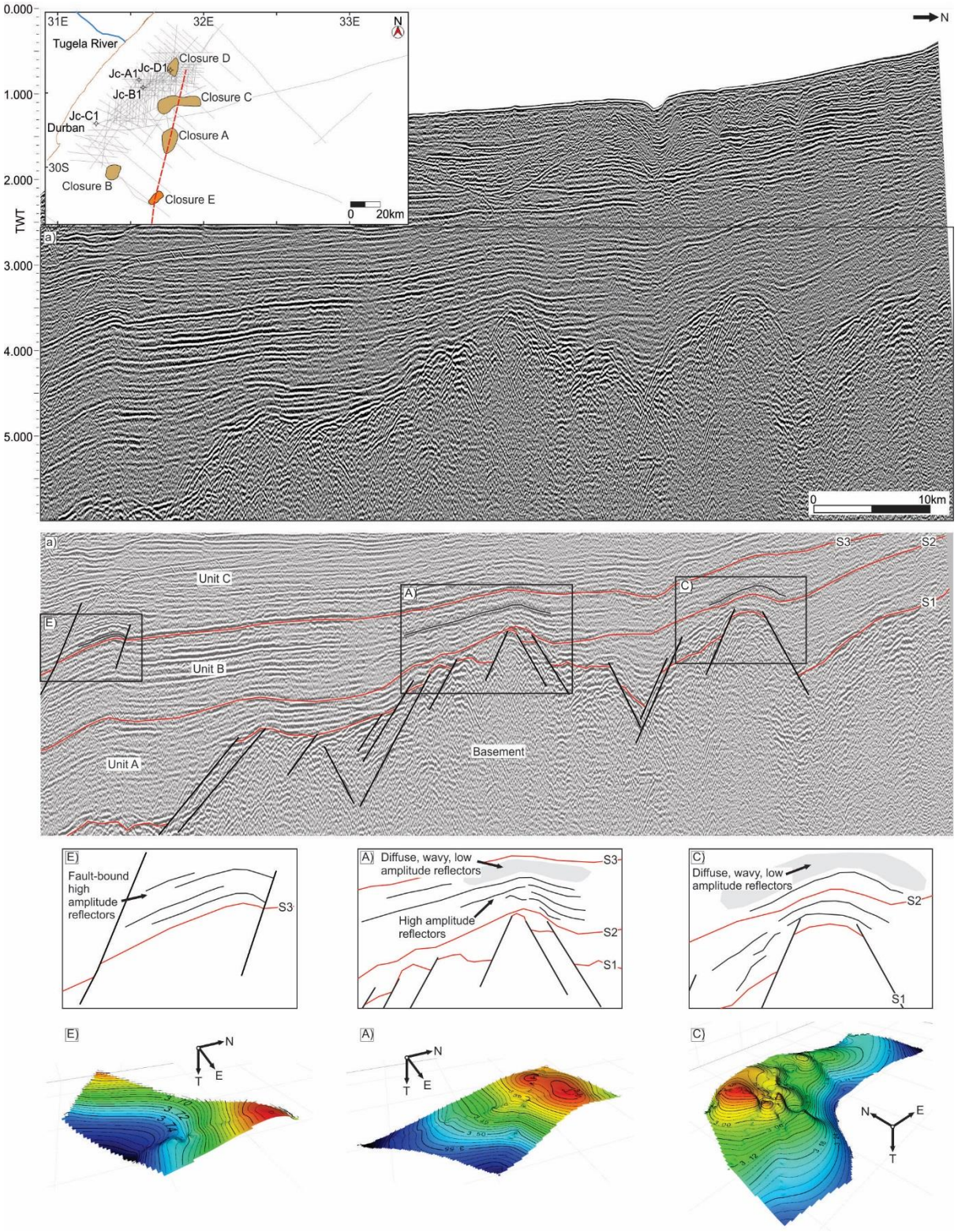

Figure 8.11: Seismic architecture of Closures A; C; E defined along seismic profile SA76-159. Closures A and C are resolved across multiple profiles, whereas Closure E is only identified in this profile. Note the roll-over structure of Closure E with the closure bound updip by a normal fault. Closures A and C define compactional anticlines overlying basement horst structures.

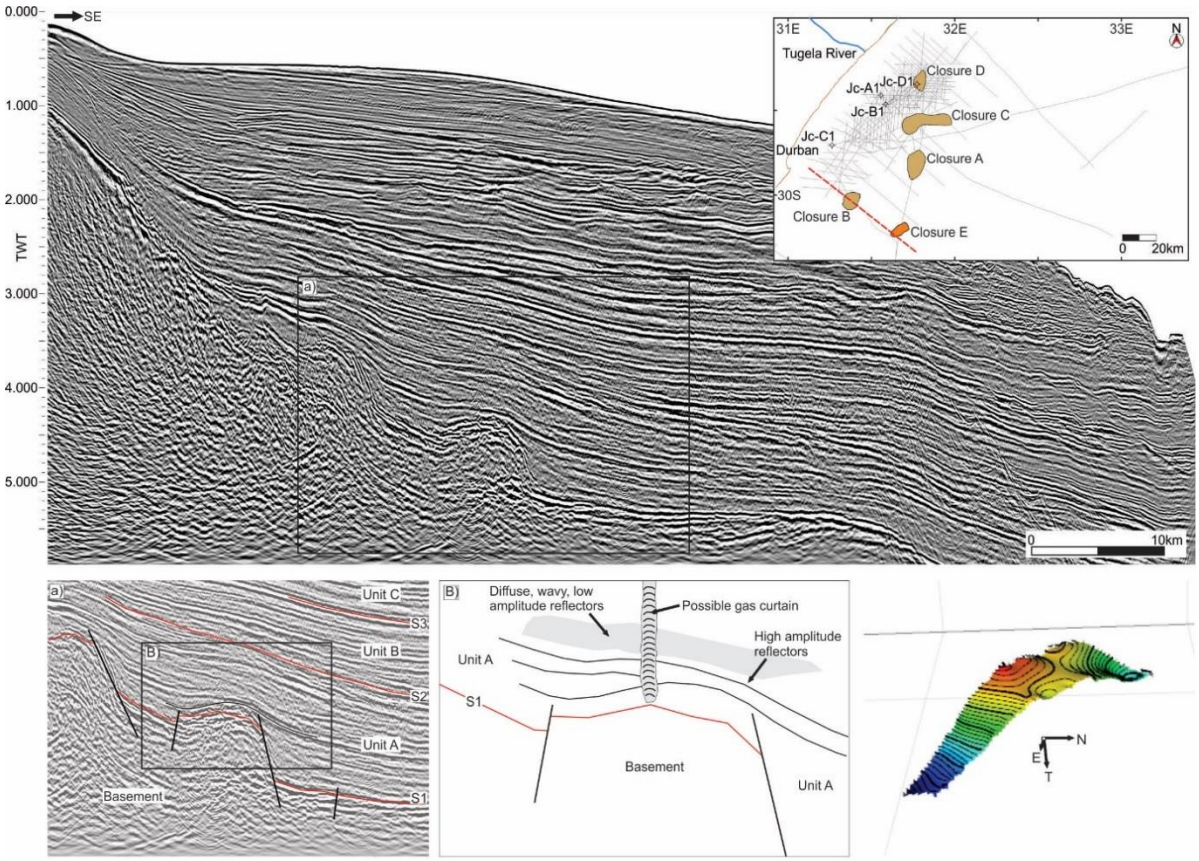

Figure 8.12: Seismic architecture of Closure B. Closure is represented by draped high amplitude reflectors overlying a basement horst structure.

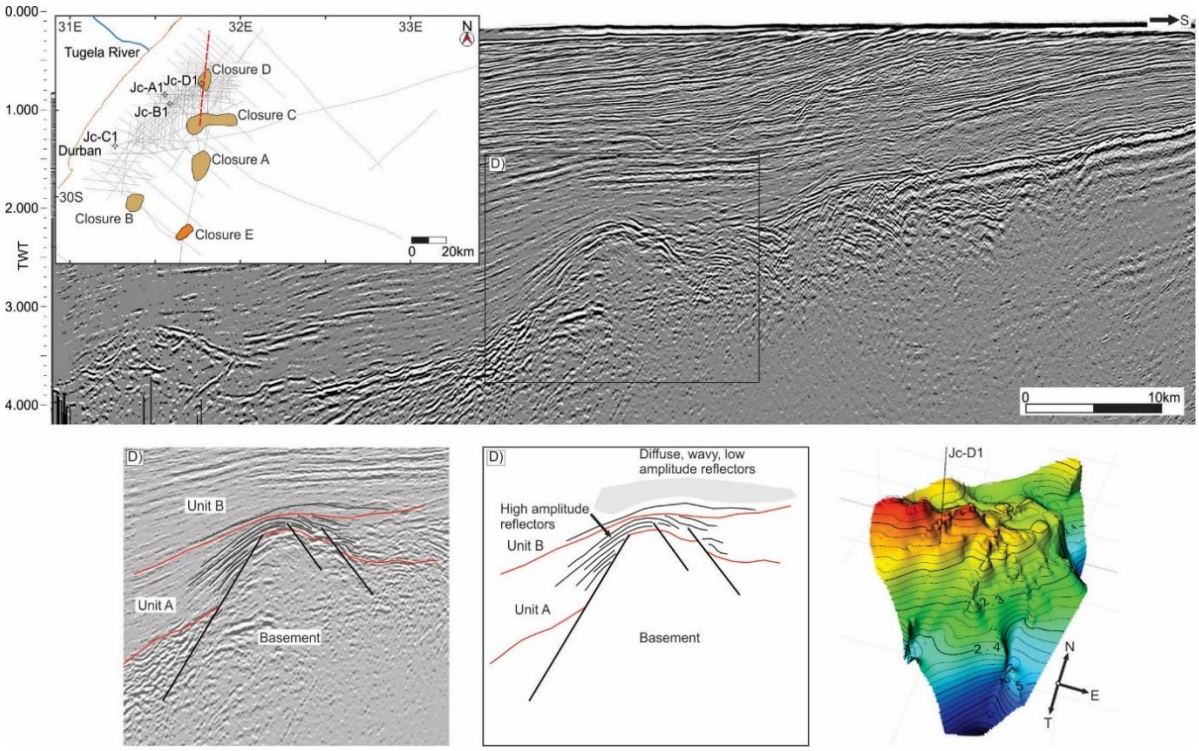

Figure 8.13: Seismic architecture of Closure D showing high amplitude reflectors forming a compactional anticline draped over a basement horst structure.

8.6 DISCUSSION STRUCTURAL TRAP SYSTEMS

Structural traps represent the most common potential targets for hydrocarbon exploration (Selley and Sonnenberg, 2015). Although structural traps are common in sedimentary basins, for a trap to be viable it must be overlain by an effective seal that hinders the upward migration of hydrocarbons through the sedimentary succession (Selley and Sonnenberg, 2015).

Structural traps form primarily through compressional tectonism active within a basin subsequent to deposition of the sedimentary pile. These can either be caused by crustal shortening, or intrusion of diapirs into the succession (Selley and Sonnenberg, 2015). Regional tectonism within the Durban Basin however, is dominated by extensional and transtensional tectonics related to the breakup of Gondwana and strike-slip movement along the AFFZ (Watkeys and Sokoutis, 1998). North of the AFFZ termination at ~30°S the basin is dominated by either coast-parallel half-graben and graben structures or arcuate NW-SE – ENE-WSW trending structural elements (Fig. 3.4) that tie with on-land faults systems (von Veh and Andersen, 1990).

The main structural elements that controlled sedimentation during Gondwana breakup from the Lower Jurassic through to the Late Cretaceous were summarized by Dingle et al. (1983) as:

- Long, approximately N-S, and NNW-SSE normal fractures bounding wide horsts and grabens on continental crust north of 30°S
- Relatively short NE-SW fractures and basement highs which offset and compartmentalise the northern Natal Valley
- Long approximately NE-SW shear fractures bounding the southern Natal Valley south of 30°S
- Arcuate fractures and E-W to NW-SE lineaments in pre-Jurassic basement rocks on the continental edge between 29 and 33°S

Subsequent to basin formation, differential compaction of basin-fill sediments has allowed for the formation of compactional anticlines with sediment drapes covering deep-seated basement horst structures. These structures, representing Closures A-E within the basin, are similar in formation to hydrocarbon plays defined by Selley and Sonnenberg, (2015) within the Forties, Montrose, and East Frigg fields in the North Sea. These structures have been the targets for all previous exploration within the basin, with the drilling of the Jc-D1 well (Phillips Petroleum, 2000) specifically examining the faulted compactional anticline (Closure D) in the upper slope.

Compactional closures within the basin occur at numerous stratigraphic levels, but are primarily observed in Aptian to Coniacian sediments (Figs 8.11; 8.12; 8.13).

8.6.1 Closures in Unit A

Closures B and D occur within unit A, with high amplitude reflectors draped over basement horst structures in the lower and middle slope. The closures occurs within sediments of possible Aptian to Barremian age (Phillips Petroleum, 2000). Closure D, prospected by the Jc-D1 borehole, comprises a 181 m thick glauconitic gritty quartz sandstone succession (Phillips Petroleum, 2000) correlative with syn-rift Barremian to Aptian sediments identified in the ZU-1/77 borehole in the Zululand Basin (Stojcic, 1979).

8.6.2 Closures in Unit B

Closures A and C occur within unit B, with potential reservoir sediments of Turonian to early Coniacian age forming compactional anticlines above two basement horst structures (Fig. 8.11). Within Closure A, Davids, (2009) suggests that the reservoir-seal pair interval comprises interbedded turbidite sandstones and bathyal shales. Potential reservoir sands within Unit B may occur within the basal portions of facies B2, associated with Turonian-age forced regression and lowstand sedimentation (McMillan, 2003).

8.6.3 Fault-related Structures

Closure E occurs within unit C, where a rollover anticline is present within the hanging wall of a listric growth fault structure (Fig. 8.11). Closure E is comparable with structures identified within the Niger Delta Basin (Adewole and Healy, 2017), where simple rollover anticlines occur within the landward extensional zone of the delta. Subsequent to rift phase termination, gravitational tectonics represent the primary deformational processes operational in passive margin basins (Tuttle et al., 1999). Within deltaic successions normal growth faulting is dominant in the landward extensional zone whilst compressional tectonics and salt diapirism occur in the seaward zone (Adewole and Healy, 2017). Weber (1987) suggests that, within the Niger Delta, the primary oil-rich belt coincides with a concentration of rollover anticlines related to growth faulting in the landward extensional zone.

Multiple growth fault structures are identified within the southern portion of the Durban Basin where gravitational tectonics are associated with instability along the edge of the continental rise (Fig. 8.14). As discussed previously (Chapters 6; 7) the Durban Basin was subject to reduced sediment supply in the late Cretaceous with the formation of a wide continental rise rather than a shelf and shelf break. Reduction in sediment supply during this period likely led to the deposition of deep marine mudstones with sediment loading resulting in instability and gravitational tectonics similar to that discussed by Carvajal et al. (2009). Unfortunately the lack of seismic profiles in this region precludes direct correlation, however it is likely that the faults identified in Figure 8.14 propagate coast-parallel, with the most landward fault likely representative of the same fault system affecting Closure E. Although Davids (2009) postulates that the reservoir rock in this closure are represented by turbidite or marine sandstones associated with the palaeo-Tugela River, a reduction in sediment supply during this period (Chapter 7) may have precluded sandy turbidite deposition, and rather thin-bedded turbidites of the Td and Te Bouma sequence would be dominant (Bouma, 1962).

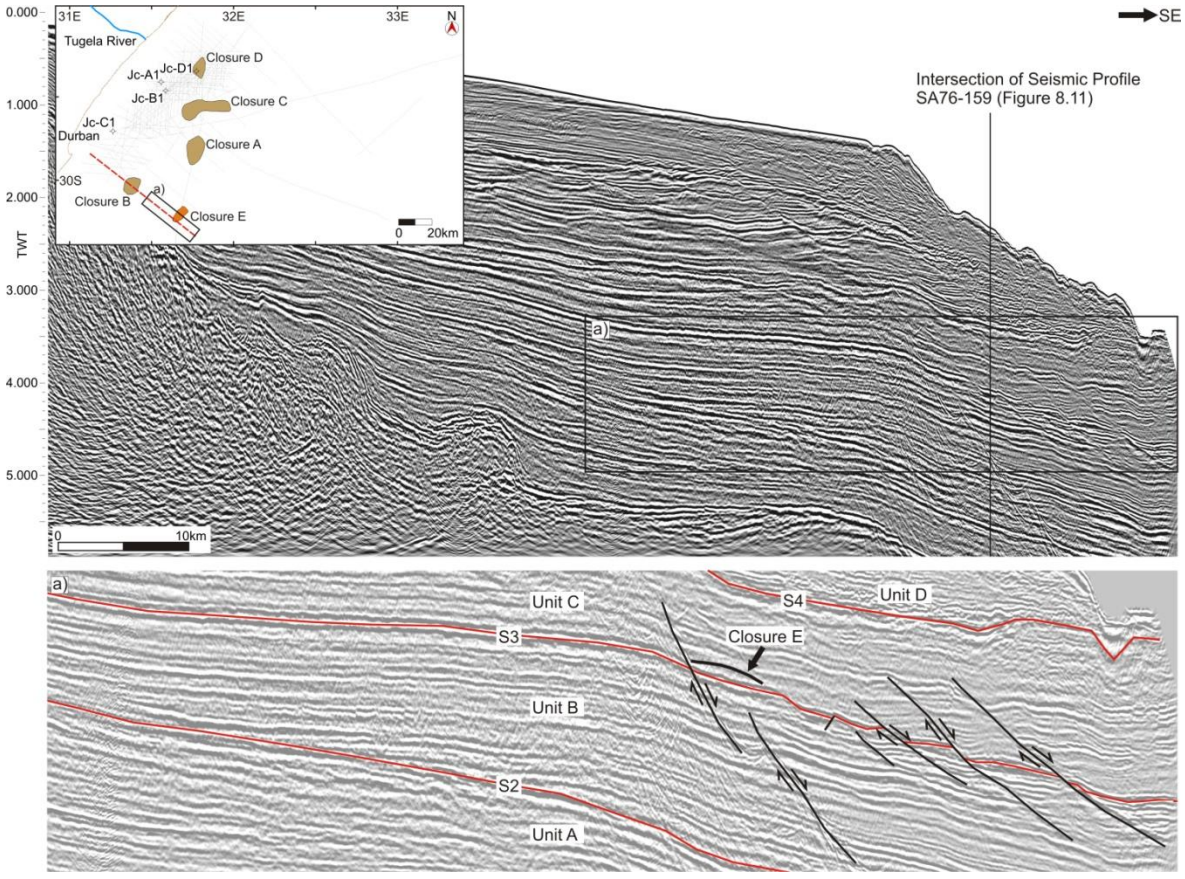

Figure 8.14: Growth faulting within the southern portion of the Durban Basin identified in coast-perpendicular section. Note the close proximity of the growth faulting to Closure E defined in seismic profile SA76-159 (Figure 8.11).

8.7 REGIONAL SEALS

Seals within the Durban Basin occur as prominent marine claystone successions at varying intervals. These include the uppermost zones of unit B (Figs 6.1; 6.2) and the uppermost zones of unit C (Figs 6.1; 6.2). These zones are laterally continuous throughout the basin as shown in Figures 8.15; 8.16; 8.17.

8.7.1 Turonian to Coniacian Seal Systems

Basin floor fan reservoirs (A-E) and sheet sands of Reservoir F are overlain by thick (>100 m) successions of deep marine claystones (Fig. 8.17 – Inset A) in Jc-A1 and Jc-B1 (Figs 8.2, 8.3). Similar marine claystones are intersected in Jc-D1 where they underlie the S3 regional reflector. In both Jc-A1 and Jc-D1 high gamma-ray geophysical anomalies are associated with this interval (Fig. 8.17 – Inset A). It is likely that these units would form potential cap rocks for both structural and stratigraphic reservoirs. Chapter 6 of this study suggests that these claystones developed during late lowstand and early transgression within the basin.

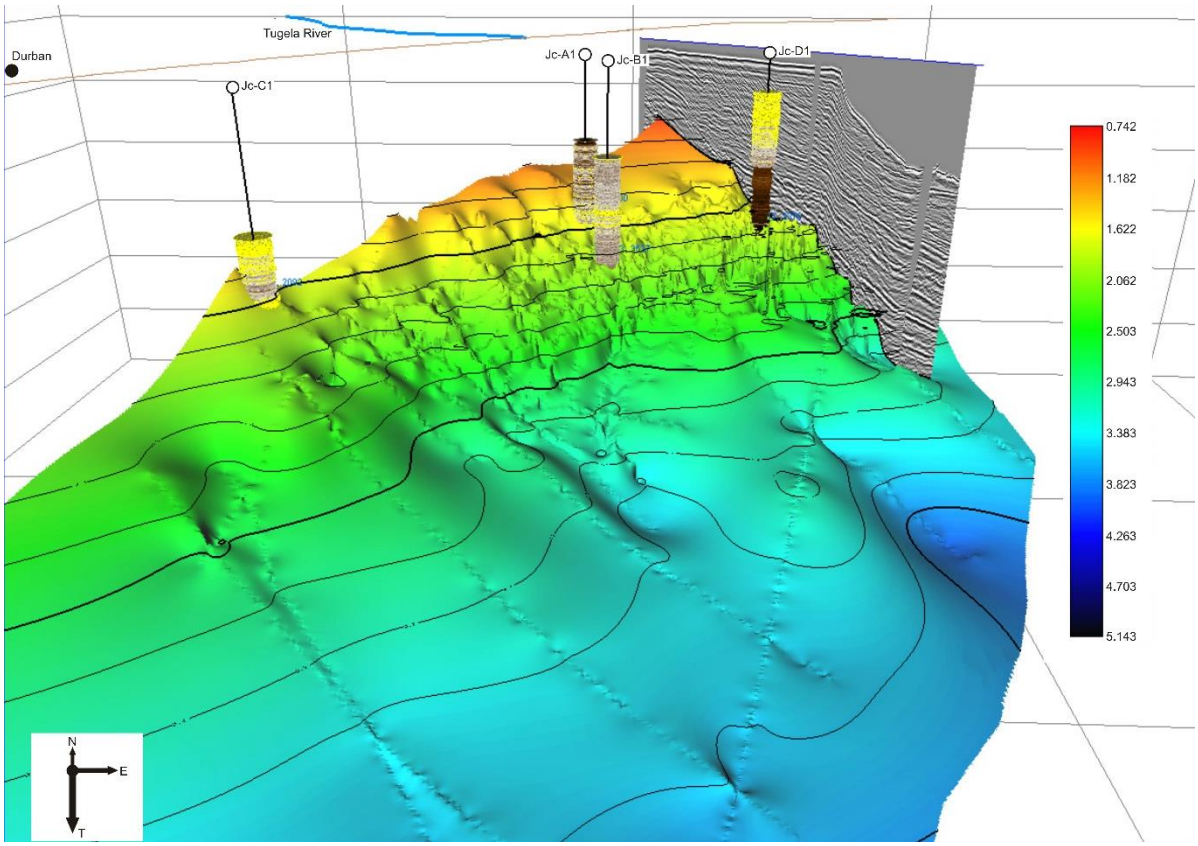

Figure 8:15: Two-way time depth structure map for the top seismic surface of the Coniacian seal system relating to the S3 regional seismic reflector.

8.7.2 Campanian Seal Systems

The basin floor fan Reservoirs (G-H) and Reservoir I deltaic sandstones of facies C1 are overlain by deep marine claystones and siltstone packages of facies C4 (Fig. 8.17 – Inset B). Intersected by boreholes Jc-A1, Jc-B1 and Jc-C1, this succession represents a transgressive systems tract capped with a maximum flooding surface 3C (cf. Chapter 6). This succession forms a regionally pervasive seal within the Durban Basin.

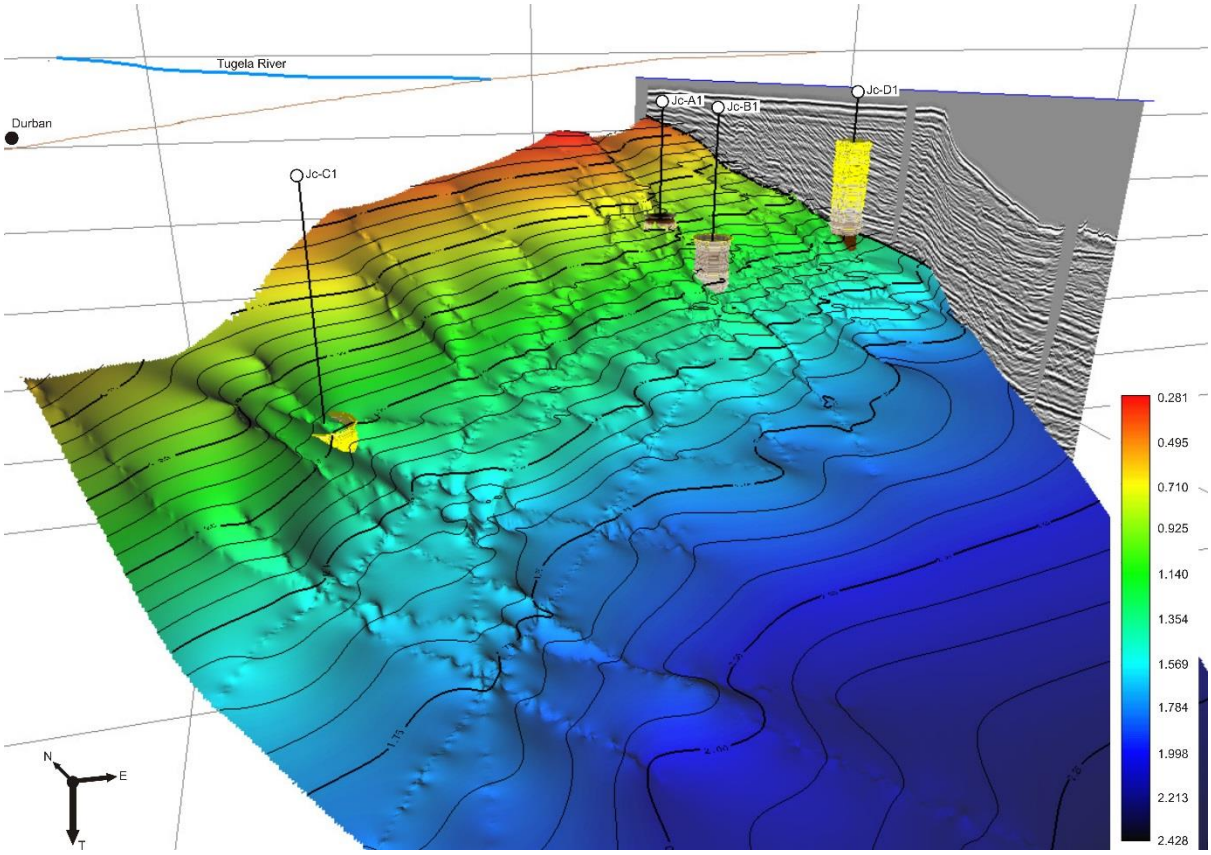

Figure 8.16: Two-way time depth structure map for the top seismic surface of the Campanian seal system relating to the maximum flooding surface 3C.

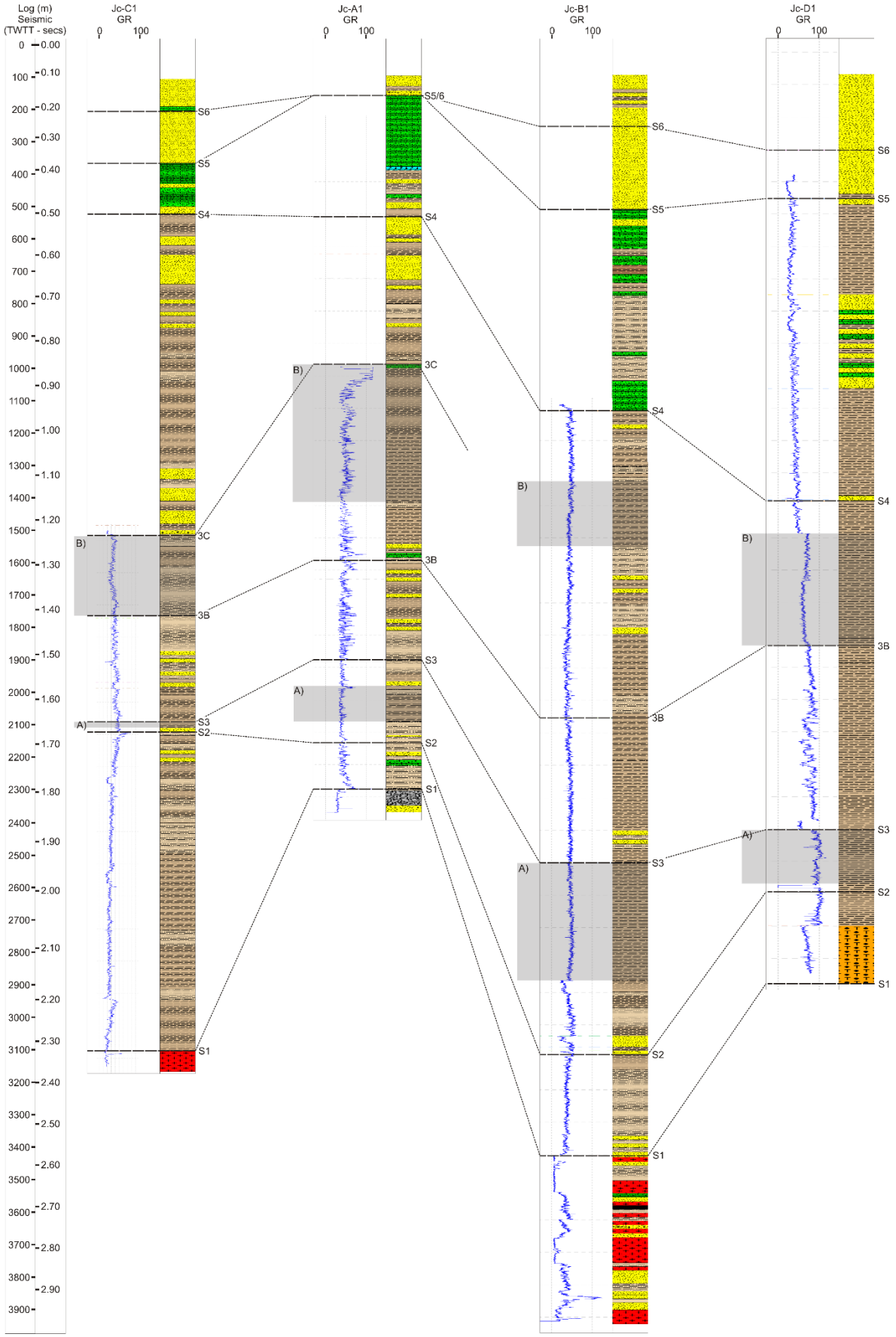

Figure 8.17: Regional seal packages intersected within the Jc-series boreholes in the Durban Basin.

CHAPTER 9

STORAGE CAPACITY ESTIMATES

9.1 INTRODUCTION

This chapter aims to assess the effective CO_2 storage potential (CSLF, 2005; Bradshaw et al., 2007) or storage efficiency (Bachu, 2015) of sandstone packages within the Durban Basin. Potential saline aquifer formations deeper than 800 m below seafloor are targeted, defined by results from seismic and sequence stratigraphic mapping and well log data discussed in Chapters 6-8. During this regional geological evaluation no attempt was made to define factors relating to CCS regulation, public perception, or economic viability.

9.2 STORAGE CAPACITY ESTIMATES

The areal extent, depth, gross and net thickness of individual mounded features, sandstone reservoirs and potential closures are presented in Table 9.1, whilst their spatial distributions are shown in Figures 8.2 and 8.10. Due to a lack of borehole intersections, no core or porosity-permeability data are available for the majority of the identified reservoirs systems. Therefore, where needed, maximum thicknesses are defined from TWTT-depth conversions based upon the Jc-D1 well shot/velocity data defined from seismic analyses and or borehole intersections. The limited data pertaining to reservoir porosity, permeability and heterogeneity has led to the utilisation of net thicknesses (50% max thickness) to account for variations within the pay zone (Table 9.1). Due to a lack of porosity data, values from analogous systems are utilised with their associated data sources referenced in Table 9.1. Porefluid pressures are defined by true depth of the reservoir top and mud weights defined by Muntingh, (1983) in borehole Jc-C1.

Porefluid pressure calculations are based upon the following equation:
Pressure (psi) = Pressure Constant (0.052) x Mud Weight (ppg) x TVD (ft)

CO_2 densities for individual reservoirs are provided in Table 9.1. The online calculator (www.energy.psu.edu/tools/CO2-EOS), based upon equation of state calculations of Span and Wagner (1996), is used to derive the CO_2 density calculations.

Overall storage resource estimates are defined by the following equation (Goodman et al., 2011). Where A is the area (m^2), h is the net thickness of the reservoir (m), $ø$ is the average porosity (%), ρ_{CO2} is the average CO_2 density, evaluated at pressures and temperatures that represent storage conditions anticipated for individual deep saline aquifers. E is a storage efficiency factor that reflects proportion of pore space that can be utilised in practice.

$$M_{CO2} = A \times h \times ø \times \rho_{CO2} \times E$$

The storage efficiency estimates for potential reservoirs and closures within the Durban Basin are summarised in Table 9.2.

Table 9.1: Reservoir extent, thickness, and physical parameters utilised for storage capacity estimates of the Durban Basin.

CO_2 Density Constant	0.052	Seafloor Temperature (°C)	14
Mud Weight (ppg)	8.6	Net/Gross Ratio	NG = 0.5
Av. Geothermal Gradient - Jc-C1 (°C/km)	26.7	Avg. Water Depth (m)	80

Reservoir	Facies	Reservoir Description	Areal Extent (km^2)	Max Thickness (m)	Net Thickness (m)	Depth of top surface (m)	Porefluid pressure (bar)	Reservoir Temperature (°C)	CO_2 Density ($kg.m^{-3}$)	Porosity %	Porosity Data Source
I	C2	Deltaic Shelf Sand	1500	100	50	1639	163	58	666	30	(Coster et al., 1989; Solomon et al., 2014)
H	C1	Basin-floor Fan	730	322	161	6817	680	196	695	15	(Coster et al., 1989)
G	C1	Basin-floor Fan	10	247	123.5	2431	242	79	679	15	(Coster et al., 1989)
F	B2	Inner Shelf Sand	1500	80	40	3050	304	95	687	30	(Gerrard, 1972a; Coster et al., 1989; Solomon et al., 2014)
E	B1	Basin-floor Fan	280	360	180	2441	243	79	681	20	(Dailly et al., 2013)
D	B1	Basin-floor Fan	38	312	156	3250	324	101	685	20	(Dailly et al., 2013)
C	B1	Basin-floor Fan	93	468	234	4992	498	147	692	20	(Dailly et al., 2013)
B	B1	Basin-floor Fan	50	250	125	3397	339	105	686	20	(Dailly et al., 2013)
A	B1	Basin-floor Fan	120	285	142.5	4828	482	143	691	20	(Dailly et al., 2013)

Closure	Unit	Reservoir Description	Areal Extent (km^2)	Max Thickness (m)	Net Thickness (m)	Depth of top surface (m)	Porefluid pressure (bar)	Reservoir Temperature (°C)	CO_2 Density ($kg.m^{-3}$)	Porosity %	Porosity Data Source
E	C	Fault Closure	30	79	40	4703	469	140	690	15	(Coster et al., 1989)
D	A	Anticline	60	132	66	2662	266	85	684	15	(Coster et al., 1989)
C	A	Anticline	210	176	88	3973	396	120	689	15	(Coster et al., 1989)
B	A	Anticline	80	109	55	5548	553	162	693	15	(Coster et al., 1989)
A	A	Anticline	130	138	69	4276	426	128	690	15	(Coster et al., 1989)

Table 9.2: CO_2 storage capacity estimates of the Durban Basin (E factors of Goodman et al., 2011).

CO_2 Storage Capacity	$MCO2 = A \times h \times \phi \times \rho CO2 \times E$	
Efficiency Factor (P90)	0.012	(Goodman et al., 2011)
Efficiency Factor (P50)	0.024	(Goodman et al., 2011)
Efficiency Factor (P10)	0.041	(Goodman et al., 2011)

Reservoir	Facies	Reservoir Description	Areal Extent (km^2)	Areal Extent (m^2)	Nett Thickness (m)	Porosity	CO_2 Density ($kg.m^{-3}$)	CO_2 Storage Capacity (Mt CO_2) (P90)	CO_2 Storage Capacity (Mt CO_2) (P50)	CO_2 Storage Capacity (Mt CO_2) (P10)
I	C2	Shelf Sand	1500	1.5E+09	50	0.30	663	180	360	614
H	C1	Basin-floor Fan	730	730000000	161	0.15	695	147	294	502
G	C1	Basin-floor Fan	10	10000000	123.5	0.15	679	2	3	5
F	B2	Shelf Sand	1500	1.5E+09	40	0.30	687	148	297	507
E	B1	Basin-floor Fan	280	280000000	180	0.2	681	82	165	281
D	B1	Basin-floor Fan	38	38000000	156	0.2	685	10	19	33
C	B1	Basin-floor Fan	93	93000000	234	0.2	692	36	72	123
B	B1	Basin-floor Fan	50	50000000	125	0.2	686	10	21	35
A	B1	Basin-floor Fan	120	120000000	142.5	0.2	691	28	57	97
					Subtotal Shelf Sand Reservoirs			328	656	1121
					Subtotal Basin Floor Fans			464	928	1585
							Total	644	1287	2199
CO_2 Storage Capacities for analogous systems										
Jubilee Field Ghana		Basin-floor Fan	110	110000000	90	0.2	695	17	33	56

CO_2 Storage Capacity	$MCO2 = A \times h \times \phi \times \rho CO2 \times E$	
Efficiency Factor (P90)	0.012	(Goodman et al., 2011)
Efficiency Factor (P50)	0.024	(Goodman et al., 2011)
Efficiency Factor (P10)	0.041	(Goodman et al., 2011)

Closure	Facies	Reservoir Description	Areal Extent (km^2)	Areal Extent (m^2)	Net Thickness (m)	Porosity	CO_2 Density ($kg.m^{-3}$)	CO_2 Storage Capacity (Mt CO_2) (P90)	CO_2 Storage Capacity (Mt CO_2) (P50)	CO_2 Storage Capacity (Mt CO_2) (P10)
E	C	Fault Closure	40	40000000	40	0.15	690	2	4	7
D	A	Anticline	60	60000000	66	0.15	684	5	10	17
C	A	Anticline	210	210000000	88	0.15	689	23	46	78
B	A	Anticline	80	80000000	55	0.15	693	5	11	19
A	A	Anticline	130	130000000	69	0.15	690	11	22	38
				Subtotal Fault Closures				2	4	7
				Subtotal Basement Anticlinal Closures				44	89	152
							Total	46	93	158

9.3 DISCUSSION

9.3.1 Storage capacities of Stratigraphic Traps within the Durban Basin

Initial storage estimates for the offshore basins of the east coast of South Africa (Viljoen et al., 2010) identified a theoretical CO_2 storage capacity of 42000 Mt (Table 9.3) based upon a net sandstone thickness of 60 m, over an area of ~81000 km^2 spanning the Durban and Zululand Basins. For their assessment, Viljoen et al. (2010) used a CO_2 density of 580 $kg.m^{-3}$, with an average porosity of 15% and an efficiency factor of 0.1. This was based upon calculations adapted from the US Department of Energy (US DOE, 2008). However, Broad et al. (2006) indicated that the Durban Basin has a total extent of only ~10000 km^2 to the 2500 m isobath, thereby leading Hicks et al. (2014) to propose a theoretical storage capacity of ~5200 Mt within the Durban Basin using Viljoen et al. (2010)'s criteria. Table 9.3 highlights a review of the identified potential storage reservoirs (this study) and previous data for the basin (Viljoen et al., 2010; Hicks et al., 2014) utilising the 0.1 E-factor of Viljoen et al. (2010). These can be compared with currently accepted E values defined by Goodman et al. (2011) which are now employed for this study (Table 9.2).

Table 9.3: CO_2 storage capacity estimates for stratigraphic traps utilising E factors of Viljoen et al. (2010).

CO_2 Storage Capacity	$MCO2 = A \times h \times \phi \times \rho CO2 \times E$
Efficiency Factor of Viljoen et al., (2010)	0.1

Reservoir	Facies	Reservoir Description	Areal Extent (km^2)	Areal Extent (m^2)	Net Thickness (m)	Porosity	CO_2 Density ($kg.m^{-3}$)	CO_2 Storage Capacity (Mt) (0.1 E)
I	C2	Shelf Sand	1500	1.5E+09	50	0.30	666	1499
H	C1	Basin-floor Fan	730	730000000	161	0.15	695	1225
G	C1	Basin-floor Fan	10	10000000	123.5	0.15	679	13
F	B2	Shelf Sand	1500	1.5E+09	40	0.30	687	1237
E	B1	Basin-floor Fan	280	280000000	180	0.2	681	686
D	B1	Basin-floor Fan	38	38000000	156	0.2	685	81
C	B1	Basin-floor Fan	93	93000000	234	0.2	692	301
B	B1	Basin-floor Fan	50	50000000	125	0.2	686	86
A	B1	Basin-floor Fan	120	120000000	142.5	0.2	691	236
							Total	5364

Reservoir	Facies	Reservoir Description	Areal Extent (km^2)	Areal Extent (m^2)	Nett Thickness (m)	Porosity	CO_2 Density ($kg.m^{-3}$)	CO_2 Storage Capacity (Mt) (0.1 E)
DBN/Zululand		Saline Aquifer	81000	8.1E+10	60	0.15	580	42282
Durban Basin		Saline Aquifer	10000	1E+10	60	0.15	580	5220

When utilising the 0.1 E-factor of Viljoen et al. (2010), a close relationship is observed between the ~5000 Mt theoretical storage capacity for the regional basin evaluation of Hicks et al. (2014) when compared with a combined storage capacity of ~5364 Mt as defined by volumetrics obtained in this study (Table 9.3). However, the initial estimates of Hicks et al. (2014) define only laterally extensive, shelf-bound saline aquifers, which here account for 2736 Mt storage at an E-factor of 0.1 (Table 9.3).

Although the estimates shown in Table 9.3 correlate well with the initial estimates of Viljoen et al. (2010) and Hicks et al. (2014), a more cautious approach (Goodman et al., 2011; Li et al., 2015) is deemed necessary for effective CO_2 storage capacity calculations. Therefore, the calculated results of this study, outlined in Table 9.2, suggest a total CO_2 storage capacity of 644 Mt at a P90 probability level (1,287 Mt at P50; 2,199 Mt at P10). These P90 estimates can be further subdivided into 328 Mt in deltaic and shelf confined sheet sands in Reservoirs F and I; and 464 Mt in delineated basin floor fan systems.

Although no capacity estimates have been undertaken on analogous basin floor fan deposits along the east African shelf, the potential basin floor fan reservoir systems identified in this study are comparable with storage capacity estimates (Table 9.2) compiled for fan systems within the Jubilee oilfield offshore Ghana (Dailly et al., 2013). In the Jubilee field, hydrocarbon plays occur in a 90 m thick, stacked succession of Turonian-age basin floor fan sandstones, with individual pay sands up to 35 m thick having porosities of ~20% (Dailly et al., 2013). Field statistics (Dailly et al., 2013) suggest that the play has an area of ~110 km^2 and net thickness of 40-90 m, comparable with dimensions defined for the facies B1 reservoirs in the Durban Basin. A determination of the effective CO_2 storage capacity of the Jubilee Field undertaken during this study, at P10 probability (Goodman et al. 2011), suggests a total storage capacity of 16 Mt CO_2, akin to the 10-36 Mt capacities defined for individual basin floor fan reservoirs in the Durban Basin (Table 9.2). As shown in analogous hydrocarbon-bearing systems within the Jubilee Field, basin floor fan systems characterize well-defined stratigraphic traps. It is therefore suggested that, dependent upon their injectivity potential (overpressure), sedimentology and net-gross ratios, the basin floor fan systems within the Durban Basin represent viable targets for CO_2 storage.

Laterally extensive inner shelf sheet sands and deltaic sandstones are confined to Reservoirs F and I respectively. Conservative (P90) storage capacity estimates for individual reservoirs (148 Mt Reservoir F; 180 Mt Reservoir I) are comparable with minimum estimates of 170 Mt CO_2 for regions of the Rotliegend sandstone in the North Sea (Wilkinson et al., 2013), as well as effective CO_2 storage capacities (160 Mt CO_2) identified for the Fushan sag within the Beibuwan Basin offshore China (Li et al., 2015).

Within the Mozambique Basin and coastal plain, the base data utilised by Solomon et al. (2014) for their basin-scale assessment, suggest a low-end, theoretical storage of 579 Mt CO_2 for sandstones of the Turonian-age Domo Formation; of which 163 Mt CO_2 storage potential is available in southern Mozambique. Similar low-end storage capacity estimates (E=0.04) of 228 Mt CO_2 (Chabangu et al., 2014) were indicated for Cenomanian-Turonian sandstones of the analogous lower St Lucia Formation in the onshore Zululand Basin in northern KwaZulu-Natal. Estimates defined for the Zululand and southern Mozambique coastal plain respectively compare well with the 148 Mt (P90) capacity defined here for the equivalent Turonian-age sandstone Reservoir F in facies B2.

A similar scenario occurs within reservoirs of the Maastrichtian-age, lower Grudja Formation in Mozambique. These occur in the context of the palaeo-Limpopo delta (Fig. 8.9). Solomon et al. (2014) indicate a low-end capacity of 1129 Mt CO_2 of which 369 Mt occurs within southern Mozambique. These values represent double the capacity when compared with the P90 estimate of 180 Mt CO_2 for Reservoir I in this study. Reservoir I however, is analogous with hydrocarbon-bearing sediments of the lower Grudja Formation in Mozambique, and it is therefore suggested that, based upon these correlations, the laterally extensive sandstone reservoirs F and I represent primary potential targets for CO_2 storage in the Durban Basin.

9.3.2 Storage capacities of Structural Traps within the Durban Basin

Although multiple structural traps are identified within the Durban Basin, these remain largely undrilled and therefore lack detailed core and volumetric data. The calculated results for potential CO_2 storage capacities within undrilled stratigraphic closures are outlined in Table 9.2. A total CO_2 storage capacity of 46 Mt CO_2 at a P90 probability level (93 Mt - P50; 158 Mt – P10) is estimated. These values can further be subdivided into two closure types. Faulted rollover anticlinal closures within the basin account for 2 Mt potential CO_2 storage at a P90 probability level (4 Mt - P50; 7 Mt – P10); whilst compactional anticlinal closures overlying basement structures account for 44 Mt potential CO_2 storage capacity at a P90 level (89 Mt – P50; 152 Mt – P10).

The identification of commercial oil and gas fields in the Mozambique coastal plain (Coster et al., 1989) and offshore fields within the Rovuma Basin (Carneiro and Alberto, 2014) to the north of the study area suggest the potential for suitable structural traps and associated reservoir systems within the Durban Basin as discussed in Chapter 8. Davids (2009) identified multiple potential leads within the Durban Basin with Roux (2009) defining a Prospective Resource (high estimate) of more than 20 Tcf gas and 3 billion barrels of oil. Viljoen et al. (2010), based upon the volumetric calculations defined by Davids (2009), suggested a theoretical storage capacity of ~205 Mt CO_2 (117 Mt – Gas reservoirs; 88 Mt – Oil Reservoirs) within potential oil and gas reservoirs within the Durban Basin. It must be noted however that, oil or gas reserves have yet to be discovered in the area.

CO_2 storage capacities defined during this study are comparable with storage capacities defined by Gibson-Poole et al. (2008) for structural closures within the Gippsland Basin, southeast Australia. The Gippsland Basin in south-eastern Australia has a similar geological evolution to the Durban Basin, represented by Early Cretaceous rifting associated with the breakup of Gondwana, followed by post-rift passive margin sediment deposition (Gibson-Poole et al., 2008). Compressional tectonism within the basin during the Eocene however, led to the formation of numerous NE trending anticlines that host large hydrocarbon accumulations and form the focus of CO_2 storage assessments (Gibson-Poole et al., 2008). Gibson-Poole (2008) propose individual storage capacities ranging from 0.6 to 577 Mt CO_2, with a total capacity of 2073.2 Mt for 32 anticlinal closures. Capacities defined in this study for the Durban Basin are comparable with values defined for the Fortescue and Kingfish oilfields within the Gippsland Basin.

Dynamic CO_2 capacities of 121 Mt defined for the voluminous Forties hydrocarbon field in the North Sea (Babaei et al., 2016) are comparable with conservative P90 estimates for Closure C in the Durban Basin. Babaei et al. (2016) further propose an additional 24 Mt CO_2 storage capacity within the Nelson Dome in the North Sea. Although far less than the capacities defined for the Forties structure, the capacities defined for the Nelson Dome are similar to conservative P90 capacities defined in this study for Closures D and E within the Durban Basin.

9.4 QUANTIFYING UNCERTAINTIES OF ANALOGOUS DATA

In the case of the Durban Basin as with similar frontier basins (cf. Green et al., 2014), uncertainties are high due to a dearth of core data. However, the use of analogous data is common practice worldwide with hydrocarbon discoveries in French Guiana utilising only seismic, gravity and magnetic data, coupled with analogous data from equatorial African discoveries (Green et al., 2014). The quantification of risk and uncertainties of reservoir conditions are commonly conducted using simplifications and conservatisms built into reservoir simulation models (Kahnt et al., 2015). In any given project a realistic degree of uncertainty must be accepted. Ringrose and Simone, (2009) suggest that at least 50% uncertainty can be defined in early project stages but this does not commonly reduce below 10% even in a mature project.

Within this study, data from analogous successions give representative estimations of the potential reservoir conditions within the Durban Basin. This can be defined through largely consistent values obtained by various authors for the Domo and Grudja Formations in Mozambique (Table 9.4). However, the potential for variations

in facies between the known analogues and the Durban Basin cannot be discounted. Furthermore core data do not exist for the basin floor fans systems mapped within the Durban Basin, thereby leading to a large uncertainty in the injectivity potential for these reservoirs.

Table 9.4: Average reservoir characteristics from known analogous systems in Mozambique and Zululand with available data shown.

Reservoir	Sand Thickness (m)	Porosity %	Permeability (mD)	Data Source
Grudja	30 - 45	20 - 30		Nairn et al., (1991)
Grudja	16	15-30		Coster et al., (1989)
Grudja		15-35		Solomon et al., (2014)
Domo Sand	40 - 45	20 - 25		Nairn et al., (1991)
Domo Sand	40	28		Coster et al., (1989)
Domo Sand		7.5 - 25		Solomon et al., (2014)
Domo Sand		15 -35	20 - 229mD	Chabangu et al., (2014)

A major risk associated with injecting large quantities of CO_2 into a subsurface reservoir is pressure build-up (Oruganti and Bryant, 2009). Cavanagh and Wildgust (2011) suggest that over-pressurization may lead to poor injectivity, caprock failure, CO_2 leakage, and brine displacement via uncontrolled migration with such impacts having major consequences upon the technical and economic viability of a project. Natural overpressure is commonly associated with thick shale/mudstone sequences in deepwater hydrocarbon systems, and may lead to a reduction in injectivity potential within a specific reservoir (Green et al., 2014). Green et al. (2014) however, suggest that feeder channels associated with basin floor fan systems act as pressure release conduits, allowing depressurization of the fan system to create a mobile aquifer similar to fan systems in the North Sea. Cavanagh and Wildgust (2011) suggest that, in general, concerns regarding pressurization and brine displacement in existing CCS projects are largely model-driven due to a scarcity of data, with pressure prediction models relying on hypothetical ranges and conceptual constraints for likely scenarios. Although reservoir conditions data are lacking for the Durban Basin, a zone of overpressure was noted in Jc-B1 within basement lithologies below the Cretaceous and Cenozoic reservoir plays (GGS, 1983). In all other wells, no overpressure was identified suggesting the possibility of open systems that may allow for good injectivity. This however, will need further modelling for both open and closed systems to define likely scenarios.

It is therefore proposed that, although data are only at a regional scale in the Durban Basin, volumetric calculations based upon detailed seismo-stratigraphic interpretations coupled with reservoir property data from analogous successions still provide new evidence of reservoir/seal pairs in saline aquifers. These may represent potential storage sites for CO_2 injection. The lack of overpressures in the Jc-series wells suggests potential injectivity for CO_2 storage within the mapped basin floor fans systems, as well as laterally extensive shallow marine shelf sands.

CHAPTER 10

CONCLUSIONS

A CO_2 storage capacity estimate of a particular sedimentary basin cannot be undertaken without detailed investigation of the active depositional regimes and evolution of the sedimentary succession. Geological characterisation is greatly enhanced through seismic sequence stratigraphic analysis, with the identification of reservoir/seal pairs and their integral association with depositional systems tracts and erosional unconformity surfaces (sequence boundaries).

The Mesozoic offshore Durban Basin, developed on the eastern margin of southern Africa, has a complex depositional history with sedimentation interrupted by protracted periods of erosion or non-deposition related to epeirogenic uplift as well as local and global sea-level fluctuations. This study provides the first comprehensive sedimentological and seismo-stratigraphic analysis of offshore data allowing for the recognition of multiple phases of margin growth within the late Mesozoic and Cenozoic including, initial sheared, syn-rift, structurally-defined sedimentation, followed by incipient ramp development, and finally progradational sedimentary shelf propagation.

Through the use of legacy, single-channel 2D seismic reflection profiles combined with well log and geophysical data from four (4) offshore wells drilled on the continental shelf, seismic stratigraphic models for the evolution of the basin are presented. These models indicate that sedimentation within the basin is represented by six individual sedimentary successions (Units A-F), separated by regional sequence boundaries. Sedimentation occurred predominantly during normal regressive conditions with the basin dominated by the progradation of the constructional submarine delta (Tugela Cone) during sea-level lowstands.

Initial deposition within the basin was controlled predominantly by tectonic events during the final stages of Gondwana breakup, with fluvial to marine deposition (Unit A) in a narrow, sheared, structurally bounded basin similar to other rifted margins globally. Unlike the continental margin of northern and southern KwaZulu-Natal, the Durban Basin is represented by major sediment input from fast flowing river systems with the construction of a shallow planar ramp margin (Unit B) in the Middle Cretaceous. This period was characterised by deep water deposition of basin floor fans systems during lowstand conditions.

Tectonism and active basin spreading had ceased by the Middle Cretaceous, resulting in the formation of a combined structural–sedimentary shelf (Unit C), with passive margin settings dominating the late Cretaceous and Cenozoic. Increased sediment supply associated with a Campanian lowstand led to the formation of the proto-shelf, nucleated close to the original structural shelf break on the Turonian ramp. The formation of this feature marked the change from ramp-dominated to shelf-edge sedimentation within the basin.

Late Cretaceous and Cenozoic sedimentation (Units C-F) is dominated by deltaic deposition through high sediment flux and off-shelf sediment-forcing during sea level lowstands. South-eastern Africa was subject to polycyclic epeirogenic uplift throughout the Cenozoic with a prominent period of uplift and associated canyon incision (erosional surface S4) occurring in the mid-Oligocene. Further uplift occurred in the mid-Miocene (erosional surface S5) and again in the Pliocene (erosional surface S6).

This study shows for the first time, a mid-Miocene seismic reflection surface S5 defining an erosional unconformity that can be correlated across the entire southern African continental shelf and slope. The formation of the S5 erosional surface and its associated submarine canyons is here inferred to relate to a mid-Miocene period of combined epeirogenic uplift and eustatic sea-level fall within the eastern portion of southern Africa.

Within the basin, the mid-Miocene sequence boundary truncates and incises a mixed carbonate-siliciclastic sediment wedge (Unit D) in the northern region of the basin. To the south however, the basin was marked by a

shallow ramp margin with a wide palaeo-continental rise. The inheritance of these geomorphological features later influenced subsequent erosion morphologies due to the antecedent control exerted by the two different gradients. Antecedent control and localised variability in depositional regimes led to the formation of two genetically variable canyon systems within the mid-Miocene palaeo-slope. Type I linear canyons (central and northern) are correlated with high sediment influx of likely coarse-grained material with downslope eroding gravity flows and turbidites causing scouring of the underlying substrate. The southern Type II canyon system has developed on a relatively sediment-starved, shallow angle slope in relation to its counterparts, dominated by mud-rich infill. The sinuous nature of the southern canyon appears to be related to subdued slope gradients in this region of the basin.

The association of canyon incision with a regionally developed, shelf/slope confined unconformity surface can be explained by changes in relative sea level as a result of global eustatic sea-level fall, combined with epeirogenic uplift of south-eastern Africa during the mid-Miocene. It is likely that the mid-Miocene event identified here is further related to rapid enlargement of the mid-Miocene Antarctic ice sheets at ~13Ma, and changes in deep oceanic current circulation patterns. The combination of these processes have had profound effects on the stratigraphic architecture of the offshore southern African basins in the form of erosion, sediment bypassing and slope sedimentation.

Through detailed seismo-sedimentary analysis of the basin-fill succession, multiple previously undefined and regionally pervasive stratigraphic traps have been delineated within Units B and C. These systems are correlated with analogous hydrocarbon-bearing sequences over a large region of the south-east African continental shelf. Increased sedimentation associated with forced regression and the formation of the S2 erosional surface during the Turonian LST, lead to the coeval deposition of potentially sand-rich distal submarine fan systems on the palaeo-slope (Reservoirs A-E) and proximal inner shelf, sheet sandstones (Reservoir F). Another sea level lowstand in the late Cretaceous lead to the deposition of a truncated, forced regressive shelf-edge delta (Reservoir I) in the inner shelf, with Reservoirs G and H formed as coeval submarine slope and basin floor fans.

Storage capacity estimates of individual reservoirs are undertaken based upon P90, P50, and P10 probability levels, with specific efficiency data obtained from Goodman et al. (2011). The initial assessment suggests a conservative total CO_2 storage capacity of 644 Mt at a P90 probability level (1287 Mt at P50; 2199 Mt at P10). This can be subdivided into 328 Mt in deltaic and shelf confined sheet sands in Reservoirs F and I; and 464 Mt in basin floor fan systems. Estimated capacities for saline formations are comparable with estimates for neighbouring sedimentary basins and others worldwide.

Potential structural traps identified within the Durban Basin include compactional anticline structures comprising sediment drapes covering deep-seated basement horst structures. Although four anticlinal features are identified within the basin most are undrilled, only Closure D has been prospected by the Jc-D1 well. Potential CO_2 storage capacities for undrilled structural closures are calculated to be 46 Mt CO_2 at a P90 probability level (93 Mt - P50; 158 Mt – P10). These values can further be subdivided into two closure types. Faulted rollover anticlinal closures within the basin account for 2 Mt potential CO_2 storage at a P90 probability level (4 Mt - P50; 7 Mt – P10); whilst compactional anticlinal closures overlying basement structures account for 44 Mt potential CO_2 storage capacity at a P90 level (89 Mt – P50; 152 Mt – P10). Estimated storage capacities defined for structural closures within the Durban Basin are comparable with estimates for similar closures in Australia and the North Sea.

Evidence of commercial-scale oil and gas fields in analogous sedimentary successions within the neighboring Mozambique Basin provides support for the potential for CO_2 storage capacities within the Durban Basin. Prospective storage sites are individually defined and are comparable with sedimentary and structural trap sites around the southern African continental shelf, as well as within CO_2 storage sites defined internationally. This study therefore provides a basin-scale, effective CO_2 storage capacity estimation with site-specific characterisation and capacity estimations for both sedimentological and stratigraphical traps within the Durban Basin, east coast of South Africa.

REFERENCES

Adewole, E.O., Healy, D., 2017. Systematic assessment of fault stability in the Northern Niger Delta Basin, Nigeria: Implication for hydrocarbon prospects and increased seismicities. Tectonophysics, 699, 227-243.

Anderson, W., 1906. On the geology of the Bluff bore, Durban, Natal. Transactions of the Geological Society of South Africa, 9, 111-116.

Babaei, M., Govindan, R., Korre, A., Shi, J.Q., Durucan, S., Quinn, M., 2016. Calculation of pressure- and migration-constrained dynamic CO_2 storage capacity of the North Sea Forties and Nelson dome structures. International Journal of Greenhouse Gas Control, 53, 127–140.

Bachu, S., 2003. Screening and ranking of sedimentary basins for sequestration of CO_2 in geological media in response to climate change. Environmental Geology, 44, 277-289.

Bachu, S., 2008. Comparison between Methodologies Recommended for Estimation of CO_2 Storage Capacity in Geological Media by the CSLF Task Force on CO_2 Storage Capacity Estimation and the USDOE Capacity and Fairways Subgroup of the Regional Carbon Sequestration Partnerships Program, Phase III Report, 21pp.

Bachu, S., 2015. Review of CO_2 storage efficiency in deep saline aquifers. International Journal of Greenhouse Gas Control, 40, 188–202.

Bachu, S., Adams, J.J., 2003. Sequestration of CO_2 in geological media in response to climate change: capacity of deep saline aquifers to sequester CO_2 in solution. Energy Conversion and Management, 44 (20), 3151-3175.

Bachu, S., Bonijoly, D., Bradshaw, J., Burruss, R., Holloway, S., Christensen, N.P., Maathiassen, O.M., 2007. CO_2 storage capacity estimation: methodology and gaps. International Journal of Greenhouse Gas Control, 1 (4), 430–443.

Ben-Avraham, Z., Hartnady, C.J.H., Kitchin, K.A., 1997. Structure and tectonics of the Agulhas-Falkland fracture zone. Tectonophysics, 282, 83-98.

Ben-Avraham, Z., Hartnady, C.J.H., Malan, J.A., 1993. Early tectonic extension between the Agulhas Bank and Falkland Plateau due to rotation of the Lafonia microplate. Earth and Planetary Science Letters, 117, 43-58.

Borissova, I., Kennard, J., Lech, M., Wang, L., Johnston, S., Lewis, C., Southby, C., 2013. Integrated approach to CO_2 storage assessment in the offshore South Perth Basin, Australia. Energy Procedia, 37, 4872-4878.

Bouma, A. H., 1962. Sedimentology of some flysch deposits: A graphic approach to facies interpretation. Amsterdam: Elsevier, 168pp.

Bouma, A.H., 2000. Coarse-grained and fine-grained turbidite systems as end member models: applicability and dangers. Marine and Petroleum Geology, 17, 137-143.

Bouma, A.H., Normark, W.R., Barnes, N.E. (Eds.), 1985. Submarine Fans and Related Turbidite Systems. Springer- Verlag, New York, 351pp.

Bradshaw, J., Bachu, S., Bonijoly, D., Burruss, R., Holloway, S., Christensen, N.P., Mathiassen, O.M., 2007. CO_2 storage capacity estimation: issues and development of standards. International Journal of Greenhouse Gas Control, 1, 62–68.

Bradshaw, J., Bradshaw, B.E., Allinson, G., Rigg, A.J., Nguyen, V., Spencer, L., 2002. The potential for geological sequestration of CO_2 in Australia: preliminary findings and implications for new gas field development. The APPEA Journal, 42 (1), 25-46.

Bradshaw, J., Dance, T., 2005. Mapping geological storage prospectivity of CO_2 for the worlds sedimentary basins and regional source to sink matching. In: Rubin, E. Keith, D. and Gilboy, C., (Eds.), Greenhouse Gas Control Technologies, 7th International Conference on Greenhouse Gas Control Technologies, 5-9 September 2004, Vancouver, 1 (4), 583-592.

Broad, D.S., Jungslager, E.H.A., McLachlan, I.R., Roux, J., 2006. Offshore Mesozoic Basins. In: Johnson, M.R., Anhaeusser, C.R., Thomas, R.J. (Eds.), The Geology of South Africa. Geological Society of South Africa, Johannesburg/Council for Geoscience, Pretoria, 553-571.

Brown, L.F. Jr., Fisher, W.L., 1977. Seismic stratigraphic interpretation of depositional systems: examples from Brazilian rift and pull apart basins. In: Payton, C.E. (Ed.) Seismic Stratigraphy–Applications to Hydrocarbon Exploration. American Association of Petroleum Geologists Memoir, 26, 213–248.

Brown, R.W., Summerfield, M.A., Gleadow, A.J.W., 2002. Denudational history along a transect across the Drakensberg Escarpment of southern Africa derived from apatite fission track thermochronology. Journal of Geophysical Research, 107, B12, 2350, 18pp.

Burke, K., Gunnell, Y., 2008. The African Erosion Surface: A continental-scale synthesis of geomorphology, tectonics, and environmental change over the past 180 Million years. Geological Society of America Memoir, 201. 66pp.

Carman, G.J., Young, R., 1981. Reservoir geology of the Forties Oilfield. Petroleum geology of the continental shelf of north-west Europe. Institute of Petroleum, London, 371-379.

Carneiro, J.F., Alberto, M., 2014. Preliminary assessment of CO_2 storage potential in the Rovuma sedimentary basin, Mozambique. Energy Procedia, 63, 5141 – 5152.

Carvajal, C., Steel, R., Petter, A., 2009. Sediment supply: The main driver of shelf-margin growth. Earth-Science Reviews, 96 (4), 221-248.

Castelino, J.A., Reichert, C., Klingelhoefer, F., Aslanian, D., Jokat, W., 2015. Mesozoic and Early Cenozoic sediment influx and morphology of the Mozambique Basin. Marine and Petroleum Geology, 66, 890-905.

Catuneanu, O., 2006. Principles of sequence stratigraphy. Elsevier, Oxford, 375pp.

Catuneanu, O., Abreu, V., Bhattacharya, J.P., Blum, M.D., Dalrymple, R.W., Eriksson, P.G., Fielding, C.R., Fisher, W.L., Galloway, W.E., Gibling, M.R., Giles, K.A., Holbrook, J.M., Jordan, R., Kendall, C.G.St.C., Macurda, B., Martinsen, O.J., Miall, A.D., Neal, J.E., Nummedal, D., Pomar, L., Posamentier, H.W., Pratt, B.R., Sarg, J.F., Shanley, K.W., Steel, R.J., Strasser, A., Tucker, M.E., Winker, C., 2009. Towards the standardization of sequence stratigraphy. Earth-Science Reviews, 92, 1-33.

Catuneanu, O., Galloway, W.E., Kendall, C.G.St. C., Miall, A.D., Posamentier, H.W., Strasser, A., Tucker, M.E., 2011. Sequence Stratigraphy: Methodology and Nomenclature. Newsletters on Stratigraphy, 44 (3), 173-245.

Catuneanu, O., Zecchin, M., 2013. High-resolution sequence stratigraphy of clastic Shelves II: Units and bounding surfaces. Marine and Petroleum Geology, 39, 26-38.

Cavanagh, A., Wildgust, N., 2011. Pressurization and brine displacement issues for deep saline formation CO_2 storage. Energy Procedia, 4, 4814-4821.

Cawthra, H.C., Neumann, F.H., Uken, R., Smith, A.M., Gauastella, L.A., Yates, A., 2012. Sedimentation on the narrow (8km wide), oceanic current-influenced continental shelf off Durban, KwaZulu-Natal, South Africa. Marine Geology 323-325, 107-122.

Chabangu, N., Beck, B., Hicks, N., Botha, G., Viljoen, J., Davids, S., Cloete, M., 2014. The investigation of CO_2 storage potential in the Zululand Basin in South Africa. Energy Procedia, 63, 2789-2799.

Cloete, M., 2010 (compiler). Atlas on the geological storage of carbon dioxide in South Africa. Council for Geoscience South Africa, 18 pp.

CO2CRC, 2008. Storage Capacity Estimation, Site Selection and Characterisation for CO_2 Storage Projects. CO2CRC Report No: RPT08-1001, 60pp.

Cook, P.J., 2012. Clean Energy, Climate and Carbon. CO2CRC, CSIRO Publishing, Australia. 215pp.

Cooper, J.A.G, Green, A.N., Smith, A.M., 2013. Vertical stacking of multiple highstand shoreline deposits from the Cretaceous to the present: facies development and preservation. Journal of Coastal Research, 65, 1904-1908.

Cornell, D.H., Thomas, R.J., Moen, H.F.G., Reid, D.L., Moore, J.M., Gibson, R.L., 2006. The Namaqua-Natal Province. In: Johnson, M.R., Anhaeusser, C.R., Thomas, R.J., (Eds.), The Geology of South Africa. Geological Society of South Africa, Johannesburg/Council for Geoscience, Pretoria, pp. 325–380.

Coster, P.W., Lawrence, S.R., Fortes, G., 1989. Mozambique: a new geological framework for hydrocarbons exploration. Journal of Petroleum Geology, 12 (2), 205-230.

Covault, J.A., Fildani, A., Romans, B.W., McHargue, T., 2011. The natural range of submarine canyon-and-channel longitudinal profiles. Geosphere, 7 (2), 313-332.

CSLF (Carbon Sequestration Leadership Forum), 2005. A Taskforce for Review and Development of Standards with Regards to Storage Capacity Measurement; CSLF-T-2005-9 15, 16pp.

CSLF (Carbon Sequestration Leadership Forum), 2008. Comparison between methodologies recommended for estimation of CO_2 storage capacity in geological media by the CSLF Task Force on CO_2 storage capacity estimation and the USDOE Capacity and Fairways Subgroup of the Regional Carbon Sequestration Partnerships Program. 17pp.

Dailly, P., Henderson, T., Hudgens, E., Kanschat, K., Lowry, P., 2013. Exploration for Cretaceous stratigraphic traps in the Gulf of Guinea, West Africa and the discovery of the Jubilee Field: a play opening discovery in the Tano Basin, Offshore Ghana. In: Mohriak, W. U., Danforth, A., Post, P. J., Brown, D. E., Tari, G. C., Nemcok, M. and Sinha, S. T. (Eds.), Conjugate Divergent Margins. Geological Society, London, Special Publications, 369, 235-248.

Davids, S., 2009. Republic of South Africa, 2009 Licence Round: Tugela Licence Area. Petroleum Agency South Africa, internal publication, 38pp.

de Almeida, N.M., Vital, H., Gomes, M.P., 2015. Morphology of submarine canyons along the continental margin of the Potiguar Basin, NE Brazil. Marine and Petroleum Geology, 68, 307-324.

de Lépinay, M.M., Loncke, L., Basile, C., Roest, W.R., Patriat, M., Maillard, A. De Clarens, P., 2016. Transform continental margins – Part 2: A worldwide review. Tectonophysics, 693, Part A, 96–115.

de Wit, M., 2007. The Kalahari Epeirogeny and climate change: differentiating cause and effect from core to space. South African Journal of Geology, 110, 367-392.

Di Celma, C., 2011. Sedimentology, architecture, and depositional evolution of a coarse-grained submarine canyon fill from the Gelasian (early Pleistocene) of the Peri-Adriatic basin, Offida, central Italy. Sedimentary Geology, 238, 233-253.

Dingle, R.V., Goodlad, S.W., Martin, A.K., 1978. Bathymetry and stratigraphy of the northern Natal Valley (SW Indian Ocean). A preliminary report. Marine Geology, 28, 89-106.

Dingle, R.V., Siesser, W.G., Newton, A.R., 1983. Mesozoic and Tertiary Geology of Southern Africa. Balkema, Rotterdam, 375pp.

Du Toit, S.R., Leith, M.J., 1974. The J(c)-1 bore-hole on the continental shelf near Stanger, Natal. Transactions of the Geological Society of South Africa, 77, 247-252.

Ehrenberg, S.N., Nadeau, P.H., 2005. Sandstone vs. carbonate petroleum reservoirs: A global perspective on porosity-depth and porosity permeability relationships. American Association of Petroleum Geologists Bulletin, 89 (4), 435-445.

Embry, A. F., Catuneanu, O., 2001. Practical Sequence Stratigraphy: Concepts and Applications. Canadian Society of Petroleum Geologists, short course notes, 167pp.

Embry, A. F., Catuneanu, O., 2002. Practical Sequence Stratigraphy: Concepts and Applications. Canadian Society of Petroleum Geologists, short course notes, 147pp.

Emery, D., Myers, K. J., 1996. Sequence Stratigraphy. Oxford, U. K., Blackwell, 297pp.

Engelbrecht, A., Golding, A., Hietkamp, S., Scholes, B., 2004. The potential for sequestration of carbon dioxide in South Africa, Process Technology Centre, CSIR, Report 86DD/HT339, 54 pp.

Flores, G., 1973. The Cretaceous and Tertiary sedimentary basins of Mozambique and Zululand. In: Blant, G. (Ed), Sedimentary Basins of the African Coasts. 2nd Part. Association of African Geological Surveys, Paris, 81-111.

Flower, B.P., Kennett, J.P., 1994. The middle Miocene climatic transition: East Antarctic ice sheet development, deep ocean circulation and global carbon cycling. Palaeogeography, Palaeoclimatology, Palaeoecology, 108, 537-555.

Flowers, R.M., Schoene, B., 2010. (U–Th)/He thermochronometry constraints on unroofing of the eastern Kaapvaal craton and significance for uplift of the southern African Plateau. Geology, 38, 827–830.

Förster, R., 1975. The geological history of the sedimentary basin of southern Mozambique, and some aspects of the origin of the Mozambique Channel. Palaeogeography Palaeoclimatology Palaeoecology, 17, 267-287.

Frankel, J.J., 1966. Basal rocks of the Tertiary at Uloa, Zululand, South Africa. Geological Magazine, 103 (3), 214-234.

Frankel, J.J., 1969. Correspondence: The ages of Tertiary Rocks at Uloa and Umkwelane, Zululand, and their Geomorphological Significance. Geological Magazine, 106 (2), 206-211.

Fulthorpe, C.S., Austin Jr, J.A., Mountain, G.S., 2000. Morphology and distribution of Miocene slope incisions off New Jersey: Are they diagnostic of sequence boundaries? GSA Bulletin, 112 (6), 817–828.

Galloway, W.E., 1989. Genetic stratigraphic sequences in basin analysis, I: Architecture and genesis of flooding-surface bounded depositional units. American Association of Petroleum Geologists Bulletin, 73, 125-142.

Galloway, W.E., 2002. Paleogeographic setting and depositional architecture of a sand-dominated shelf depositional system, Miocene Utsira Formation, North Sea Basin. Journal of Sedimentary Research, 72 (4), 476-490.

Geological Survey, 1984. 1:000000 scale geological map sheets (NE & SE sheets), Pretoria, Government Printer.

Gerber, T.P., Amblas, D., Wolinsky, M.A., Pratson, L.F., Canals, M., 2009. A model for the long-profile shape of submarine canyons. Journal of Geophysical Research, 114, F03002.

Gerrard, I., 1972a. Report on progress on the evaluation of the Zululand Basin. Report, SOEKOR, PSV 1325 (unpubl.)

Gerrard, I., 1972b. Depth-pressure, salinity and potentiometric surface data from the onshore Cretaceous Zululand Basin. Report, SOEKOR, PSV 2274 (unpubl.), 79pp.

Gerrard, I., Wood, M., 1978. Recommendation to drill Borehole Jc-B1 in Block Jc on the Tugela Bank, Republic of South Africa. Report, SOEKOR (unpubl.), 70pp.

GGS (Gearhart Geodata Services), 1983. Well completion report, Jc-B1 Durban Basin, East Coast, R.S.A. Soekor report No. ACT-2, 7pp.

Gibson-Poole, C.M., 2009. Site Characterisation for Geological Storage of Carbon Dioxide: Examples of Potential Sites from the North West Shelf, Australia. Unpublished PhD Thesis, Australian School of Petroleum, University of Adelaide, 422pp.

Gibson-Poole, C.M., Svendsen, L., Underschultz, J.R., Watson, M.N., Ennis-King, J., van Ruth, P.J., Nelson, E.J., Daniel, R.F., Cinar, Y., 2008. Site characterisation of a basin-scale CO_2 geological storage system: Gippsland Basin, southeast Australia. Environmental Geology, 54 (8), 1583-1606.

Global CCS Institute, 2015. The Global Status of CCS: 2015, Summary Report, Melbourne, Australia. 18pp.

Global CCS Institute, 2016. The Global Status of CCS: 2016. Summary Report, Australia. 28pp.

Gong, C., Wang, Y., Steel, R. J., Olariu, C., Xu, Q., Liu, X., Zhao, Q., 2015. Growth styles of shelf-margin clinoforms: Prediction of sand- and sediment-budget partitioning into and across the shelf. Journal of Sedimentary Research, 85 (3), 209-229.

Goodlad, S.W., 1986. Tectonic and sedimentary history of the mid-Natal Valley (S.W. Indian Ocean).Bulletin of Joint Geological Survey/University of Cape Town Marine Geoscience Unit, 15, 415pp.

Goodlad, S.W., Martin, A.K., Hartnady, C.J.H., 1982. Mesozoic magnetic anomalies in the southern Natal Valley. Nature, 295, 686-688.

Goodman, A., Hakala, A., Bromhal G., Deel, D., Rodosta, T., Frailey, S., Small, M., Allen, D., Romanov, V., Fazio, J., Huerta, N., McIntyre, D., Kutchko, B., Guthrie, G., 2011. U.S. DOE methodology for the development of geologic storage potential for carbon dioxide at the national and regional scale. International Journal of Greenhouse Gas Control, 5, 952-965.

Goudie, A., 2005. The drainage of Africa since the Cretaceous. Geomorphology, 67, 437–456.

Green, A.N., 2009a. Sediment dynamics on the narrow, canyon-incised and current swept shelf of the northern KwaZulu-Natal continental shelf, South Africa, Geo-Marine Letters, 29 (4), 201-219.

Green, A.N. 2009b. Palaeo-drainage, incised valley fills and transgressive systems tract sedimentation of the northern KwaZulu-Natal continental shelf, South Africa, SW Indian Ocean. Marine Geology, 263, 46-63.

Green, A.N., 2011a. The late Cretaceous to Holocene sequence stratigraphy of a sheared passive upper continental margin, northern KwaZulu-Natal, South Africa. Marine Geology, 289, 17-28.

Green, A.N., 2011b. Submarine canyons associated with alternating sediment starvation and shelf-edge wedge development: Northern KwaZulu-Natal continental margin, South Africa. Marine Geology, 284, 114-126.

Green, A.N., Garlick, L.G., 2011. A sequence stratigraphic framework for a narrow, current-swept continental shelf: The Durban Bight, central KwaZulu-Natal, South Africa. Journal of African Earth Sciences, 60, 303-314.

Green, A.N., Dladla, N., Garlick, G.L., 2013. Spatial and temporal variations in incised valley systems from the Durban continental shelf, KwaZulu-Natal, South Africa. Marine Geology, 335, 148-161.

Green, A.N., Goff, J.A., Uken, R., 2007, Geomorphological evidence for upslope canyon-forming processes on the northern KwaZulu-Natal shelf, South Africa, SW Indian Ocean, Geo-Marine Letters, 27, 399–409.

Green, A.N., Ovechkina, M., Uken, R., 2008. Nannofossil age constraints for the northern KwaZulu-Natal shelf-edge wedge: Implications for continental margin dynamics, South Africa, SW Indian Ocean. Continental Shelf Research, 28, 2442-2449.

Green, A.N., Uken, R., 2008. Submarine landsliding and canyon evolution from the northern KwaZulu-Natal continental shelf, South Africa, SW Indian Ocean, Marine Geology, 254, 152-170.

Green, C.P., Ennis-King, J., 2013. Convective mixing in geological storage of CO_2. Earth Science and Resource Engineering, CSIRO, ANLEC project 7-1011-1090, 24pp.

Green, S., O'Connor, S.A., Edwards, A.P., Carter, J.E., Cameron, D.E.L., Wright, R., 2014. Understanding potential pressure regimes in undrilled Labrador deep water by use of global analogues. Leading Edge, 33 (4), 414–416.

Guillocheau, F., Rouby, D., Robin, C., Helm, C., Rolland, N., Le Carlier de Veslud, C., Braun, J., 2012. Quantification and causes of the terrigenous sediment budget at the scale of a continental margin: a new method applied to the Namibia- South Africa margin. Basin Research, 24, 3-30.

Haddon, I.G., McCarthy, T.S., 2005. The Mesozoic–Cenozoic interior sag basins of Central Africa: The Late-Cretaceous–Cenozoic Kalahari and Okavango basins. Journal of African Earth Sciences, 43, 316-333.

Hagen, R.A., Bergersen, D.D., Moberly, R., Coulbourn, W.T., 1994. Morphology of a large meandering submarine canyon system on the Peru-Chile forearc. Marine Geology, 119, 7-38.

Haq, B.U., Hardenbol, J., Vail, P.R., 1987. Chronology of Fluctuating Sea Levels since the Triassic. Science, 235, 1156-1167.

Haq, B.U., Hardenbol, J., Vail, P.R., 1988. Mesozoic and Cenozoic Chronostratigraphy and cycle of sea-level change. In: Wigus, C.K., Hastings, B.S., Posamentier, H., Van Wagoner, J., Ross, C.A., Kendall, C.G.St. C. (Eds.), Sea-level changes – An integrated approach. Society of Economic Paleontologists and Mineralogists Special Publication No 42. 411pp.

Harris, P.T., Whiteway, T., 2011. Global distribution of large submarine canyons: Geomorphic differences between active and passive continental margins. Marine Geology, 285, 69–86.

Hartnady, C.J.H., 1990. Seismicity and plate boundary evolution in southeastern Africa. South African Journal of Geology, 93(3), 473–484.

Heezen, B.C., Hollister, C.D., Ruddiman,W.F., 1966. Shaping of the continental rise by deep geostrophic contour currents. Science, 152, 502-508.

Helland-Hansen, W., Steel, R.J., Sømme, T.O., 2012. Shelf genesis revisited. Journal of Sedimentary Research, 82, 133–148.

Heller, P.L., Dickinson, W.R., 1985. Submarine ramp facies model for delta-fed, sand-rich turbidite systems. American Association of Petroleum Geologists Bulletin, 69 (6), 960-976.

Hicks, N., Davids, S., Beck, B., Green, A.N., 2014. Investigation of CO_2 storage potential of the Durban basin in South Africa. Energy Procedia, 63, 5200-5210.

Hicks, N., Green, A.N., 2016. Sedimentology and depositional architecture of a submarine delta-fan complex in the Durban Basin, South Africa. Marine and Petroleum Geology, 78, 390-404.

Hicks, N., Green, A.N., 2017a. A Mid-Miocene erosional unconformity from the Durban Basin, SE African margin: A combination of global eustatic sea level change, epeirogenic uplift, and ocean current initiation. Marine and Petroleum Geology, 86, 798-811.

Hicks, N., Green, A.N., 2017b. A first assessment of potential stratigraphic traps for geological storage of CO_2 in the Durban Basin, South Africa. International Journal of Greenhouse Gas Control, 64, 73-86.

Holbourn, A., Kuhnt, W., Schulz, M., Flores, J.A., Andersen, N., 2007. Orbitally-paced climate evolution during the middle Miocene "Monterey" carbon-isotope excursion. Earth and Planetary Science Letters, 261, 534-550.

Hunt, D., Tucker, M.E., 1992. Stranded parasequences and the forced regressive wedge systems tract: deposition during base level fall. Sedimentary Geology, 81, 1-9.

Hutcheon, I., Shevalier, M., Durocher, K., Bloch, J., Johnson, G., Nightingale, M., Mayer, B., 2016. Interactions of CO_2 with formation waters, oil and minerals and CO_2 storage at the Weyburn IEA EOR site, Saskatchewan, Canada. International Journal of Greenhouse Gas Control, 53, 354–370.

International Energy Agency, 2012. Energy technology perspectives: 2012: Pathways to a clean energy system. OECD/IEA, France. 63pp.

International Energy Agency, 2014. World Energy Outlook 2014, Paris: OECD/IEA.

International Energy Agency, 2016. 20 Years of Carbon Capture and Storage; Accelerating Future Development. IEA Publications, Paris, France. 115pp.

IEAGHG, 2009. Development of storage coefficients for carbon dioxide storage in deep saline formations. International Energy Agency Greenhouse Gas R&D Programme Report 2009/13, 118pp.

Iliffe, J.E., Lerche, I., DeBuyl, M., 1991. Basin analysis and hydrocarbon generation of the South Mozambique Graben using extensional models of heat flow. Marine and Petroleum Geology, 8, 152-162.

IPCC, 2005. IPCC Special report on Carbon Dioxide Capture and Storage. Prepared by Working Group III of the Intergovernmental Panel on Climate Change. Metz, B., Davidson, O., de Coninck, H., Loos, M. and Meyer, L. (Eds.), Cambridge University Press, Cambridge United Kingdom and New York, NY, USA, 442pp.

IPCC, 2014: Climate Change 2014: Mitigation of Climate Change. Contribution of Working Group III to the Fifth Assessment Report of the Intergovernmental Panel on Climate Change. Edenhofer, O., R. Pichs-Madruga, Y. Sokona, E. Farahani, S. Kadner, K. Seyboth, A. Adler, I. Baum, S. Brunner, P. Eickemeier, B. Kriemann, J. Savolainen, S. Schlömer, C. von Stechow, T. Zwickel and J.C. Minx (Eds.), Cambridge University Press, Cambridge, United Kingdom and New York, NY, USA, 1454pp.

Jobe, Z.R., Lowe, D.R., Uchytilb, S.J., 2011. Two fundamentally different types of submarine canyons along the continental margin of Equatorial Guinea. Marine and Petroleum Geology, 28, 843-860.

John, C.M., Karner, G.D., Browning, E., Leckie, R.M., Mateo, Z., Carson, B., Lowery, C., 2011. Timing and magnitude of Miocene eustacy derived from the mixed siliciclastic-carbonate stratigraphic record of the northeastern Australian margin. Earth and Planetary Science Letters, 304, 455-467.

Johnson, M. R., Van Vuuren, C. J., Visser, J. N. J., Cole, D. I., Wickens, H. d. V., Christie, A. D. M., Roberts, D. L., Brandl, G., 2006. Sedimentary Rocks of the Karoo Supergroup. In: Johnson, M. R., Anhaeusser, C. R., Thomas, R. J. (Eds.), The Geology of South Africa. Geological Society of South Africa / Council for Geoscience. 461-500.

Kahnt, R., Kutzke, A., Martin, M., Eckart, M., Schlüter, R., Kempa, T., Tillner, E., Hildenbrand, A., Krooss, B.M., Gensterblum, Y., Adams, M., Feinendegen, M., Klebingat, S., Neukum, C., 2015. CO2RINA CO_2 storage risk integrated analysis. In: Liebscher, A., Münch, U. (Eds.), Geological Storage of CO_2 Long Term Security Aspects. Geotechnologien Science Report No. 22. Springer, Switzerland, pp. 139-166.

Kennedy, W.J., Klinger, H.C., 1975. Cretaceous faunas from Zululand and Natal, South Africa. Introduction, Stratigraphy. Bulletin of the British Museum of Natural History (Geology), 25, 265–315.

Kennett, J.P., 1982. Marine Geology: Englewood Cliffs, N.J., Prentice-Hall, 813pp.

King, L., 1953. A Miocene marine fauna from Zululand. Transactions of the Geological Society of South Africa, 56, 59-91.

King, L., 1969. Correspondence: The ages of Tertiary Rocks at Uloa and Umkwelane, Zululand, and their Geomorphological Significance. Geological Magazine, 106 (2), 206-211.

Kitchin, K.A., 1995. Tectonics related to the northern termination of the Agulhas-Falkland Fracture Zone offshore Southern Natal. Geological Society of South Africa, Centennial Geocongress Abstracts, Rand Afrikaans Univ., Johannesburg, 1, 460-463.

Kitchin, K., McLachlan, I.R., 1996. Tectonics and hydrocarbon potential of the east coast of South Africa. Soekor Petroleum Licencing Unit, Document SOE-PLU-RPT-001. 49pp.

Kuhlmann, G., Adams, S., Campher, C., van der Spuy, D., di Primio, R., Horsfield, B., 2010. Passive margin evolution and its controls on natural gas leakage in the southern Orange Basin, blocks 3/4, offshore South Africa. Marine and Petroleum Geology, 27, 973-992.

Lastras, G., Arzola, R.G., Masson, D.G., Wynn, R.B., Huvenne, V.A.I., Hühnerbach, V., Canals, M., 2009. Geomorphology and sedimentary features in the Central Portuguese submarine canyons, Western Iberian margin. Geomorphology, 103, 310–329.

Lastras, G., Acosta, J., Muñoz, A., Canals, M., 2011. Submarine canyon formation and evolution in the Argentine Continental Margin between 44°30'S and 48°S. Geomorphology, 128, 116–136.

Leetaru, H.E., Freiburg, J.T., 2014. Perspective: Litho-facies and reservoir characterization of the Mt Simon Sandstone at the Illinois Basin – Decatur Project. Greenhouse Gases: Science and Technology, 4, 580–595.

Leinweber, V.T., Jokat, W., 2011. Is there continental crust underneath the northern Natal Valley and the Mozambique Coastal Plains? Geophysical Research Letters, 38, L14303.

Leith, M.J., 1971. Jc-A1 geological well completion report. SOEKOR internal report. SOE-DRG-WCR-346. 19pp.

Lester, M.J., 2000. A biostratigraphic study of the Jc-D1 (Rhino) well, Durban Basin, Republic of South Africa. Timetrax Limited, unpublished internal report, 49pp.

Li, P., Zhou, D., Zhang, C., Chen, G., 2015. Assessment of the effective CO_2 storage capacity in the Beibuwan Basin, offshore of southwestern P. R. China. International Journal of Greenhouse Gas Control, 37, 325-339.

Liu, C., Fulthorpe, C.S., Austin Jr., J.A., Sanchez, C.M., 2011. Geomorphologic indicators of sea level and lowstand paleo-shelf exposure on early-middle Miocene sequence boundaries. Marine Geology, 280, 182-194.

Lowe, D.R., 1982. Sediment gravity flows; II. Depositional models with special reference to the deposits of high-density turbidity currents. Journal of Sedimentary Petrology, 52, 279-297.

Martin, A.K., 1984. Plate tectonic status and sedimentary basin in-fill of the Natal Valley (SW Indian Ocean). Bulletin of the Joint Geological Survey/University of Cape Town, Marine Geoscience Unit 14, 209pp.

Martin, A.K., 1987. Comparison of sedimentation rates in the Natal Valley, southwest Indian Ocean, with modern sediment yields in east coast rivers of Southern Africa. South African Journal of Science, 83, 716-724.

Martin, A.K., Flemming, B.W., 1986. The Holocene shelf sediment wedge off the south and east coast of South Africa. In: Knight, R.J. and McLean, J.R. (Eds.), Shelf Sands and Sandstones. Canadian Society of Petroleum Geologists, Memoir II, 27-44.

Martin, A.K., Goodlad, S.W., Salmon, D.A., 1982. Sedimentary basin in-fill in the northernmost Natal Valley, hiatus development and Agulhas Current palaeo-oceanography. Journal of the Geological Society, London, 139, 183-201.

Martin, A.K., Hartnady, C.J.H., Goodlad, S.W., 1981. A revised fit of South America and south central Africa, Earth and Planetary Science Letters, 54, 293-305.

Martins-Neto, M.A., Catuneanu, O., 2010. Rift sequence stratigraphy. Marine and Petroleum Geology, 27, 247-253.

Mashaba, V., Altermann, W., 2015. Calculation of water saturation in low resistivity gas reservoirs and pay-zones of the Cretaceous Grudja Formation, onshore Mozambique basin. Marine and Petroleum Geology, 67, 249-261.

Mayall, M., Jones, E., Casey, M., 2006. Turbidite channel reservoirs – Key elements in facies prediction and effective development. Marine and Petroleum Geology, 23, 821-841.

McCormick, S., Cooper, J.A.G., Mason, T.R., 1992. Fluvial sediment yield to the Natal coast: a review. Southern African Journal of Aquatic Science, 18, 74-88.

McGregor, B.A., Bennett, R.H., 1979. Mass movement of sediment on the continental slope and rise seaward of the Baltimore Canyon trough. Marine Geology, 33, 163-174.

McLachlan, I.R., McMillan, I.K. 1979. Microfaunal biostratigraphy, chronostratigraphy and history of Mesozoic and Cenozoic deposits on the coastal margin of South Africa. In: Anderson, A.M., Van Biljon, W.J. (Eds.), Some Sedimentary Basins and Associated Ore Deposits of South Africa (Geokongres ‘77), Geological Society of South Africa, Special Publication, 6, 161-181.

McMillan, I.K., 2003. Foraminiferally defined biostratigraphic episodes and sedimentation pattern of the Cretaceous drift succession (Early Barremian to Late Maastrichtian) in seven basins on the South African and southern Namibian continental margin. South African Journal of Science, 99, 537–576.

McMillan, I.K., Dale, D., 2000. Final report on the foraminiferal biostratigraphy of Borehole Jc-D1 (Rhino). 43pp.

Miller, K.G., 2009. Sea Level Change, Last 250 Million Years. In: Gornitz, V. (Ed.) Encyclopedia of Paleoclimatology and Ancient Environments, 879-887.

Miller, K.G., Kominz, M.A., Browning, J.V., Wright, J.D., Mountain, G.S., Katz, M.E., Sugarman, P.J., Cramer, B.S., Christie-Blick, N., Pekar, S.F., 2005. The Phanerozoic record of global sea-level change. Science, 310, 1293-1298.

Miller, K.G., Melillo, A.J., Mountain, G.S., Farre, J.A., Poag, C.W., 1987. Middle to late Miocene canyon cutting on the New Jersey continental slope: biostratigraphic and seismic stratigraphic evidence. Geology, 15, 509-512.

Mitchum, R.M. Jr., Vail, P.R., Thompson, S., III, 1977. Seismic stratigraphy and global changes of sea-level, part 2: the depositional sequence as a basic unit for stratigraphic analysis. In: Payton, C.E. (Ed.). Seismic Stratigraphy–Applications to Hydrocarbon Exploration. American Association of Petroleum Geologists Memoir 26, 53–62.

Moore, A.E., 1999. A reappraisal of epeirogenic flexure axes in southern Africa. South African Journal of Geology, 102 (4), 363-376.

Moore, A.E., Larkin, P.A., 2001. Drainage evolution in south-central Africa since the break-up of Gondwana. South African Journal of Geology, 104, 47-68.

Mountain, G.S., Burger, R.L., Delius, H., Fulthorpe, C.S., Austin, J.A., Goldberg, D.S., Steckler, M.S., McHugh, C.M., Miller, K.G., Montverde, D.H., Orange, D.L., Pratson, L.F., 2007. The long-term stratigraphic record on continental margins. Special Publication 37. In: Nittrouer, C.A., Austin, J.A., Field, M.E., Kravitz, J.H., Syvitski, J.P.M., Wiberg, P.L. (Eds.), Continental margin Sedimentation: from Sediment Transport to Sequence Stratigraphy. International Association of Sedimentologists, Blackwell, Oxford, pp. 275-339.

Muntingh, A., 1983. Geological well completion report of borehole Jc-C1. SOEKOR internal report. SOE-DRG-WCR-363. 23pp.

Nairn, A.E.M., Lerche, I., Iliffe, J.E., 1991. Geology, basin analysis, and hydrocarbon potential of Mozambique and the Mozambique Channel. Earth-Science Reviews, 30, 81-123.

NETL, 2010. Carbon Dioxide Enhanced Oil Recovery. Untapped Domestic Energy Supply and Long Term Carbon Storage Solution. National Energy Technology Laboratory. 32pp.

Niemi, T.M., Ben-Avraham, Z., Hartnady, C.J.H., Reznikov, M., 2000. Post-Eocene seismic stratigraphy of the deep ocean basin adjacent to the southeast African continental margin: a record of geostrophic bottom current systems. Marine Geology, 162, 237–258.

Nittrouer, C.A., Austin Jr., J.A., Field, M.E., Kravitz, J.H., Syvitski, J.P.M., Wiberg, P.L., 2007. Writing a Rosetta stone: insights into continental-margin sedimentary processes and strata. In: Nittrouer, C.A., Austin Jr., J.A., Field, M.E., Kravitz, J.H., Syvitski, J.P.M., Wiberg, P.L. (Eds.), Continental Margin Sedimentation: from Sediment Transport to Sequence Stratigraphy. International Association of Sedimentologists, pp. 1-48. Special Volume.

Norden, B., Frykman. P., 2013. Geological modelling of the Triassic Stuttgart Formation at the Ketzin CO_2 storage site, Germany. International Journal of Greenhouse Gas Control, 19, 756-774.

Nordfjord, S., Goff, J.A., Austin Jr, J.A., Sommerfield, C.K., 2005. Seismic geomorphology of buried channel systems on the New Jersey outer shelf: assessing past environmental conditions. Marine Geology, 214, 339-364.

Nordfjord, S., Goff, J.A., Austin Jr, J.A. Gulick, S.P.S., Galloway, W.E., 2006. Seismic facies of incised valley-fills, New Jersey continental shelf: implications for erosion and preservation processes acting during late Pleistocene/Holocene transgression. Journal of Sedimentary Research, 76, 1284-1303.

Nordfjord, S., Goff, J.A., Austin Jr, J.A., Duncan, L.S., 2009. Shallow stratigraphy and complex transgressive ravinement on the New Jersey middle and outer continental shelf. Marine Geology, 266, 232-243.

Normark, W.R., 1970. Growth patterns of deep sea fans. AAPG Bulletin, 54, 2170-2195.

Noy, D.J., Holloway, S., Chadwick, R.A., Williams, J.D.O., Hannis, S.A., Lahann, R.W., 2012. Modelling large-scale carbon dioxide injection into the Bunter Sandstone in the UK Southern North Sea. International Journal of Greenhouse Gas Control, 9, 220–233.

O'Grady, D.B., Syvitski, J.P.M., Pratson, L.F., Sarg, J.F., 2000. Categorizing the morphologic variability of siliciclastic passive continental margins. Geology, 28 (3), 207–210.

Oruganti, Y.D., Bryant, S.L., 2009. Pressure build-up during CO_2 storage in partially confined aquifers. Energy Procedia, 1, 3315–3322.

Palermo, D., Galbiati, M., Famiglietti, M., Marchesini, M., Mezzapesa, D., Fonnesu, F., 2014. Insights into a New Super-Giant Gas Field - Sedimentology and Reservoir Modelling of the Coral Complex, Offshore Northern Mozambique. Offshore Technology Conference Asia, Kuala Lumpur, Malaysia, 25-28 March 2014. 8pp.

Partridge, T.C., 1997. Cainozoic environmental change in southern Africa, with special emphasis on the last 200 000 years. Progress in Physical Geography, 21 (1), 3-22.

Partridge T.C., 1998. Of diamonds, dinosaurs and diastrophism: 150 million years of landscape evolution in southern Africa. South African Journal of Geology, 101 (3), 167-184.

Partridge, T.C., Botha, G.A., Haddon, I.G. 2006. Cenozoic deposits of the Interior. In: Johnson, M.R., Anhaeusser, C.R., Thomas, R.J., (Eds.), The Geology of South Africa. Geological Society of South Africa and Council for Geoscience, 585-604.

Partridge, T.C., Maud, R.R., 1987. Geomorphic evolution of southern Africa since the Mesozoic. South African Journal of Geology, 90, 179-208.

Partridge, T.C., Maud, R.R., 2000. Macro-scale geomorphic evolution of southern Africa. In: Partridge, T.C., Maud, R.R. (Eds.), The Cenozoic of Southern Africa. Oxford University Press, New York, 3-18.

Pattier, F., Loncke, L., Imbert, P., Gaullier, V., Basile, C., Maillard, A., Roest, W.R., Patriat, M., Vendeville, B.C., IGUANES Scientific Party, 2015. Origin of an enigmatic regional Mio-Pliocene unconformity on the Demerara plateau. Marine Geology, 365, 21-35.

Pau, G.S.H., Bell, J.B., Pruess, K., Almgren, A.S., Lijewski, M.J., Zhang, K., 2010. High-resolution simulation and characterization of density-driven flow in CO_2 storage in saline aquifers. Advances in Water Resources, 33, 443-455.

Petroleum Agency SA, 2008. Petroleum Exploration: Information and opportunities 2008. Petroleum Agency SA, 30 pp.

Petroleum Agency SA, 2012. Petroleum exploration in South Africa. Information and opportunities. Petroleum Agency SA Booklet. 32pp.

Petroleum Agency SA, 2015. Republic of South Africa, Petroleum potential of the East Coast. Petroleum Agency SA Booklet. 4pp

Phillips Petroleum South Africa Ltd. 2000. Jc-D1 (Rhino)-1 Final Geologic report. Petroleum Agency South Africa, POF 11846 (unpubl.) 261pp.

Pisaniec, K., Abu, C., Barlass, D., Kornpihl, D., Kanrar, A., Tyagi, C., Hollebeek, E., 2017. Unlocking the potential of the Durban Basin, South Africa, using modern 3D seismic data interpretation. 79th EAGE Conference and Exhibition, Paris, France 12-15 June 2017. 5pp.

Porat, N., Botha, G.A., 2008. The luminescence chronology of dune development on the Maputaland coastal plain, southeast Africa. Quaternary Science Reviews, 27, 1024-1046.

Porebski, S.J., Steel, R.J., 2003. Shelf-margin deltas: their stratigraphic significance and relation to deepwater sands. Earth-Science Reviews, 62, 283-326.

Posamentier, H.W., Allen, G.P., 1999. Siliciclastic sequence stratigraphy: concepts and applications. SEPM Concepts in Sedimentology and Paleontology, 7, 210pp.

Posamentier, H.W., Morris, W.R., 2000. Aspects of the strata architecture of forced regressive deposits. In: Hunt, D., Gawthorpe, R.L. (Eds.), Sedimentary Responses to Forced Regressions, Geological Society Special Publication, Geological Society of London, 172, 19-46.

Posamentier, H.W., Walker, R.G., 2006. Deep-Water Turbidites and Submarine Fans. In: Posamentier, H.W., Walker, R.G., (Eds.), Facies Models Revisited. SEPM Special Publication, 84, 397-520.

Pratson, L.F., Ryan, W.B.F., Mountain, G.S., Twichell, D.C., 1994. Submarine canyon initiation by downslope-eroding sediment flows: Evidence in late Cenozoic strata on the New Jersey continental slope. Geological Society of America Bulletin, 106, 395-412.

Preu, B., Spieß, V., Schwenk, T., Schneider, R., 2011. Evidence for current-controlled sedimentation along the southern Mozambique continental margin since Early Miocene times. Geo-Marine Letters, 31, 427-435.

Prosser, S., 1993. Rift-related linked depositional systems and their seismic expression. In: Williams, G.D., Dobb, A., (Eds.), Tectonics and seismic sequence stratigraphy. Geological Society Special Publication, 71, 35-66.

Ramsay, P.J., 1994. Marine geology of the Sodwana Bay shelf, Southeast Africa. Marine Geology, 120, 225-247.

Ramsay, P.J., 1996. Quaternary marine geology of the Sodwana Bay shelf, northern Kwazulu-Natal. Bulletin of the Geological Survey of South Africa 117, 154pp.

Reading, H. G., Richards, M., 1994. Turbidite systems in deep-water basin margins classified by grain size and feeder system. Bulletin of the American Association of Petroleum Geologists, 78, 792-822.

Ringrose, P., Simone, A., 2009. Site selection. In: Cooper, C. (Ed.), A Technical Basins for Carbon Dioxide Storage. CO_2 Capture Project. CPL Press, United Kingdom 92 pp.

Robb, L.J., Brandl, G., Anhaeusser, C.R., Poujol, M., 2006. Archaean Granitoid Intrusions. In: Johnson, M.R., Anhaeusser C.R., Thomas, R.J., (Eds.), The Geology of South Africa. Geological Society of South Africa, Johannesburg/Council for Geoscience, Pretoria, 57–94.

Roberts, D.L., Botha, G.A., Maud, R.R., Pether, J., 2006. Coastal Cenozoic deposits. In: Johnson, M.R., Anhaeusser, C.R., Thomas, R.J. (Eds.), The Geology of South Africa. Geological Society of South Africa and Council for Geoscience, Johannesburg/Pretoria, 605-628.

Roux, J., 2009. Estimates of oil and gas resources offshore South Africa. Petroleum Agency SA, August 2009.

Said, A., Moder, C., Clark, S., Ghorbal, B., 2015. Cretaceous–Cenozoic sedimentary budgets of the Southern Mozambique Basin: Implications for uplift history of the South African Plateau. Journal of African Earth Sciences, 109, 1-10.

Salman, G., Abdula, I., 1995. Development of the Mozambique and Ruvuma sedimentary basins, offshore Mozambique. Sedimentary Geology, 96, 7-41.

Santra, M., Goff, J.A., Steel, R.J., Austin Jr., J.A., 2013. Forced regressive and lowstand Hudson paleo-Delta system: Latest Pliocene growth of the outer New Jersey shelf. Marine Geology, 339, 57-70.

Schlüter, P., Uenzelmann-Neben, G., 2007. Seismostratigraphic analysis of the Transkei Basin: A history of deep sea current controlled sedimentation. Marine Geology, 240, 99-111.

Schlüter, P., Uenzelmann-Neben, G., 2008. Indications for bottom current activity since Eocene times: The climate and ocean gateway archive of the Transkei Basin, South Africa. Global and Planetary Change, 60, 416-428

Seyedmehdi, Z., George, A.D., Tucker, M.E., 2016. Sequence development of a latest Devonian-Tournaisian distally-steepened mixed carbonate-siliciclastic ramp, Canning Basin, Australia. Sedimentary Geology, 333, 164-183.

Shackleton, N.J., Kennett, J.P., 1975. Initial Reports. Deep Sea Drilling Project 29, 743pp.

Shanmugam, G., 2000. 50 years of the turbidite paradigm (1950s-1990s): deep-water processes and facies models - a critical perspective. Marine and Petroleum Geology, 17, 285-342.

Shanmugam, G., 2016. Submarine fans: A critical retrospective (1950–2015). Journal of Palaeogeography, 5 (2), 110-184.

Shanmugam, G., Bloch, R.B., Mitchell, S.M., Beamish, G.W.J., Hodgkinson, R.J., Damuth, J.E., Straume, T., Syvertsen, S.E., Shields, K.E., 1995. Basin-floor fans in the North Sea: Sequence stratigraphic models vs. sedimentary facies. American Association of Petroleum Geologists Bulletin, 79 (4), 477-512.

Shaw, M.J., 1998. Seismic stratigraphy of the northern KwaZulu-Natal upper continental margin. MSc Thesis, University of Natal, Durban, 190pp.

Shepard, F.P., 1963. Submarine Geology. Harper and Row, New York, 557pp.

Shepard, F.P., 1981. Submarine canyons: multiple causes and long-time persistence. American Association of Petroleum Geologists, Bulletin 65 (6), 1062-1077.

Shevenell., A.E., Kennett, J.P., Lea, D.W., 2004. Middle Miocene southern ocean cooling and Antarctic cryosphere expansion. Science, 305, 1766-1770.

Shone, R.W., 2006. Onshore Post-Karoo Mesozoic Deposits. In: Johnson, M.R., Anhaeusser, C.R., Thomas, R.J. (Eds.), The Geology of South Africa. Geological Society of South Africa, Johannesburg/Council for Geoscience, Pretoria, 541-552.

Siesser, W.G., Dingle, R.V., 1981. Tertiary sea-level movements around southern Africa. Journal of Geology, 89 (4), 523-536.

Singh, V., McLachlan, I., 2003. South Africa's east coast frontier offers untested mid to deepwater potential. Oil and Gas Journal, 101 (22), 40-45.

Solomon, S., Bureau-Cauchois, G., Ahmed, N., Aarnes, J., Holtedahl, P., 2014. CO_2 storage capacity assessment of deep saline aquifers in the Mozambique Basin. Energy Procedia, 63, 5266-5283.

Soulet, Q., Migeon, S., Gorini, C., Rubino, J-L., Raisson, F., Bourges, P., 2016. Erosional versus aggradational canyons along a tectonically-active margin: The northeastern Ligurian margin (western Mediterranean Sea). Marine Geology, 382, 17-36.

Span, R., Wagner, W., 1996. A new equation of state for carbon dioxide covering the fluid region from the triple-point temperature to 1100K at pressures up to 800 MPa. Journal of Physical and Chemical Reference Data, 25, 1509-1596.

Stojcic, B., 1979. Geological well completion report of Zululand 1 (ZU-1/77).Report, SOEKOR, PSV 1960 (unpubl.) 32pp.

Stow, D.A.V., Mayall, M., 2000. Deep-water sedimentary systems: New models for the 21st century. Marine and Petroleum Geology, 17, 125-135.

Stow, D.A.V., Reading, H.G., Collinson, J.D., 1996. Deep Seas. In: Reading, H.G. (Ed.), Sedimentary Environments: Processes, Facies and Stratigraphy. Third Edition, Blackwell Publishing, Australia, 395-453.

Sydow, C.J., 1988. Stratigraphic control of slumping and canyon development on the continental margin, east coast, South Africa. BSc Hons Thesis, University of Cape Town. 55pp.

Tikku, A.A., Marks, K.M., Kovacs, L.C., 2002. An Early Cretaceous extinct spreading centre in the northern Natal valley. Tectonophysics, 347, 87-108.

Tinker, J., de Wit, M., Brown, R., 2008. Mesozoic exhumation of the southern Cape, South Africa, quantified using apatite fission track thermochronology. Tectonophysics, 455, 77-93.

Tuttle, M.L.W., Charpentier, R.R., Brownfield, M.E., 1999. The Niger Delta Petroleum System: Niger Delta Province, Nigeria, Cameroon, and Equatorial Guinea, Africa. U.S. Geological Survey, Open-File Report 99-50-H, 71pp.

Uenzelmann-Neben, G., Clift, P.D., 2015. A sediment budget for the Transkei Basin, Southwest Indian Ocean. Marine Geophysical Research, 36, 281-291.

Underschultz, J., Boreham, C., Dance, T., Stalker, L., Freifeld, B., Kirste, D., Ennis-King, J., 2011. CO_2 storage in a depleted gas field: An overview of the CO2CRC Otway Project and initial results. International Journal of Greenhouse Gas Control, 5 (4), 922–932.

UNFCCC, 1992. United Nations Framework Convention on Climate Change. United Nations, FCCC/INFORMAL/84 GE.05-62220 (E) 200705, 25pp.

Unstead, P.J., Muntingh, A., Mills, S.R., McLachlan, I.R., 1983. Jc-B1 Geological well completion report. SOEKOR internal report, unpublished. 15pp.

US DOE, 2008. Carbon Sequestration Atlas of the United States and Canada, Second Edition: Appendix A − Methodology for Development of Carbon Sequestration Capacity Estimates. National Energy Technology Laboratory, United States Department of Energy, Office of Fossil Energy, 37pp

Vail, P.R., Mitchum, R.M., Thompson, S., 1977. Seismic stratigraphy and global changes of sea level. Part 4: global cycles of relative changes of sea level. In: Payton, C.E. (Ed.), Seismic Stratigraphy - Applications to Hydrocarbon Exploration: American Association of Petroleum Geologists Memoir, 26, pp. 83–97.

Van Aken, H.M., Ridderinkof, H., de Ruijter, W.P.M., 2004. North Atlantic deep water in the south-western Indian Ocean. Deep-Sea Research I, 51, 755-776.

Van Bergen, F. Tambach, T., Pagnier, H., 2011. The role of CO_2-Enhanced Coalbed Methane production in the global CCS strategy. Energy Procedia, 4, 3112-3116.

Van Vuuren, C.J., Broad, D.S., Jungslager, E.H.A., Roux, J., McLachlan, I.R., 1998. Oil and gas, In: Wilson, M.G.C., Anhaeusser, C.R., (Eds.), The Mineral Resources of South Africa. Handbook, Council for Geoscience, 16, 483-494.

Varban, B.L., Plint, A.G., 2008. Palaeoenvironments, palaeogeography, and physiography of a large, shallow, muddy ramp: Late Cenomanian-Turonian Kaskapau Formation, Western Canada foreland basin. Sedimentology, 55, 201-233.

Viljoen, J.H.A., Stapelberg, F.D.J., Cloete, M., 2010. Technical report on the geological storage of carbon dioxide in South Africa. Report, Council for Geoscience, 236pp.

Visser, D.J.L., 1998. The geotectonic evolution of South Africa and offshore areas. Explanation: Structure map (1:1 000 000) Council for Geoscience, 319pp.

Von Veh, M.W., Andersen, N.J.B., 1990. Normal-slip faulting in the coastal areas of northern Natal and Zululand. South African Journal of Geology, 93 (4), 574-582.

Walford, H.L., White, N.J., Sydow, J.C., 2005. Solid sediment load history of the Zambezi Delta. Earth and Planetary Science Letters, 238, 49-63.

Watkeys, M.K., 2006. Gondwana Break-Up: A South African Perspective. In: Johnson, M.R., Anhaeusser C.R., Thomas, R.J., (Eds.), The Geology of South Africa. Geological Society of South Africa, Johannesburg/Council for Geoscience, Pretoria, 531-539.

Watkeys, M.K., Sokoutis, D., 1998. Transtension in southeastern Africa associated with Gondwana breakup. In: Holdsworth, R.E., Strachan, R.A., Dewey, J.F (Eds.), Continental Transpressional and Transtensional Tectonics, Geological Society, London, Special Publications, 135, 203-214.

Weber, K.J., 1987. Hydrocarbon distribution patterns in Nigerian growth fault structures controlled by structural style and stratigraphy. Journal of Petroleum Science and Engineering, 1, 91-104.

Weigelt, E., Uenzelmann-Neben, G., 2004. Sediment deposits in the Cape Basin: Indications for shifting ocean currents? American Association of Petroleum Geologists, Bulletin, 88 (6), 765–780.

Wigley, R.A., Compton, J.S., 2006. Late Cenozoic evolution of the outer continental shelf at the head of the Cape Canyon, South Africa. Marine Geology, 226, 1-23.

Wiles, E., Green, A.N., Watkeys, M., Jokat, W., Krocker, R., 2013. The evolution of the Tugela canyon and submarine fan: A complex interaction between margin erosion and bottom current sweeping, southwest Indian Ocean, South Africa. Marine and Petroleum Geology, 44, 60-70.

Wiles, E., Green, A.N, Watkeys, M., Jokat, W., Krocker, R., 2014. A new pathway for Deep water exchange between the Natal Valley and Mozambique Basin? Geo-Marine Letters, 34, 525-540.

Wilkinson, M., Haszeldine, R.S., Mackay, E., Smith, K., Sargeant, S., 2013. A new stratigraphic trap for CO_2 in the UK North Sea: Appraisal using legacy information. International Journal of Greenhouse Gas Control, 12, 310-322.

Würdemann, H., Möller, F., Kühn, M., Heidug, W., Christensen, N.P., Borm, G., Schilling, F.R., The CO_2SINK Group. 2010. CO2SINK - From site characterisation and risk assessment to monitoring and verification: One year of operational experience with the field laboratory for CO_2 storage at Ketzin, Germany. International Journal of Greenhouse Gas Control, 4, 938–951.

Zachos, J.C., Flower, B.P., Paul, H., 1997. Orbitally paced climate oscillations across the Oligocene/Miocene boundary. Nature, 388, 567-570.

Zachos, J., Pagani, M., Sloan, L., Thomas, E., Billups, K., 2001. Trends, rhythms, and aberrations in global climate 65Ma to Present. Science, 292, 686-693.

Zecchin, M., Caffau, M., Roda, C., 2011. Relationships between high-magnitude relative sea-level changes and filling of a coarse-grained submarine canyon (Pleistocene, Ionian Calabria, Southern Italy). Sedimentology, 58, 1030-1064

Zecchin, M., Catuneanu, O., 2013. High-resolution sequence stratigraphy of clastic Shelves I: Units and bounding surfaces. Marine and Petroleum Geology, 39, 1-25.

Zecchin, M., Catuneanu, O., 2015. High-resolution sequence stratigraphy of clastic shelves III: Applications to reservoir geology. Marine and Petroleum Geology, 62, 161-175.

Zecchin, M., Praeg, D., Ceramicola, S., Muto, F., 2015. Onshore to offshore correlation of regional unconformities in the Plio-Pleistocene sedimentary successions of the Calabrian Arc (central Mediterranean). Earth-Science Reviews, 142, 60–78.

Zhu, M., Graham, S.A., Pang, X., McHargue, T., 2009. Characteristics of migrating submarine canyons from the middle Miocene to present: implications for paleo-oceanographic circulation, northern South China Sea. Marine and Petroleum Geology, 27 (1), 307-319.

APPENDIX I

Available online at www.sciencedirect.com

ScienceDirect

Energy Procedia 63 (2014) 5200 – 5210

Energy Procedia

GHGT-12

Investigation of CO_2 storage potential of the Durban basin in South Africa

Nigel Hicks[1, 4]*, Sean Davids[2], Brendan Beck[3], and Andrew Green[4]

[1]*Council for Geoscience, 139 Jabu Ndlovu Street, Pietermaritzburg, RSA*
[2]*Petroleum Agency South Africa, 7 Mispel Street, Bellville, 7530, Cape Town, RSA*
[3]*South African Centre for Carbon Capture and Storage, Johannesburg 2146, South Africa*
[4]*Discipline of Geological Sciences, School of Agricultural, Earth and Environmental Sciences, University of KwaZulu-Natal, Westville, Private Bag X54001, South Africa*

Abstract

The mitigation of anthropogenic carbon dioxide (CO_2) emissions through technologies such as Carbon Capture and Storage (CCS) has been internationally identified as one of the major technical approaches that can be used to combat global climate change in fossil fuel dominated countries. The South African Centre of Carbon Capture and Storage (SACCCS) was established in 2009 to investigate the potential for CCS in the country. Results from a country-scale assessment of CO_2 storage potential suggest that South Africa has a theoretical storage capacity of ~150 Gt, of which 98% occurs offshore in Mesozoic sedimentary basins preserved on the submerged continental shelf. This paper will discuss the progress associated with the ongoing investigation of CO_2 storage potential in the 10 000 km^2, offshore Durban basin on the east coast of South Africa.

With the use of existing data and information the geological development and CO_2 storage suitability of the offshore Durban basin is assessed. The basin is structurally complex, hosting a number of horst and graben structures but is dominated by the Tugela Cone, a Tertiary-age, deep-water fan complex that is located seaward of the continental shelf. Although not formally given formation status, sequence stratigraphic correlation can be applied to the Jurassic to Cretaceous succession, separating it into four formations based upon onshore sequences in the Zululand basin to the north. Formations are namely; Syn-Rift, Makatini, Mzinene, St Lucia. Cenozoic sediments range in thickness from ~1300 m to ~2000 m comprising a variety of lithologies that cap the sequence. Re-analysis of existing legacy 2D seismic and exploration borehole data has been undertaken in the context of CCS to assess the CO_2 prospectivity, geological evolution, and depositional architecture of this portion of the South African continental shelf.

* Corresponding author. Tel.: +27 (0) 333456265; fax: +27 (0) 333949342.
E-mail address: nhicks@geoscience.org.za

Peer-review under responsibility of the Organizing Committee of GHGT-12
doi:10.1016/j.egypro.2014.11.551

Peer-review under responsibility of the Organizing Committee of GHGT-12

Keywords: CO_2; CCS; South Africa; SACCCS; Council for Geoscience

1. Introduction

The mitigation of anthropogenic carbon dioxide (CO_2) emissions has been internationally identified as a major technical approach within climate change technologies. Although other anthropogenic greenhouse gas emissions do contribute to towards global warming, CO_2 is defined as a primary contributor. A variety of mitigation options have been experimented, with the capture, transportation and storage of anthropogenic CO_2 in geological formations being at the forefront of available methodologies. Storage of CO_2, either as a condensed, supercritical fluid phase, or as a gas, has previously been undertaken in a number of geological formations such as depleted oil or gas reservoirs, unmineable coal beds, deep saline-water saturated reservoirs, and basaltic formations [1]. Deep saline reservoirs occur throughout the world and provide large, potentially accessible storage opportunities for Carbon Capture and Storage (CCS) technologies.

The South African Centre for Carbon Capture and Storage (SACCCS) was formed in 2009 as a division of the South African National Energy Development Institute (SANEDI) and undertakes "CCS research and development to attain a state of country readiness for the implementation of CCS in South Africa". A multidisciplinary scientific programme is underway to identify and study the possibilities for CCS in South Africa. A country-scale assessment of the storage potential of South Africa's sedimentary basins was undertaken by Viljoen et al., [2], which concluded in the publication of the "Atlas on geological storage of carbon dioxide in South Africa" [3]. This assessment identified five Mesozoic sedimentary basins with possible storage potential, two of which were onshore and the remaining three located on the submerged continental shelf (Figure 1). The current paper documents a component of this research with an ongoing project detailing the geological evolution and storage prospectivity of the offshore Durban basin in KwaZulu-Natal.

The investigated area occurs in a fault-bounded sedimentary basin of Mesozoic age, preserved along the eastern continental margin of South Africa. Previous exploration focused upon possible traps in the Tugela Cone with a minor gas show in the Jc-B1 well, and the Jc-D1 well providing evidence for an active petroleum system [4]. Analysis of legacy 2D seismic and exploration borehole data in a CCS context has been undertaken to provide a better understanding of the depositional architecture and CO_2 storage prospectivity of the basin.

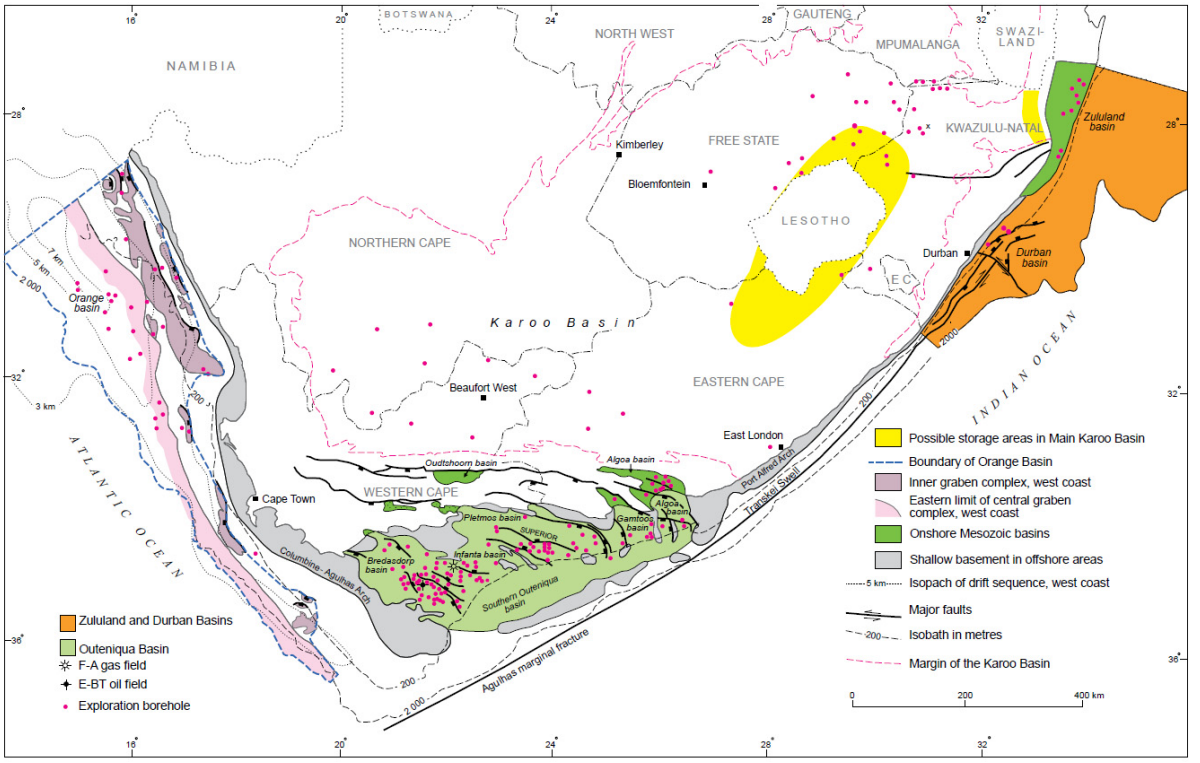

Figure 1: Possible storage opportunities within deep saline formations in South Africa. Data confidence ranked out of 5 is represented by purple figures in each basin. [modified after 3].

2. Methodology

Available data are restricted to legacy oil and gas surveys obtained between 1960 and 2000, during limited exploration programmes along the eastern seaboard of South Africa. The east coast continental shelf is traversed by approximately 13 000 km of legacy 2D seismic profiles with limited distinction between the Durban and offshore Zululand basins. Previous exploration focused primarily upon the Tugela Cone (Figure 2) with acquisition of close grid-spacing seismic profiles across the shallow continental shelf. Limited deep sea seismics were acquired during this phase.

The basins hydrocarbon potential has been tested by only four unsuccessful wildcat wells (Figure 2), drilled on the continental shelf. Wells intersected approximately 2000 m of Cretaceous and late Jurassic sediments representing drift and syn-rift phase sedimentation. All available data are held by the Petroleum Agency SA, with well completion reports, engineering reports, lithology logs, geophysical (density, sonic, gamma) logs and log analysis reports being available. Limited coring was undertaking during the exploration drilling and no downhole testing for reservoir quality or oil or gas potential were undertaken.

Exploration in 2012 and 2013 by Impact Oil and Gas (in partnership with Silver Wave Energy) and CGGVeritas respectively saw the acquisition of 5000 km of 2D seismic profiles across the Tugela Fan complex, and 10 000 km of 2D seismic acquisition within the deep Durban basin and offshore Zululand basin in water depths from 500-2500 m. Unfortunately during the timeframes of the current project this data was proprietary and not available for

analysis, but may form a valuable database for future projects. Although a wealth of legacy 2D seismic data exist, the limited borehole array within the basin causes a dearth of detailed reservoir, and geophysical data with no reservoir tests (porosity or permeability) being undertaken during exploration and therefore little to no qualitative data being available.

Although depths at which supercritical phase CO_2 is reached fluctuate dependent upon the geothermal regime and stratigraphy of the basin [5], the depth limits for the assessment were set at optimum depths of greater than 800 m. The study utilized existing seismic and well log information to delineate potential sandstone reservoirs as well as their potential rock volume for the safe storage of CO_2.

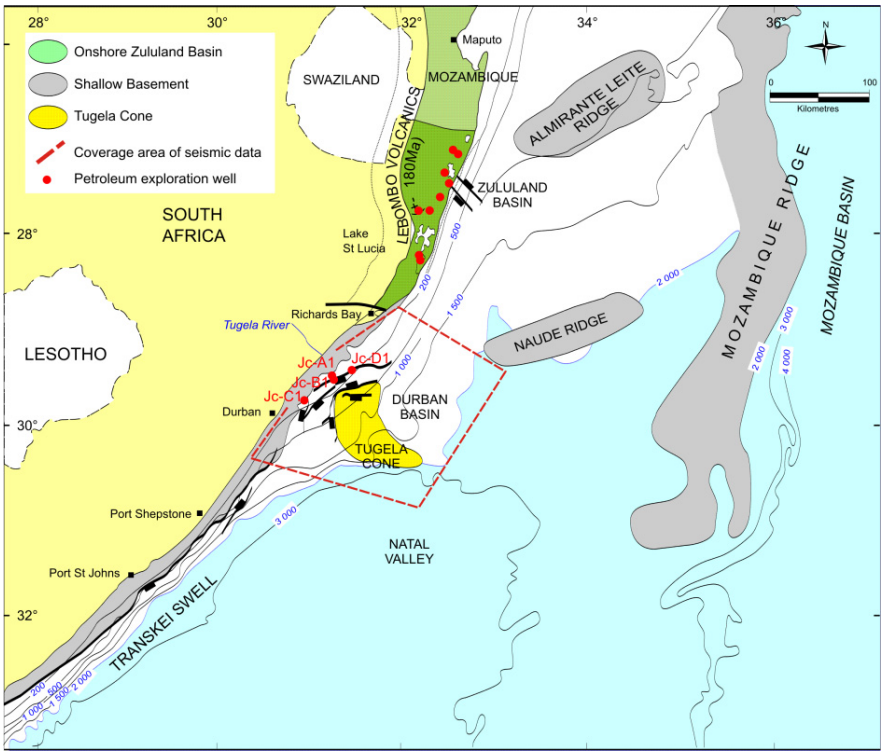

Figure 2: Offshore coverage of legacy seismic data and associated well positions data acquired within the Durban and Zululand basins [after 4].

A detailed analysis of the stratigraphy and basin genesis was initially undertaken to define the basin sedimentology characteristics and its CO_2 storage prospectivity. Currently all available stratigraphic logs are being remapped, with sandstone units below 800 m depth targeted for analysis. Sandstone bodies identified from borehole and geophysical logs are correlated with seismic reflectors and their extent mapped across the basin. The lack of exploratory boreholes within the deeper portions of the basin has forced some mapping to be undertaken upon purely seismic identification with potential structures mapped on intersection seismic lines. This process is currently ongoing, with the potential for sandstone units within the identified structures still to be defined. No detailed basin-scale 2D or 3D cross sections have been completed for the Durban basin

In most instances, only seismic data are available for selected areas within the basin, with many identified structures remaining undrilled, thereby hampering definition of potential reservoirs. The lack of drilling within the basin has also resulted in no detailed geological data on caprock being available.

3. Results

3.1. Evolution and Stratigraphy of the Durban basin

The Durban basin, occurs as a 10 000 km^2 offshore rift basin [6], preserved on the eastern continental shelf of South Africa. It is bounded to the south by a major transform fault that marks the beginning of the Natal Valley and the Agulhas-Falklands Fracture Zone (AFFZ), whilst to the east the basin is separated from the Mozambique basin

by the Mozambique Ridge. The basin is structurally complex hosting a number of horst and graben structures upon which syn-rift and early drift phase sediments have been deposited. Overlying the syn-rift and early drift sediments are thick successions of late drift phase shelf sediments. Since the Mesozoic, the geometry of the continental margin of southern Africa has been defined by structures relating to continental-scale tectonism associated with rifting and separation of the Gondwana supercontinent. At the time of continental separation southern Africa had high mean surface elevations between 2000 to 2500 m amsl (above mean sea level) due to its relative position in Gondwanaland, and the deposition and extrusion of the Karoo Supergroup [7]. During breakup, the marginal escarpment along the newly forming continental margins was rapidly eroded to the base level of the newly forming Indian and Atlantic Oceans with this rapid erosion providing much of the sediment that was deposited along the southern African continental shelf during the Cretaceous [7].

Basin-fill consists of Kimmeridgian to Cenozoic sediments, which can be subdivided into five successions bounded by major unconformities. The dominant zone of sedimentation occurs within the Tugela Cone, a Tertiary-age, deep-water fan complex that is located seaward of the continental shelf. It is within the Tugela Cone that Petroleum Agency SA identified prospective structures, as well as oil and gas leads and play concepts [4]. Sediment thicknesses vary between 2300 m and 3940 m based upon drilling depths of the Jc-A1 and Jc-B1 wells respectively, however thicknesses may increase to ~7250 m [8].

Syn-rift sediments of Kimmeridgian to late Valanginian age are identified in individual graben fill successions. Syn-rift sediments have only been intersected in three boreholes, Jc-B1 and Jc-D1 in the Durban basin, and ZU 1/77 in the onshore Zululand basin. The non-fossiliferous green-grey and red-brown silty to clayey sandstones are correlated with conglomeratic continental red-bed successions identified at the base of the Zululand Group in the onshore Zululand basin to the north. Within the JC-B1 well, drilled on the shelf edge offshore Durban, the syn-rift interval has been heavily intruded by dolerite sills causing alteration of the surrounding sandstones, siltstones and claystones. The sediments consist of ~40 m thick upward coarsening, regressive cycles of claystone, siltstone and sandstone. Sandstones can reach 10 m in thickness [9] and are commonly carbonaceous with calcareous cement [10]. It is proposed by Kitchin and McLachlan [9] that the syn-rift interval from the basement horizon D up to the 6At1 horizon represents a major transgressional event along the eastern seaboard, which is terminated by a major erosional unconformity (6At1) thought to be related to major uplift. The 6At1 reflector marks the termination of syn-rift sedimentation and the onset of drift-stage deposition within the Durban and Zululand basins.

Early drift phase sedimentation is represented by a ~30 m thick succession of mid-Barremian to early Aptian, marine, high-gamma claystones and shelfal sandstones of the Makatini Formation in borehole Jc-C1 and Jc-B1. Early drift sedimentation within the Durban basin is exceptionally localised with units occurring in the deeper portions of the basin, thinning against basement high features. The basal claystones are overlain by late Barremian to early Aptian, shelfal sandstones of variable thickness (Jc-C1 – 890 m and Jc-B1 – 290 m). This unit thins to the north of the Durban basin, where it is identified as a localised, but sandstone-rich horizon in the Jc-B1 well interbedded with minor claystone. The sandstone is very fine- to fine-grained, with subordinate grains of coarse-grained, angular quartz [10]. Gearhart Geodata Services [10] indicate that the sandstone is non-glauconitic, unlike glauconitic sandstones identified higher up in the succession between the Y and Z horizons and therefore suggest a major unconformity correlated with the Z horizon.

The Makatini Formation is overlain unconformably by the Mzinene Formation, deposited between the late Aptian/early Albian to late Cenomanian/early Turonian. Within the basin the formation consists of a localized succession of siltstone and claystone deposited on the palaeo-middle to -outer shelf with minor shallow marine sandstones capping the succession. The contact between the Mzinene Formation and overlying St Lucia Formation is marked by a ~30 m thick, laterally extensive, wave-sorted, gritty, quartz sandstone which represents a forced-regressive shoreline deposit that covered most of the early Turonian palaeo-shelf of southern Africa. Although this unit is not represented in boreholes within the Durban basin, seismic analysis has postulated its existence in the undrilled, proximal region of the basin.

The St Lucia Formation forms the uppermost Cretaceous succession in the basin, represented by sporadic Turonian to Maastrichtian deposition of deep-water claystone and mid- to outer-shelf siltstones, with subordinate tight marine sandstone [11]. Syn-rift and early drift sediments are overlain by a succession of late drift shelf sediments, which form part of the Tugela Cone, a Cenozoic-age, deep-water fan complex that is located seaward of the continental shelf. Seismic interpretation of the undrilled Tugela Cone suggest potential for turbidite sands being deposited within the upper fan on levees and within channel infills, whilst the middle fan potentially hosts bedded distal turbidites and possible supra fan lobes. Late Cretaceous sedimentation in the basin is dominated by grey claystones with minimal coarse clastics providing a potential cap rock for the underlying units.

Cenozoic sediments range in thickness from ~1300 m to ~2000 m with basal units comprising deep marine anoxic shales deposited in the early Palaeogene. Continental uplift during the Oligocene allowed for the deposition of coarse-grained sandstone in fluvial to deltaic channels identified from seismic interpretation along the continental shelf. The upper Tertiary is dominated by claystone, calcarenite, and subordinate siltstone and sandstone.

3.2. Storage Prospects of the Durban basin

Previous exploration within the basin focused upon possible traps in the Tugela Cone with a minor gas show in the Jc-B1 well, and the Jc-D1 well providing evidence for an active petroleum system [4]. It must be noted however that all wells were poorly positioned, with no appreciable sandstone reservoirs of Cretaceous age encountered as the wells were drilled upon basement highs along the shelf-edge in sediment by-pass zones. Davids [12] suggests that none of the wells tested traps with demonstrable closures. Re-analysis of the Durban basin data focuses upon both structural and stratigraphic traps and reservoir systems as prospective analysis sites.

3.2.1. Reservoir sandstones with structural traps

Preliminary analysis of TIFF and SEG-Y format seismic imagery has identified a number of structural traps within the basin, which are in accordance with trap sites identified by Petroleum Agency South Africa reservoir engineers during previous oil and gas seismic interpretation. None of the trap sites have been drilled however, and further analysis is needed to define the potential for reservoir sands within the zones. Two anticlinal structures are identified along seismic lines S76-159 and S74-006, representing a sequence of draped sediments overlying basement horst structures (Figure 3 – A and B). The sediments overlie the 15At1 reflector [4], representing sandstones of possible Turonian age within the St Lucia Formation. The structure (B) is evident at all stratigraphic levels between the Cenomanian-Turonian reflector (15At1) and the Cretaceous-Tertiary boundary (22At1). The structure represents a closed structure with potential 4-way closure over an area of ~100 km^2. Down-dip of this structure along S76-159, a secondary closure is evident below the Cretaceous-Tertiary unconformity (C), with sediments draped over a potential fault structure (Figure 3).

Within the syn-rift succession, a number of structural fault traps are evident in graben structures, where sediments of syn-rift and possibly Makatini Formation association abut basement lithologies. As no downhole pressure testing has been undertaken within the wells in the basin, the sealing potential of the faults is unknown. However the basement lithologies within the region are represented either by Natal Group siltstone and shale, Dwyka Group tillite, or Karoo Supergroup volcanics. In most instances these lithologies have the potential to form good seals due to limited porosity and permeability related primarily to fractures and jointing. Seismic evidence suggests that faulting ceased prior to deposition of the Mzinene Formation, with thick successions of unfaulted siltstone and marine claystone potentially acting as overlying seals for faults with potential transmissivity.

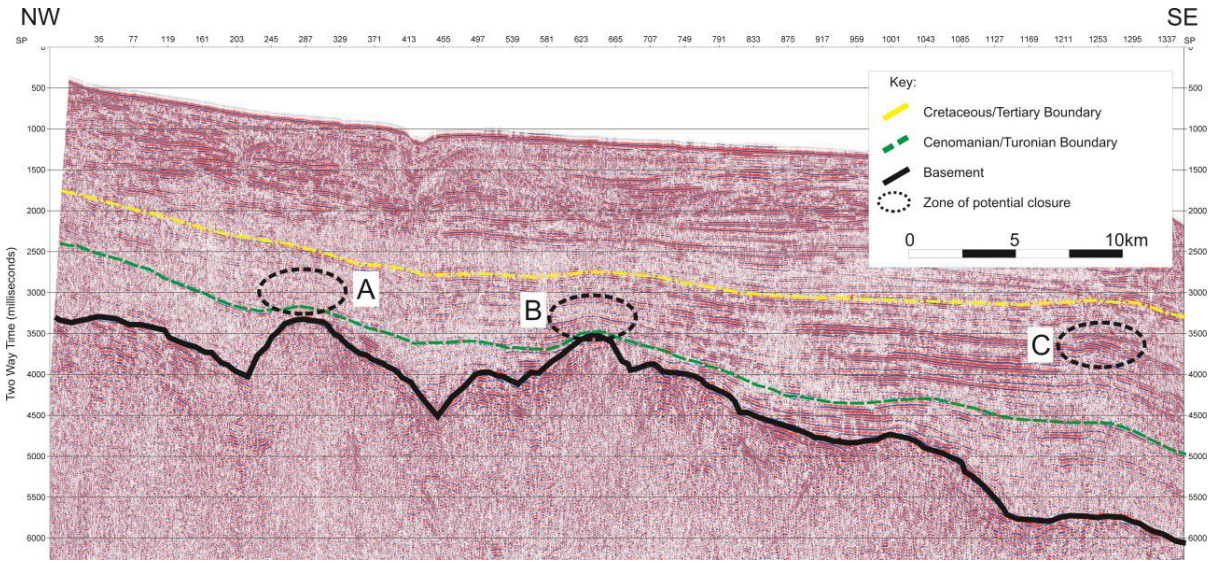

Figure 3: Seismic section SA76-159 with approximate levels of major boundary reflectors indicated. Note the anticlinal structure with associated sediment draping at A and B. Note the anticlinal structure below the Cretaceous-Tertiary boundary at C.

Two such traps are evident in seismic line S74-007 (Figure 4), where syn-rift graben fill thins out and is truncated against basement high zones. Zone (A) occurs on the landward side of a major graben structure where syn-rift and early drift sediments (potentially correlated with the Makatini Formation) thin out and are truncated up-dip against a major normal fault. Zone B is identified down-dip of "A" where sediments of potentially similar age are truncated against a large horst structure.

In both instances these zones are undrilled; with the nearest well (Jc-A1) sited up-dip of zone A. Jc-A1 intersected only upper Cretaceous units, with the oldest sediments being of late Cenomanian to Turonian age [13]. This suggests that ~1500 m of early Cretaceous sediment preserved within the graben structure down-dip of Jc-A1 is likely to be truncated against the basement horizon updip creating a potential structural trap zone if reservoir sandstones are developed. Sandstones identified in the Makatini Formation to the north are represented by ~50 to 100 m tight sandstones of Aptian age, with similar deposits identified in Jc-B1 and Jc-D1, suggesting that the potential for sandstone development in these zones is high.

3.2.2. Reservoir sandstones with stratigraphic traps

Preliminary seismic analysis has identified a number of potential basin floor fans present at varying stratigraphic levels within the basin. Zone C in Figure 4 represents a ~10 km long basin floor fan developed upon the Cenomanian/Turonian unconformity with lateral pinch out up- and down-dip against the palaeo-slope. The fan attains a maximum thickness of ~300 m but its lateral extent parallel to the coast cannot be defined as no seismic intersections are available along its profile. It is assumed by Petroleum Agency SA [4] that the fan has an area of closure of ~100 km^2. It is suggested by Petroleum Agency SA [4] that the reservoir lithologies are potential turbidite sandstones with stratigraphic pinchout traps against shale slope facies.

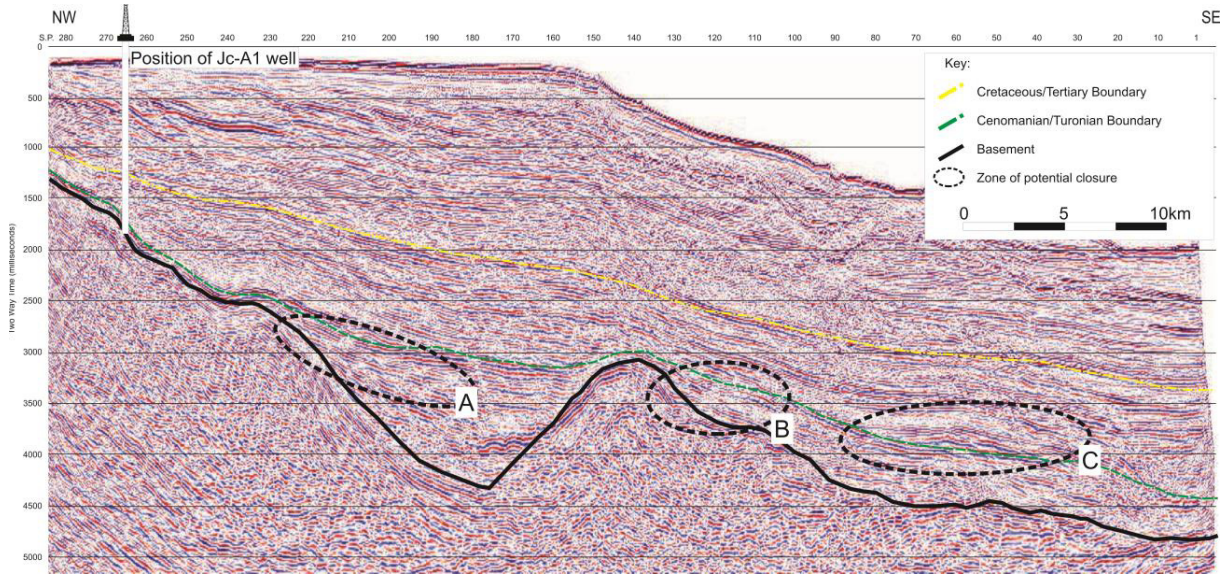

Figure 4: Seismic section S74-007. Major reflectors are shown with potential structural and stratigraphic trap zones identified. Zones A and B represent up-dip structural fault traps within syn-rift and Makatini Formation sediments, whilst Zone C represents a well-developed basin floor fan complex within the St Lucia Formation, directly overlying the Cenomanian/Turonian unconformity.

Although Viljoen et al., [2] suggest that sandstone of Cretaceous age represent the target horizons within the offshore basins, a ~300 m thick succession of interbedded sandstone, limestone and minor claystone is intersected in the Jc-D1 well between 770 m and 1060 m depth from KB (KB to seafloor is 110 m). Although the formation top of this unit occurs above ~800 m depth, the overlying lithologies form a potentially good seal, dominated by ~300 m of claystone with subordinate thin stringers of limestone and silty sandstone. The sandstones are of Miocene age, overlying the Miocene/Oligocene unconformity [14]. Individual sandstones range in thickness from ~5 to 17 m interbedded with shales ranging from 2 to ~6 m in thickness. The thickest reservoir package occurs between ~920 and 990 m, represented by an interbedded succession of sandstone (40%) and limestone (60%). The lowermost zone within the package occurs between 1010 m and 1060 m and is represented by sandstone (60%) interbedded with minor limestone (15%) and claystone (25%). The sandstone is generally light to medium grey, fine- to very fine-grained, moderate- to poorly-sorted with a weak calcite cement [14]. The limestone is often sandy, commonly grading into sandstone in places, true limestones are generally firm to hard with a cryptocrystalline to finely crystalline matrix. Claystones are generally soft and commonly silty, amorphous, and often calcareous.

Although work on the lateral extent of this unit has yet to be undertaken, the zone represents a prospective reservoir that may occur in other portions of the basin.

4. Discussion

4.1. CCS Reservoir Capability

Although the potential for reservoir sandstones within the Durban basin is good, no intersections of considerable thickness were made in the Jc-Series wells. McMillian [11] suggests that the Durban basin is dominated by claystone within only minor sandstone lenses identified within the Early Aptian and late Campanian.

Despite the lack of identified sandstones, seismic evidence and lateral facies correlation with the onshore Zululand basin to the north suggests the potential for shallow marine sandstones at depth within the basin. McMillian [11] indicates that the "11" sandstone which marks the top of the early Turonian appears to cover almost the entire Turonian palaeo-shelf of South Africa. The only basin where it has yet to be drilled is the Durban basin, but identification of extensive, clean, gritty and locally pebbly, quartz sandstone within the onshore Zululand basin suggests that this unit is likely present within the undrilled portions of the Durban basin. This unit has porosities of 30 to 40% with permeabilities (Horizontal in air) varying between 20 – 230 mD [15]. Although it is proposed by McMillian [11] that the sandstones occur within the undrilled region of the Durban basin their reservoir properties are unknown with stratigraphic heterogeneity probable.

Early Aptian sedimentation within the onshore Zululand basin also produced thick sandstone/siltstone successions deposited in estuarine, tidal flat and shallow-marine environments [16] and/or deltaic deposits [15]. The sandstones are represented by a 121 m thick succession of siltstone and fine-grained sandstone in borehole ZA but thin out rapidly against basement highs. This thinning of the Aptian sandstones is also identified within the Durban basin, where seismic profiles suggest thick Aptian age sedimentation in the downdip, undrilled portion of the basin with think successions preserved against the basement highs. Porosity and permeability analysis undertaken by Gerrard [15] in the Zululand basin indicated that the Aptian sandstone, although having porosities of 10 – 20% has exceptionally poor permeabilities (<1 mD) due to a high percentage of clay matrix. Although cored within the Jc-B1 well, uncertainty exists regarding the potential Aptian-age reservoirs within the Durban basin as these sandstones have been heavily intruded by dolerite and their reservoir capabilities reduced by contact metamorphism.

Although the drilled portion of the Durban basin is dominated by a thick claystone interval [11], the potential for reservoir sandstones exists within undrilled grabens in the Durban basin. These data are therefore subject to uncertainty as the potential sites identified within the Durban basin remain undrilled. The sandstone potential although theorised, is yet to be proven, increasing the risk of the current project. The lack of exploration drilling within the region poses a second issue to current CCS calculations with a lack of reservoir quality data within the basin reducing the accuracy of proposed reservoir storage calculations. Porosity and permeability data was therefore obtained from analogue formations within the onshore Zululand basin to the north [15]. Injectivity potential at potential sites within the basin is a large issue as this requires detailed reservoir property measurements which have not been undertaken for the basin. Although analogues such as those in the Zululand basin can be utilised [15], facies variations or changes in porosity and permeabilities may severely affect the injectivity potential of some zones.

4.2. Storage Capacity Estimate of the Durban basin

Although a large amount of vital reservoir data are lacking within the basin, a static method calculation based upon the CO_2 storage capacity of deep saline reservoirs [17] was undertaken to estimate the potential capacity of the identified sandstone reservoirs within the mapped areas.

It must be noted that inaccuracy is inherent within the calculations as the estimate depends on specific reservoir data, some of which is limited or not available. It is therefore suggested that if additional information be acquired, the estimates be recalculated accordingly. Although a geometrical factor is used in the formula when storage occurs in a depleted oil and gas reservoir, it is usually not used for storage in saline reservoirs, since it is incorporated in the efficiency factor. CO_2 trapping mechanisms such as, structural/stratigraphic trapping, hydrodynamic trapping, residual trapping, solubility trapping and mineral trapping [18], are important factors as they influence the storage volume and storage volume assessment method [19]. A further important factor to take into account is whether storage occurs in a closed, open or semi-closed system. No refinement of calculations was made in this study to incorporate the different trapping mechanisms, permeability and pressure conditions in the reservoir [20; 21; 19].

The following formula was utilized or calculation purposes:

$M_{CO2} = A_t\, h_g\, \varphi_{tot}\, \rho\, E$ (see Table 1).

Table 1. Volumetric equation parameters for calculation of CO_2 storage capacity in deep saline formations [17].

Parameter	Units*	Description
M_{CO2}	M	Mass estimate of saline formation CO_2 storage capacity.
A_t	L^2	Geographical area that defines the basin or region being assessed for CO_2 storage calculation.
h_g	L	Gross thickness of saline formations for which CO_2 storage is assessed within the basin or region defined by A.
φ_{tot}	L^3/L^3	Average porosity of entire saline formation over thickness h_g or total porosity of saline formations within each geological unit's gross thickness divided by h_g.
P	M/L^3	Density of CO_2 evaluated at pressure and temperature that represents storage conditions anticipated for a specific geological unit averaged over h_g. See Figure 3.1.
E**	L^3/L^3	CO_2 storage efficiency factor that reflects a fraction of the total pore volume that is filled by CO_2 ([2] stipulates that for South African basins for which net storage areas and thicknesses data are used, this factor should vary from 0,04 to 0,16 for deep saline reservoir storage.)

* L is length; M is mass.

Viljoen et al., [2] combined their storage capacity estimates of the offshore Durban and Zululand basins giving a potential area of ~81 000 km^2 and a potential CO_2 storage capacity of 42 282 Mt based upon a net sandstone thickness of 60 m over the area. However, the 10 000 km^2 extent of the Durban basin indicated by [6] is far smaller than that assumed by Viljoen et al., [2] in their calculations. Therefore if only the 10 000km^2 Durban basin were selected, calculations based upon Viljoen et al. [2] data suggest that the theoretical storage capacity of the Durban basin alone is ~5 000 Mt.

5. Conclusions

Initial evaluation of the offshore Durban basin on the eastern seaboard of South Africa suggests that a thick succession of late Jurassic to Cretaceous sediment is preserved, overlain by a ~1800 m thick Cenozoic interval of Palaeocene, Early to Late Eocene, Early Oligocene and Early to Middle Miocene age. The drilled sequence is dominated by shelfal claystone and minor sandstone with syn-rift and drift phase sedimentation defined throughout the basin. Although limited sandstone reservoirs have been intersected in boreholes drilled along the continental shelf, the potential for reservoir sandstones downdip is high, with numerous structural and stratigraphic trap sites defined through first pass seismic mapping. First-pass storage calculations within the Durban basin are modified from previous work undertaken by Viljoen et al., [2], with a proposed 5000 Mt of potential storage capacity.

6. Acknowledgements

Mr. Nigel Hicks would like to thank the South African Centre for Carbon Capture and Storage for supplying the bursary funding for the current project. The Council for Geoscience is also thanked for its contributions towards the project through its Statutory Project ST-2013-1183, and the permission to publish.

7. References

[1] IPCC, 2005. IPCC Special report on Carbon Dioxide Capture and Storage. Prepared by Working Group III of the Intergovernmental Panel on Climate Change. [B. Metz, O. Davidson, H. de Coninck, M. Loos and L. Meyer (eds)]. Cambridge University Press, Cambridge United Kingdom and New York, NY, USA, 442pp.

[2] Viljoen, J.H.A., Stapelberg, F.D.J. and Cloete, M., 2010. Technical report on the geological storage of carbon dioxide in South Africa. *Report,* Council for Geoscience, 236 pp.

[3] Cloete, M. 2010. Atlas on geological storage of carbon dioxide in South Africa. Council for Geoscience, Pretoria, South Africa, 60 pp.

[4] Petroleum Agency SA, 2013. Republic of South Africa East Coast Summary Brochure. 4pp. http://www.petroleumagencysa.com/Libraries/Brochures.aspx

[5] Bachu, S., 2003. Screening and ranking of sedimentary basins for sequestration of CO_2 in geological media in response to climate change. *Environmental Geology*, 44, 277–289. DOI 10.1007/s00254-003-0762-9

[6] Broad, D.S., Jungslager, E.H.A., McLachlan, I.R., and Roux, J. 2006. Offshore Mesozoic basins, In: Johnson, M.R., Anhaeusser, C.R. and Thomas, R.J., (Eds). *The Geology of South Africa*. Geological Society of South Africa and Council for Geoscience, 553 – 571.

[7] Patridge, T.C., Botha, G.A. and Haddon, I.G. 2006. Cenozoic deposits of the Interior. In: Johnson, M.R., Anhaeusser, C.R. and Thomas, R.J., (Eds). *The Geology of South Africa*. Geological Society of South Africa and Council for Geoscience, 585-604.

[8] Goodlad, S.W. 1986. Tectonic and sedimentary history of the mid-Natal Valley (S.W. Indian Ocean). Bulletin of Joint Geological Survey/University of Cape Town Marine Geoscience Unit, 15, 415pp.

[9] Kitchin, K. and McLachlan, I.R., 1996. Tectonics and hydrocarbon potential of the east coast of South Africa. Soekor Petroleum Licencing Unit, *Document* SOE-PLU-RPT-001. 49pp.

[10] GGS – Gearhart Geodata Services, 1983. Well completion report, Jc-B1 Durban Basin, East Coast, R.S.A. *Soekor report* No. ACT-2, 7pp.

[11] McMillan, I.K. 2003. Foraminiferally defined biostratigraphic episodes and sedimentation pattern of the Cretaceous drift succession (Early Barremian to Late Maastrichtian) in seven basins on the South African and southern Namibian continental margin. *South African Journal of Science*, 99, 537–576.

[12] Davids, S. 2009. Tugela licence area, Republic of South Africa 2009 *Licence round. Petroleum Agency SA internal report*. 38pp.

[13] Leith, M.J. 1971. Jc-A1 geological well completion report. SOE-DRG-WCR-346. *Petroleum Agency SA report* POF7796, 19pp.

[14] Phillips Petroleum. 2000. Jc-D1 (Rhino) – 1 Final Geologic Report. *Phillips Petroleum South Africa LTD, internal report*. Petroleum Agency SA Report No POF 11846, 261 pp.

[15] Gerrard, I. 1972. Report on progress on the evaluation of the Zululand Basin. *Report*, SOEKOR, PSV 1325 (unpubl.).

[16] Shone, R.W., 2006. Onshore post-Karoo Mesozoic deposits, In: Johnson, M.R., Anhaeusser, C.R. and Thomas, R.J., (Eds). *The Geology of South Africa*. Geological Society of South Africa and Council for Geoscience, 541 – 552.

[17] DOE, 2008. Carbon Sequestration Atlas of the United States and Canada, Second Edition: Appendix A − Methodology for Development of Carbon Sequestration Capacity Estimates. National Energy Technology Laboratory, United States Department of Energy, Office of Fossil Energy. http://www.netl.doe.gov/technologies/carbon_seq/ refshelf/atlasII/atlasII.pdf.

[18] Kaldi, J.G. and Gibson-Poole, C.M. (eds), 2008. Storage Capacity Estimation, Site Selection and Characterisation for CO_2 Storage Projects. Cooperative Research Centre for Greenhouse Gas Technologies, Canberra, CO2CRC, Report No. RPT08-1001, March 2008, 52 pp.

[19] Bachu, S., Bonijoly, D., Bradshaw, J., Burruss, R., Holloway, S., Christensen, N.P. and Mathiassen, O.M. 2007. CO_2 storage capacity estimation: Methodology and gaps. *International Journal of Greenhouse Gas Control*, 1, 430–443.

[20] Kopp, A., Class, H. and Helmig, R., 2009. Investigations on CO_2 storage capacity in saline aquifers — Part 2: Estimation of storage capacity coefficients. *International Journal of Greenhouse Gas Control*, 3, 277–287.

[21] Quanlin, Z., Birkholzer, J.T., Tsang, C-F. and Rutqvist, J. 2008. A method for quick assessment of CO_2 storage capacity I closed and semi-closed saline formations. *International Journal of Greenhouse Gas Control*, 2, 626–639.

APPENDIX II

Marine and Petroleum Geology 78 (2016) 390–404

Contents lists available at ScienceDirect

Marine and Petroleum Geology

journal homepage: www.elsevier.com/locate/marpetgeo

Research paper

Sedimentology and depositional architecture of a submarine delta-fan complex in the Durban Basin, South Africa

Nigel Hicks [a, b, *], Andrew Green [b]

[a] Council for Geoscience, 139 Jabu Ndlovu Street, Pietermaritzburg 3200, South Africa
[b] Discipline of Geological Sciences, School of Agricultural, Earth and Environmental Sciences, University of KwaZulu-Natal, Westville, Private Bag X54001, South Africa

ARTICLE INFO

Article history:
Received 27 July 2016
Received in revised form
28 September 2016
Accepted 28 September 2016
Available online 30 September 2016

Keywords:
Sequence stratigraphy
Shelf edge
Delta
Rift basins

ABSTRACT

The seismic stratigraphy, evolution and depositional framework of a sheared-passive margin, the Durban Basin, of South East Africa are described. Based on single-channel 2D seismic reflection data, six seismic units (A-F) are revealed, separated by major sequence boundaries. These are compared to well logs associated with the seismic data set. Internal seismic reflector geometries and sedimentology suggest a range of depositional regimes from syn-rift to upper slope and outer shelf. Nearshore and continental facies are not preserved, with episodic shelf and slope sedimentation related to periods of tectonic-induced base level fall. The sedimentary architecture shows a change from a structurally defined shelf (shearing phase), to shallow ramp and then terminal passive margin sedimentary shelf settings. Sedimentation occurred predominantly during normal regressive conditions with the basin dominated by the progradation of a constructional submarine delta (Tugela Cone) during sea-level lowstands (LST). The earlier phases of sedimentation are tectonic-controlled, however later stages appear to be linked to global eustatic changes.

1. Introduction

Globally, passive continental margins are defined by broad (~50 km - Shepard, 1963; ~80 km - Helland-Hansen et al., 2012) gently sloping (0.05°; Kennett, 1982) shallow water regions comprising thick sedimentary successions derived from onshore erosion. These have been the object of intense sequence stratigraphic analyses, namely due to their potential hydrocarbon reserves. The sequence stratigraphic analyses of sheared, or structurally controlled passive margins are less conspicuous in the literature (cf. de Lépinay et al., 2016). As de Lépinay et al. (2016) point out, a number of questions arise regarding their evolution in the context of gradient and geodynamic and/or sedimentary setting. It is in this context that the Durban Basin, a portion of the sheared-passive KwaZulu-Natal margin of SE Africa is investigated.

The eastern continental margin of South Africa is unique. It has been subject to prolonged periods of sediment starvation, coupled with tectonic-induced periods of abundant sediment supply (Green, 2011a). It is also dominated by an extremely narrow (~2–12 km) shelf (Martin, 1984; Martin and Flemming, 1986; Green and Garlick, 2011; Cawthra et al., 2012), considered a morphologically inherited feature of the initial shearing phase during margin development (Martin, 1984). In this study, we examine the Durban Basin of the SE African margin, a north-south trending, sediment-filled, sheared-rift basin (Dingle et al., 1978). The basin itself is conspicuous by the development of the Tugela Cone, an anomalous deep-water fan complex of late Cretaceous to Tertiary-age (McMillian, 2003), that occurs beneath and seaward of the present shelf break.

This paper aims to assess the sedimentology and sequence stratigraphic history of the Durban Basin, highlighting controls on sedimentation as the margin evolved from a sheared-rift to drift sequence. We propose a model for the basin, and compare and contrast to the current models for structurally controlled (Martins-Neto and Catuneanu, 2010; Helland-Hansen et al., 2012) and passive margin (Catuneanu et al., 2011) basins.

2. Regional setting

2.1. Geology

The Mesozoic evolution of the Durban Basin is poorly

* Corresponding author. Council for Geoscience, 139 Jabu Ndlovu Street, Pietermaritzburg 3200, South Africa.
E-mail address: nigel.hicks101@gmail.com (N. Hicks).

http://dx.doi.org/10.1016/j.marpetgeo.2016.09.032
0264-8172/

documented (Du Toit and Leith, 1974; McMillian, 2003); with work focussed on either low resolution single-channel seismic reflection data (Dingle et al., 1978; Martin, 1984; Goodlad, 1986), or seafloor sediment dynamics, submarine canyon formation and Holocene geology (Green and Garlick, 2011; Cawthra et al., 2012; Green et al., 2013; Wiles et al., 2013). The basin is structurally complex with basement comprising rifted Carboniferous-Jurassic sedimentary and volcanic lithologies of the Karoo Supergroup (Johnson et al., 2006). The basin owes its existence to continental rifting during early Gondwana break-up ~183-159 Ma (Leinweber and Jokat, 2011), bounded to the north by the Naude Ridge, the east by the Mozambique Ridge, and to the south by the Southern Natal Valley (Fig. 1) (Martin et al., 1981; Goodlad et al., 1982). The southern boundary coincides with a major east-west trending fault system that forms the limit of the Agulhas-Falkland Fracture Zone (AFFZ) (Broad et al., 2006). The final stages of rifting in the basin occurred between 115 and 90 Ma Watkeys and Sokoutis (1998), with passive margin conditions prevailing since ~90Ma (Ben Avraham et al., 1993; Watkeys, 2006).

Kimmeridgian to Cenozoic age sediments (Broad et al., 2006) comprise the basin-fill with the main focus of sedimentation occurring within the Tugela Cone (Fig. 1). Based on regional unconformities identified from the biostratigraphy of the Jc-series boreholes and 2D seismic reflection data, Dingle et al. (1978) and McMillian (2003) subdivided the units into syn-rift and drift sequences broadly correlated with the coeval Zululand Group in the onshore Zululand Basin to the north of the study area (Fig. 1) (Broad et al., 2006). Since the late Cretaceous, deposition along the continental shelf is marked by several hiatuses which have resulted in incomplete preservation of the drift stratigraphy (Green, 2011a).

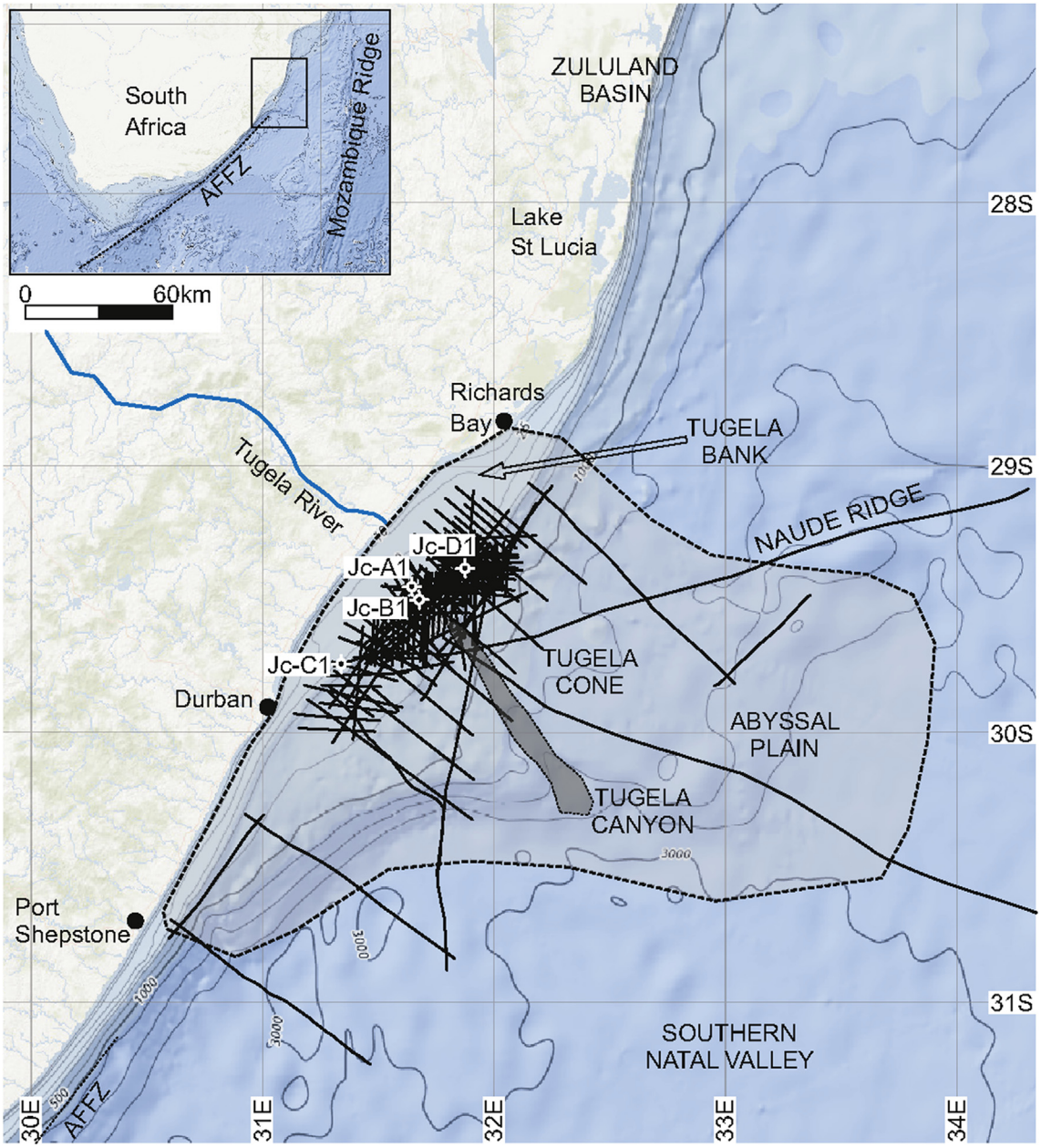

Fig. 1. Locality map detailing study area location with National Oceanic and Atmospheric Administration (1 min grid) UTM showing study area and Indian Ocean bathymetry. The areal extent of the Durban Basin is shown within the shaded polygon. Note the relative position of the Jc-series boreholes drilled on the continental shelf to that of the deep water Tugela Cone and the Abyssal Plain.

Early Cenozoic deposition within the Durban Basin has no lateral correlation with onshore deposits, strictly associated with the construction of the Tugela Cone, an asymmetric submarine delta-fan complex seaward of the Tugela River (Goodlad, 1986). A regional seismic reflector Jimmy (Goodlad, 1986) represents a late Pliocene/early Pleistocene unconformity which is traceable throughout the Natal Valley (Green, 2011a) but not in the Jc-series boreholes. Post-Jimmy deposits reflect sediment starvation of the upper margin, with late Pleistocene deposits occurring as remnant palaeo-dune cordons and coast-parallel reef systems (Green, 2011b), and Holocene sedimentation occurring as ~20 m thick unconsolidated sediment wedges and valley fills (Green and Garlick, 2011; Cawthra et al., 2012).

2.2. Physiography

Extending between the coastline and the 2000m isobath, the Durban Basin covers an area of ~10,000 km^2 (Broad et al., 2006) with the ~5000 m thick sedimentary succession derived from rapid erosion and high sediment influx via short, fast flowing river systems draining the high hinterland (2000–2500 m amsl) and marginal escarpment which have been in existence from the mid Cretaceous (Dingle et al., 1978; Partridge and Maud, 2000; Partridge et al., 2006; Green et al., 2013). The KwaZulu-Natal continental margin is bounded by a narrow shelf, except in the region of the Tugela Bank where it broadens to ~45 km due to the progradation of the Tugela Cone (Martin, 1984; Martin and Flemming, 1986). The Tugela Bank comprises a shallowly dipping, 0.2° (Goodlad, 1986) continental shelf with the shelf-break at −100 m. The upper slope is defined by shallow gradients of 1.7°–2.1°, compared with world averages of 4.28° (Goodlad, 1986). The slope and rise are dissected by the Tugela Canyon (Fig. 1) which obliquely crosscuts the Tugela Cone from the upper slope, 50 km offshore, in a NW to SE orientation (Goodlad, 1986; Wiles et al., 2013). To the west of the Tugela Cone, the continental rise is separated from the Mozambique Ridge by a deep abyssal plain which deepens to the south, finally merging with the Transkei Basin at 4000 m depth.

3. Methods

3.1. Data collection and processing

The Durban Basin is traversed by 2761 km of legacy, reprocessed, migrated stack 2D seismic reflection profiles obtained over a period spanning the 1970's to 1990's. Two thousand kilometres of single-channel 2D seismic were obtained from the Petroleum Agency of South Africa (PASA) in SEGY format. These span an area of 175 000 km^2 and cover the continental shelf, slope and abyssal plain between the KwaZulu-Natal coastline and the Mozambique Ridge. Seismic data comprise eleven exploration programmes which form a 32 000 km^2 grid at ~4 km^2 grid spacing on the continental shelf.

Well log and downhole geophysical data were obtained for the four Jc-series exploration wells that were drilled on the continental shelf offshore between 1970 and 2000 (Figs. 1 and 2). Well completion reports, engineering reports, lithology logs and log analysis reports were obtained from the Council for Geoscience and PASA.

3.2. Data interpretation

SEGY data and log data were interpreted in IHS Global Inc. Kingdom Advanced V2015.0. Digital well shoot/velocity data from the Jc-D1 well were utilised by PASA to define two-way time vs measured depth (m) in order to tie well bore data to the seismic data. Sequence stratigraphic nomenclature and interpretation in this paper are based upon the recent sequence stratigraphic procedures defined by Catuneanu et al. (2009); Martins-Neto and Catuneanu (2010) and Catuneanu et al. (2011).

4. Results

Six seismic units are delineated within the Durban Basin. These are based upon seismic bounding features, impedance, and internal-reflection characteristics (Table 1). The units characterised represent sedimentation within the basin that occurred after the formation of the post-Karoo Supergroup basement unconformity.

4.1. Unit A

The deepest resolved unit within the basin, unit A, occurs as a discontinuous succession unconformably overlying acoustic basement along a high amplitude reflector S1. The unit terminates updip against faulted pre-breakup basement (Fig. 2a–b) but thickens substantially downdip, increasing from 0 to 1sec two-way time in thickness (Fig. 2b). In the north of the basin, unit A thins substantially, occurring as a ~0.2sec thick succession defined by high impedance reflectors in small graben-fill successions (Fig. 2c). Unit thickness is dependent upon palaeo-topography, with the unit onlapping against basement horst structures (Fig. 3) and is best developed in Jc-C1 (Fig. 2) where ~900 m of siltstone and claystone with subordinate sandstone is intersected. An upward increase in reflector impedance is noted in the succession (Fig. 3), and this can be correlated with sandy to conglomeratic units intersected in Jc-B1 and Jc-D1 (Fig. 2c – Jc-D1 Inset a) with the gamma ray logs in Jc-B1 showing an upward coarsening of facies at the top of the unit (Fig. 2b – Jc-B1 Inset a).

Within unit A, two seismic facies occur beneath the Tugela Cone, best defined from coast-parallel seismic reflection profiles (Fig. 4). Facies A1 is an aggradational succession of low impedance reflectors which increase in impedance strength with stratigraphic height (Fig. 4). Reflector architecture is dominated by parallel to sub-parallel internal reflectors which parallel the basement-cover interface. Facies A2 overlies A1, separated by a discontinuous high amplitude surface identified in coast-parallel profiles (Fig. 4). The surface hosts numerous incisions (arrows in Fig. 4) which are commonly U-shaped and range from 800 to 1100 m wide and 20–30 m (0.30–0.4 s TWTT) deep. Although the internal architecture of the facies is the same as facies A1, the base of facies A2 is defined by low impedance reflectors which appear to onlap the incision surface (Fig. 4).

4.2. Unit B

Unit B overlies unit A along an erosional, high amplitude seismic reflector S2, which can be traced through much of the distal portions of the basin. Proximally, the reflector truncates against faulted basement, with unit B unconformably overlying seismic basement in the updip profile (Fig. 2a–b). Two facies are defined (B1-2) with facies B1 represented by a series of laterally discontinuous, high impedance reflectors that occur as mounded zones onlapping and downlapping onto the underlying unit (Figs 5 and 6). The positions of the mounds relative to the contemporary shoreline are shown as polygons on the seismic grid map insets in Figs. 5 and 6. Two dominant architecture styles, *single* and *retrograde*, are identified. Single mounds have a basal progradational structure with seaward-dipping reflectors downlapping the underlying reflector S2 whilst landward dipping reflectors are seen to migrate updip and onlap surface S2 (Fig. 5). Where multiple mounds are developed (Fig. 6a–b), an overall retrogradational architecture is recognised as

Table 1
Simplified sequence stratigraphic framework for the continental margin within the Durban basin, describing seismic units, facies, bounding surfaces, interpreted depositional environment and the age of each unit (ages based upon McMillian, and Dale, 2000; McMillian, 2003; Green et al., 2008).

Unit	Facies	Surface	Modern description	Stratal relationship	Thickness (two-way time)	Interpreted depositional environment	Systems tract	Age
F	F4			Transparent reflector package	0.2s	na	na	Holocene?
	F3		Chaotic Reflector Package	Wavy to chaotic moderate to low amp reflectors	0–0.2s	na	na	Pleistocene to Pliocene?
	F2		Progradational wedge	High impedance, sub-parallel, progradational reflectors	0–0.2s	Lowstand shelf edge delta	LST	Pliocene
	F1		Channel Fill	Onlapping and lateral accretion fills, chaotic, high amplitude reflectors	0–0.2s	Incised Valley Fill	LST	Pliocene
		S6	Shelf-confined erosional reflector					
E	E3		Aggradational package	Low impedance, sub-parallel, aggradational reflectors	0–0.2s	Inner to Mid Shelf	TST	Miocene
	E2		Progradational wedge	High impedance, sigmoid, progradational reflectors	0–0.3s	Lowstand shelf edge delta	LST	Miocene
	E1		Channel Fill	Onlapping and lateral accretion fills, chaotic, moderate amplitude reflectors	0–0.2s	Incised Valley Fill	LST	Miocene
		S5	Shelf-confined erosional reflector					
D	D2		Progradational wedge	Moderate impedance, steeply dipping, progradational reflectors	1s	Lowstand shelf edge delta	LST	Miocene to Oligocene
	D1		Channel Fill	Onlapping and lateral accretion fills, chaotic, moderate amplitude reflectors	0–0.2s	Incised Valley Fill	LST	Oligocene
		S4	Basin-wide Erosional Reflector					
C	C5		Progradational wedge	Moderate impedance, steeply dipping, progradational reflectors	0–0.3s	Highstand wedge	HST	Eocene
		3C	Maximum Flooding Surface					
	C4		Aggradational to Retrogradational package	Low impedance aggrading reflectors, backstep and onlap 3B landward	0.1–0.3s	Healing Phase wedge	TST	Palaeocene
		3B	Maximum Regressive Surface					
	C3		Aggradational to Progradational Wedge	Low to moderate impedance, sub parallel, aggradational reflectors, onlap S3	0–0.5s	Delta Margin	LST	Maastrichtian to Campanian
	C2		Progradational wedge	Moderate impedance, steeply dipping, progradational reflectors	0–0.5s	Falling stage wedge	FSST	Maastrichtian to Campanian
	C1		Slope Fan	Moderate impedance, progradational reflectors, downlap and onlap S3	0 to 0.3s	Falling stage slope fan apron	FSST	Campanian
		S3	Shelf-confined erosional reflector					
B	B2		Aggradational ramp	Low to moderate amp, sub parallel reflectors, onlap S2 updip.	0–0.5s	Lowstand ramp	LST	Turonian
	B1		Retrogradational Basin-floor Fan	High impedance progradational reflectors that downlap and onlap S2, individual mounds show internal progradation but retrograde as packages.	0–0.3s	Falling stage basin floor fan	FSST	Turonian
		S2	Basin-wide Erosional Reflector					
A	A2		Syn-rift valley fill	Aggradational to Progradational packages that onlap S1 against basement highs	0–1s	Syn-rift valley fill	Syn-rift TST/HST	Cenomanian to Aptian
	A1		Syn-rift valley fill	Aggradational to Progradational packages that onlap S1 against basement highs		Syn-rift valley fill	Syn-rift TST/HST	Aptian to Kimmeridgian
		S1	Basin-wide Erosional Reflector					
BASEMENT			Acoustic Basement					Jurassic

younger features onlap successively landwards onto the underlying feature.

Where facies B1 does not occur, reflectors of facies B2 onlap S2 progressively landward, with downdip reflectors occurring in an aggradational stacking arrangement (Fig. 2a). This comprises a succession of high impedance reflectors aggradationally stacked above either facies B1 or unit A (Fig. 2a). Facies B2 is represented by a succession of siltstones and claystones of variable thickness

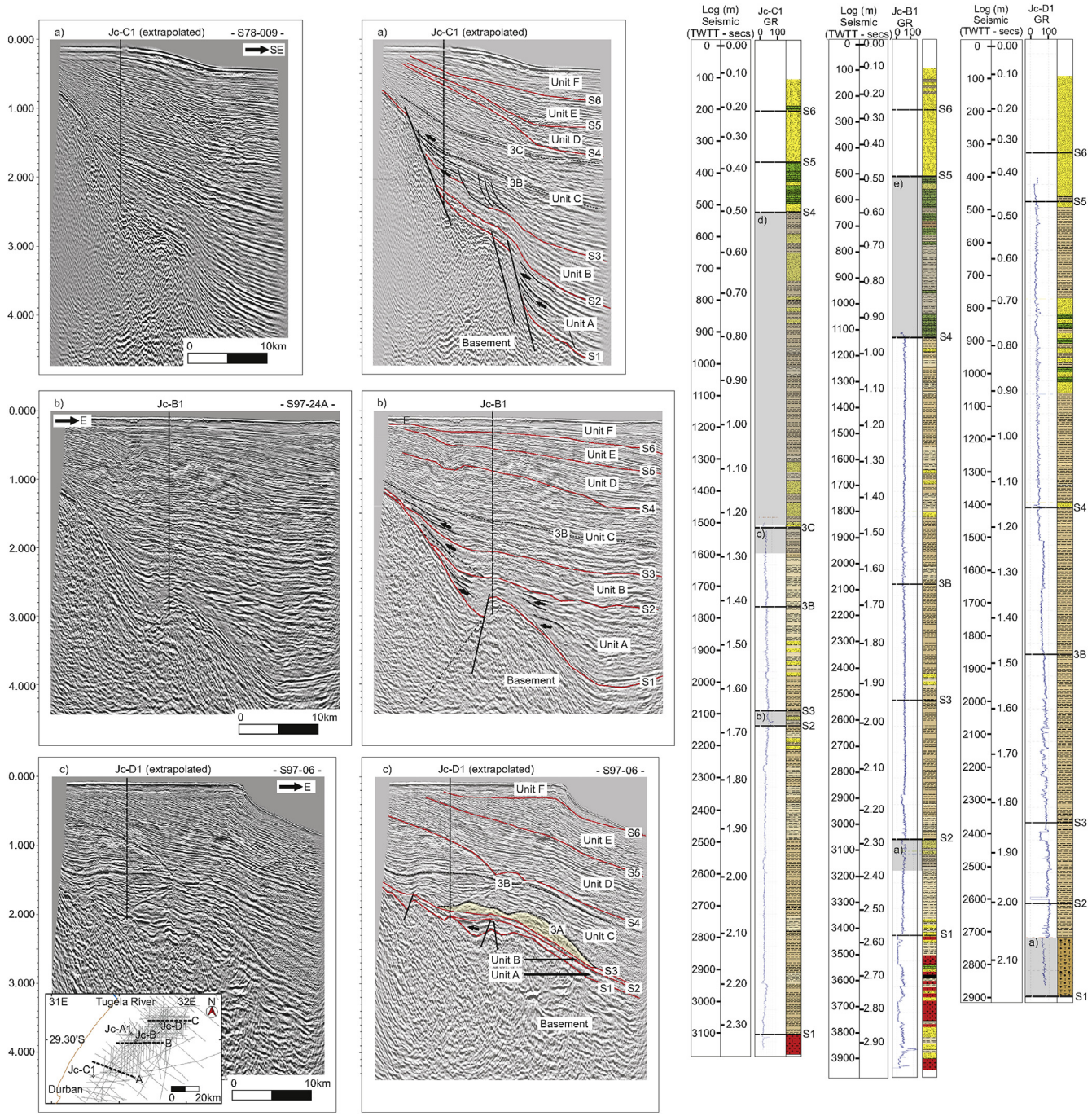

Fig. 2. Seismic profiles and associated well logs showing sediment architecture and lithological and geophysical properties (gamma-ray log) of units beneath the present continental shelf within the Durban basin. Zones of discussion within the well logs are highlighted by greyed insets. a) Seismic profile through the southern basin. Arrows show onlap of seismic reflectors against antecedent basement structures. The extrapolated position of Jc-C1 is shown. b) Profile through the central basin. Arrows show onlap of seismic reflectors against antecedent basement structures. The position of Jc-B1 is shown. c) Profile through the northern basin. Note the shaded area of potential basin floor fan development overlying S3 in the northern basin. The extrapolated position of Jc-D1 is shown.

within the Jc-Series wells (Fig. 2 – Jc-C1 Inset b). Within Jc-B1 and Jc-C1 (Fig. 2), gamma ray logs indicate coarsening upwards sequences capped by thin sandstone packages.

4.3. Unit C

Unit C occurs as a prograding package with an offlapping reflector configuration, separated from the underlying unit by an erosional, moderate amplitude reflector (S3). Under the Tugela Cone (Fig. 7) five facies (C1-5) are resolved. Facies C1 is represented by mounded reflectors that prograde internally, downlapping the underlying reflector S3 (Fig. 2c). This facies is laterally discontinuous, developed along the lower slope in the north of the basin where it is capped by a moderate amplitude reflector surface "3A" (Fig. 2c). Where facies C1 is not developed, reflector S3 is overlain by either facies C2 in the proximal basin, or C3 in the distal basin (Fig. 7). Internal reflector architecture for facies C2 is dominantly progradational, with pronounced downlap on surface S3 (Fig. 7).

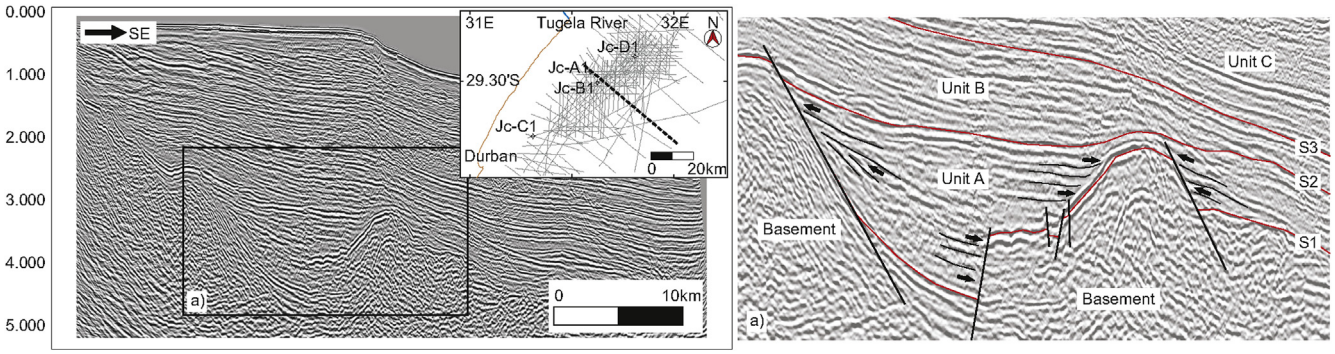

Fig. 3. Syn-rift infill within a graben system in the central Durban basin. Note the onlap and truncation of reflectors against basement structures in both directions.

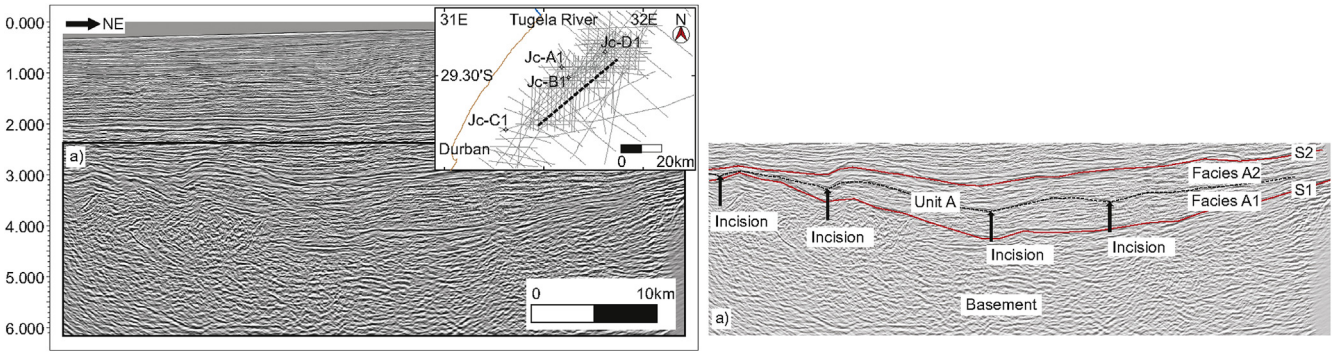

Fig. 4. Coast-parallel seismic profile of unit A showing possible incisions into seismic surface separating facies A1 from A2.

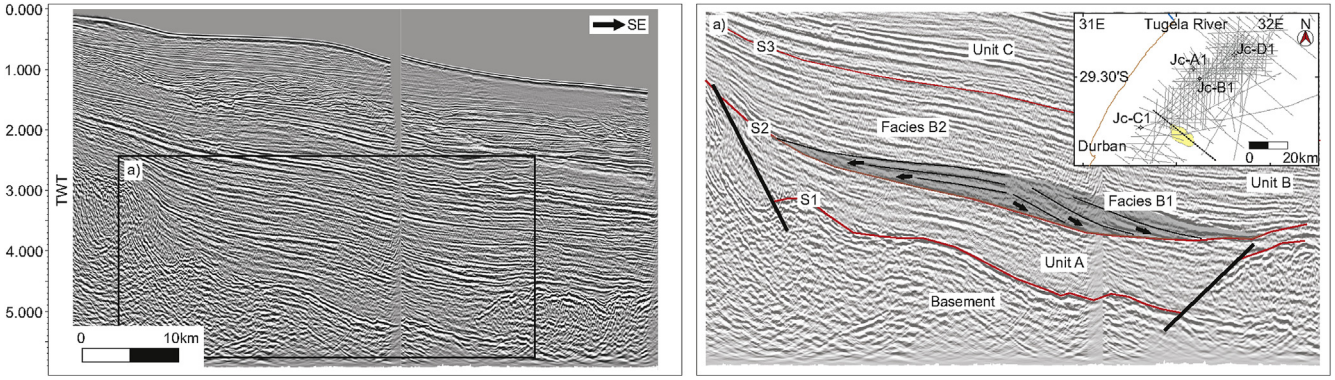

Fig. 5. Singular, mounded structure constituting facies B1, overlying seismic surface S2 in the southern basin. Note the pronounced onlap updip and downlap of reflectors (arrows) onto the underlying surface.

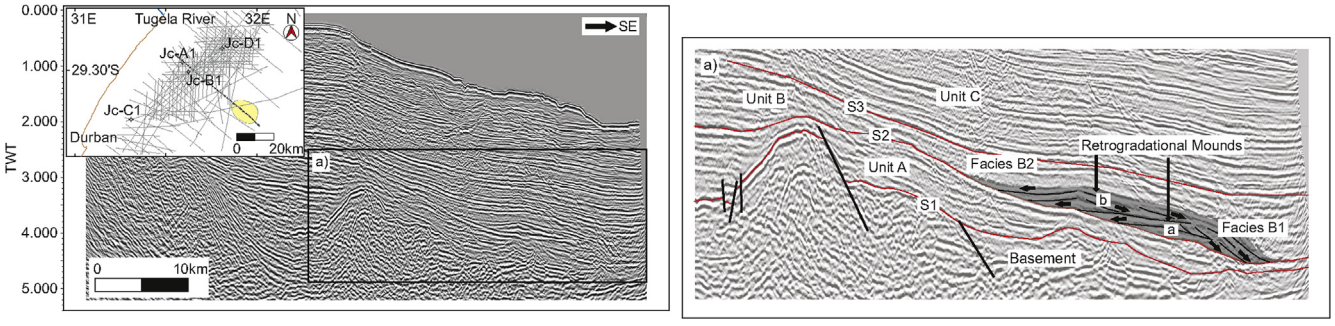

Fig. 6. Multiple, retrogradational mounded structures overlying seismic surface S2, constituting facies B1 in the central basin. Note the pronounced onlap and downlap of reflectors onto the underlying surface. Note the retrogradational stacking pattern of mound a) vs mound b), with mound b) reflectors downlapping upper surfaces in mound a).

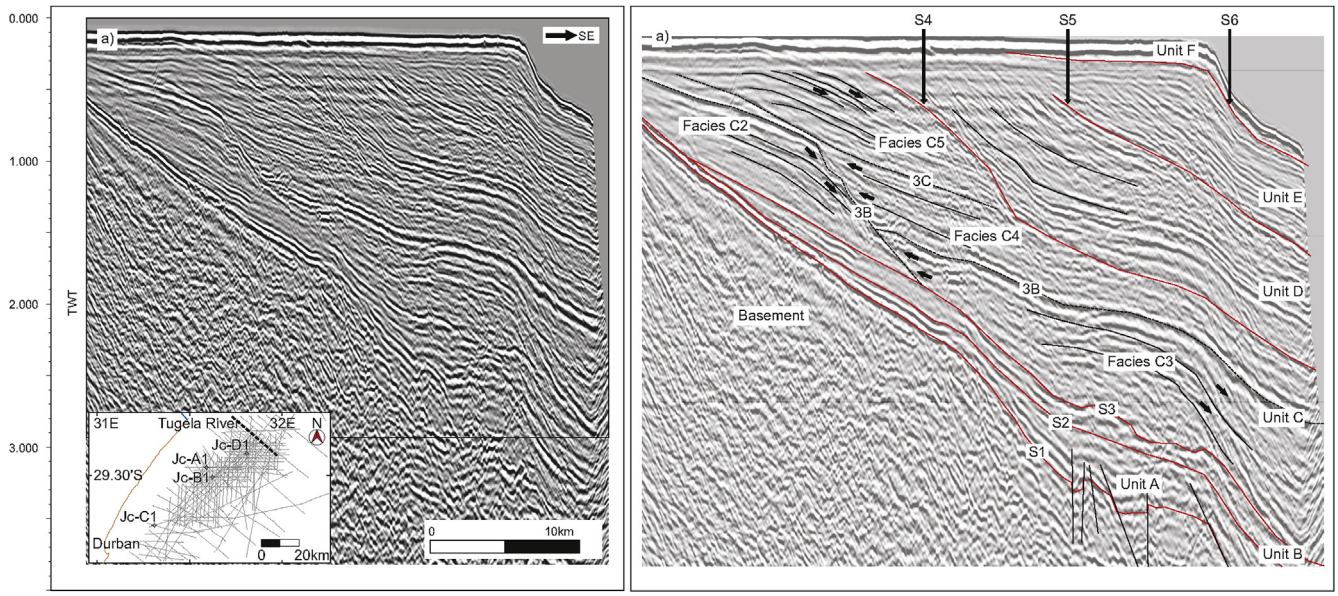

Fig. 7. Seismic architecture of unit C in the northern basin. Note the downlapping progradational reflector package of facies C2 in the inner shelf with progradational reflectors of facies C3 preserved in the deeper portion of the basin. Note the aggradational to retrogradational "healing phase" deposits of facies C4 that progressively onlap facies C2 updip. Note the final progradational reflector package C5 which caps the sequence.

Facies C3 shows aggradational to progradational internal reflectors (Fig. 7). Facies C3 is not well developed in the southern basin, where unit C is dominated by aggradational reflector architectures (Fig. 2a–b). Gamma ray and lithological logs (Fig. 2) indicate that facies C3 is composed of siltstones and claystones with subordinate sandstone stringers which cap upward-coarsening cycles.

Facies C4 is observed throughout the study area, overlying facies C2 and C3 along a high amplitude reflector surface "3B" that marks the base of the most prominent onlap. The facies comprises low impedance, sub-parallel to parallel aggradational to weakly retrogradational reflectors that distinctly onlap the underlying facies C2 updip (Fig. 7). Within the wells, the facies is dominated by claystones and siltstones, capped by a moderate to high gamma ray signature claystone in Jc-C1 (Fig. 2 – Jc-C1 Inset c) and by a 6 m thick limestone in Jc-A1 (Fig. 8 – Jc-A1 Inset e).

Facies C5 is confined to the proximal basin and occurs as a prograding wedge which oversteps facies C5 seaward along a downlap surface"3C" (Fig. 7). The facies is intersected only in Jc-C1 where the package is dominated by coarse-to medium-grained sandstones and subordinate claystones (Fig. 2 Jc-C1 Inset d). No geophysical logs are available for this facies. Thicknesses of facies C5 are variable, with the sequence truncated by a major erosional reflector (S4).

4.4. Unit D

Along coastal strike, unit D overlies a pronounced erosional surface (S4) that delineates a series of U and V-shaped incisions up to 70 m (0.9 s TWTT) deep. Unit D can be separated into two facies which together represent a seaward thickening succession in the northern portion of the study area, but a relatively thin succession in the southern portion of the basin. Facies D1 is an infilling facies with onlapping high amplitude reflectors restricted to coast-perpendicular incisions (Fig. 9). Facies D1 is overlain by facies D2, a seaward dipping, aggradational to progradational set of high impedance, low amplitude reflectors. This facies is laterally continuous along strike (Fig. 2b–c) and comprises calcarenite and coquina interbedded with sandstone and siltstones in all wells (Fig. 2 – Jc-B1 Inset e).

4.5. Unit E

Although unit E is similar in its internal reflector architecture to unit D, the two are separated by an erosional surface S5 that is identifiable in coast-parallel section and delimits a series of U and V-shaped incisions up to 50 m (0.6 s TWTT) deep (Fig. 10). In the northern portion of the Tugela Cone, unit E occurs as a seaward prograding reflector package with pronounced downlap on the underlying S5 surface (Fig. 11). Three facies are identified within unit E, with facies E1 having a similar architecture to that of facies D1, represented by incision fill with high amplitude reflectors onlapping the incision flanks. Incisions and associated fills are identified along both the palaeo-shelf and slope, with both drape fill and flank-attached deposits (Fig. 10). Facies E2 overlies either facies E1 or unit D if E1 is not preserved. Facies E2 consists of high impedance reflectors that in downdip section occur as a seaward prograding set of high impedance reflectors which exhibit pronounced downlap on the underlying S7 surface. Facies E3 forms the uppermost facies, represented by low impedance parallel reflectors that show aggradational stacking patterns. Facies E3 is separated from the underlying facies by a moderate amplitude reflector.

4.6. Unit F

Unit F corresponds to a prograding sediment wedge that occurs on the continental shelf and at the shelf break. The unit is bounded at the base by an erosional high amplitude reflector, S6, with incisions into the underlying unit. In many instances the internal architecture of the unit is obscured by seafloor multiples, but in coast-parallel section (Fig. 10) the succession can be delineated and comprises four facies (F1–F4). Facies F1 represents incision fill where onlapping high amplitude reflectors are restricted to incisions on the palaeo-shelf and slope (Fig. 10a–b). Facies F2 represents high impedance sub-parallel to parallel reflectors. In coast perpendicular section, this facies occurs as a prograding wedge of seaward dipping reflectors, with facies F2 occurring as a distal

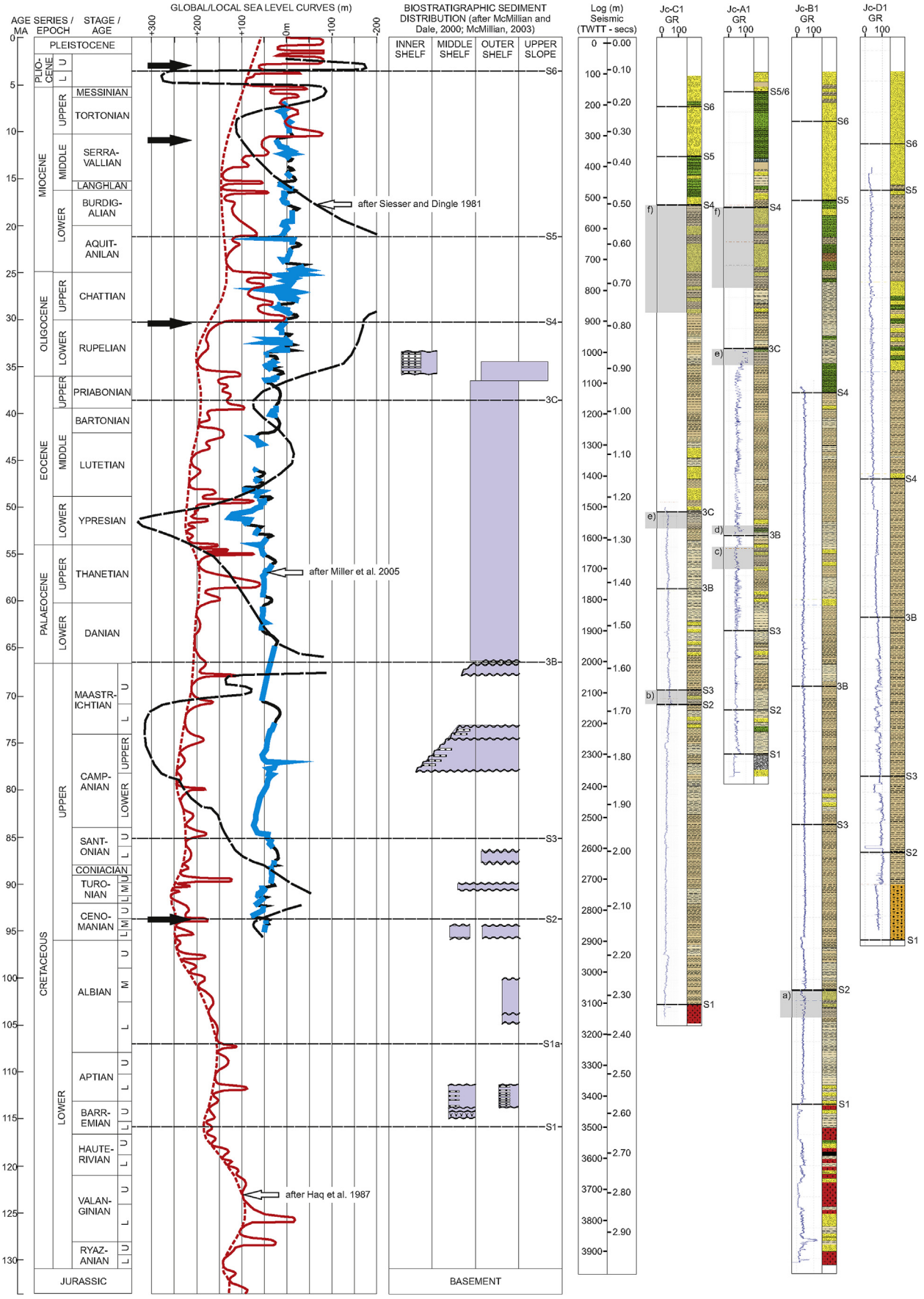

Fig. 8. Biostratigraphy of the Durban basin (after McMillian and Dale, 2000; McMillian, 2003) compared with Jurassic to Pliocene sea-level curves in southern Africa (modified after Siesser and Dingle, 1981) and global eustatic sea-level curves (modified after Haq et al., 1987; Millar et al., 2005). Filled arrows denote uplift episodes of Siesser and Dingle, 1981; Dingle et al., 1983; Partridge and Maud, 2000). Geological and gamma ray logs for all Jc-series boreholes are presented with depths in m and TWTT (sec). Logs are correlated with sea level curve graphs via mapped seismic surfaces (S2; S3 etc.). Areas of interest discussed in log data are shown in greyed areas.

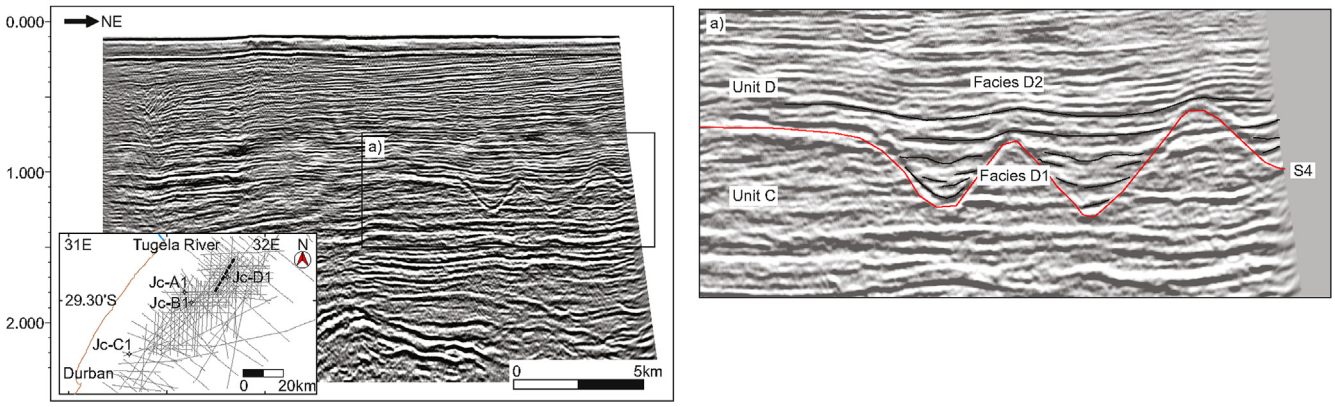

Fig. 9. Coast-parallel seismic profile indicating multiple incisions and associated incision-fill along seismic surface S4 in the northern basin.

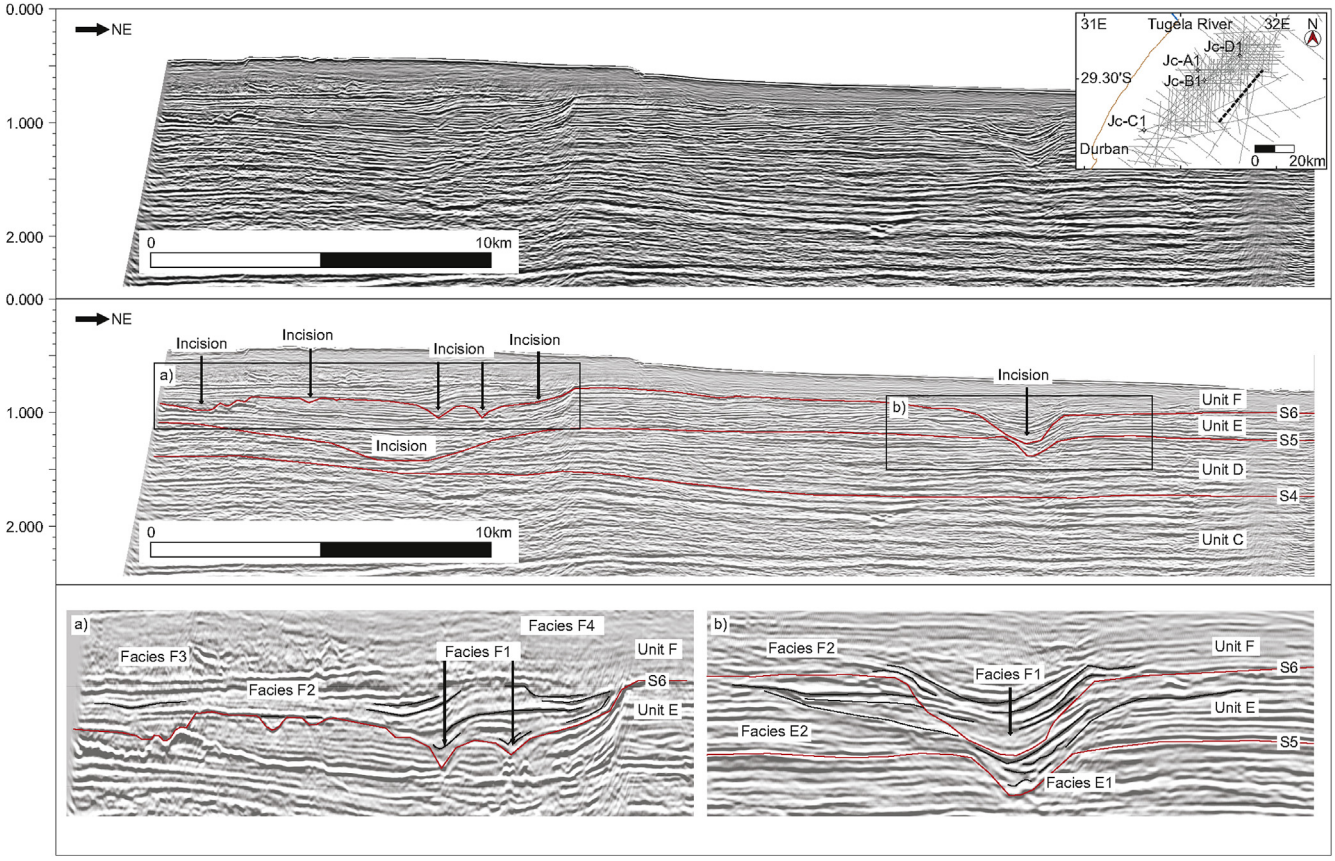

Fig. 10. Coast-parallel seismic profile indicating multiple incisions and associated incision-fill along multiple seismic surfaces S5 and S6 in the southern basin. Note the multiple incision episodes in singular incisions as shown in inset b).

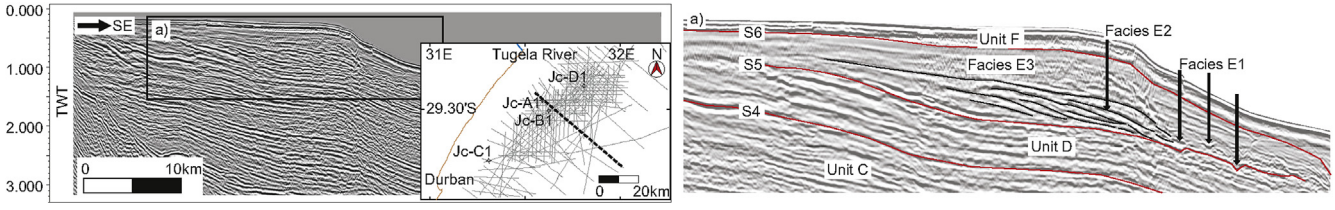

Fig. 11. Progradational reflector package comprising facies E2 overlying seismic surface S5.

succession of aggradational reflectors underlying the seafloor (Fig. 10b). Facies F3 is only evident in coast-parallel section, occurring as chaotic low impedance reflectors (Fig. 10a). Unit F is capped by facies F4 which occurs as low impedance sub-parallel to parallel reflectors.

5. Sedimentary facies and associated depositional regimes

Sedimentation within the Durban Basin is represented by both syn-rift and drift phase sequences. Although conventional sequence stratigraphic analysis (cf. Catuneanu et al., 2011; Zecchin and Catuneanu, 2013) is generally focussed on drift phase sediments in passive margin basins, for rifted sequences separate models need to be utilised with typical rift sequences comprising transgressive and highstand system tracts (cf. Martins-Neto and Catuneanu, 2010).

5.1. Early syn-rift infillings

The spatial distribution of unit A is irregular (Fig. 12a), and represents syn-rift, graben fill of likely lacustrine to fluvial origin (Stojcic, 1979; McMillian, 2003). Seismic reflector architecture in individual grabens shows onlap of chaotic reflectors against fault scarps similar to that defined by Prosser (1993) for “rift initiation” fluvial sedimentation. The identification of continental syn-rift sediments (Fig. 2c – Jc-D1 Inset a) in facies A1 (Stojcic, 1979; McMillian, 2003), overlain by lacustrine facies A2 sediments in the Jc-B1 and Jc-D1 wells (McMillian, 2003) supports Kitchin and McLachlan (1996) proposal that the interval represents a major marine transgression which can be correlated with global sea level rise in the early Albian (Haq et al., 1987) (Fig. 8). Facies A2 likely correlates with “rift climax” sedimentation of subaerial alluvial fans and shoal-type deltas as defined by Prosser (1993).

The increase in reflector impedance upwards in the facies (Fig. 3) suggests a succession of coarsening upward packages bounded by flooding surfaces similar to that defined by Martins-Neto and Catuneanu (2010) for active rift basins. Here a thin transgressive systems tract (TST) of retrogradational reflectors is overlain by aggradational to progradational facies of the highstand systems tract (HST) (Martins-Neto and Catuneanu, 2010). This fits well with the syn-rift deposits identified in Jc-B1 (Figs. 2b and 8 – Inset a), which comprise ~40 m thick upward coarsening, regressive cycles of claystone, siltstone and sandstone (Kitchin and McLachlan, 1996). This facies is likely the equivalent of the Makatini and Mzinene Formations from the adjoining Zululand Basin (Broad et al., 2006) which span the late Barremian to middle Cenomanian.

5.2. Ramp margin deposition

The syn-rift succession is overlain by deposits of unit B, which are bounded at their base by regional seismic reflector S2. This surface marks a major regional hiatus [McDuff – (Goodlad, 1986); 15At1 – (McMillian, 2003)] that, through biostratigraphical data (McMillian and Dale, 2000; McMillian, 2003), is shown to span the late Cenomanian to early Turonian (Fig. 8). This period coincides with marked forced regression and sea level fall around southern Africa as defined by Dingle et al. (1983) (Fig. 8). In the proximal basin, S2 represents a subaerial unconformity (Fig. 12b) with erosion of the underlying units and sediment bypass into the deep basin. Within the deeper basin, facies B1 sediments show progradation and downlap on reflector S2 with mounded, prograding structures (Figs. 5 and 6) representative of deep water, basin floor fans formed by off-shelf sediment forcing and the deposition of high density turbidites (cf. Catuneanu et al., 2011). Fig. 12b shows a zone of proximal bypass and the deposition of isolated fans of facies B1. It is thus postulated that these fans were deposited during forced regression of the falling stage systems tract (FSST) along the palaeo-shelf (sensu Catuneanu et al., 2009, 2011). Due to the downlap evident in reflectors overlying surface S2, we propose that, in the deep basin, S2 represents a basal surface of forced regression “BSFR” (sensu Posamentier and Allen, 1999) with facies B1 separated from facies B2 by a correlative conformity (Hunt and Tucker, 1992) separating FSST and lowstand systems tracts (LST) deposits on the basin floor.

Facies B2 is dominated by aggradational reflectors, and as such represents deposition during a phase of normal regression during the ensuing LST (Catuneanu et al., 2011) with the corresponding sedimentology from Jc-B1 (Fig. 2b) suggesting deposition of deep marine shales in a slope environment (Kitchin and McLachlan, 1996) (Fig. 8). The architecture of facies B2 is dominated by gently dipping, parallel reflector patterns suggestive of deep water deposition within a narrow, 10 km wide, ramp margin (Fig. 12b), similar to that defined by Seyedmehdi et al. (2016) in the Canning Basin, Australia. Antecedent topography defines the mid ramp depositional characteristics with units pinching out laterally updip against surface S2 (Figs. 2,7 and 12b), whilst the landward section of the basin is dominated by a rugged erosional unconformity which we interpret as a subaerial unconformity based upon a biostratigraphical hiatus (Muntingh, 1983) and limited sedimentation in Jc-C1 (Figs. 2a,8 – Inset b).

5.3. Proximal erosional hiatuses and distally focussed deposition

Although outer shelf deposits of Early Santonian age are identified onshore (Anderson, 1906; McMillian, 2003) and beneath the inner continental shelf (Green and Garlick, 2011), representing remnants of the TST and HST correlated with a period of sea-level high within the Durban Basin (Dingle et al., 1983), post-unit B TST and HST successionsw are not preserved distally offshore. In this study, we consider that this period marked non-deposition in the distal basin between the late Turonian and early Campanian as identified in the biostratigraphy (McMillian, 2003), with a laterally extensive bounding surface S3 separating unit B from the overlying unit C.

Based upon biostratigraphical ages defined by McMillian and Dale (2000) and McMillian (2003) (Fig. 8) unit C represents a period of almost continuous distal basin deposition from the Maastrichtian to Eocene. Five facies are resolved, with mounded structures of facies C1 downlapping the underlying surface S3 with progradational internal reflectors similar to retrogressive turbidite lobes identified by Shanmugam (2016); we thus consider them to represent deposition as slope and basin floor fans within the late FSST (Fig. 12c). These were focussed offshore of the position of the contemporary Tugela River (Fig. 12c). Furthermore, in the northern portion of the basin, reflector architecture of facies C2 shows marked progradation with pronounced offlap and limited topset development (Fig. 7) and is truncated above by a subaerial unconformity, a reflector architecture synonymous with forced regressive conditions in the proximal FSST (Zecchin and Catuneanu, 2013). The C2 sequence has been identified along much of the KwaZulu-Natal margin (Fig. 12c) (Green, 2011b; Green and Garlick, 2011) and has been correlated with the relative sea level fall of the late Campanian and early Maastrichtian (Dingle et al., 1983), with sedimentation a product of deltaic deposition from large river systems (Dingle et al., 1983; Goodlad, 1986). In this regard, we interpret Facies C2 as a truncated shelf-edge delta (Fig. 12c) within the FSST as defined by Hunt and Tucker (1992) with Facies C1 representing coeval forced regressive submarine fans. This marks the early stages in construction of the nascent shelf edge.

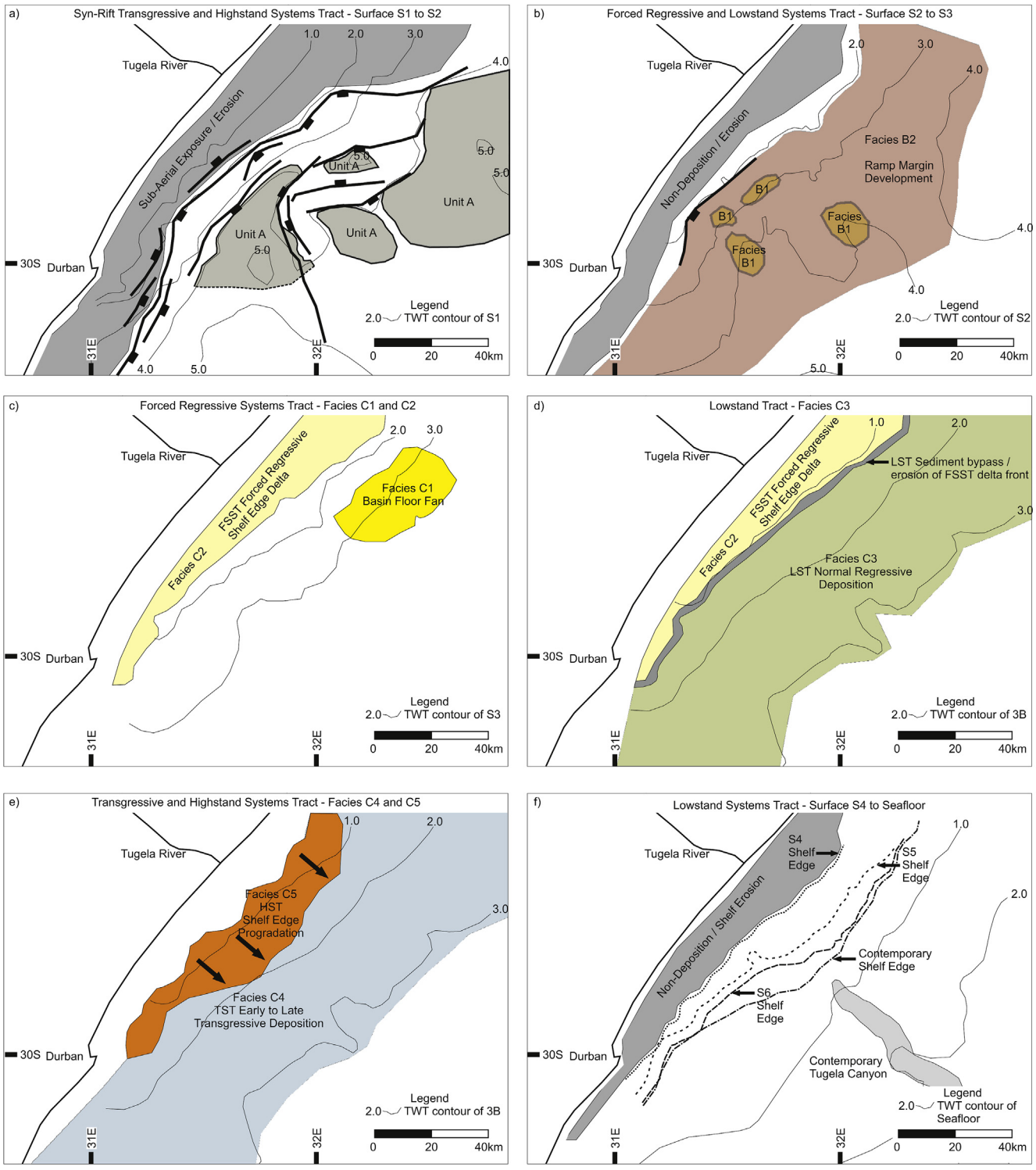

Fig. 12. Spatial distribution for each unit within the Durban basin. a) Syn-rift, transgressive to highstand systems tract sedimentation of unit A in restricted structurally-defined depocentres. b) Position of falling stage and lowstand basin floor fans (facies B1) overlain by ramp margin sedimentation of facies B2. c) Position of basin floor fan relative to facies C2 shelf edge delta. d) Deposition of facies C3 basinward of the palaeo-shelf edge. e) Transgressive systems tract deposition of facies C4 overlain by progradational (arrows) shelf edge delta facies C5. f) Lowstand shelf edge progradation of units D-F defined by relative positions of the palaeo-shelf edge associated with horizons S4, S5 and S6 relative to the contemporary shelf break.

Facies C3 is resolved seaward of the facies C2 FSST (Fig. 12d) and occurs as a seaward thickening wedge of aggradational to progradational reflectors (Fig. 7). The wedge tapers landward, onlapping the underlying S3 surface in the mid-shelf (Fig. 7). The forestepping nature of the reflectors is similar to that of wedges produced during the late LST (cf. Posamentier and Allen, 1999), suggesting stable accommodation space change relative to sediment supply. The C3 lowstand wedge is intersected in Jc-A1, where numerous coarsening-upwards parasequences of claystone and sandstone are identified (Fig. 8 – Inset c). Deposition in a

prograding delta margin setting similar to that discussed by Porebski and Steel (2003) is thus envisioned, with LST sedimentation overlying the FSST slope component. Truncated clinoforms within the FSST shelf-edge delta suggest that this facies has been prone to erosion through current activity, shelf-edge slumping and/or sediment bypass during early lowstand (Fig. 7).

The seismic reflector (3B) which overlies facies C2 and C3 (Fig. 7) is coincident with Cretaceous-Tertiary boundary and forms the base of a distinct retrograding parasequence set in the slope environment. Although difficult to identify in the borehole logs which show limited sedimentological variation due to their location in the deeper shelf settings (Figs. 2 and 8), in Jc-A1, the surface is overlain by a ~6 m thick carbonate that exhibits a marked high gamma ray signal (Fig. 8 – Inset d). The reflector is often not well defined in seismic section, and is not mapped by previous studies (Dingle et al., 1978; Martin, 1984; Goodlad, 1986). Although a limited biostratigraphical hiatus is defined by McMillian (2003), biostratigraphy within the Jc-D1 well (Lester, 2000) suggests continued deposition across the boundary, with a change from more proximal LST deposits to distal TST Tertiary sedimentation. This is corroborated by the sea level curves of Siesser and Dingle (1981), which show a change from regressive to transgressive conditions across the boundary (Fig. 8). Due to the seismic architecture of the parasequences above and below this surface (Fig. 7) combined with sedimentological and biostratigraphical well log data, we propose that surface 3C represents the maximum regressive surface marking the change from lowstand normal regression to transgression (cf. Catuneanu et al., 2009).

Overlying surface 3B, facies C4 is recognised from borehole studies (Du Toit and Leith, 1974) as a ~440 m thick Palaeocene and Eocene-age (Lester, 2000) succession of marine claystones. This occurs throughout the study area (Fig. 12e). The seismic architecture of facies C4 is best represented in the northern Tugela Cone (Fig. 7) where reflectors show consistent retrogradation landward over the underlying FSST (facies C2), with prominent onlap against the 3B surface. The succession thins to the south, identified in Jc-C1 as a ~200 m thick succession of claystone which fines upwards to siltstone (Fig. 8). The stratal architecture bears similarity to the architecture of "healing phase" TST wedges as defined by other authors (sensu Catuneanu, 2006). The limited occurrence of Palaeocene and Eocene sediments on the inner shelf is discussed by Siesser and Dingle (1981), Green and Garlick (2011), and Green (2011a), who consider it a function of non-preservation due to intervening episodes of sediment bypass and later erosion.

Facies C4 is capped by surface 3C (Fig. 7) which correlates with a 5 m thick limestone horizon (Fig. 8 - Inset e) evident at 975 m depth in Jc-A1 (Du Toit and Leith, 1974). The overlying facies C5 (Fig. 7) is intersected by borehole Jc-A1 where three Palaeocene age coarsening upward packages of shale to sandstone are identified (Du Toit and Leith, 1974). Sandstones vary in thickness from 5 to 40 m (Fig. 8 – Inset f) and the progradational nature of the seismic reflections suggests that these are likely representative of shallow marine shoreface sands (Catuneanu, 2006). Siesser and Dingle (1981) suggest that the Palaeogene was a period of protracted sea level rise along the east coast (Fig. 8) with TST deposits identified along the northern KZN shelf (Green, 2009). Although a minor regressive phase in the early Eocene is postulated by Siesser and Dingle (1981), this study shows continued marine transgression throughout the Palaeogene with highstand conditions prevailing in the late Eocene consistent with sea level curves of Siesser and Dingle (1981).

As surface 3C caps the TST in Jc-A1, with the corresponding limestone in Jc-A1 having a high gamma ray signature typical of condensed sections (Fig. 8 – Inset e), we propose that the surface is representative of a maximum flooding surface that caps the healing phase wedge (Fig. 7). The progradational facies C5, which overlies this surface is correlated with inner shelf sands and thus considered the subsequent HST wedge (Fig. 12e) (Catuneanu et al., 2011). This mantles the underlying C4 and spans almost the entire study area along-strike (Fig. 12e).

5.4. Large scale sediment influx, cone development and shelf construction

Unit C is truncated by a regional unconformity surface S4 (Angus – Goodlad, 1986), which correlates with a basin-wide early Oligocene hiatus identified in the Jc-A1 well (Du Toit and Leith, 1974). The Oligocene hiatus correlates with hinterland uplift (Partridge and Maud, 1987), as well as a global sea level lowstand during the middle Oligocene (Fig. 8) (Haq et al., 1987; Millar et al., 2005; Millar, 2009). Siesser and Dingle (1981) suggest sea level fall around southern Africa of −500 m during the early to middle Oligocene (Fig. 8), whilst Dingle et al. (1983) propose −100 to −200 m sea level fall along the east coast. Within the Durban Basin, the Oligocene sequence boundary S4 is marked by numerous channel incisions on the palaeo-shelf (Fig. 9). This boundary thus represents the subaerial unconformity and its seaward extension (correlative conformity cf. Posamentier and Allen, 1999), with lower shelf and slope incisions formed by off-shelf sediment forcing and turbidity current incision. At this time, deepwater slope fans would have been deposited (Catuneanu, 2006), however Wiles et al. (2013) suggest that these deposits have been subsequently reworked and removed by bottom currents active in the adjoining Natal Valley.

The overlying unit D represents periodic, but voluminous deposition by short, fast-flowing and entrenched river systems that drained the nearby coastal escarpment during the late Oligocene to early Miocene. Periods of hinterland uplift and denudation are notable during this time period (Partridge and Maud, 1987; Walford et al., 2005; Green, 2011b; Said et al., 2015), producing a zone of erosion/sediment bypass in the shelf and deposition near the contemporary shelf edge (Fig. 12f). The dominantly progradational reflectors of unit D depict the associated basinward advance of a large, normal regressive, constructional, submarine delta (Tugela Cone) during sea-level lowstand. Facies D1 represents the LST fill of submarine canyons preserved in the underlying erosional unconformity. The higher amplitude seismic reflections relative to the adjacent incised units, suggest coarser-grained sedimentary infill along the lines of canyons described by Di Celma (2011). Posamentier and Walker (2006) suggest that, in active continental margin settings, coarse-grained canyon fill is common with deepwater canyon systems linked directly to short and steep fluvial systems similar to that identified in the Durban Basin. Although no canyon/channel systems are intersected by the boreholes offshore, the increase in sediment supply during this period is identified in Jc-C1 and Jc-D1 and best shown in Jc-A1. Fossil assemblages within the sandstone packages of Jc-A1 (Leith, 1971) suggest a similar middle shelf environment to that outlined by Zecchin et al. (2011) for the early stages of submarine canyon fills in the Crotone Basin, Italy. Although not recognised in the northern portion of the basin (Green, 2011b), an architecturally similar, though undated, canyon fill is identified by Wiles et al. (2013) within the adjoining Tugela Canyon. Our data corroborate this and we consider that initial canyon incision corresponded with the mid Oligocene hiatus, with subsequent canyon quiescence and infilling related to late Oligocene to Miocene transgression (Fig. 9).

Facies D2, the overlying moderate amplitude, aggradational-progradational offlapping seismic reflections, constitute a LST shelf-edge wedge deposit (sensu Santra et al., 2013). This marks the development of the shelf-break system which characterises the

area to date.

Truncating unit D is a second highly erosional surface (S5), which shows large-scale channel incision along the shelf (Fig. 10), correlated with subaerial erosion and sediment bypass. The complete lack of TST or HST post unit D, has been discussed by Green (2011a, 2011b) who suggests that the continental shelf was subject to alternating periods of sediment influx (FSST and LST) and sediment starvation with ensuing erosion/non deposition (TST and HST). This is corroborated by Green and Garlick (2011) and Green et al. (2013) who identify a prolonged hiatus on the inner shelf spanning the late Eocene to Pliocene; and further suggests the deposition of deep water slope fans and turbidites during this period. The lack of preserved FSST deposits within Unit E is however due to reworking by bottom currents as described by Wiles et al. (2013) within the Natal Valley since the Oligocene.

Unit E is architecturally similar to unit D, characterised by progradational to aggradational reflections which form an offlapping LST wedge on the shelf-edge (Fig. 12f). Within the progradational shelf-edge wedge, facies E1 occurs as high amplitude channel/valley fill deposits (Fig. 10b) similar to that of the early LST facies D1. Facies E2 consists of progradational offlapping seismic reflections forming a seaward dipping LST shelf-edge wedge similar to that of facies D2. Updip these reflectors pass into the diffusely reflective facies E3 in the proximal portion of the wedge. Due to the wedging out updip of the unit, no boreholes intersect these deposits. However, the transparent nature of facies E3 is likely associated with uniform mud-rich lithologies as discussed by Santra et al. (2013) for the New Jersey continental shelf wedge.

5.5. Sediment starvation

Unit F represents the uppermost resolvable seismic unit. The base of the unit is a highly erosional surface (S6), which we correlate to the early Pliocene seismic reflector “Jimmy” (Martin, 1984; Goodlad, 1986). Green (2011b) suggests that, along the northern KwaZulu-Natal continental shelf, an extended hiatus correlated with this reflector spans the late Palaeocene to early Pliocene, having occurred through a combination of sediment starvation, non-deposition, and sediment bypass. Channel incision has occurred both on the continental shelf through erosion and sediment bypass during forced regression, as well as on the upper slope where canyon formation is identified beneath the present Tugela Canyon. Like the repeating units beneath, unit F comprises an early LST channel fill facies F1 with high impedance reflections which onlap against the channel/canyon flanks (Fig. 10). Green et al. (2008) dated the wedge, which is continuous along-strike, at the late Pliocene. These deposits thus coincide with local sea-level rise following rapid sea-level fall in the early Pliocene (Dingle et al., 1983). The progradational nature of the overlying facies F2 suggests normal regressive deposition during early sea level rise as part of a lowstand shelf-edge delta (e.g. Fig. 12f). Green (2011b), showed that this final phase of shelf-edge wedge aggradation formed the contemporary shelf break of the Zululand Basin, with which we ascribe a similar situation in the Durban Basin. Subsequent sediment starvation (e.g. Green, 2011b) has left this feature preserved as a moribund shelf break.

6. Shelf evolution– a combination of structural and sedimentary shelf dominance

The Durban Basin and its associated sediments have a complex depositional history with sedimentation interrupted by protracted periods of erosion or non-deposition. In all cases however, sedimentation can be related to both local and global sea-level fluctuations (Haq et al., 1987, 1988; Siesser and Dingle, 1981; Dingle et al., 1983) with sedimentation following closely (albeit not completely) with currently accepted sequence stratigraphic principles (Posamentier and Allen, 1999; Catuneanu, 2006; Catuneanu et al., 2011). Unlike the continental margin to the north and south, the area investigated in this study is represented by major sediment input from the Tugela and Umgeni Rivers with bypass of the shelf and proximal ramp areas and deposition initially dominant on the upper slope as the construction of the shelf ensued.

The formation of the shelf is however unlike that described for other passive margin settings (Carvajal et al., 2009; Catuneanu et al., 2011; Santra et al., 2013), as early sedimentation was controlled by fluvial deposition in a narrow, sheared, structurally bounded basin (Figs. 12a and 13a) similar to sedimentation styles in rifted margins (Martins-Neto and Catuneanu, 2010). The result is a combined structural–sedimentary shelf (Fig. 13a) similar to that defined by Helland-Hansen et al. (2012).

Sedimentation styles within the basin changed dramatically during the mid-Cretaceous, with deep water deposition of basin floor fans in the Turonian (Fig. 13b) followed by the formation of a shallow, planar ramp during lowstand conditions (Fig. 13c). Although ramp margins are commonly related to carbonate geology (Helland-Hansen et al., 2012), the Durban Basin represents a siliciclastic ramp margin similar to those discussed by Varban and Plint (2008).

Tectonism and active spreading had ceased by the Cenomanian (Ben Avraham et al., 1993; Watkeys, 2006), however the formation of the proto-shelf on the Turonian ramp was still nucleated close to the original structural shelf break (Fig. 13c) similar to that seen in active structural shelves (Helland-Hansen et al., 2012). Increased sediment supply and base-level fall during the Campanian saw the initial formation of a shelf break (facies C2) in the basin defined by a narrow, forced regressive shelf-edge wedge (Fig. 13d) marking a change from ramp-dominated to shelf-edge sedimentation. The change in depositional style from structural-sedimentary shelf to progradational sedimentary shelf (Helland-Hansen et al., 2012) coincides with McMillian (2003) suggestion that basin began acting as a single depo-centre during this period. Continuous deposition through lowstand, transgressive (Fig. 13e) and highstand (Fig. 13f) conditions dominated the Maastrichtian to Eocene, with the Eocene highstand wedge prograding from the incipient shelf break, initially defined by facies C2. This highstand shelf-edge wedge later controlled the positioning of the future shelf breaks by providing an anchor point from which successive episodes of protracted lowstand sediment delivery could build succeeding aggrading and prograding shelf-edge wedges (unit D-F). This transformed the shelf edge into the sharp feature that currently marks the contemporary shelf break (Fig. 13g–h). The progradational units D and E are similar in architecture to moderately deep water margins defined by Carvajal et al. (2009) and progradational to aggradational shelf margins defined by Gong et al. (2015) in the South China Sea. Clinoform architecture and the absence of large sediment aprons at the base of the slope suggests modest sediment input regimes during this period when compared with similar margins defined by Carvajal et al. (2009).

Subsequent to the final stages of sediment influx during the late Miocene, the basin has experienced renewed sediment starvation, with a thin veneer of Pleistocene to Holocene sediment preserved on the shelf and shelf edge (McMillian, 2003; Green, 2011b), suggesting that the major phases of hinterland uplift and attendant sediment supply drove the construction of main basin almost in its entirety. Unlike other authors suggestions (e.g. Martin, 1984; Martin and Flemming, 1986), the overall narrowness of the adjoining shelf in the basin is not a product of the initial rifting of the margin, but rather a fortuitous alternation between an overabundance of uplift-driven sediment delivery and normal

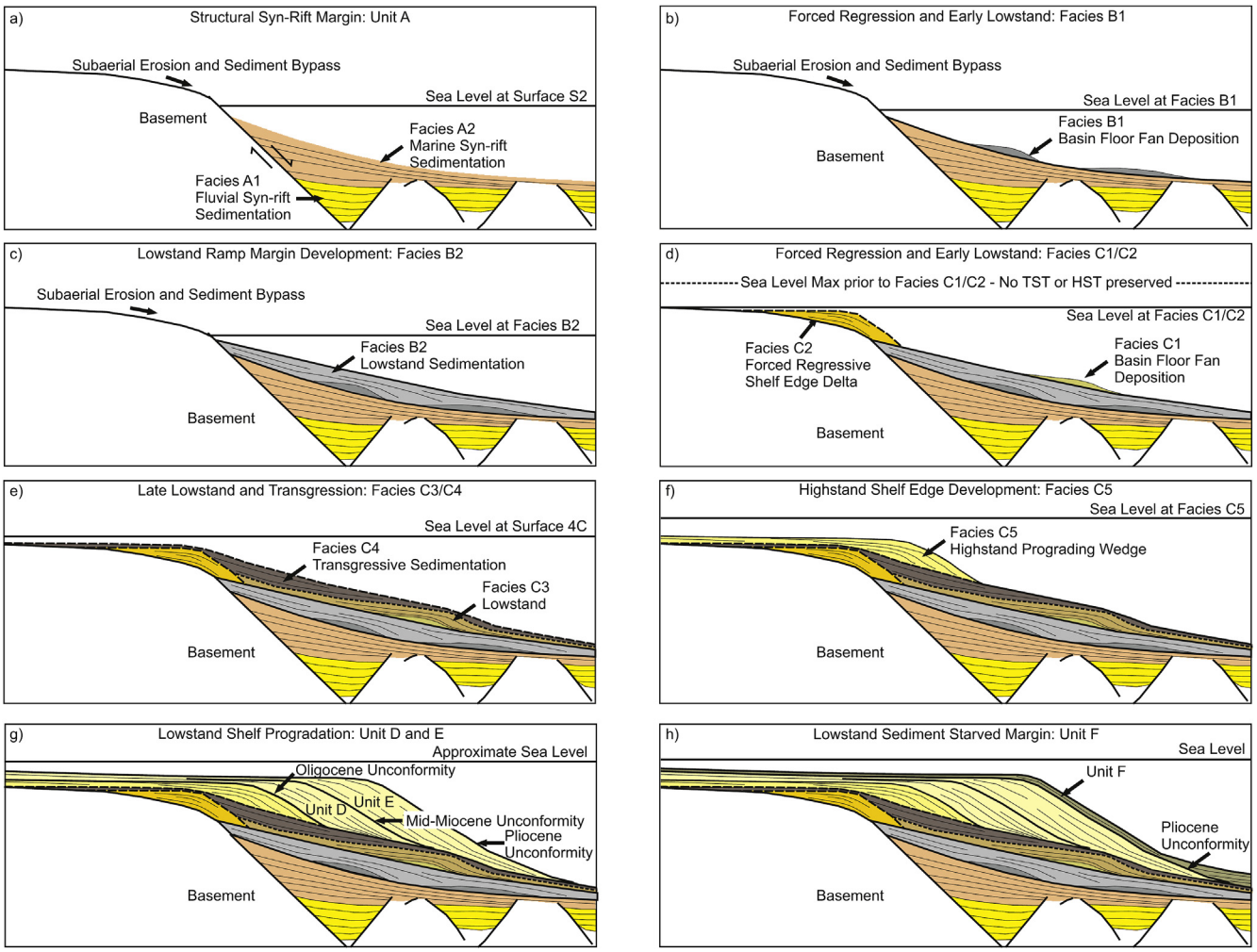

Fig. 13. Schematic model of the evolution of the Durban basin defining syn-rift structural-sedimentary deposition followed by ramp margin development and finally sedimentary shelf progradation (modified after Helland-Hansen et al., 2012).

regression, followed by generally quiescent conditions until today.

Although combined structural-sedimentary shelves generally form in young seascapes related to active extensional regimes (Helland-Hansen et al., 2012), the Durban Basin represents a unique case where structurally controlled deposition and later sedimentary shelf progradation is related to base level fluctuations and sediment supply regimes rather than tectonically induced accommodation space creation.

7. Conclusions

This study provides the first comprehensive sedimentological and seismic analysis of offshore data within the Mesozoic Durban Basin, eastern margin of southern Africa. The review has allowed for the recognition of multiple phases of margin growth within the late Mesozoic and Cenozoic including, initial sheared, syn-rift, structurally-defined sedimentation, followed by incipient ramp development, and finally progradational sedimentary shelf propagation. Depositional evolution of the basin is represented by six individual sedimentary successions (Units A-F), separated by regional sequence boundaries. Sedimentation occurred predominantly during normal regressive conditions with the basin dominated by the progradation of the constructional submarine delta (Tugela Cone) during sea-level lowstands (LST). Although initial deposition within the basin was controlled predominantly by tectonic events during the final stages of Gondwana breakup in the region, passive margin sedimentation dominates, with cycles of deposition or erosion correlated to local and global sea-level fluctuations and sediment supply.

Acknowledgements

The authors are grateful to the two anonymous reviewers, and editor-in-chief, Prof. Massimo Zecchin for their input that helped improve the manuscript scope and clarity. This research was funded by a PhD bursary from the South African Centre for Carbon Capture and Storage (SACCCS), a division of the South African National Energy Development Institute (SANEDI), and comprises part of a Council for Geoscience (CGS) statutory programme (ST-2013-1183). NH thanks the CGS and SANEDI/SACCCS for their financial and technical support towards the project. We acknowledge the Petroleum Agency South Africa for supplying data to the University of KwaZulu-Natal.

References

Anderson, W., 1906. On the geology of the bluff bore, Durban, natal. Trans. Geol. Soc. S. Afr. 9, 111–116.

Ben Avraham, Z., Hartnady, C.H.J., Malan, J.A., 1993. Early tectonic extension between the Agulhas bank and Falkland plateau due to rotation of the lafonia microplate. Earth Planet. Sci. Lett. 117, 43–58.

Broad, D.S., Jungslager, E.H.A., McLachlan, I.R., Roux, J., 2006. Offshore Mesozoic basins. In: Johnson, M.R., Anhaeusser, C.R., Thomas, R.J. (Eds.), The Geology of South Africa. Geological Society of South Africa. Johannesburg/Council for Geoscience, Pretoria, pp. 553–571.
Carvajal, C., Steel, R., Petter, A., 2009. Sediment supply: the main driver of shelf-margin growth. Earth Sci. Rev. 96 (4), 221–248.
Catuneanu, O., 2006. Principles of Sequence Stratigraphy. Elsevier, Oxford, 375pp.
Catuneanu, O., Abreu, V., Bhattacharya, J.P., Blum, M.D., Dalrymple, R.W., Eriksson, P.G., Fielding, C.R., Fisher, W.L., Galloway, W.E., Gibling, M.R., Giles, K.A., Holbrook, J.M., Jordan, R., Kendall, C.G.St.C., Macurda, B., Martinsen, O.J., Miall, A.D., Neal, J.E., Nummedal, D., Pomar, L., Posamentier, H.W., Pratt, B.R., Sarg, J.F., Shanley, K.W., Steel, R.J., Strasser, A., Tucker, M.E., Winker, C., 2009. Towards the standardization of sequence stratigraphy. Earth Sci. Rev. 92, 1–33.
Catuneanu, O., Galloway, W.E., Kendall, C.G.St.C., Miall, A.D., Posamentier, H.W., Strasser, A., Tucker, M.E., 2011. Sequence stratigraphy: methodology and nomenclature. Newsl. Stratigr. 44 (3), 173–245.
Cawthra, H.C., Neumann, F.H., Uken, R., Smith, A.M., Gauastella, L.A., Yates, A., 2012. Sedimentation on the narrow (8km wide), oceanic current-influenced continental shelf off Durban, KwaZulu-Natal, South Africa. Mar. Geol. 323–325, 107–122.
de Lépinay, M.M., Loncke, L., Basile, C., Roest, W.R., Patriat, M., Maillard, A., De Clarens, P., 2016. Transform continental margins – Part 2: a worldwide review. Tectonophysics. http://dx.doi.org/10.1016/j.tecto.2016.05.038 (accepted manuscript).
Di Celma, C., 2011. Sedimentology, architecture, and depositional evolution of a coarse-grained submarine canyon fill from the Gelasian (early Pleistocene) of the Peri-Adriatic basin, Offida, central Italy. Sediment. Geol. 238, 233–253.
Dingle, R.V., Goodlad, S.W., Martin, A.K., 1978. Bathymetry and stratigraphy of the northern Natal Valley (SW Indian Ocean). A preliminary report. Mar. Geol. 28, 89–106.
Dingle, R.V., Siesser, W.G., Newton, A.R., 1983. Mesozoic and Tertiary Geology of Southern Africa. Balkema, Rotterdam, 375pp.
Du Toit, S.R., Leith, M.J., 1974. The J(c)-1 bore-hole on the continental shelf near Stanger, Natal. Trans. Geol. Soc. S. Afr. 77, 247–252.
Gong, C., Wang, Y., Steel, R.J., Olariu, C., Xu, Q., Liu, X., Zhao, Q., 2015. Growth styles of shelf-margin clinoforms: prediction of sand- and sediment-budget partitioning into and across the shelf. J. Sediment. Res. 85 (3), 209–229.
Goodlad, S.W., 1986. Tectonic and sedimentary history of the mid-Natal Valley (S.W. Indian Ocean). Bull. Jt. Geol. Survey Univ. Cape Town Mar. Geoscience. Unit, 15, 415pp.
Goodlad, S.W., Martin, A.K., Hartnady, C.J.H., 1982. Mesozoic magnetic anomalies in the southern Natal Valley. Nature 295, 686–688.
Green, A.N., 2009. Palaeo-drainage, incised valley fills and transgressive systems tract sedimentation of the northern KwaZulu-Natal continental shelf, South Africa, SW Indian Ocean. Mar. Geol. 263, 46–63.
Green, A.N., 2011a. The late Cretaceous to Holocene sequence stratigraphy of a sheared passive upper continental margin, northern KwaZulu-Natal, South Africa. Mar. Geol. 289, 17–28.
Green, A.N., 2011b. Submarine canyons associated with alternating sediment starvation and shelf-edge wedge development: northern KwaZulu-Natal continental margin, South Africa. Mar. Geol. 284, 114–126.
Green, A.N., Dladla, N., Garlick, G.L., 2013. Spatial and temporal variations in incised valley systems from the Durban continental shelf, KwaZulu-Natal, South Africa. Mar. Geol. 335, 148–161.
Green, A.N., Garlick, L.G., 2011. A sequence stratigraphic framework for a narrow, current-swept continental shelf: the Durban Bight, central KwaZulu-Natal, South Africa. J. Afr. Earth Sci. 60, 303–314.
Green, A.N., Ovechkina, M., Uken, R., 2008. Nannofossil age constraints for the northern KwaZulu-Natal shelf-edge wedge: implications for continental margin dynamics, South Africa, SW Indian Ocean. Cont. Shelf Res. 28, 2442–2449.
Haq, B.U., Hardenbol, J., Vail, P.R., 1987. Chronology of fluctuating sea levels since the triassic. Science 235, 1156–1167.
Haq, B.U., Hardenbol, J., Vail, P.R., 1988. Mesozoic and Cenozoic Chronostratigraphy and cycle of sea-level change. In: Wigus, C.K., Hastings, B.S., Posamentier, H., Van Wagoner, J., Ross, C.A., Kendall, C.G.St.C. (Eds.), Sea-level Changes – an Integrated Approach. Society of Economic Paleontologists and Mineralogists Special Publication No 42, 411pp.
Helland-Hansen, W., Steel, R.J., Sømme, T.O., 2012. Shelf genesis revisited. J. Sediment. Res. 82, 133–148.
Hunt, D., Tucker, M.E., 1992. Stranded parasequences and the forced regressive wedge systems tract: deposition during baselevel fall. Sediment. Geol. 81, 1–9.
Johnson, M.R., van Vuuren, C.J., Visser, J.N.J., Cole, D.I., Wickens, H.D.V., Christie, A.D.M., Roberts, D.L., Brandl, G., 2006. Sedimentary rocks of the Karoo Supergroup. In: Johnson, M.R., Anhaeusser, C.R., Thomas, R.J. (Eds.), The Geology of South Africa. Geological Society of South Africa/Council for Geoscience, pp. 461–500.
Kennett, J.P., 1982. Marine Geology: Englewood Cliffs. Prentice-Hall, N.J, 813 pp.
Kitchin, K., McLachlan, I.R., 1996. Tectonics and Hydrocarbon Potential of the East Coast of South Africa. Soekor Petroleum Licencing Unit. Document SOE-PLU-RPT-001. 49pp.
Leinweber, V.T., Jokat, W., 2011. Is there continental crust underneath the northern Natal Valley and the Mozambique coastal plains? Geophys. Res. Lett. 38, L14303.
Leith, M.J., 1971. Jc-A1 Geological Well Completion Report. SOEKOR internal report. SOE-DRG-WCR-346. 19pp.
Lester, M.J., 2000. A Biostratigraphic Study of the Jc-D1 (Rhino) Well, Durban Basin, Republic of South Africa. Timetrax Limited unpublished internal report, 49pp.
Martin, A.K., 1984. Plate tectonic status and sedimentary basin in-fill of the Natal Valley (SW Indian Ocean). Unit 14 Bull. Jt. Geol. Survey Univ. Cape Town, Mar. Geoscience 209.
Martin, A.K., Flemming, B.W., 1986. The Holocene shelf sediment wedge off the south and east coast of South Africa. In: Knight, R.J., McLean, J.R. (Eds.), Shelf Sands and Sandstones. Canadian Society of Petroleum Geologists, Memoir II, pp. 27–44.
Martin, A.K., Hartnady, C.J.H., Goodlad, S.W., 1981. A revised fit of South America and south central Africa. Earth Planet. Sci. Lett. 54, 293–305.
Martins-Neto, M.A., Catuneanu, O., 2010. Rift sequence stratigraphy. Mar. Petroleum Geol. 27, 247–253.
McMillian, I.K., 2003. Foraminiferally defined biostratigraphic episodes and sedimentation pattern of the Cretaceous drift succession (Early Barremian to Late Maastrichtian) in seven basins on the South African and southern Namibian continental margin. South Afr. J. Sci. 99, 537–576.
McMillian, I.K., Dale, D., 2000. Final Report on the Foraminiferal Biostratigraphy of Borehole Jc-D1 (Rhino).
Millar, K.G., 2009. Sea level change, last 250 million years. In: Gornitz, V. (Ed.), Encyclopedia of Paleoclimatology and Ancient Environments, pp. 879–887.
Millar, K.G., Kominz, M.A., Browning, J.V., Wright, J.D., Mountain, G.S., Katz, M.E., Sugarman, P.J., Cramer, B.S., Christie-Blick, N., Pekar, S.F., 2005. The Phanerozoic record of global sea-level change. Science 310, 1293–1298.
Muntingh, A., 1983. Geological Well Completion Report of Borehole Jc-C1. SOEKOR internal report. SOE-DRG-WCR-363. 23pp.
Partridge, T.C., Botha, G.A., Haddon, I.G., 2006. Cenozoic deposits of the interior. In: Johnson, M.R., Anhaeusser, C.R., Thomas, R.J. (Eds.), The Geology of South Africa. Geological Society of South Africa and Council for Geoscience, pp. 585–604.
Partridge, T.C., Maud, R.R., 1987. Geomorphic evolution of southern Africa since the Mesozoic. South Afr. J. Geol. 90, 179–208.
Partridge, T.C., Maud, R.R., 2000. Macro-scale geomorphic evolution of southern Africa. In: Partridge, T.C., Maud, R.R. (Eds.), The Cenozoic of Southern Africa. Oxford University Press, New York, pp. 3–18.
Porebski, S.J., Steel, R.J., 2003. Shelf-margin deltas: their stratigraphic significance and relation to deepwater sands. Earth Sci. Rev. 62, 283–326.
Posamentier, H.W., Allen, G.P., 1999. Siliciclastic Sequence Stratigraphy: Concepts and Applications, vol. 7. SEPM Concepts in Sedimentology and Paleontology, 210pp.
Posamentier, H.W., Walker, R.G., 2006. Deep-water turbidites and submarine fans. In: Posamentier, H.W., Walker, R.G. (Eds.), Facies Models Revisited, vol. 84. SEPM Special Publication, pp. 397–520.
Prosser, S., 1993. Rift-related linked depositional systems and their seismic expression. In: Williams, G.D., Dobb, A. (Eds.), Tectonics and Seismic Sequence Stratigraphy, vol. 71. Geological Society Special Publication, pp. 35–66.
Said, A., Moder, C., Clark, S., Ghorbal, B., 2015. Cretaceous–cenozoic sedimentary budgets of the Southern Mozambique basin: implications for uplift history of the South African plateau. J. Afr. Earth Sci. 109, 1–10.
Santra, M., Goff, J.A., Steel, R.J., Austin Jr., J.A., 2013. Forced regressive and lowstand Hudson paleo-Delta system: latest Pliocene growth of the outer New Jersey shelf. Mar. Geol. 339, 57–70.
Seyedmehdi, Z., George, A.D., Tucker, M.E., 2016. Sequence development of a latest Devonian-Tournaisian distally-steepened mixed carbonate-siliciclastic ramp, Canning Basin, Australia. Sediment. Geol. 333, 164–183.
Shanmugam, G., 2016. Submarine fans: a critical retrospective (1950–2015). J. Palaeogeogr. 5 (2), 110–184.
Shepard, F.P., 1963. Submarine Geology. Harper and Row, New York, 557pp.
Siesser, W.G., Dingle, R.V., 1981. Tertiary sea-level movements around southern Africa. J. Geol. 89 (4), 523–536.
Stojcic, B., 1979. Geological Well Completion Report of Zululand 1 (ZU-1/77). Report, SOEKOR, PSV 1960 (unpubl.).
Varban, B.L., Plint, A.G., 2008. Palaeoenvironments, palaeogeography, and Physiography of a large, shallow, muddy ramp: late Cenomanian-Turonian Kaskapau Formation, Western Canada foreland basin. Sedimentology 55, 201–233.
Walford, H.L., White, N.J., Sydow, J.C., 2005. Solid sediment load history of the Zambezi Delta. Earth Planet. Sci. Lett. 238, 49–63.
Watkeys, M.K., 2006. Gondwana break-up: a South African perspective. In: Johnson, M.R., Anhaeusser, C.R., Thomas, R.J. (Eds.), The Geology of South Africa. Geological Society of South Africa. Johannesburg/Council for Geoscience, Pretoria, pp. 531–539.
Watkeys, M.K., Sokoutis, D., 1998. Transtension in southeastern Africa associated with Gondwana breakup. In: Holdsworth, R.E., Strachan, R.A., Dewey, J.F. (Eds.), Continental Transpressional and Transtensional Tectonics, vol. 135. Geological Society, London, Special Publications, pp. 203–214.
Wiles, E., Green, A., Watkeys, M., Jokat, W., Krocker, R., 2013. The evolution of the Tugela canyon and submarine fan: a complex interaction between margin erosion and bottom current sweeping, southwest Indian Ocean, South Africa. Mar. Pet. Geol. 44, 60–70.
Zecchin, M., Caffau, M., Roda, C., 2011. Relationships between high-magnitude relative sea-level changes and filling of a coarse-grained submarine canyon (Pleistocene, Ionian Calabria, Southern Italy). Sedimentology 58, 1030–1064.
Zecchin, M., Catuneanu, O., 2013. High-resolution sequence stratigraphy of clastic Shelves I: units and bounding surfaces. Mar. Pet. Geol. 39, 1–25.

APPENDIX III

Marine and Petroleum Geology 86 (2017) 798–811

Contents lists available at ScienceDirect

Marine and Petroleum Geology

journal homepage: www.elsevier.com/locate/marpetgeo

Research paper

A Mid-Miocene erosional unconformity from the Durban Basin, SE African margin: A combination of global eustatic sea level change, epeirogenic uplift, and ocean current initiation

Nigel Hicks [a, b, *], Andrew Green [b]

[a] Council for Geoscience, 139 Jabu Ndlovu Street, Pietermaritzburg 3200, South Africa
[b] Discipline of Geological Sciences, School of Agricultural, Earth and Environmental Sciences, University of KwaZulu-Natal, Westville, Private Bag X54001, South Africa

ARTICLE INFO

Article history:
Received 19 January 2017
Received in revised form
23 June 2017
Accepted 23 June 2017
Available online 27 June 2017

Keywords:
Passive margin
Epeirogenic uplift
Submarine canyon
Sequence boundary
South Africa
Durban Basin

ABSTRACT

Erosional unconformity surfaces are key indicators for the variations in eustatic sea level, ocean dynamics and climatic conditions which significantly affect depositional environments of sedimentary successions. Using a dense grid of 2D seismic data, we present new evidence from a frontier basin, the offshore Durban Basin, of a mid-Miocene age erosional unconformity that can be correlated with analogous horizons around the entire southern African continental margin.

In the Durban Basin, this unconformity is typified by the incision of a mixed carbonate-siliciclastic wedge and ramp margin by a series of submarine canyons. Epeirogenic uplift of southern Africa characterised this period, with erosion and sediment bypass offshore concomitant with increases in offshore sedimentation rates. Although epeirogenic uplift appears to be the dominant mechanism affecting formation of the identified sequence boundary, it is postulated that an interplay between global eustatic sea-level fall, expansion of the east Antarctic ice sheets, and changes in deep oceanic current circulation patterns may have substantially contributed to erosion during this period.

1. Introduction

Continental shelves in passive margin settings commonly comprise thick sedimentary successions, allowing for documentation of variations in sediment supply regimes, eustatic sea level, ocean dynamics and climatic conditions (Mountain et al., 2007; Nittrouer et al., 2007; Zecchin et al., 2015). The recognition of palaeo-geomorphic features including progradational clinoform architecture (Liu et al., 2011), submarine canyon incision (Fulthorpe et al., 2000; Jobe et al., 2011; de Almeida et al., 2015), and basin-scale erosional surfaces (sequence boundaries) (Fulthorpe et al., 2000; Zecchin et al., 2015) have been utilised to define relative sea-level changes (Vail et al., 1977; Haq et al., 1987, 1988) or variations in oceanic and global climatic conditions (Zachos et al., 1997, 2001).

The Durban Basin, developed along the eastern continental margin of South Africa, has been subject to protracted hiatus events since the late Jurassic. Previous studies of the continental shelf (Dingle et al., 1983; Green, 2011a,b; Green and Garlick, 2011; Green et al., 2013) suggest that erosional/non-depositional regimes were dominant between the Maastrichtian and latest Pliocene. A recent study by Hicks and Green (2016) has however, identified prolonged Cenozoic depositional periods beneath the outer continental shelf and slope, separated by regional unconformities (sequence boundaries) related to eustatic sea-level fall. Utilising existing seismic and borehole data we identify a previously undefined mid-Miocene erosional unconformity preserved beneath the outer shelf and slope offshore Durban. This research represents the first detailed examination of this erosional event within the Durban Basin, with correlation between analogous mid-Miocene sequence boundaries around the southern African continental shelf, as well as in the global context.

The southeast African continental margin currently represents a major frontier basin region for hydrocarbon exploration, with the Durban Basin located south of the gas-rich Mozambique Basin (Singh and McLachlan, 2003). Although the Durban Basin margin is under-explored, recent 3D seismic acquisition within the

* Corresponding author. Council for Geoscience, 139 Jabu Ndlovu Street, Pietermaritzburg 3200, South Africa.
E-mail address: nhicks@geoscience.org.za (N. Hicks).

http://dx.doi.org/10.1016/j.marpetgeo.2017.06.037
0264-8172/

deepwater Natal Valley (Pisaniec et al., 2017) suggests the potential for additional work in this region. The hydrocarbon potential of the east African margin is further highlighted by the super-giant (80 TCF) discoveries made offshore northern Mozambique within the Mamba Field, a Lower Eocene fan complex affected by strong, deep water bottom currents that influenced gravity-flow deposition (Palermo et al., 2014). This paper focuses on the identification and interpretation of previously unrecognised unconformities that span these basins, an outcome that may prove valuable to the future hydrocarbon exploration in the region.

2. Regional setting

Along the coastal margin of the KwaZulu-Natal Province, South Africa, Cretaceous and Cenozoic lithologies are largely absent (Dingle et al., 1983). Cretaceous deposits are however preserved in Maputaland, northern KwaZulu-Natal, where a >2000m thick succession (Shone, 2006) occurs within the onshore Zululand Basin (Fig. 1). Palaeocene and Eocene sedimentation is absent throughout the coastal margin, with early Miocene to early Pliocene sediments occurring as a marine regressional package (Uloa and Umkwelane Formations) overlying Cretaceous sediments northwards of Richards Bay in northern KwaZulu-Natal (Roberts et al., 2006). The Uloa Formation is represented by an upward shoaling sequence of shallow marine coquina and sandstone overlain by aeolianite, calcarenite and decalcified red soils (Roberts et al., 2006; Porat and Botha, 2008). The lack of preservation of Cenozoic deposits along the KwaZulu-Natal coastline is due to a chain of compounded hiatuses that together span the late Palaeocene to early Pliocene (McLachlan and McMillian, 1979; Dingle et al., 1983). Flores (1973) and Förster (1975) however, indicate substantial Cenozoic deposition to the north in onshore Mozambique, with individual hiatus periods correlated with the early Oligocene, mid-Miocene and early Pliocene (Martin, 1984).

As with the onshore deposits, the inner continental shelf along the KwaZulu-Natal coast is dominated primarily by a major hiatus spanning the late Palaeocene to early Pliocene (Green, 2011a; Green and Garlick, 2011). Green (2011a) proposed that this protracted hiatus occurred through compounded hinterland uplift episodes within south-eastern Africa during the early-Oligocene, mid-Miocene and Pliocene.

The Durban Basin (Fig. 1), developed offshore of southeast Africa, derives from continental rifting during early Gondwana breakup ~183-159 Ma (Leinweber and Jokat, 2011) and the opening of the western Indian Ocean (Ben Avraham et al., 1993; Watkeys and Sokoutis, 1998). It forms a structurally complex, sheared, passive margin basin (Broad et al., 2006), comprising early Cretaceous and Cenozoic sedimentary successions (McMillian, 2003) dominated by a Cenozoic deep-water fan complex, the Tugela Cone, developed beneath and seaward of the present shelf (Hicks and Green, 2016).

Prior to the hydrocarbon exploration of the mid 1980's to 2000's, detailed descriptions of the seismic and well data within

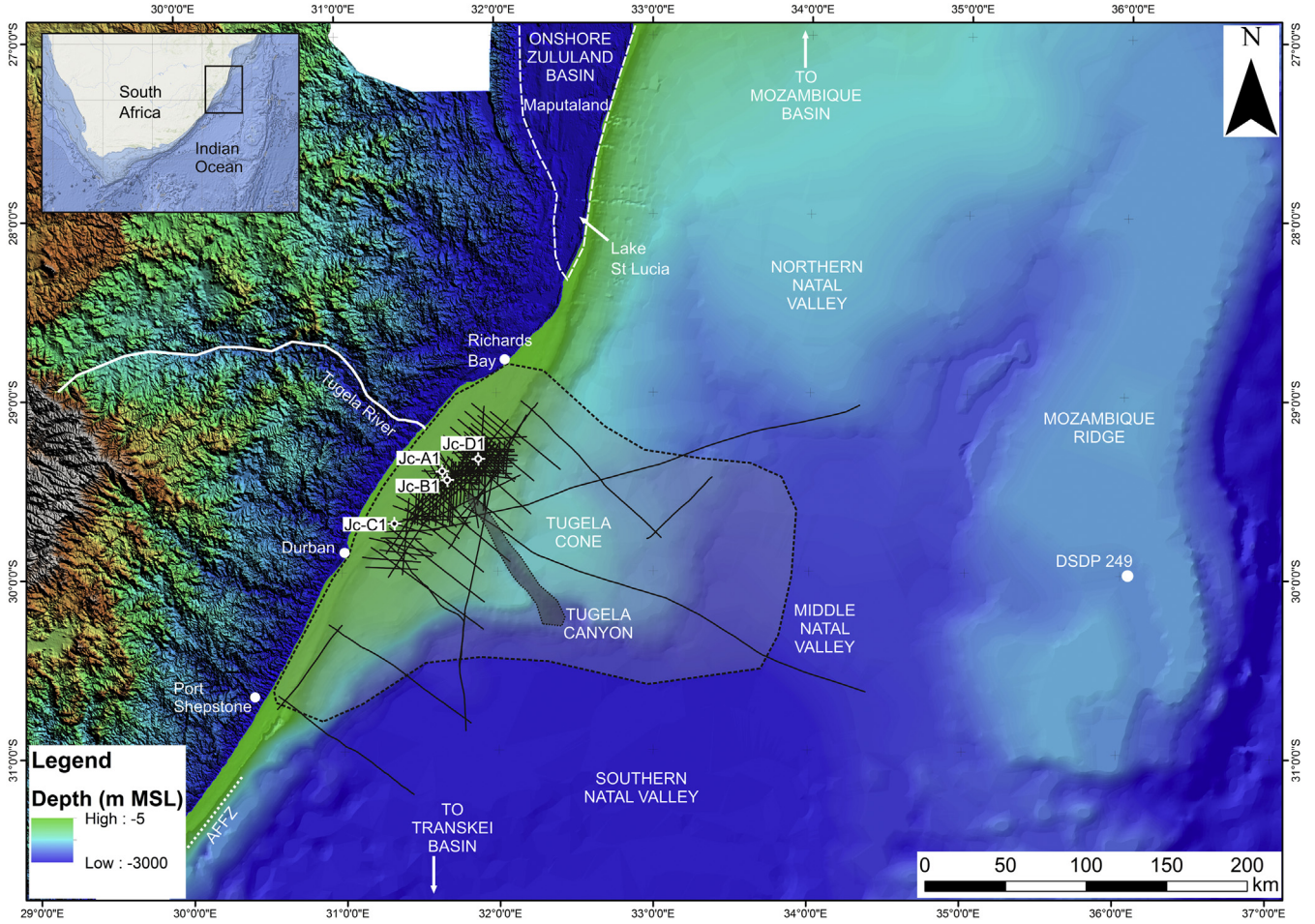

Fig. 1. Hillshade/bathymetry map detailing study area location. The areal extent of the Durban Basin is shown within the shaded polygon. Note the relative position of the Jc-series boreholes drilled on the continental shelf to that of the deep water Tugela Cone, the Natal Valley, and Transkei, Zululand and Mozambique Basins.

the basin were lacking. The work of Martin et al. (1982) and Goodlad (1986) used limited biostratigraphical data (Du Toit and Leith, 1974) and regional seismic profiles to define three regional reflecting horizons within the mid-Cretaceous (McDuff), Oligocene (Angus), and Pliocene (Jimmy). These were correlated with major hiatuses in the northern Natal Valley (Fig. 1). Reflector McDuff (S2; Table 1) is correlated with a Cenomanian/Turonian hiatus present in all Cretaceous basins around southern Africa (McMillian, 2003). However, as this reflector occurs within the acoustic basement for this study, it is not discussed further. Reflector Angus (S4; Table 1) correlates with an early Oligocene hiatus identified by Du Toit and Leith (1974) in Jc-A1, whilst reflector Jimmy (S6; Table 1), correlates with an early Pliocene hiatus in the offshore Durban Basin (Dingle et al., 1983; Goodlad, 1986). Until now, a mid-Miocene erosional event within the basin has not yet been defined.

3. Methods

3.1. Data collection and processing

The Durban Basin is traversed by 2 761 km of legacy, 2D seismic profiles of 1970's to 1990's vintage, obtained over an area of 175

Table 1
Simplified sequence stratigraphic framework for the study area. Seismic units, facies, bounding surfaces, interpreted depositional environments and the age of each unit are described. Ages are based on previous work (McMillian and Dale, 2000; McMillian, 2003; Green et al., 2008).

Unit	Facies	Surface	Interpreted depositional environment	Thickness (two-way time)	Average Shelf Sediment Thickness (m)	Sedimentology	Systems Tract	Age	Time Period (Myr)	Sediment Accumulation Rate (m/Myr)	Areal Extent of Sedimentation (km^2)	Sediment Flux ($x10^3 km^3/Myr$)	This Study
F	F4		na	0.2s			na	Holocene?					
	F3		na	0 to 0.2s	80		na	Pleistocene to Pliocene?	5.3	15.1	2000	5.7	
	F2		Lowstand shelf edge delta	0 to 0.2s			LST	Pliocene					
	F1		Incised valley fill	0 to 0.2s			LST	Pliocene					
		S6	Shelf-confined erosional reflector										
E	E3		Inner to mid shelf	0 to 0.2s	200	Glauconitic sandstones subordinate claystone	TST	Miocene	8.5	23.5	2000	5.5	
	E2		Lowstand shelf edge delta	0 to 0.3s			LST	Miocene					
	E1		Incised valley fill	0 to 0.2s		Sandstone, subordinate claystone	LST	Miocene					
		S5	Shelf and slope-confined, regionally developed erosional reflector										
D	D3		Lowstand shelf edge delta	0.5	200	Carbonate-rich calcarenite and limestone	LST	Miocene to Oligocene	10.1	19.8	2000	3.9	
		S4a	Confined northern shelf reflector within Unit D										
	D2		Lowstand shelf edge delta	0.5	350	Carbonate-rich calcarenite and limestone	LST	Miocene to Oligocene	10	35.0	2000	7.0	
	D1		Incised valley fill	0 to 0.2s		Sandstone, calcarenite and limestone	LST	Oligocene					
		S4	Basin-wide erosional reflector										
C	C5		Highstand wedge	0 to 0.3s	250	Interbedded sandstone and siltstone	HST	Eocene	22.1	11.3	3000	1.5	
		3C	Maximum flooding surface										
	C4		Healing phase wedge	0.1 to 0.3s	250	Deep marine claystone	TST	Palaeocene					
		3B	Maximum regressive surface										
	C3		Delta margin	0 to 0.5s	350		LST	Maastrichtian to Campanian	17.6	19.9	3000	3.4	
	C2		Falling stage wedge	0 to 0.5s	200		FSST	Coniacian to Santonian	10	20.0	2000	4.0	
	C1		Falling stage slope fan apron	0 to 0.3s	200		FSST	Coniacian to Santonian					
		S3	Shelf-confined erosional reflector										
B	B2		Lowstand ramp	0 to 0.5s	200		LST	Turonian	7.6	26.3	2000	6.9	
	B1		Falling stage basin floor fan	0 to 0.3s			FSST	Turonian					
		S2	Basin-wide Erosional Reflector										
A	A2		Syn-rift valley fill	0 to 1s	200		Syn-rift TST/HST	Cenomanian to Aptian	19.1	10.5	3000	1.6	
	A1		Syn-rift valley fill	0 to 1s	100		Syn-rift TST/HST	Aptian to Barremian	16.4	6.1	3000	1.1	
		S1	Basin-wide Erosional Reflector										
BASEMENT			Acoustic Basement					Jurassic					

000 km^2 covering the continental shelf, slope and abyssal plain. All seismic data utilised in this study were pre-processed, stacked and migrated by the Petroleum Agency SA (PASA) or the associated exploration companies, and were obtained in SEGY format. For this study, an area of approximately 5700 km^2 was mapped with 2D seismic profiles paired with lithostratigraphic well log and downhole geophysical data from four wildcat exploration wells (Jc-series) drilled on the continental shelf (Fig. 1).

3.2. Data interpretation

Digital seismic data and log data were interpreted utilising IHS Global Inc., Kingdom Advanced V2015.0. Digital well shoot/velocity data from the Jc-D1 well were utilised by PASA to define two-way time vs measured depth (m). Seismic reflectors representing erosional surfaces were tied to known biostratigraphical and lithological variances obtained from the four Jc-Series well data. Seismic profile mapping was subsequently undertaken in Kingdom Suite 2D/3D PAK allowing for the formation and interpretation of individual seismic facies. Once seismic horizons were mapped and correlated, these were exported as grid files and imported into Kingdom Suite VuPAK for export as contoured horizon maps (Figs. 4 and 6). Sequence stratigraphic nomenclature and interpretation in this paper are based upon current sequence stratigraphic procedures summarized by Catuneanu et al. (2011).

3.3. Sedimentation rate interpretation

For the purpose of this study, rates of sedimentation are deduced for the Cenozoic succession based upon mean sediment package thicknesses derived from well data, and overall areal extents derived from seismic interpretations (Table 1). A similar approach to that defined by Walford et al. (2005) and Said et al. (2015) is utilised. Absolute age constraints for the bounding surfaces of individual units are defined by biostratigraphic ages obtained from the Jc-series wells (Du Toit and Leith, 1974; Unstead et al., 1983; Muntingh, 1983; Lester, 2000). Ages are correlated with the currently accepted International Commission on Stratigraphy Time Chart (v2017/02).

4. Results

4.1. Seismic reflection architecture

The basement to the current study comprises syn-rift and early drift phase sedimentary infill (Units A-B; Table 1) which defines a low-angle marine ramp margin in the Durban Basin. Within this study, the basal unit “C” into which erosional surface S4 incises (Fig. 2), forms the incipient shelf, shelf edge and slope within the basin (Fig. 3). The palaeo-shelf edge at S4 time is defined by the offlap break of the most-seaward reflector of Unit C (Fig. 3). Although largely removed by later erosional episodes, where preserved, the palaeo-shelf break forms a linear feature orientated northeast-southwest approximately 20 km offshore of the contemporary coastline (Fig. 4).

Unit D immediately overlying erosional surface S4, is defined by a north-eastward thickening sediment wedge, most prominent between Jc-B1 and Jc-D1 (Fig. 2). The inflection point of the most-seaward clinoforms of Unit D occurs at ~0.4s TWT (Fig. 3), and outlines the seaward progradation of an approximately 10 km wide and 30 km long, mixed carbonate/siliciclastic wedge between boreholes Jc-B1 and Jc-D1 (Figs. 2 and 3). The intercalated succession of carbonate and siliciclastic sediments (Figs. 2 and 3) can be subdivided into three seismic facies. D1-3. Facies D1 occurs as a discontinuous infilling basal facies confined to incisions along the S4 surface (Figs. 2 and 3).

Facies D2 and D3, which constitute the main components of the sediment wedge, are separated by a local reflector “S4a” (Figs. 2 and 3). Facies D2 attains a maximum thickness of ~600 m and comprises high amplitude, wavy reflectors. These constitute interbedded siltstones and calcarenites in Jc-B1 and a coarsening upward succession of siltstones and interbedded sandstone and limestone in Jc-D1 (Fig. 2). Facies D3 attains a maximum thickness of ~350 m in the vicinity of Jc-D1 (Fig. 2) but is truncated to the south of Jc-B1 by an overlying erosional surface “S5”. Diffuse low amplitude reflectors in the southern portion of the wedge are defined by calcarenites in Jc-B1 (Fig. 2). Northward, in the vicinity of Jc-D1, Facies D3 is defined by medium to high amplitude north-easterly dipping reflectors (Fig. 3) that comprise a succession of siltstone with limited carbonates (Fig. 2).

In contrast to the central and northern parts of the basin, Facies D2 and D3 are not resolved in the southern basin (Fig. 2). Instead, an amalgamated succession of “Unit D” is preserved. In this region aggradation, as opposed to progradation, is dominant on the shelf and slope (Fig. 5). The distal southern basin is dominated by the development of a ~20 km wide continental rise which is not identified in the northern basin (Fig. 6).

The upper reflectors of Unit D are incised by a number of dip-orientated lows associated with a high amplitude reflector corresponding to an erosional surface “S5”. From time-depth reconstructions, this surface is resolved across an area of 5000 km^2 (Fig. 6). The surface is however confined to the mid- and outer shelf, truncated updip by a younger erosional surface “S6”. The S5 surface has an undulatory geometry forming three V and U-shaped incisions (southern, central and northern) best observed in the coast-parallel sections (Fig. 2). In proximal areas, these incisions have a relief of 150–300 m, with a maximum width of 2.8 km (Fig. 2), but broaden and increase in relief downslope up to 500–600 m deep and ~7 km wide (Fig. 6–8). The geometry of the southern and central incisions exhibit multiple erosional episodes within these regions, affecting the S4, S5 and S6 surfaces (Figs. 2 and 8). Multiple incision episodes are defined by vertically stacked U- and V-shaped incisions as shown in Fig. 8, with little to no lateral migration evident. The northern incision however, has no stacked pattern (Figs. 2 and 8) and represents only a single incision episode.

The variable nature of these incisions is evident from the time-depth reconstruction of surface S5 (Fig. 6). The U-shaped southern incision, confined to the upper and middle slope, is a sinuous feature with a total length of ~25 km. It incises into an area characterised by a subdued slope gradient profile (Fig. 5), terminating on the continental rise in the southern part of the basin (Figs. 6 and 8). The V-shaped, linear, central incision is the most prominent, with a total length of ~45 km, incising along the southern margin of the Unit D wedge (Fig. 6). This incision underlies the contemporary Tugela Canyon in the distal basin (Figs. 7 and 8). The V-shaped northern incision is particularly linear, attaining a total length of ~30 km and incising the steep slope associated with the underlying Unit D sediment wedge (Fig. 6). Only the central and northern incisions indent the palaeo-shelf edge (Fig. 6), defined by the inflection point of the most-seaward clinoforms of Unit D.

Unit E, comprising predominantly fine-grained, glauconitic sandstone and minor siltstone overlies reflector S5 throughout the study area. Three seismic facies (E1-3) are resolved. Facies E1 consists of incision infill, with an internal reflector architecture that varies from south to north. The southern incision infill is defined by basal, diffuse, wavy reflectors, overlain by laterally continuous, high amplitude, draped reflectors (Fig. 2). The central incision's fill comprises basal, high amplitude, onlapping, wavy reflectors, overlain by diffuse wavy reflectors (Fig. 2). This is capped by a series of draped, laterally continuous, high amplitude reflectors (Fig. 2).

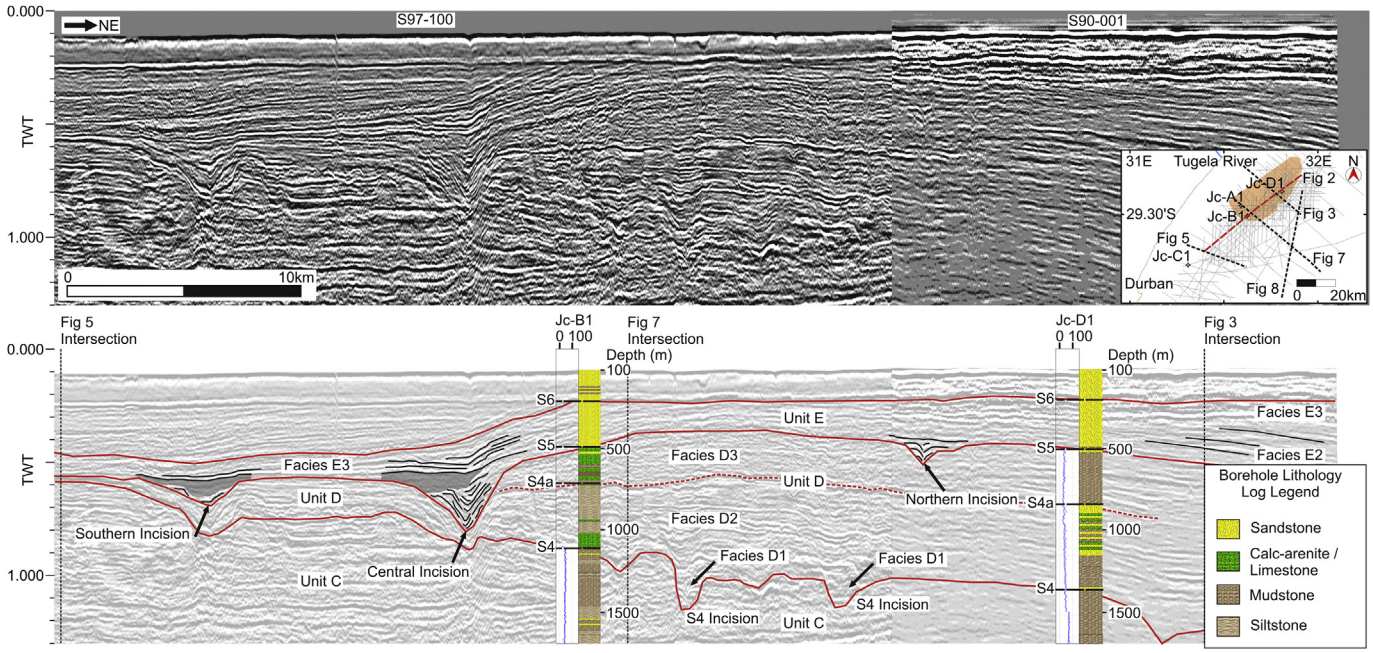

Fig. 2. Coast-parallel, composite seismic profile of seismic lines S97-100 (South) and S90-001 (North) indicating multiple incisions and associated incision-fill along multiple seismic surfaces "S4, S5, S6". Stratigraphic control is given by borehole intersections with Jc-B1 and Jc-D1. Lithological and gamma ray logs are displayed. The spatial position and extent of Unit D's siliciclastic-carbonate wedge is defined by the shaded polygon in the spatial inset box on the un-interpreted figure.

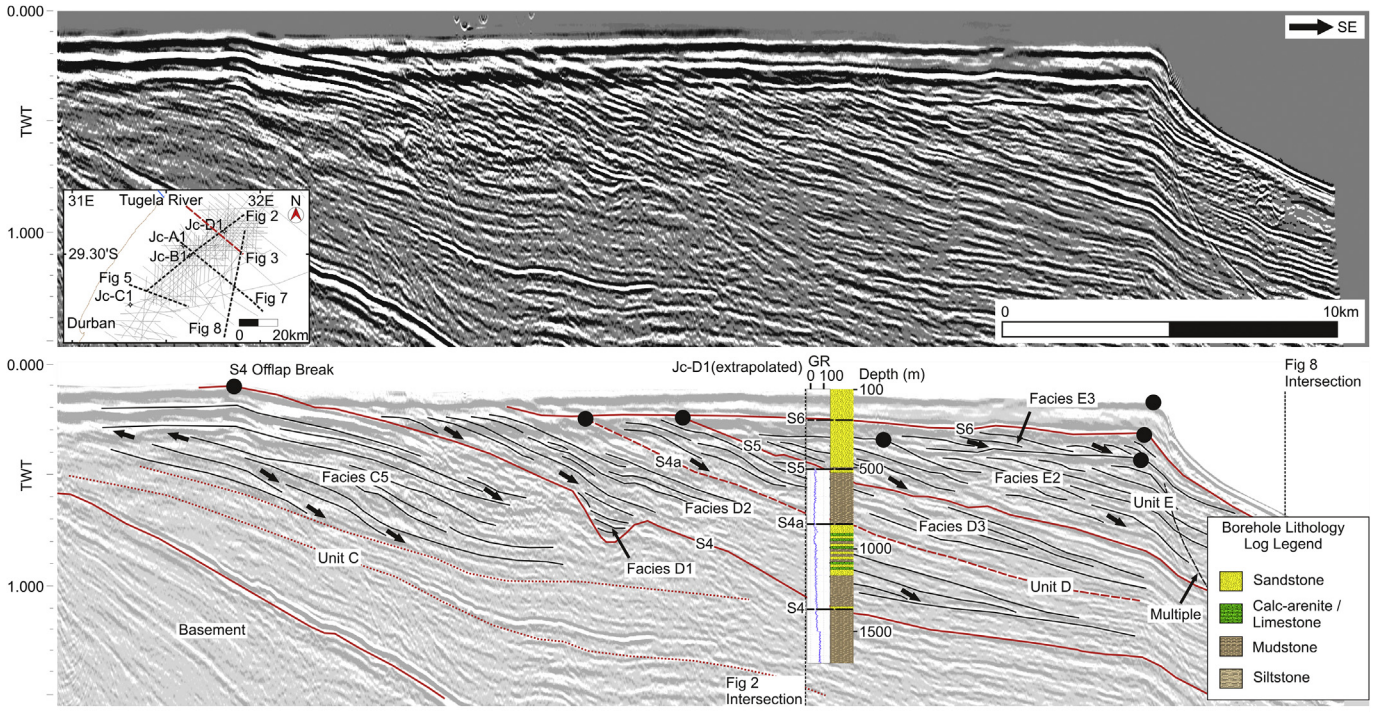

Fig. 3. Dip-orientated profile of seismic line S76-009 intersecting Unit D's siliciclastic-carbonate wedge. Note the well-defined palaeo-shelf edge of the underlying Unit C. Incision within the S4 unconformity surface can be identified. Stratigraphic control is given by extrapolated borehole intersection with Jc-D1. Note the progradational nature of the clinoforms within Units D-E.

The northern incision has only flank-attached, onlapping, high amplitude reflectors (Fig. 2).

In the northern portion of the basin, northward of Jc-B1, seaward dipping, aggradational to progradational reflectors of high impedance, and low amplitude (Facies E2) overlie S5 adjacent to, and updip of, the central and northern incisions (Figs. 3 and 7). This facies is laterally continuous along strike to the north, with a basinward-prograding clinoform architecture that defines successive migration of the dip inflection point and the clinoform toe of the clinoform front (Figs. 3 and 7).

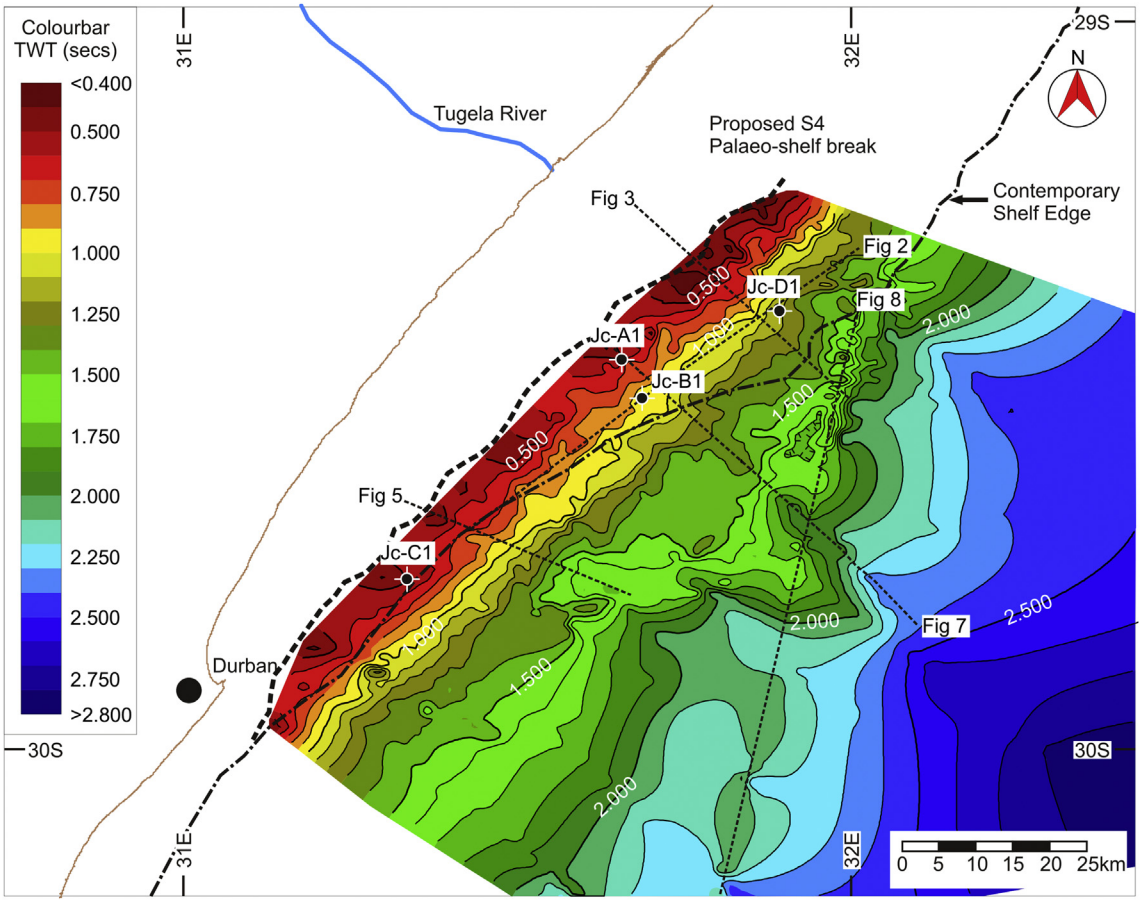

Fig. 4. Two-way time contour map of the S4 (Oligocene) erosional surface. Note the proposed linear shelf break (thick dashed line) as shown in Fig. 3.

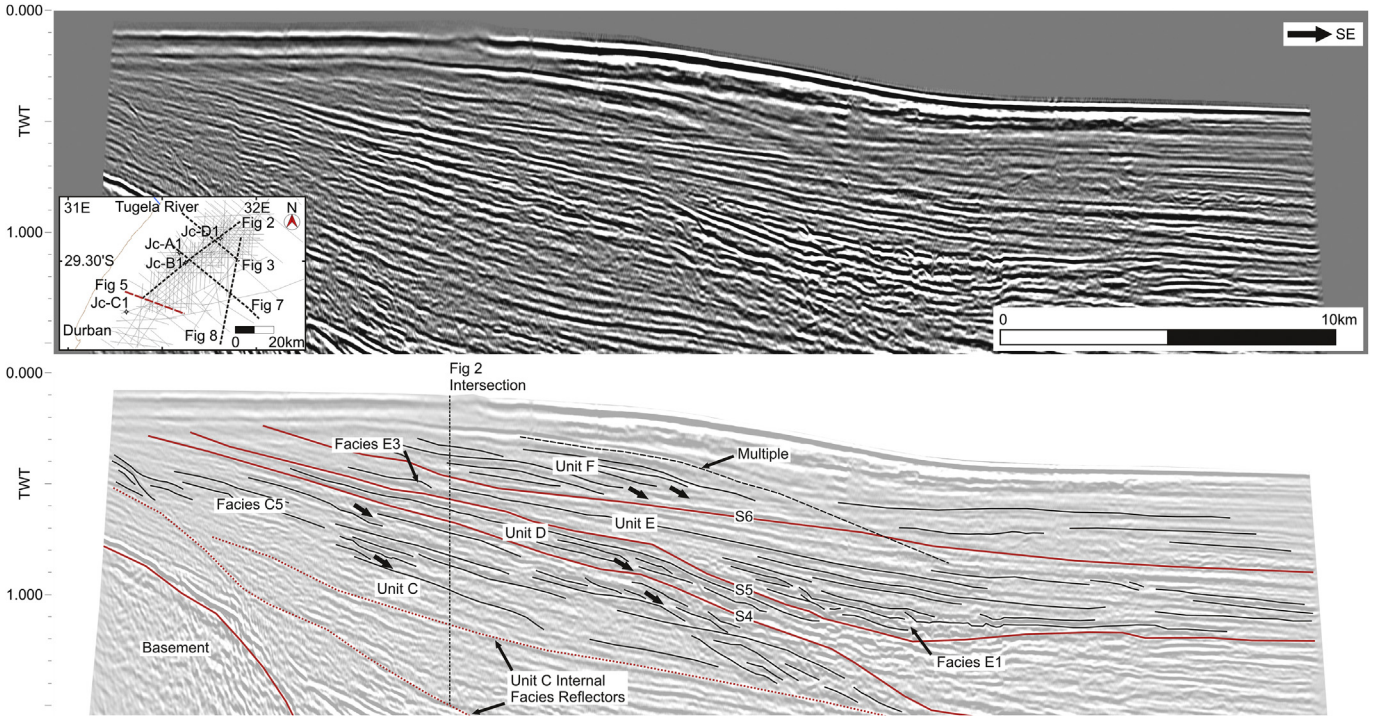

Fig. 5. Dip-orientated profile of seismic line S78-009 intersecting the southern region of the Durban Basin. Note the limited thickness of Units D and E, suggesting sediment starvation in this portion of the basin. Note the lack of a well-defined palaeo-shelf edge, suggesting a ramp, as opposed to shelf-break, type margin.

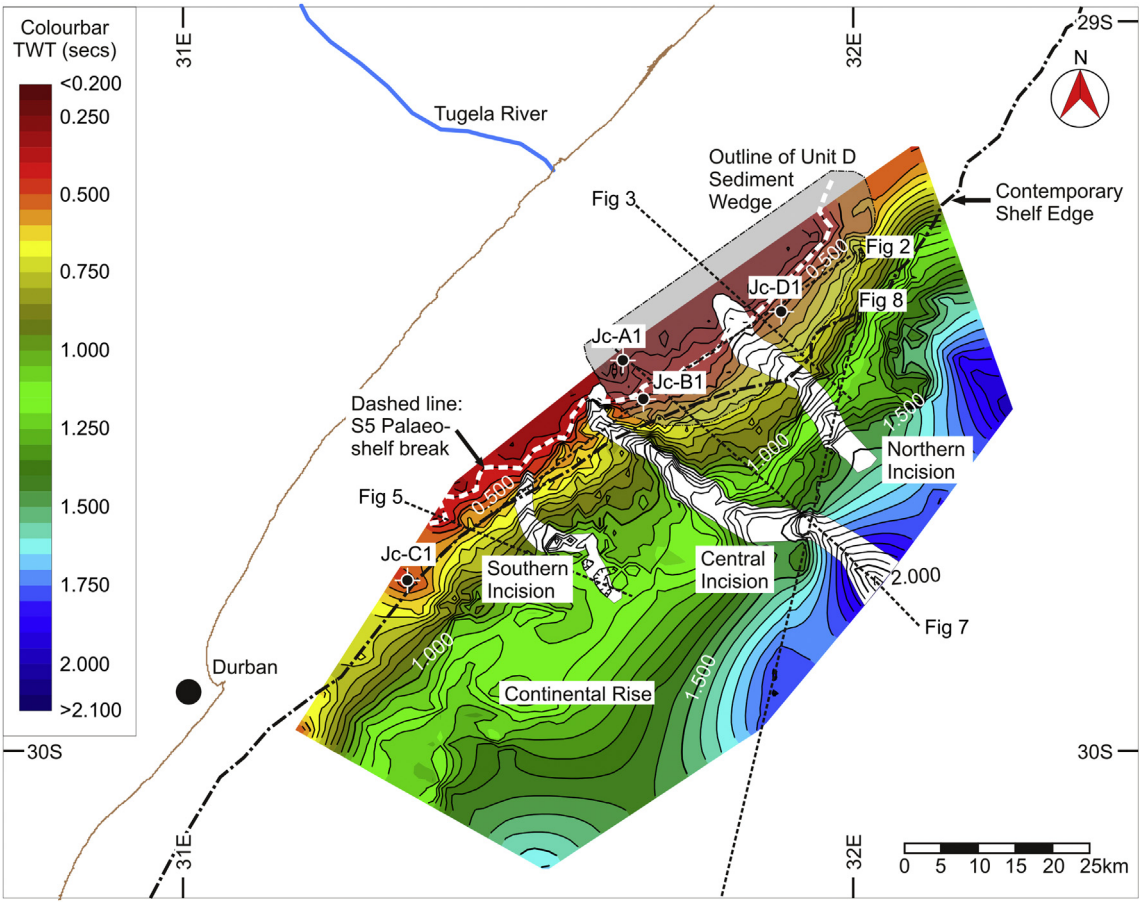

Fig. 6. Two-way time contour map of the S5 (mid-Miocene) erosional surface. Note the prograded shelf edge north of Jc-B1, related to the deposition of Unit D. White polygons denote position and orientation of canyon systems incised into surface S5. Note the sinuous nature of the slope-confined southern canyon, compared with the linear palaeo-shelf indenting central and northern canyons, and the relatively shallow slope gradient between 1.0 and 1.5s TWT across the southern basin compared with the steep gradients north of Jc-B1.

In the southern portion of the basin however, Unit E, as with the underlying Unit D, is poorly developed, with sediment fill defined by aggradational reflectors of Facies E3 (Fig. 5). In all areas, Unit E reflectors are erosionally truncated by regional reflector S6, which marks the third phase of erosion within the study area (Figs. 2, 5, 7 and 8).

4.2. Sedimentation rates

Although well data within the basin are limited, and distances between data are large, all wells intersect the entire succession. Average sediment thicknesses of individual units with average sedimentation rates in m/Myr are outlined in Table 1. The Oligocene is represented by an increase in sedimentation within the basin from 11.3 m/Myr to 35 m/Myr across the S4 erosional boundary. Sedimentation rates diminished slightly in the late Oligocene and early Miocene (Table 1). Sedimentation rates defined for Jc-B1 and Jc-C1 in Table 2 suggest that, during the Oligocene and early Miocene, the southern basin was subject to sediment starvation with a sedimentation rate of 5 m/Myr, compared to 38 m/Myr and 23.8 m/Myr for facies D2 and D3 respectively. Renewed sedimentation throughout the basin is noted across the S5 erosional boundary with the late Miocene defined by elevated rates of 23.5 m/Myr (Table 1).

5. Discussion

5.1. Sediment supply regimes

Since the initiation of Gondwana breakup in the mid-Jurassic (Watkeys and Sokoutis, 1998), several hundred thousand cubic kilometres of material have been eroded from the southern African continent (Said et al., 2015). Voluminous denudation in southern Africa lead to the formation of the Great Escarpment (Partridge and Maud, 1987; Partridge 1997, 1998; Moore 1999; Partridge and Maud, 2000; Guillocheau et al., 2012) which separates a high altitude (1000–1500 m) interior plateau from deeply incised coastal regions (Figs. 1 and 9). During the Cenozoic, south-eastern Africa was subject to multiple phases of epeirogenic uplift (Partridge and Maud, 1987; Partridge, 1998; Moore, 1999; Walford et al., 2005), leading to the development of the African planation surface, fluvial incision and increased sediment supply to the offshore areas (McCormick et al., 1992; Burke and Gunnell, 2008). Although the most prominent period of uplift was during the Oligocene, Walford et al. (2005) propose two periods of Neogene uplift, the smaller of which is thought to have begun in Early Miocene times, whilst a second, greater-magnitude event occurred in the Pliocene.

Within South Africa, Partridge and Maud (1987) propose that moderate uplift and westward tilting of the sub-continent during the early Miocene was accompanied by minor coastal monoclinal

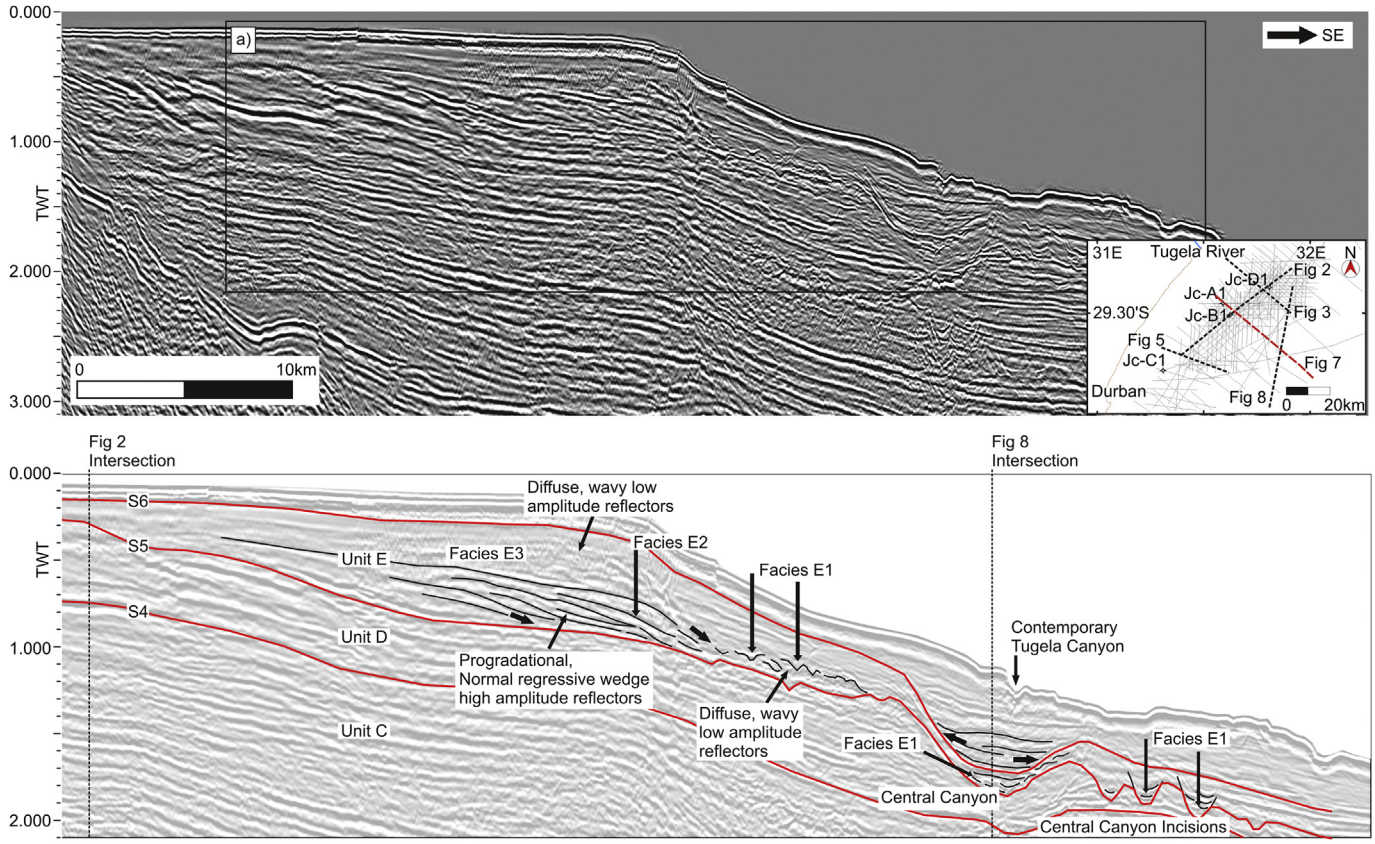

Fig. 7. Dip-orientated seismic profile S74-007 indicating progradational reflector package "Facies E2" overlying seismic surface S5. Note the slope confined canyon incisions of the central canyon, and associated canyon fill, downdip of the progradational shelf-edge wedge.

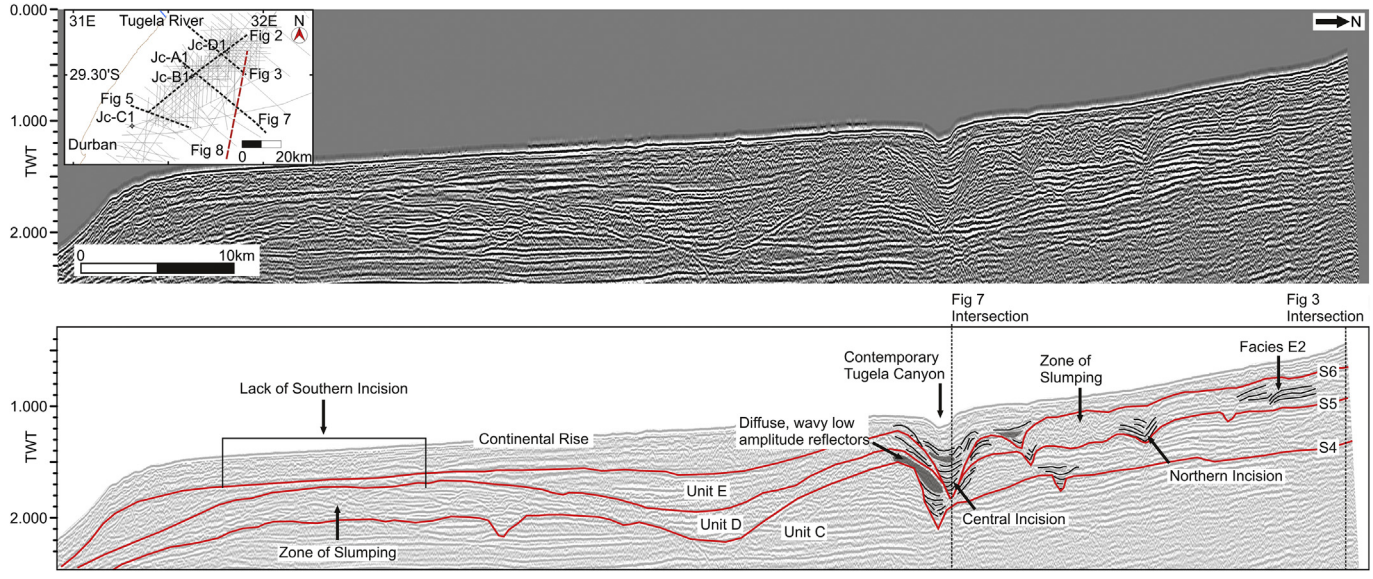

Fig. 8. Dip-orientated seismic profile SA76-159 indicating multiple canyon incision episodes within the central and northern canyon systems. Note the absence of multiple canyons beneath the southern canyon of the shallower gradient, lower slope area.

warping with maximum uplift occurring along the Ciskei-Swaziland Axis in KwaZulu-Natal (Fig. 9). This episode accounts for the development of the Post-African I erosion surface, with renewed sedimentation to the coastal zone via short, fast flowing minor river systems allowing for the deposition of the Uloa Formation (Partridge and Maud, 1987). Only the palaeo-Tugela River (Fig. 1) represented a major point of sediment flux. However, as defined by the geometry of the seismic reflectors associated with Units D and E, sediment supply appears to have been imbalanced (Fig. 3), with abundant supply to the north and sediment

Table 2
Sediment accumulation rates within the Jc-B1 and Jc-C1 wells offshore Durban.

Unit	Facies	Surface	Time Period (Myr)	Jc-B1 Average Sediment Thickness (m)	Jc-B1 - Sediment Accumulation Rate (m/Myr)	Jc-C1 Average Sediment Thickness (m)	Jc-C1 - Sediment Accumulation Rate (m/Myr)	This Study
F	F4							
	F3		5.3	50	9.4	60	11.3	
	F2							
	F1							
		S6						
E	E3		8.5	230	27.1	180	21.2	
	E2							
	E1							
		S5						
D	D3		10.1	240	23.8	50	5.0	
		S4a						
	D2		10	380	38.0	50	5.0	
	D1							
		S4						
C	C5		22.1	1000	45.2	700	31.7	
		3C						
	C4		10	210	21.0	250	25.0	
		3B						
	C3		17.6		0.0		0.0	
	C2		10	300	30.0	450	45.0	
	C1		10		0.0		0.0	
		S3						
B	B2		7.6	50	6.6	550	72.4	
	B1							
		S2						
A	A2		19.1	400	20.9	150	7.9	
	A1		16.4	450	27.4	200	12.2	
		S1						
BASEMENT								

starvation of the shelf in the southern portions of the basin (Figs. 2 and 5).

Partridge and Maud (1987) and Burke and Gunnell (2008) suggest that Miocene uplift during the post African Surface I cycle caused erosional rejuvenation with active deltaic and deep marine fan deposition along the east African margin through the lower to mid-Miocene. Seismic reflection analysis from the current study suggests that mid-Miocene sedimentation occurred predominantly on the slope, with zones of sediment bypass and erosion dominant within the shelfal region of the basin (Fig. 3). Although Burke and Gunnell (2008) suggest that deep water slope fans would have been deposited during this lowstand event, Goodlad (1986) and Wiles et al. (2013) propose that flow initiation, winnowing and reworking by North Atlantic Deep Water (NADW) since the early Miocene may have led to removal of such features in the deep basin (Figs. 1, 7 and 9). These sedimentation patterns appear similar to systems defined by Palermo et al. (2014) for the Eocene deep water fan system of the Coral Sequence in Mozambique.

5.2. Sedimentation rates

Detailed analyses of sedimentation rates for various regions of the southeast African continental margin have been undertaken (Martin, 1987; McCormick et al., 1992; Walford et al., 2005; Said et al., 2015; Uenzelmann-Neben and Clift, 2015). Although many studies deal primarily with recent sedimentation, Walford et al. (2005) and Said et al. (2015) depict sedimentation in Mozambique from the early Cretaceous (Fig. 9). Results from these studies are largely similar to results obtained here, with peak sedimentation rates (Fig. 9; Table 1 and 2) coinciding with periods of epeirogenic uplift in southeast Africa (Partridge and Maud, 1987). Similar to the rates defined by Said et al. (2015) for the southern Mozambique Basin, sedimentation within the Durban Basin reflects a ~20 m/Myr increase across the S4 erosional reflector (Fig. 9). Sedimentation rates, although high, declined marginally through the late Oligocene and early Miocene. An increase of ~4 m/Myr occurred across the mid-Miocene S5 erosional surface (Table 1), suggests increased denudation within the southeast African hinterland during this period (cf. Partridge and Maud, 1987; Burke and

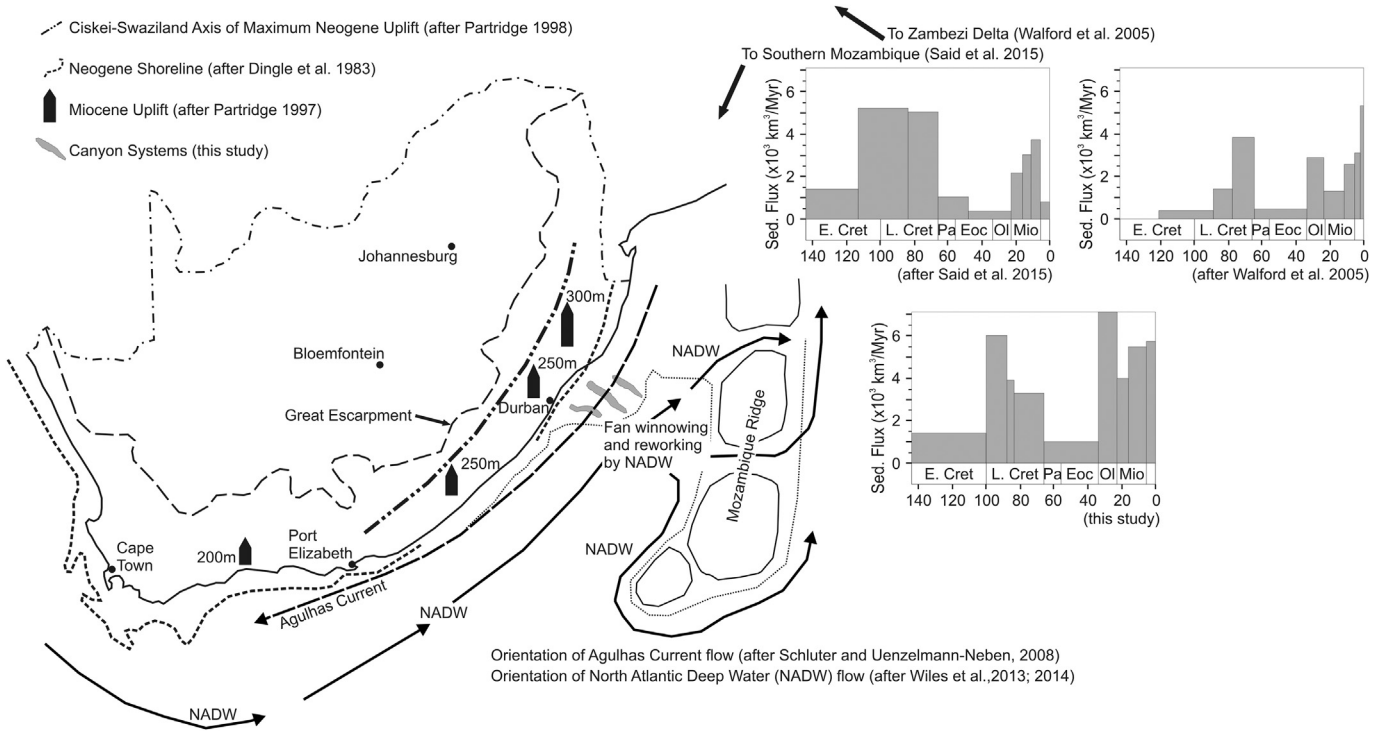

Fig. 9. Schematic map depicting changes in sedimentation rates, submarine canyon systems, tectonic events, and oceanographic activities that occurred during the mid-Miocene. Amplitudes of epeirogenic uplift along the southeast African margin after Partridge (1997). Axis of maximum Neogene uplift after Partridge (1998). Regional oceanographic currents are adapted from Schlüter and Uenzelmann-Neben (2008) and Wiles et al. (2013, 2014). Sedimentation rates for southern Mozambique and the Zambezi Delta after Said et al. (2015) and Walford et al. (2005) respectively.

Gunnell, 2008). We therefore propose that, within the Durban Basin, increased sedimentation rates within the Neogene occur following erosional episodes in the early-Oligocene, and mid-Miocene.

5.3. Incipient shelf development

Neogene sedimentation within the Durban Basin is dominated by the basinward advance of the Tugela Cone delta during normal-regressive sea level lowstands (Hicks and Green, 2016). The moderate amplitude, aggradational to progradational offlapping seismic reflectors of Facies C5 (Unit C) in the northern basin (Fig. 3), represent initial progradation of the Tugela Cone delta (sensu Santra et al., 2013). An initial Eocene pulse of lowstand sedimentation (McMillian and Dale, 2000) led to the formation of the incipient shelf edge, from which the contemporary shelf has prograded. This sedimentation pattern is analogous to the lower-Eocene Coral Sequence of the Mamba gas field, Mozambique, which is interpreted as a lowstand deepwater fan deposit overlying a channelized basal erosive unconformity (Palermo et al., 2014).

Deposition of Unit D, subsequent to the early Oligocene "S4" hiatus event (McMillian and Dale, 2000; Hicks and Green, 2016), is correlated with a late Oligocene to early Miocene, asymmetrical, mixed siliciclastic-carbonate sediment wedge. Intercalated carbonate (low terrigenous sediment input) and siliciclastic (high terrigenous sediment input) sediments (Figs. 2, 3 and 6) were possibly fed by occasional discharge from the palaeo-Tugela River (siliciclastic input). The southern basin however, is defined by a shallow ramp margin and wide continental rise, the succession of which is carbonate-dominated (e.g. Jc-C1 borehole), with a ~100 m thick succession of coquina observed (Muntingh, 1983; Hicks and Green, 2016). We propose that this variability in sedimentation is related to oceanic current circulation controlled sedimentation patterns within the Durban Basin as defined by Green (2009) and Wiles et al. (2014).

In northern KwaZulu-Natal and Mozambique, lower Miocene lagoonal to shallow marine coquina and sandy limestone of the Uloa (Roberts et al., 2006) and Temane Formations (Flores, 1973) crop out as isolated outliers. Cooper et al. (2013) suggest that, within the vicinity of Lake St Lucia, the Uloa Formation represents a multiple stack of normal regressive shoreline deposits. Du Toit and Leith (1974) correlated the Uloa Formation with a ~140 m thick coquina identified in the Jc-A1 borehole, and with the identification of early Miocene coquina in all wells within the Durban Basin, we further propose that Unit D represents the lateral equivalent of the Temane Formation and the offshore equivalent of the Uloa Formation. The unit likely represents a mixed siliciclastic-carbonate wedge deposited during normal regressive, late highstand to lowstand conditions similar to that described by Catuneanu et al. (2011).

In both northern KwaZulu-Natal (King, 1969) and Mozambique (Flores, 1973; Förster, 1975), the early Miocene succession is truncated by a mid-Miocene erosional surface, overlain by glauconitic sandstones or calcarenites of late Miocene to early Pliocene age (King, 1953, 1969; Frankel 1966, 1969). We therefore propose that the erosional episode (Surface S5) which incises Unit D within the Durban Basin (Figs. 2 and 3) is correlative with this erosional surface. This surface marks the termination of the calcarenite succession in borehole Jc-B1, overlain by late Miocene to early Pliocene glauconitic sandstones (Unstead et al., 1983). A similar succession has been identified on the west coast of South Africa (Wigley and Compton, 2006) where a transition from carbonate-dominant to glauconitic sandstone assemblages is identified across a mid-Miocene erosional surface (Weigelt and Uenzelmann-Neben,

2004; Kuhlmann et al., 2010). The identification and correlation of such erosional surfaces around southern Africa suggests that sediment bypass and submarine erosion was dominant throughout the southern African continental shelves during this period.

5.4. Development and architecture of submarine canyon systems

The stratigraphy of the Durban Basin is interspersed by regional unconformity surfaces representative of sequence boundaries (Martin, 1984; Goodlad, 1986; Hicks and Green, 2016). Wiles et al. (2013) identified three erosional surfaces (S4–S6 of this study) related to episodes of uplift and associated marine regression, manifested as a series of incision events within the palaeo-Tugela Canyon (central incision: Figs. 7 and 8). Wiles et al. (2013) were however unable to correlate these regionally across the palaeo-shelf and slope. Like Wiles et al. (2013), we propose the incisions of surface S5 in our dataset represent a series of palaeo-canyons that have incised the upper slope and outer shelf of the Durban Basin. We further consider that the S5 erosional surface identified in this study correlates with the Miocene sequence boundary and incision episode proposed by Wiles et al. (2013).

New shelf-wide analyses of seismic and well data presented in this study clearly define three canyon systems that are morphologically similar to systems that incise continental margins elsewhere (e.g. Pratson et al., 1994; Wigley and Compton, 2006; Covault et al., 2011; Harris and Whiteway, 2011; Jobe et al., 2011). Cross-slope incision relief profiles of the S5 erosional surface are comparable with a series of buried, U and V shaped, Miocene palaeo-canyon systems on the New Jersey continental shelf (Miller et al., 1987; Fulthorpe et al., 2000). Two canyon morphologies are evident within the Durban Basin; the classically-described Type I canyons (Shepard, 1981; Pratson et al., 1994; Green and Uken, 2008; Lastras et al., 2009, 2011; Pattier et al., 2015) with erosional morphologies and a coarse-grained fill; and Type II canyons (Hagen et al., 1994; Zhu et al., 2009; Jobe et al., 2011; Soulet et al., 2016), defined by aggradation and mud-dominated fills.

We suggest that the northern and central incisions represent "Type I" canyons which indent the shelf edge (Fig. 6) and are similar to the canyons defined by Pratson et al. (1994) and Fulthorpe et al. (2000). These systems have linear trajectories with concave longitudinal profiles comparable with systems along erosional or immature continental margins (Covault et al., 2011). Covault et al. (2011) associate these profiles with steep continental slopes, narrow shelves and short hinterland river systems analogous with the east coast of South Africa. Although no boreholes intersect the canyon systems within the Durban Basin, high amplitude, wavy, onlapping seismic reflection architecture (shown as annotated reflectors in Figs. 2, 7 and 8) suggests deposition of coarse-grained canyon fill through either debris flow (Shanmugam, 2000), high energy erosive turbidity currents (Jobe et al., 2011) or mass wasting (Harris and Whiteway, 2011). Gerber et al. (2009) demonstrated that similar linear canyon systems within the narrow Catalan margin formed through erosion by coarse-grained sediment gravity flows on steep slopes terminating in basin floor fan system lobes. The Durban Basin however, is unique as although basin floor fan systems would likely have developed, Wiles et al. (2013) suggest that bottom current winnowing and reworking led to removal/non-deposition of these features.

The southern incision we consider representative of a "Type II" canyon (Fig. 6), exhibiting a sinuous to meandering path, similar to the canyon systems defined by Hagen et al. (1994). We consider the aggradational, smooth, U-shaped seismic reflection architecture and diffuse reflector zones (Fig. 2) to be related to the low energy deposition of (possibly) mud-dominant channel-fill lithologies (Figs. 2 and 8 – grey shade). Jobe et al. (2011) infer similar processes at play in canyons they identified. The southward thinning of the "high-supply" Units D and E into the southern basin suggest the formation of a sinuous Type II canyon in a sediment-starved portion of the margin.

The southern canyon system exhibits a slightly concave longitudinal profile, similar to profiles defined by Covault et al. (2011) for mud-rich systems. Although these systems are commonly associated with supply-dominated passive margins (Covault et al., 2011), we propose that the southern canyon in this study is associated with sediment starvation and limited shelf development with incision likely a response to slumping and slope failure (e.g. Harris and Whiteway, 2011). Hagen et al. (1994) propose that the sinuosity of submarine canyons is a function of slope gradient, with Harris and Whiteway (2011) and O'Grady et al. (2000) suggesting that higher sinuosity canyons occur on gentle, subdued continental margins. Here it appears that the southern canyon fed sediment to a low-gradient continental rise (Fig. 6), similar to mud-rich canyon systems (e.g. McGregor and Bennett, 1979).

For the Durban Basin, we suggest that erosional processes caused instability of the shelf-edge wedge, providing the driving force for canyon inception similar to that defined by Green (2011b) for the northern KwaZulu-Natal continental shelf. Green (2009) however indicates that contemporary and palaeo-shelf development along the KwaZulu-Natal continental margin is a result of a complex interaction between and submarine canyon topography and strong geostrophic ocean current systems (Fig. 9).

5.5. Ocean current control on sedimentation and hiatus development

Heezen et al. (1966) were the first to propose that geostrophic bottom currents are principal processes that shape continental margins worldwide. Palermo et al. (2014) suggest that, within the deepwater Mamba gas field Mozambique, deposition and sediment winnowing of channelized sand bodies was largely affected by bottom current flow perpendicular to channelized, high volume, sand-rich turbidites. Bottom flow processes are likely related to the equatorward flowing North Atlantic Deep Water (cf. Van Aken et al., 2004), which prompted the dispersion of the turbulent fine-grained suspension cloud in asymmetric drift successions with mud-free facies preserved in the channel system. Similarly within the Natal Valley, circulation is dominated by bottom current circulation of the equatorward flowing North Atlantic Deep Water (Wiles et al., 2014), whilst upper ocean flow is controlled by the polewards flowing Agulhas Current (Fig. 9) (Preu et al., 2011; Wiles et al., 2013).

South of the study area in the Transkei Basin (Fig. 1), Niemi et al. (2000) and Schlüter and Uenzelmann-Neben (2007, 2008); proposed that mid-Miocene sequence boundary initiation was the result of a shift in Antarctic Bottom Water (AABW) (Fig. 9) which coincided with global cooling (Zachos et al., 2001). Deep water cooling, an increase in global oceanic $\delta^{18}O$ concentrations and ice-growth events within the east Antarctic ice sheet during the mid-Miocene climatic transition (Shackleton and Kennett, 1975; Flower and Kennett, 1994; Miller et al., 2005) were associated with eustatic sea-level change in the Southern Ocean (Shevenell et al., 2004). We therefore propose that changes in global oceanic conditions across the mid-Miocene climatic transition account, in part, for S5 sequence boundary development in the Durban Basin.

Sequence boundary development during the mid-Miocene climatic transition is not restricted to southeast Africa. Weigelt and Uenzelmann-Neben (2004) identified a mid-Miocene erosional surface that they correlated with the onset of modern deep oceanic current circulation patterns on the west coast of southern Africa. Liu et al. (2011) identified age correlative surfaces along the

western Australian margin. Further evidence for global shifts in eustatic sea levels are identified by John et al. (2011) on the east Australian margin, where a marked shift in foraminifera concentrations, as well as a positive shift in oceanic $\delta^{18}O$ concentrations correspond with a major sequence boundary at ~13.9Ma. We therefore postulate that, as the timing of this global oceanic event is coincident with epeirogenic uplift in southern Africa, variations in oceanic circulation across the mid-Miocene climate transition may account for a Miocene unconformity identified in the Durban Basin.

In accordance with Siesser and Dingle (1981) and Kuhlmann et al. (2010), we thus suggest that Cenozoic epeirogenesis (Partridge and Maud, 1987) combined with global changes in eustatic sea level (Haq et al., 1987, 1988; Miller et al., 2005; Miller, 2009 and John et al., 2011) and changes in global oceanic conditions (Shevenell et al., 2004; Holbourn et al., 2007) have had a profound effect on local sea level around southern Africa. These processes have shaped the stratigraphic architecture of the continental shelves through episodes of erosion and sediment bypass or marine deposition. We propose that these events lead to submarine canyon incision and the formation of a pronounced offshore erosional surface (S5).

6. Conclusions

New evidence from the offshore Durban Basin, east southern African continental margin, supports sequence stratigraphic models of submarine canyon incision and sequence boundary development during sea level lowstands (Van Wagoner et al., 1988; Fulthorpe et al., 2000). We show for the first time, a mid-Miocene seismic reflection surface defining an erosional unconformity that can be correlated across the entire southern African continental shelf and slope. The formation of the S5 surface and its associated submarine canyons is here inferred to relate to a mid-Miocene period of combined epeirogenic uplift and eustatic sea-level fall within the eastern portion of southern Africa.

Within the Durban Basin, the mid-Miocene sequence boundary truncates and incises a mixed carbonate-siliciclastic sediment wedge in the northern region of the basin. To the south however, the basin was marked by a shallow ramp margin with a wide palaeo-continental rise. The inheritance of these geomorphological features later influenced subsequent erosion morphologies due to the antecedent control exerted by the two different gradients.

Antecedent control and localised variability in depositional regimes led to the formation of two genetically variable canyon systems within the mid-Miocene palaeo-slope. Type I linear canyons (central and northern) are correlated with high sediment influx of likely coarse-grained material with downslope eroding gravity flows and turbidites causing scouring of the underlying substrate. The southern, Type II, canyon system has developed on a relatively sediment-starved, shallow angle slope in relation to its counterparts, dominated by mud-rich infill. The sinuous nature of the southern canyon appears to be related to subdued slope gradients in this region of the basin.

The association of canyon incision with a regionally developed, shelf/slope confined unconformity surface can be explained by changes in relative sea-level as a result of global eustatic sea-level fall, combined with epeirogenic uplift of south-eastern Africa during the mid-Miocene. It is likely that the mid-Miocene event identified here is further related to rapid enlargement of the middle Miocene Antarctic ice sheets at ~13Ma, and changes in deep oceanic current circulation patterns. The combination of these processes have had profound effects on the stratigraphic architecture of the offshore southern African basins in the form of erosion, sediment bypassing and slope sedimentation.

Acknowledgements

This research was funded by a PhD bursary from the South African Centre for Carbon Capture and Storage (SACCCS), a division of the South African National Energy Development Institute (SANEDI), as well as being part of a statutory programme (ST-2013-1183) at the Council for Geoscience (CGS). The financial assistance of the South African Centre for Carbon Capture and Storage towards this research is hereby acknowledged. Opinions expressed and conclusions arrived at, are those of the author and are not necessarily to be attributed to SACCCS. Mr Hicks would like to thank both the CGS and SANEDI/SACCCS for their financial and technical support towards the project. Petroleum Agency South Africa is thanked for supplying the data for the project. IHS Global Inc. is acknowledged for its support through an academic licence grant for Kingdom Suite 2015 software. We finally thank the three anonymous reviewers and associate editor Francisco Lobo, for their constructive comments and suggestions which helped to improve the manuscript.

References

Ben Avraham, Z., Hartnady, C.H.J., Malan, J.A., 1993. Early tectonic extension between the Agulhas bank and falkland plateau due to rotation of the lafonia microplate. Earth Planet. Sci. Lett. 117, 43–58.

Broad, D.S., Jungslager, E.H.A., McLachlan, I.R., Roux, J., 2006. Offshore mesozoic basins. In: Johnson, M.R., Anhaeusser, C.R., Thomas, R.J. (Eds.), The Geology of South Africa. Geological Society of South Africa, Johannesburg/Council for Geoscience, Pretoria, pp. 553–571.

Burke, K., Gunnell, Y., 2008. The African Erosion Surface: a continental-scale synthesis of geomorphology, tectonics, and environmental change over the past 180 Million years. Geol. Soc. Am. Mem. 201, 66.

Catuneanu, O., Galloway, W.E., Kendall, C.G.St C., Miall, A.D., Posamentier, H.W., Strasser, A., Tucker, M.E., 2011. Sequence stratigraphy: methodology and nomenclature. Newsletters Stratigr. 44 (3), 173–245.

Cooper, J.A.G., Green, A.N., Smith, A.M., 2013. Vertical stacking of multiple highstand shoreline deposits from the Cretaceous to the present: facies development and preservation. J. Coast. Res. SI65, 1904–1908.

Covault, J.A., Fildani, A., Romans, B.W., McHargue, T., 2011. The natural range of submarine canyon-and-channel longitudinal profiles. Geosphere 7 (2), 313–332.

de Almeida, N.M., Vital, H., Gomes, M.P., 2015. Morphology of submarine canyons along the continental margin of the Potiguar Basin, NE Brazil. Mar. Petroleum Geol. 68, 307–324.

Dingle, R.V., Siesser, W.G., Newton, A.R., 1983. Mesozoic and Tertiary Geology of Southern Africa. Balkema, Rotterdam, 375pp.

Du Toit, S.R., Leith, M.J., 1974. The J(c)-1 bore-hole on the continental shelf near Stanger, Natal. Trans. Geol. Soc. S. Afr. 77, 247–252.

Flores, G., 1973. The cretaceous and tertiary sedimentary basins of Mozambique and Zululand. In: Blant, G. (Ed.), Sedimentary Basins of the African Coasts, 2nd Part. Association of African Geological Surveys, Paris, pp. 81–111.

Flower, B.P., Kennett, J.P., 1994. The middle Miocene climatic transition: east Antarctic ice sheet development, deep ocean circulation and global carbon cycling. Palaeogeogr. Palaeoclimatol. Palaeoecol. 108, 537–555.

Förster, R., 1975. The geological history of the sedimentary basin of southern Mozambique, and some aspects of the origin of the Mozambique Channel. Palaeogeogr. Palaeoclimatol. Palaeoecol. 17, 267–287.

Frankel, J.J., 1966. Basal rocks of the tertiary at Uloa, Zululand, South Africa. Geol. Mag. 103 (3), 214–234.

Frankel, J.J., 1969. Correspondence: the ages of tertiary rocks at Uloa and Umkwelane, Zululand, and their geomorphological significance. Geol. Mag. 106 (2), 206–211.

Fulthorpe, C.S., Austin Jr., J.A., Mountain, G.S., 2000. Morphology and distribution of Miocene slope incisions off New Jersey: are they diagnostic of sequence boundaries? GSA Bull. 112 (6), 817–828.

Gerber, T.P., Amblas, D., Wolinsky, M.A., Pratson, L.F., Canals, M., 2009. A model for the long-profile shape of submarine canyons. J. Geophys. Res. 114, F03002.

Goodlad, S.W., 1986. Tectonic and sedimentary history of the mid-Natal Valley (S.W. Indian Ocean). Bull. Jt. Geol. Survey/University Cape Town Mar. Geoscience Unit 15, 415.

Green, A.N., 2009. Sediment dynamics on the narrow, canyon-incised and current-swept shelf of the northern KwaZulu-Natal continental shelf, South Africa. GeoMarine Lett. 29, 201–219.

Green, A.N., 2011a. The late Cretaceous to Holocene sequence stratigraphy of a sheared passive upper continental margin, northern KwaZulu-Natal, South Africa. Mar. Geol. 289, 17–28.

Green, A.N., 2011b. Submarine canyons associated with alternating sediment starvation and shelf-edge wedge development: northern KwaZulu-Natal continental margin, South Africa. Mar. Geol. 284, 114–126.

Green, A.N., Garlick, G.L., 2011. A sequence stratigraphic framework for a narrow, current-swept continental shelf: the Durban Bight, central KwaZulu-Natal, South Africa. J. Afr. Earth Sci. 60, 303–314.
Green, A.N., Uken, R., 2008. Submarine landsliding and canyon evolution on the northern KwaZulu-Natal continental shelf, South Africa, SW Indian Ocean. Mar. Geol. 254 (3–4), 152–170.
Green, A.N., Ovechkina, M., Uken, R., 2008. Nannofossil age constraints for the northern KwaZulu-Natal shelf-edge wedge: implications for continental margin dynamics, South Africa, SW Indian Ocean. Cont. Shelf Res. 28 (17), 2442–2449.
Green, A.N., Dladla, N., Garlick, G.L., 2013. Spatial and temporal variations in incised valley systems from the Durban continental shelf, KwaZulu-Natal, South Africa. Mar. Geol. 335, 148–161.
Guillocheau, F., Rouby, D., Robin, C., Helm, C., Rolland, N., Le Carlier de Veslud, C., Braun, J., 2012. Quantification and causes of the terrigeneous sediment budget at the scale of a continental margin: a new method applied to the Namibia-South Africa margin. Basin Res. 24, 3–30.
Hagen, R.A., Bergersen, D.D., Moberly, R., Coulbourn, W.T., 1994. Morphology of a large meandering submarine canyon system on the Peru-Chile forearc. Mar. Geol. 119, 7–38.
Haq, B.U., Hardenbol, J., Vail, P.R., 1987. Chronology of fluctuating sea levels since the triassic. Science 235, 1156–1167.
Haq, B.U., Hardenbol, J., Vail, P.R., 1988. Mesozoic and Cenozoic Chronostratigraphy and cycle of sea-level change. In: Wigus, C.K., Hastings, B.S., Posamentier, H., Van Wagoner, J., Ross, C.A., Kendall, C.G.St C. (Eds.), Sea-level Changes – an Integrated Approach. Society of Economic Paleontologists and Mineralogists, p. 411. Special Publication No 42.
Harris, P.T., Whiteway, T., 2011. Global distribution of large submarine canyons: geomorphic differences between active and passive continental margins. Mar. Geol. 285, 69–86.
Heezen, B.C., Hollister, C.D., Ruddiman, W.F., 1966. Shaping of the continental rise by deep geostrophic contour currents. Science 152, 502–508.
Hicks, N., Green, A.N., 2016. Sedimentology and depositional architecture of a submarine delta-fan complex in the Durban Basin, South Africa. Mar. Petroleum Geol. 78, 390–404.
Holbourn, A., Kuhnt, W., Schulz, M., Flores, J.A., Andersen, N., 2007. Orbitally-paced climate evolution during the middle Miocene "Monterey" carbon-isotope excursion. Earth Planet. Sci. Lett. 261, 534–550.
Jobe, Z.R., Lowe, D.R., Uchytilb, S.J., 2011. Two fundamentally different types of submarine canyons along the continental margin of Equatorial Guinea. Mar. Petroleum Geol. 28, 843–860.
John, C.M., Karner, G.D., Browning, E., Leckie, R.M., Mateo, Z., Carson, B., Lowery, C., 2011. Timing and magnitude of Miocene eustacy derived from the mixed siliciclastic-carbonate stratigraphic record of the northeastern Australian margin. Earth Planet. Sci. Lett. 304, 455–467.
King, L., 1953. A Miocene marine fauna from Zululand. Trans. Geol. Soc. S. Afr. 56, 59–91.
King, L., 1969. Correspondence: the ages of tertiary rocks at Uloa and Umkwelane, Zululand, and their geomorphological significance. Geol. Mag. 106 (2), 206–211.
Kuhlmann, G., Adams, S., Campher, C., van der Spuy, D., di Primio, R., Horsfield, B., 2010. Passive margin evolution and its controls on natural gas leakage in the southern Orange Basin, blocks 3/4, offshore South Africa. Mar. Petroleum Geol. 27, 973–992.
Lastras, G., Arzola, R.G., Masson, D.G., Wynn, R.B., Huvenne, V.A.I., Hühnerbach, V., Canals, M., 2009. Geomorphology and sedimentary features in the Central Portuguese submarine canyons, Western Iberian margin. Geomorphology 103, 310–329.
Lastras, G., Acosta, J., Muñoz, A., Canals, M., 2011. Submarine canyon Formation and evolution in the argentine continental margin between 44°30'S and 48°S. Geomorphology 128, 116–136.
Leinweber, V.T., Jokat, W., 2011. Is there continental crust underneath the northern Natal Valley and the Mozambique coastal plains? Geophys. Res. Lett. 38, L14303.
Lester, M.J., 2000. A Biostratigraphic Study of the Jc-D1 (Rhino) Well, Durban Basin, Republic of South Africa. Phillips Petroleum internal report, 54pp.
Liu, C., Fulthorpe, C.S., Austin Jr., J.A., Sanchez, C.M., 2011. Geomorphologic indicators of sea level and lowstand paleo-shelf exposure on early–middle Miocene sequence boundaries. Mar. Geol. 280, 182–194.
Martin, A.K., 1984. Plate Tectonic Status and Sedimentary Basin In-fill of the Natal Valley (SW Indian Ocean). Bulletin of the Joint Geological Survey/University of Cape Town, p. 209. Marine Geoscience Unit 14.
Martin, A.K., 1987. Comparison of sedimentation rates in the Natal Valley, southwest Indian Ocean, with modern sediment yields in east coast rivers of Southern Africa. South Afr. J. Sci. 83, 716–724.
Martin, A.K., Goodlad, S.W., Salmon, D.A., 1982. Sedimentary Basin In-fill in the Northernmost Natal Valley, Hiatus Development and Agulhas Current Palaeoceanography, vol. 139. Journal of the Geological Society, London, pp. 183–201.
McCormick, S., Cooper, J.A.G., Mason, T.R., 1992. Fluvial sediment yield to the Natal coast: a review. South. Afr. J. Aquatic Sci. 18, 74–88.
McGregor, B.A., Bennett, R.H., 1979. Mass movement of sediment on the continental slope and rise seaward of the Baltimore Canyon trough. Mar. Geol. 33, 163–174.
McLachlan, I.R., McMillan, I.K., 1979. In: Anderson, A.M., van Biljon, W.J. (Eds.), Microfaunal Biostratigraphy, Chronostratigraphy and History of Mesozoic and Cenozoic Deposits on the Coastal Margin of South Africa, vol. 6. Geological Society of South Africa Special Publication, pp. 161–181.
McMillian, I.K., 2003. Foraminiferally defined biostratigraphic episodes and sedimentation pattern of the Cretaceous drift succession (Early Barremian to Late Maastrichtian) in seven basins on the South African and southern Namibian continental margin. South Afr. J. Sci. 99, 537–576.
McMillian, I.K., Dale, D., 2000. Final Report on the Foraminiferal Biostratigraphy of Borehole Jc-D1 (Rhino). Phillips Petroleum South Africa Ltd., 43pp.
Miller, K.G., 2009. Sea level change, last 250 Million years. In: Gornitz, V. (Ed.), Encyclopedia of Paleoclimatology and Ancient Environments. Springer, Netherlands, pp. 879–887.
Miller, K.G., Melillo, A.J., Mountain, G.S., Farre, J.A., Poag, C.W., 1987. Middle to late Miocene canyon cutting on the New Jersey continental slope: biostratigraphic and seismic stratigraphic evidence. Geology 15, 509–512.
Miller, K.G., Kominz, M.A., Browning, J.V., Wright, J.D., Mountain, G.S., Katz, M.E., Sugarman, P.J., Cramer, B.S., Christie-Blick, N., Pekar, S.F., 2005. The phanerozoic record of global sea-level change. Science 310, 1293–1298.
Moore, A.E., 1999. A reappraisal of epeirogenic flexure axes in southern Africa. South Afr. J. Geol. 102 (4), 363–376.
Mountain, G.S., Burger, R.L., Delius, H., Fulthorpe, C.S., Austin, J.A., Goldberg, D.S., Steckler, M.S., McHugh, C.M., Miller, K.G., Montverde, D.H., Orange, D.L., Pratson, L.F., 2007. The long-term stratigraphic record on continental margins. Special Publication 37. In: Nittrouer, C.A., Austin, J.A., Field, M.E., Kravitz, J.H., Syvitski, J.P.M., Wiberg, P.L. (Eds.), Continental margin Sedimentation: from Sediment Transport to Sequence Stratigraphy. International Association of Sedimentologists, Blackwell, Oxford, pp. 275–339.
Muntingh, A., 1983. Geological Well Completion Report of Borehole. Jc-C1. SOEKOR internal report. SOE-DRG-WCR-363. 23pp.
Niemi, T.M., Ben-Avraham, Z., Hartnady, C.J.H., Reznikov, M., 2000. Post-Eocene seismic stratigraphy of the deep ocean basin adjacent to the southeast African continental margin: a record of geostrophic bottom current systems. Mar. Geol. 162, 237–258.
Nittrouer, C.A., Austin Jr., J.A., Field, M.E., Kravitz, J.H., Syvitski, J.P.M., Wiberg, P.L., 2007. Writing a Rosetta stone: insights into continental-margin sedimentary processes and strata. In: Nittrouer, C.A., Austin Jr., J.A., Field, M.E., Kravitz, J.H., Syvitski, J.P.M., Wiberg, P.L. (Eds.), Continental Margin Sedimentation: from Sediment Transport to Sequence Stratigraphy. International Association of Sedimentologists, pp. 1–48. Special Volume.
O'Grady, D.B., Syvitski, J.P.M., Pratson, L.F., Sarg, J.F., 2000. Categorizing the morphologic variability of siliciclastic passive continental margins. Geology 28 (3), 207–210.
Palermo, D., Galbiati, M., Famiglietti, M., Marchesini, M., Mezzapesa, D., Fonnesu, F., 2014. Insights into a New Super-Giant Gas Field – Sedimentology and Reservoir Modeling of the Coral Complex, Offshore Northern Mozambique. Offshore Technology Conference Asia, Kuala Lumpur, Malaysia, 25–28 March 2014. 8pp.
Partridge, T.C., 1997. Cainozoic environmental change in southern Africa, with special emphasis on the last 200 000 years. Prog. Phys. Geogr. 21 (1), 3–22.
Partridge, T.C., 1998. Of diamonds, dinosaurs and diastrophism: 150 million years of landscape evolution in southern Africa. South Afr. J. Geol. 101 (3), 167–184.
Partridge, T.C., Maud, R.R., 1987. Geomorphic evolution of southern Africa since the mesozoic. South Afr. J. Geol. 90, 179–208.
Partridge, T.C., Maud, R.R., 2000. Macro-scale geomorphic evolution of southern Africa. In: Partridge, T.C., Maud, R.R. (Eds.), The Cenozoic of Southern Africa. Oxford University Press, New York, pp. 3–18.
Pattier, F., Loncke, L., Imbert, P., Gaullier, V., Basile, C., Maillard, A., Roest, W.R., Patriat, M., Vendeville, B.C., IGUANES Scientific Party, 2015. Origin of an enigmatic regional Mio-Pliocene unconformity on the Demerara plateau. Mar. Geol. 365, 21–35.
Pisaniec, K., Abu, C., Barlass, D., Kornpihl, D., Kanrar, A., Tyagi, C., Hollebeek, E., 2017. Unlocking the potential of the Durban Basin, South Africa, using modern 3D seismic data interpretation. 79th EAGE Conference and Exhibition, Paris, France 12–15 June 2017. 5pp.
Porat, N., Botha, G.A., 2008. The luminescence chronology of dune development on the Maputaland coastal plain, southeast Africa. Quat. Sci. Rev. 27, 1024–1046.
Pratson, L.F., Ryan, W.B.F., Mountain, G.S., Twichell, D.C., 1994. Submarine canyon initiation by downslope-eroding sediment flows: evidence in late Cenozoic strata on the New Jersey continental slope. Geol. Soc. Am. Bull. 106, 395–412.
Preu, B., Spieß, V., Schwenk, T., Schneider, R., 2011. Evidence for current-controlled sedimentation along the southern Mozambique continental margin since Early Miocene times. Geo-Marine Lett. 31, 427–435.
Roberts, D.L., Botha, G.A., Maud, R.R., Pether, J., 2006. Coastal cenozoic deposits. In: Johnson, M.R., Anhaeusser, C.R., Thomas, R.J. (Eds.), The Geology of South Africa. Geological Society of South Africa and Council for Geoscience, Johannesburg/Pretoria, pp. 605–628.
Said, A., Moder, C., Clark, S., Ghorbal, B., 2015. Cretaceous-Cenozoic sedimentary budgets of the Southern Mozambique basin: implications for uplift history of the South African plateau. J. Afr. Earth Sci. 109, 1–10.
Santra, M., Goff, J.A., Steel, R.J., Austin Jr., J.A., 2013. Forced regressive and lowstand Hudson paleo-Delta system: latest Pliocene growth of the outer New Jersey shelf. Mar. Geol. 339, 57–70.
Schlüter, P., Uenzelmann-Neben, G., 2007. Seismostratigraphic analysis of the Transkei Basin: a history of deep sea current controlled sedimentation. Mar. Geol. 240, 99–111.
Schlüter, P., Uenzelmann-Neben, G., 2008. Indications for bottom current activity since Eocene times: the climate and ocean gateway archive of the Transkei Basin, South Africa. Glob. Planet. Change 60, 416–428.
Shackleton, N.J., Kennett, J.P., 1975. Initial reports. Deep Sea Drill. Proj. 29, 743.
Shanmugam, G., 2000. 50 years of the turbidite paradigm (1950s-1990â€™): deep-

water processes and facies models - a critical perspective. Mar. Petroleum Geol. 17, 285–342.
Shepard, F.P., 1981. Submarine canyons: multiple causes and long-time persistence. Am. Assoc. Petroleum Geol. Bull. 65 (6), 1062–1077.
Shevenell, A.E., Kennett, J.P., Lea, D.W., 2004. Middle Miocene southern ocean cooling and Antarctic cryosphere expansion. Science 305, 1766–1770.
Shone, R.W., 2006. Onshore post-karoo mesozoic deposits. In: Johnson, M.R., Anhaeusser, C.R., Thomas, R.J. (Eds.), The Geology of South Africa. Geological Society of South Africa, Johannesburg/Council for Geoscience, Pretoria, pp. 541–552.
Siesser, W.G., Dingle, R.V., 1981. Tertiary sea-level movements around southern Africa. J. Geol. 89 (4), 523–536.
Singh, V., McLachlan, I., 2003. South Africa's east coast frontier offers untested mid to deepwater potential. Oil Gas J. 101 (22), 40–45.
Soulet, Q., Migeon, S., Gorini, C., Rubino, J.-L., Raisson, F., Bourges, P., 2016. Erosional versus aggradational canyons along a tectonically-active margin: the north-eastern Ligurian margin (western Mediterranean Sea). Mar. Geol. 382, 17–36.
Uenzelmann-Neben, G., Clift, P.D., 2015. A sediment budget for the Transkei Basin, southwest Indian Ocean. Mar. Geophys. Res. 36, 281–291.
Unstead, P.J., Muntingh, A., Mills, S.R., McLachlan, I.R., 1983. Jc-B1 Geological Well Completion Report. Soekor internal report. 15pp.
Vail, P.R., Mitchum, R.M., Thompson, S., 1977. Seismic stratigraphy and global changes of sea level. Part 4: global cycles of relative changes of sea level. In: Payton, C.E. (Ed.), Seismic Stratigraphy - Applications to Hydrocarbon Exploration, vol. 26. American Association of Petroleum Geologists Memoir, pp. 83–97.
Van Aken, H.M., Ridderinkof, H., de Ruijter, W.P.M., 2004. North Atlantic deep water in the South-western Indian Ocean. Deep-Sea Res. I 51, 755–776.
Van Wagoner, J.C., Posamentier, H.W., Mitchum, R.M., Vail, P.R., Sarg, J.F., Loutit, T.S., Hardenbol, J., 1988. An overview of sequence stratigraphy and key definitions. In: Wilgus, C.K., Hastings, B.S., Kendall, C.G.StC., Posamentier, H.W., Ross, C.A., Van Wagoner, J.C. (Eds.), Sea Level Changes – an Integrated Approach, vol. 42. Society of Economic Paleontologists and Mineralogists (SEPM), pp. 39–45. Special Publication.
Walford, H.L., White, N.J., Sydow, J.C., 2005. Solid sediment load history of the Zambezi Delta. Earth Planet. Sci. Lett. 238, 49–63.
Watkeys, M.K., Sokoutis, D., 1998. Transtension in south-east Africa during Gondwana break-up. In: Holdsworth, R.E., Strachan, R., Dewey, J.F. (Eds.), Continental Transpressional and Transtensional Tectonics, vol. 135. Geological Society of London, pp. 203–214. Special Publication.
Weigelt, E., Uenzelmann-Neben, G., 2004. Sediment deposits in the Cape Basin: indications for shifting ocean currents? Am. Assoc. Petroleum Geol. Bull. 88 (6), 765–780.
Wigley, R.A., Compton, J.S., 2006. Late Cenozoic evolution of the outer continental shelf at the head of the Cape Canyon, South Africa. Mar. Geol. 226, 1–23.
Wiles, E., Green, A.N., Watkeys, M., Jokat, W., Krocker, R., 2013. The evolution of the Tugela canyon and submarine fan: a complex interaction between margin erosion and bottom current sweeping, southwest Indian Ocean, South Africa. Mar. Petroleum Geol. 44, 60–70.
Wiles, E., Green, A.N., Watkeys, M., Jokat, W., Krocker, R., 2014. A new pathway for Deep water exchange between the Natal Valley and Mozambique Basin? Geo-Marine Lett. 34, 525–540.
Zachos, J.C., Flower, B.P., Paul, H., 1997. Orbitally paced climate oscillations across the Oligocene/Miocene boundary. Nature 388, 567–570.
Zachos, J., Pagani, M., Sloan, L., Thomas, E., Billups, K., 2001. Trends, rhythms, and aberrations in global climate 65Ma to Present. Science 292, 686–693.
Zecchin, M., Praeg, D., Ceramicola, S., Muto, F., 2015. Onshore to offshore correlation of regional unconformities in the Plio-Pleistocene sedimentary successions of the Calabrian Arc (central Mediterranean). Earth-Science Rev. 142, 60–78.
Zhu, M., Graham, S.A., Pang, X., McHargue, T., 2009. Characteristics of migrating submarine canyons from the middle Miocene to present: implications for paleo-oceanographic circulation, northern South China Sea. Mar. Petroleum Geol. 27 (1), 307–319.

APPENDIX IV

International Journal of Greenhouse Gas Control 64 (2017) 73–86

Contents lists available at ScienceDirect

International Journal of Greenhouse Gas Control

journal homepage: www.elsevier.com/locate/ijggc

A first assessment of potential stratigraphic traps for geological storage of CO_2 in the Durban Basin, South Africa

Nigel Hicks[a,b,*], Andrew Green[b]

[a] Council for Geoscience, 139 Jabu Ndlovu Street, Pietermaritzburg 3200, South Africa
[b] Discipline of Geological Sciences, School of Agricultural, Earth and Environmental Sciences, University of KwaZulu-Natal, Westville, Private Bag X54001, South Africa

ARTICLE INFO

Keywords:
South Africa
Offshore
Sedimentary basins
Geological CO_2 storage
Durban basin

ABSTRACT

Within offshore frontier sedimentary basins, legacy data are important tools in basin-scale exploration for potential CO_2 storage. We utilise single-channel 2D seismic reflection and well data obtained from the offshore Durban Basin, east coast South Africa, to provide new evidence of reservoir/seal pairs in saline aquifers that may represent potential storage sites for CO_2 injection. Multiple, previously undefined and regionally pervasive stratigraphic traps have been mapped through a detailed seismo-sedimentary analysis. These include shelf-bound shallow-marine-sheet and deltaic sandstone packages of Turonian and Maastrichtian age respectively. Coeval with these laterally extensive shelf packages, multiple basin floor fan systems have been identified on the palaeo-slope. We further correlate these systems with analogous hydrocarbon-bearing sequences throughout a large region of the south-east African continental shelf. Using conservative assumptions, we propose that ~327 Mt CO_2 could potentially be stored in two laterally extensive shelf sand sequences, with a further potential for ~464 Mt CO_2 storage in basin floor fan systems in the distal basin.

1. Introduction

Geological storage of anthropogenic CO_2 via Carbon Capture and Storage (CCS) technologies represents a crucial component to the mitigation of global climate change. For the geological storage of CO_2 to be optimised, suitable strata and reservoir conditions need to be identified. Whilst a wealth of knowledge exists for CCS projects associated with hydrocarbon provinces (IPCC, 2005; US DOE, 2008; Würdemann et al., 2010; Underschultz et al., 2011; Hutcheon et al., 2016), saline aquifer storage, specifically in under-explored frontier basins, is commonly hampered by a lack of physical data needed to define CO_2 storage reservoirs and their storage capacity due to limited exploration activities (Wilkinson et al., 2013).

South Africa, like many countries worldwide, is heavily reliant on fossil fuels for energy supply, with about 90% of primary energy derived from either coal, oil or gas (Engelbrecht et al., 2004). A country-scale analysis of the geological storage potential of CO_2 was undertaken by Viljoen et al. (2010) and culminated in an atlas of CO_2 storage potential (Cloete, 2010). During their technical review, Viljoen et al. (2010) identified potential storage capacity in multiple onshore and offshore Mesozoic sedimentary basins (Fig. 1). On the eastern seaboard of South Africa, a theoretical storage capacity of 42,000 Mt CO_2 was assigned to the combined offshore Durban and Zululand Basins (Fig. 1) (Viljoen et al., 2010). Although a low confidence ranking of "1" was given to the Durban Basin based upon data density and sub-surface heterogeneities (Cloete, 2010), it was selected for study due to the following factors:

1. its proximity to potential CO_2 transport pipelines from major CO_2 sources
2. large storage potential as defined by Viljoen et al. (2010)
3. geological storage potential within stratigraphic and structural settings.

The ~10,000 km^2 Durban Basin that borders the Zululand Basin to the north (Fig. 1), represents a poorly explored frontier basin (Singh and McLachlan, 2003). Hydrocarbon exploration is limited to low resolution single-channel seismic reflection data sets (Du Toit and Leith, 1974; Dingle et al., 1978; Martin, 1984; Goodlad, 1986) and four wildcat wells that focused upon potential structural plays beneath the continental shelf.

This paper aims to provide the first effective assessment of the CO_2 storage potential (CSLF, 2005; Bradshaw et al., 2007; Bachu, 2015) of sandstone packages within the Durban Basin, through analysis of regional seismic and well log data. Interpretations of the sedimentary architecture of potential stratigraphic traps are discussed. It should be

* Corresponding author at: Council for Geoscience, 139 Jabu Ndlovu Street, Pietermaritzburg 3200, South Africa.
E-mail address: nigel.hicks101@gmail.com (N. Hicks).

http://dx.doi.org/10.1016/j.ijggc.2017.06.015
Received 9 March 2017; Received in revised form 20 June 2017; Accepted 24 June 2017

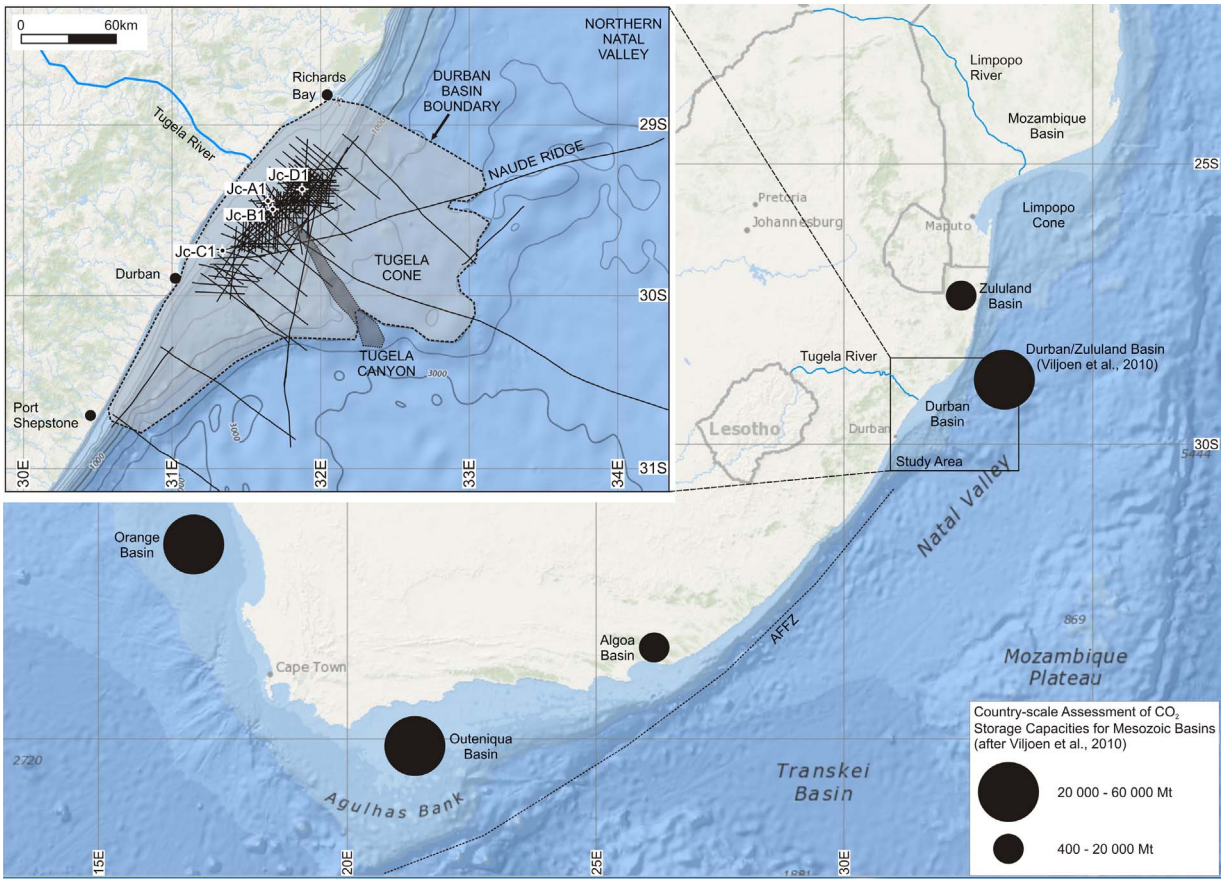

Fig. 1. Locality map detailing the study area location with National Oceanic and Atmospheric Administration (1 min grid) UTM bathymetric grid. The areal extent of the Durban Basin is depicted within the shaded polygon. Note the relative position of the Jc-series boreholes drilled on the continental shelf to that of the deep water Tugela Cone. The CO_2 storage estimates of Mesozoic basins defined by Viljoen et al. (2010) are shown.

noted that this paper makes no attempt to define factors relating to CCS regulation, public perception, or economic viability.

2. Regional and geological setting

The Durban Basin is a sheared rift basin (Broad et al., 2006; Hicks and Green, 2016) that developed between the coastline and the 2500 m isobath, from Port Shepstone in the south to Richards Bay in the north (Fig. 1). The continental margin of this region is unique, dominated by an extremely narrow (~2–12 km) sheared margin (Martin, 1984; Martin and Flemming, 1986; Green and Garlick, 2011), resulting from periods of alternating sediment starvation or abundant sediment supply (Green, 2011a; Hicks and Green, 2016). Offshore Durban, the shelf broadens to ~45 km, defining the spatial extent of the Tugela Cone (Fig. 1), a submarine delta that has prograded into the basin since Eocene times (Hicks and Green, 2016).

The sedimentology and evolution of the basin was recently discussed by Hicks and Green (2016) who highlighted several phases of margin growth that were defined by six main seismo-sedimentary units (A–F) as shown in Table 1. The depositional history of the basin-fill is complex and comprises syn-rift, ramp margin, and progradational shelf margin sediments (Table 1; Fig. 2) that were deposited predominantly during periods of sea-level lowstand (Hicks and Green, 2016).

3. Methods

3.1. Data collection and processing

The Durban Basin is traversed by 2761 km of legacy, reprocessed, migrated stack 2D seismic reflection profiles (Fig. 1) obtained from eleven exploration programmes over a period spanning the 1970's to 1990's. For this study two thousand kilometres of pre-migrated and stacked single-channel 2D seismic spanning an area of 15000 km^2 across the continental shelf, and slope were obtained from the Petroleum Agency of South Africa (PASA) in SEGY format. Well log and downhole geophysical data were obtained for the four Jc-series exploration wells that were drilled on the continental shelf offshore between 1970 and 2000 (Fig. 1).

3.2. Data interpretation

SEGY data and LAS log data were interpreted in IHS Global Inc. Kingdom Advanced V2015.0. Digital well shoot/velocity data from the Jc-D1 well were obtained from PASA in order to define two-way time vs measured depth (m) so as to tie the well data to the seismic data. The seismic stratigraphic interpretations are based upon the currently accepted seismic and sequence stratigraphic frameworks for passive margins defined by Catuneanu et al. (2009) and Catuneanu et al. (2011).

3.3. Estimation of processing parameters

No core, porosity permeability or water saturation data are available for any wells within the basin and therefore values from analogous formations within the southern African east and west coasts are utilised for volumetric calculations. Data from analogous successions in Ghana (Dailly et al., 2013) are utilised for basin floor fan reservoir systems, whilst data from the onshore Zululand (Gerrard, 1972) and Mozambique Basins (Coster et al., 1989; Solomon et al., 2014) are utilised for the shelf sand reservoirs. As limited data are available for the basin,

Table 1
Simplified sequence stratigraphic framework for the continental margin of the Durban Basin. Seismic units, facies, bounding surfaces, interpreted depositional environment and reservoir/seal potential of each unit are provided.

Unit	Facies	Surface	Modern Description	Stratal Relationship	Borehole Lithology Summary	Net Thickness	Reservoir and Seal Potential
F			Progradational wedge	Moderate impedance, sub-parallel, progradational reflectors	Unconsolidated sands		None – Too Shallow
		S6	Shelf-confined erosional reflector				
E			Progradational wedge	Moderate impedance, sigmoid, progradational reflectors overlain by aggradational reflectors	Sandstone and coquina	200 m	None – No seal
		S5	Shelf-confined erosional reflector				
D			Progradational wedge	Moderate impedance, steeply dipping, progradational reflectors	Calcarenite, siltstone and claystone	900 m	None – No seal
		S4	Basin-wide Erosional Reflector				
C	C5		Progradational wedge	Moderate impedance, steeply dipping, progradational reflectors	Inner shelf sandstones and siltstones	950 m	None – seal unknown
		3C	Maximum Flooding Surface				
	C4		Retrogradational package	Low impedance aggrading reflectors, backstep and onlap 3B landward	Deep water mudstones	600 m	Seal
		3B	Maximum Regressive Surface				
	C3		Aggradational to Retrogradational Wedge	Low to moderate impedance, sub parallel, aggradational reflectors, onlap S3	Deep water mudstones and sandy turbidites	500 m	Seal
	C2		Progradational wedge	Moderate impedance, steeply dipping, progradational reflectors	Mudstone and interbedded well-sorted shelf sandstones	300 m	Good – Possible Reservoir
	C1		Slope Fan	Moderate impedance, progradational reflectors, downlap and onlap S3	Unknown – possibly sandy turbidites	250 m	Good – Possible Reservoir
		S3	Shelf-confined erosional reflector				
B	B2		Aggradational ramp	Low to moderate amp, sub parallel reflectors, onlap S2 updip.	Mudstone dominated top		Seal – Upper facies
					Sandstone dominated base	250 m	Good – Basal Facies – Possible Reservoir
	B1		Basin-floor Fan	High impedance progradational reflectors that downlap and onlap S2, individual mounds show internal progradation but retrograde as packages.	Unknown – possibly sandy turbidites	250 m	Good – Possible Reservoir
		S2	Basin-wide Erosional Reflector				
A			Syn-rift valley fill	Aggradational to Progradational packages that onlap S1 against basement highs	Clay-rich sandstone and conglomerate	950 m	Not Investigated
		S1	Basin-wide Erosional Reflector				
BASEMENT			Acoustic Basement		Diamictite, sandstone and/or volcanics	Unknown	None – Basement

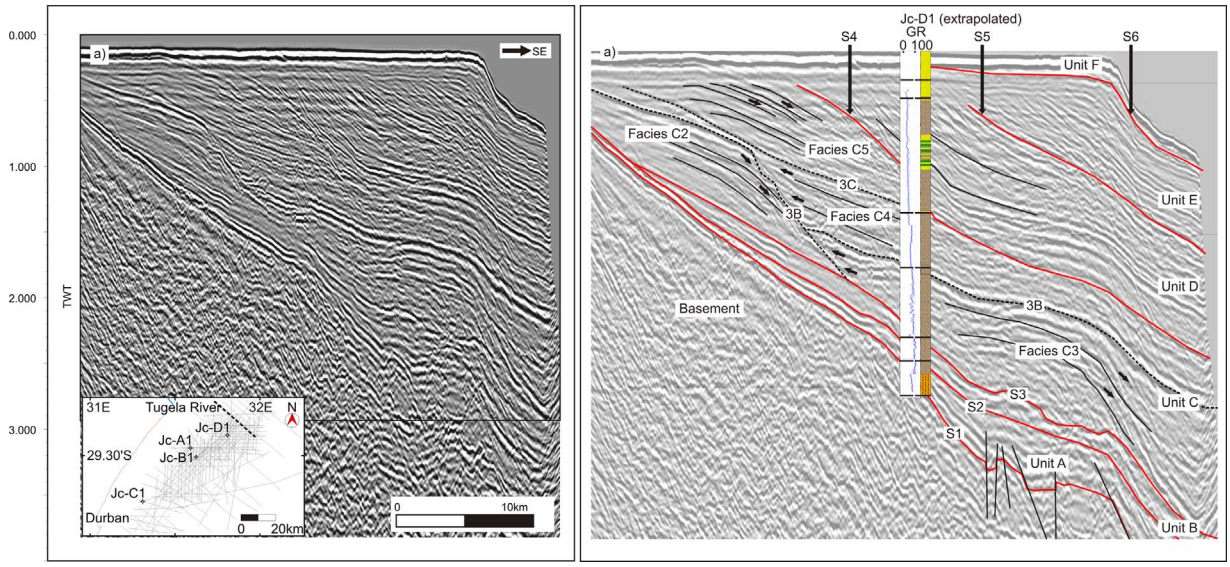

Fig. 2. General overview of the seismic stratigraphy of the Durban Basin (modified after Hicks and Green, 2016).

50% net thicknesses of reservoirs are utilised for this study. CO_2 density values are calculated based upon depths of individual formation tops defined from seismic profiles, combined with a pore fluid pressure of 8.6 ppg and a geothermal gradient of 2.67 °C/100 m as considered for borehole Jc-C1 (Muntingh, 1983). The online calculator (www.energy.psu.edu/tools/CO2-EOS), employing the equation of state calculations of Span and Wagner (1996), is used to derive the CO_2 density calculations.

3.4. Effective storage capacity estimations

The effective storage capacity of individual reservoir units is assessed using calculations based upon currently accepted storage capacity estimations as defined by numerous authors (IPCC, 2005; Bachu et al., 2007; Bachu, 2008; US DOE, 2008; Goodman et al., 2011; Bachu, 2015). Here the United States Department of Energy (US DOE) methodology (Goodman et al., 2011) is used, whereby the effective storage capacity in a saline formation, M_{CO2}, is given by:

$$M_{CO2} = A \times h \times \phi \times \rho_{CO2} \times E$$

Where A is the area (m^2), h is the net thickness of the reservoir (m), ϕ is the average porosity (%), ρ_{CO2} is the average CO_2 density, evaluated at pressures and temperatures that represent storage conditions anticipated for individual deep saline aquifers. E is a storage efficiency factor that reflects the total pore volume filled with CO_2. Efficiency factors at a formation scale have been defined by the IEAGHG (2009) and by Goodman et al. (2011) for different lithologies over P10, P50 and P90 probabilities. For this work the formation-scale values defined by Goodman et al. (2011) are used. We base our work on an upper depth cut-off of 800 m below the seafloor as per the criteria for supercritical CO_2 storage defined by the IPCC (2005).

Although the Efficiency factor (E) adjusts total gross thickness to net gross thickness, total area to net area, and total porosity to effective porosity (cf. Cook, 2012), the "net" thicknesses shown in Table 2 are based on 50% of the maximum thickness measured for an individual reservoir. This was done in order to account for 1) lateral thickness variations and wedge-out up- and down-dip in the case of basin floor fan deposits, and 2) variation in thickness of the shelf sediment wedges due to erosional surfaces and package thinning/pinching into the deep basin.

4. Results

Within the Durban Basin, six seismic units (A–F) are delineated. These are defined by seismic bounding surfaces, reflector and unit impedance, and internal-reflector characteristics (Table 1; Fig. 2). Unit A represents a syn-rift sedimentary succession (not discussed further but discussed in detail by Hicks and Green, 2016) whilst the overlying units (B–F) were deposited during passive margin construction. Individual units are separated by regionally pervasive, high amplitude, erosional seismic reflectors (Fig. 2). Units are commonly characterised by multiple seismic facies defined by specific seismic characteristics and architectures (Fig. 2).

On the basis of depth below seafloor, sedimentology, seismic architecture and reservoir properties, sedimentary units within four facies are identified as having CO_2 storage potential with well-defined reservoir-seal pairs. These include facies B1 and the basal zone of facies B2 (of unit B), and facies C1 and C2 within unit C (Table 1).

4.1. Sedimentology of reservoir-seal pairs

4.1.1. Unit B

Unit B overlies unit A along an erosional, high amplitude seismic reflector "S2" (Figs. 2 and 3). Unit B, comprises two facies, B1 and B2 (Fig. 3), and is developed on a shallowly dipping proto-margin (Fig. 2). Facies B1 is laterally discontinuous, characterised by mounded, high amplitude seismic reflectors (Fig. 3). The positions of the mounds (Reservoirs A–E) relative to the contemporary shoreline are shown in Fig. 4. The seismic architecture of facies B1 is defined by progradational, seaward-dipping reflectors which downlap the underlying reflector S2 (Fig. 5). The mound architecture varies between sheet mounds as in Reservoir C, (Fig. 5) and stacked mounds such as in Reservoir A (Fig. 6). Stacked mounds exhibit a progradational internal clinoform architecture separated by sheet-like High Amplitude Reflection Packages (HARPs) (Figs. 6 and 7). In coast-perpendicular section, the upper mound retrogrades over the lower fan with successive updip migration of the internal clinoforms (Fig. 6). These clinoforms onlap successively landwards onto the underlying surface S2 (Fig. 6). Along strike, the mounds exhibit erosional internal architectures separating bright, high amplitude reflectors from diffuse, low amplitude zones (Fig. 7).

Although mounded structures of facies B1 are not intersected by the boreholes, a 28 m thick, coarsening upward, medium- to coarse-grained sandstone unit is intersected in Jc-B1, 3.8 km updip of a mounded

Table 2
Reservoir characteristics: extent, thickness, and physical parameters for the Durban Basin. Porosity data shown from analogous plays in neighbouring basins.

Reservoir	Facies	Reservoir Description	Areal Extent (km^2)	Max Thickness (m)	Net/Gross Thickness (m)	Depth of top surface (m)	Hydrostatic Pressure (bar)	Reservoir Temperature (°C)	CO_2 Density ($g\ cm^{-3}$)	CO_2 Density ($kg\ m^{-3}$)	Porosity%	Porosity Data Source
I	C2	Deltaic Shelf Sand	1500	100	50	1639	163	58	0.663	663	30	(Coster et al., 1989; Solomon et al., 2014)
H	C1	Basin-floor Fan	730	322	161	6817	680	196	0.695	695	15	(Coster et al., 1989)
G	C1	Basin-floor Fan	10	247	123.5	2431	242	79	0.679	679	15	(Coster et al., 1989)
F	B2	Inner Shelf Sand	1500	80	40	3050	304	95	0.687	687	30	(Gerrard, 1972; Coster et al., 1989; Solomon et al., 2014)
E	B1	Basin-floor Fan	280	360	180	2441	243	79	0.681	681	20	(Dailly et al., 2013)
D	B1	Basin-floor Fan	38	312	156	3250	324	101	0.685	685	20	(Dailly et al., 2013)
C	B1	Basin-floor Fan	93	468	234	4992	498	147	0.692	692	20	(Dailly et al., 2013)
B	B1	Basin-floor Fan	50	250	125	3397	339	105	0.686	686	20	(Dailly et al., 2013)
A	B1	Basin-floor Fan	120	285	142.5	4828	482	143	0.691	691	20	(Dailly et al., 2013)

CO_2 Density Constant—0.052.
Mud Weight (ppg)—8.6.
Av. Geothermal Gradient – Jc-C1 (°C/km)—26.7.
Seafloor Temperature (°C)—14.
Net/Gross Ratio—NG = 0.5.
Avg. Water Depth (m)—80.

feature (Fig. 3). This unit (Reservoir F) represents a basal package of facies B2, identified in all but the Jc-D1 borehole. A low gamma signature is however noted at this zone in the corresponding petrophysical log of Jc-D1 (Fig. 4). The material is a fine- to coarse-grained, very well-sorted sandstone with thicknesses that vary from 5 to 28m. Overlying the basal package, the seismic reflectors of facies B2 comprise a stacked succession of aggradational, high impedance reflectors best represented in Jc-B1 and Jc-C1 where it is associated with a succession of claystone and subordinate siltstone (Fig. 3).

4.1.2. Unit C

Unit C, erosionally separated from the underlying successions by reflector S3, is defined by moderate amplitude, offlapping, progradational reflectors that downlap the underlying units seaward. Five facies (C1-5) (Fig. 2) are resolved beneath the contemporary shelf and slope, separated by diffuse to pronounced reflectors.

Facies C1 is laterally discontinuous, comprising mounded reflectors with prograding internal architectures which downlap the underlying reflector S3 (Fig. 8). Along the lower slope, in the south of the basin, a pronounced mounded feature (Reservoir H) that exhibits variable internal reflectors including incision fills, HARPs, and inter-leveed bright to diffuse wavy reflectors is developed (Fig. 8).

Facies C2 is confined to the proximal basin where it is defined by a wedge of predominantly progradational seismic reflectors that downlap the underlying surface S3 (Fig. 2). Facies C2 is intersected in three wells (Jc-A1, Jc-B1 and Jc-C1) where it comprises an interbedded succession of sandstone and claystone defined as Reservoir I (Figs. 3 and 4). This facies attains a thickness of ~87 m in Jc-C1 (Fig. 4). Sandstones are fine- to coarse-grained, and well sorted with individual sandstone thicknesses varying from 5 to 20m.

Facies C3 is resolved seaward of facies C2, in the distal basin, where it overlies either facies C1 or reflector S3 (Fig. 2). The facies is defined by aggradational to progradational internal reflectors. The gamma ray and lithological logs suggest siltstone and claystone deposits, with subordinate sandstones lenses capping upward-coarsening cycles (Fig. 4). Facies C4 comprises low impedance, sub-parallel to parallel, aggradational to weakly retrogradational reflectors which overlie facies C2 and C3 along a marked high amplitude reflector surface “3B” that defines the base of the most prominent onlap (Fig. 2). In this facies, the corresponding lithostratigraphy is dominated by marine claystone and siltstone with the facies capped by a moderate to high gamma ray signature claystone in Jc-C1 (Fig. 4).

Facies C5 is confined to the proximal basin, only intersected by the Jc-C1 borehole, where it caps unit C as a prograding wedge. This wedge oversteps facies C4 seaward along a downlap surface“3C” (Fig. 7). This facies comprises an overall coarsening upward succession of claystone to medium-grained sandstones (Figs. 2 and 4). The succession is truncated by a major regional erosional reflector (S4) that incises facies C5 in the proximal basin and facies C4 in the distal basin.

4.2. Storage capacity of saline formations

The areal extent, depth, gross and net thickness of individual mounded features and sandstone reservoirs are presented in Table 2, whilst their spatial distributions are shown in Fig. 4. As none of the above described mounded features were intersected by boreholes, their maximum thicknesses are instead defined from TWTT-depth conversions based upon the Jc-D1 well shot/velocity data. The thicknesses of individual reservoirs are defined from seismic analyses and or borehole intersections with the net thickness utilised for storage potential calculations. CO_2 densities for individual reservoirs are provided in Table 2.

As previously mentioned, overall storage resource estimates are defined by the following equation (Goodman et al., 2011).

$$M_{CO2} = A \times h \times \phi \times \rho_{CO2} \times E$$

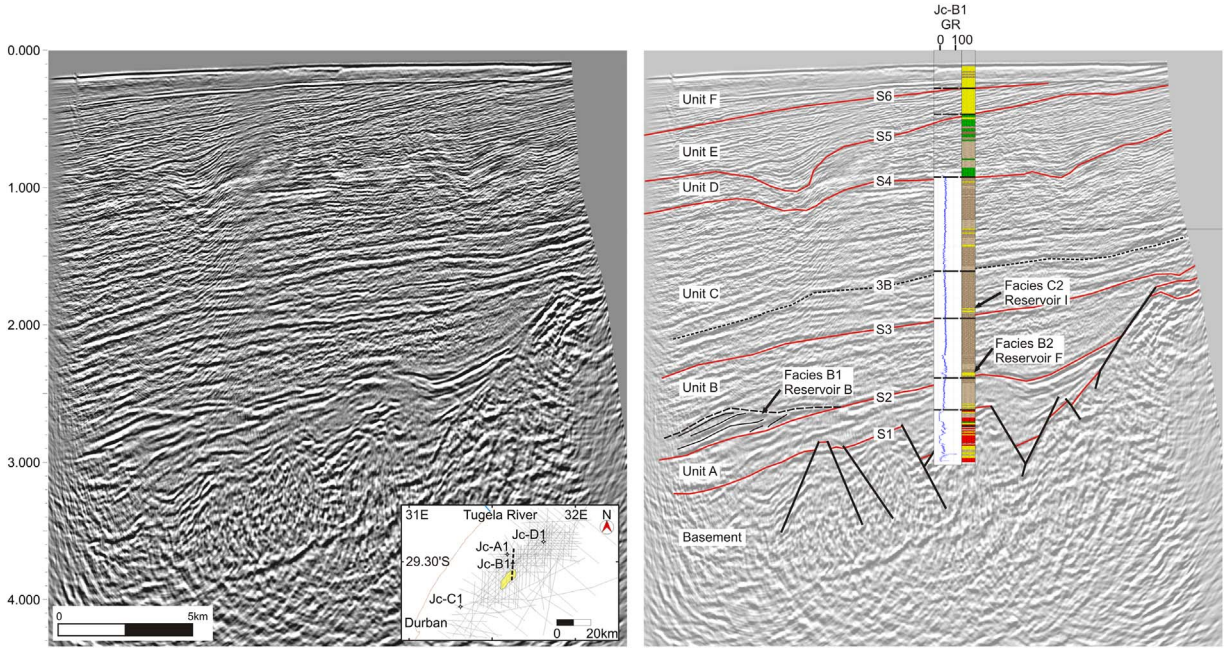

Fig. 3. Seismic stratigraphy of Reservoirs B, F and I with intersections within Jc-B1 shown. Position of Reservoir B shown as polygon in inset.

The storage capacity estimates for individual mounded features identified in facies B1 and C1; as well as the shelf sands identified in facies B2 and C2 are summarised in Table 3.

5. Discussion

5.1. Reservoirs

Although CO_2 storage is commonly focused on laterally extensive saline aquifers formed by either shallow marine sand-rich shelf systems (Galloway, 2002) or fluvial braid-plain sandstone deposition (Noy et al., 2012; Leetaru and Freiburg, 2014), deep-water hydrocarbon-bearing reservoir systems are commonly associated with stacked basin floor fan systems similar to those described by Carman and Young (1981) in the North Sea, and Dailly et al. (2013) offshore Ghana. Such systems have become targets for potential CO_2 storage, as outlined by Gibson-Poole (2009) and Borissova et al. (2013) for basin floor fan systems in Australia. Reservoir packages within the Durban Basin are confined to units B and C with multiple targets identified in basin floor fan systems as well as laterally extensive shallow marine shelf, and deltaic sands.

5.1.1. Cenomanian-Turonian reservoirs – Domo Formation equivalents

5.1.1.1. Distal Basin reservoir systems. Reservoir systems A–E within facies B1 occur as a series of progradational, mounded features () similar in geometry to the basin floor fan systems defined by Bouma (2000) and Shanmugam (2016). Internal clinoform orientations suggest interaction between progradational sheet sand (Fig. 5) and erosional channel and channel-levee structures (Figs. 6 and 7) as discussed by Shanmugam et al. (1995), Mayall et al. (2006), and Shanmugam (2016). It is likely these deposits formed by off-shelf sediment forcing of high-density turbidite currents (Lowe, 1982; Heller and Dickinson, 1985; Catuneanu et al., 2011) or sandy debris flows (Shanmugam, 2016). We therefore propose that Reservoirs A-E comprise basin floor fan systems deposited during late forced regression and early normal regression, related to global and local sea-level fall during the late Cenomanian and early Turonian (Dingle et al., 1983; Haq et al., 1987, 1988; Miller et al., 2005; Miller, 2009).

Unlike classic submarine canyon-associated fan systems (e.g. Normark, 1970; Bouma et al., 1985; Posamentier and Allen, 1999; Shanmugam, 2016), the Durban Basin at first comprised a ramp margin with no associated single-point canyon feeder system (Hicks and Green, 2016). Heller and Dickinson (1985), Stow and Mayall (2000) and Porebski and Steel (2003) suggest that, in ramp margin settings where multiple shelf sediment sources are available, proximal fan systems develop with no defined canyon feeder systems. In direct comparison with the fan systems identified in this study, Castelino et al. (2015) indicate a similar lack of shelf indenting, feeder canyons for submarine fan systems of the distal Domo Formation within the Turonian-age Zambezi Delta of the Mozambique Basin (Fig. 9). We therefore propose that similar depositional regimes must have been active and spanned the sum of the Durban and Mozambique Basins during this period.

5.1.1.2. Proximal Basin reservoir systems. In the proximal Durban Basin, a laterally extensive sandstone package (Reservoir F) of Turonian age (Leith, 1971; Unstead et al., 1983; McMillian, 2003; Hicks and Green, 2016) is identified in Jc-A1, Jc-B1 and Jc-C1 (Figs. 3 and 4). McMillian (2003) suggests that a comparable unit from onshore, in the adjacent Zululand Basin (Fig. 1), represents a Cenomanian-Turonian forced regressive shoreline deposit equivalent to the proximal Domo Formation sandstones in southern Mozambique (Fig. 9). Coster et al. (1989) and Salman and Abdula (1995) postulated that the Domo Formation developed as a proximal inner shelf, sheet sandstone with coeval distal submarine fan deposition on the upper palaeo-slope (Fig. 9). Coster et al. (1989) further propose that the widespread Domo Formation represents a major target for hydrocarbon exploration within the basin. We therefore consider that, within the Durban Basin, unit B represents the coeval deposition of proximal, forced regressive, shelf sheet sands (Reservoir F), with distal accumulation of deep water, slope and basin floor fan systems (Reservoirs A–E) in a ramp margin setting. These conditions are identical to age-equivalent depositional environments described by Coster et al. (1989) and Castelino et al. (2015) in Mozambique. This suggests a regional connectivity in response to local sea-level variability around this region of south-eastern Africa; along-strike deposition of a series of coeval deep-water sandy turbidite fan systems, offshore of the major river systems, was active during this period.

5.1.2. Campanian reservoir systems – lower Grudja formation equivalents

5.1.2.1. Distal Basin reservoir systems. The Reservoirs G-H and I of unit

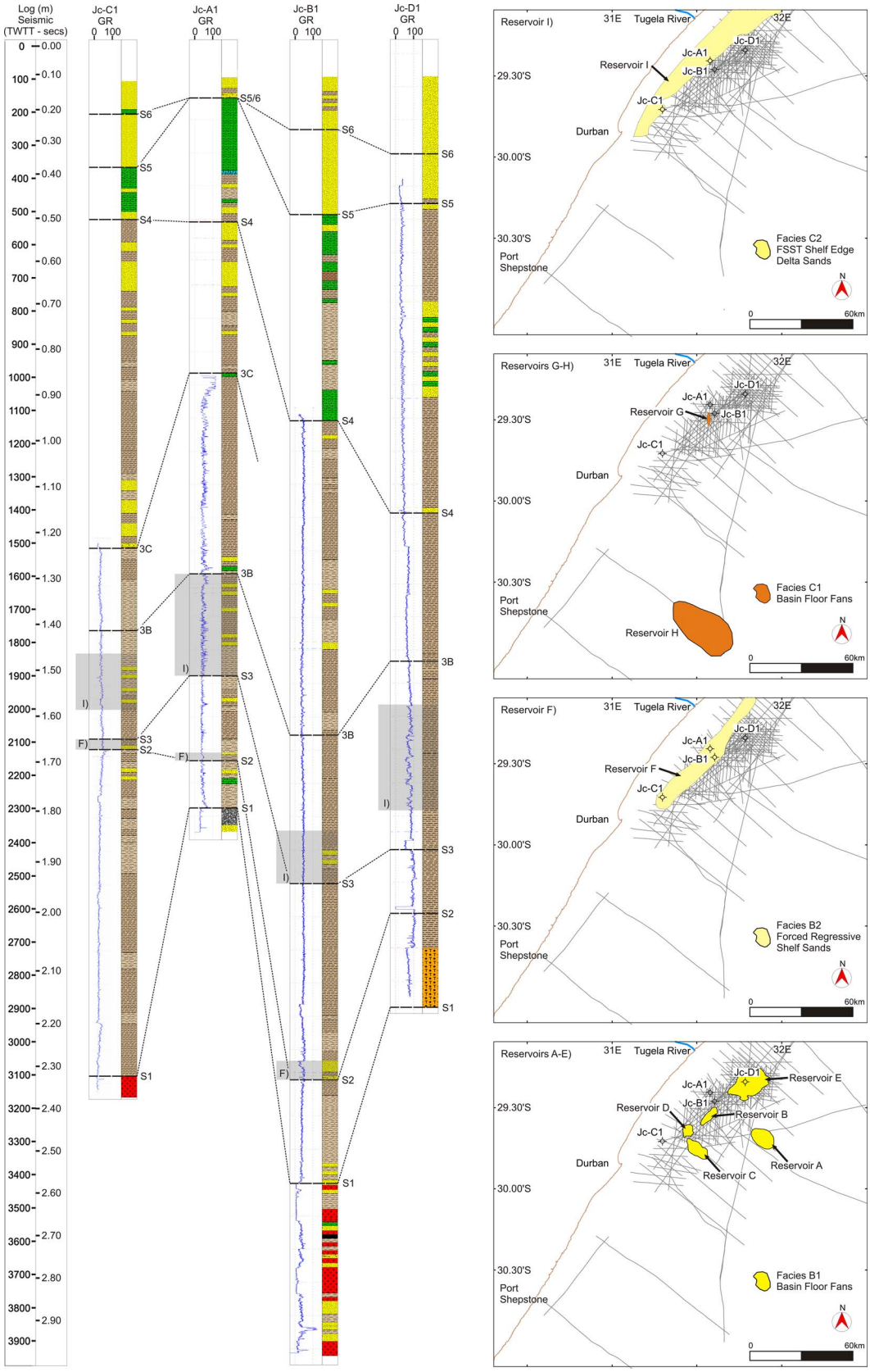

Fig. 4. Lithological logs and associated lithostratigraphic correlations of the Jc-series wells drilled within the Durban Basin. Spatial positions of all identified reservoirs are shown in insets.

C were deposited during forced regressive and lowstand conditions in the late Cretaceous (McMillian, 2003; Hicks and Green, 2016). Facies C1 and C2 were deposited on the palaeo-slope and shelf edge respectively, and are considered coeval (cf. Hicks and Green, 2016). Reservoirs G and H formed as submarine slope and basin floor fans, with Reservoir H in the southern basin (Figs. 4 and 8) the largest of

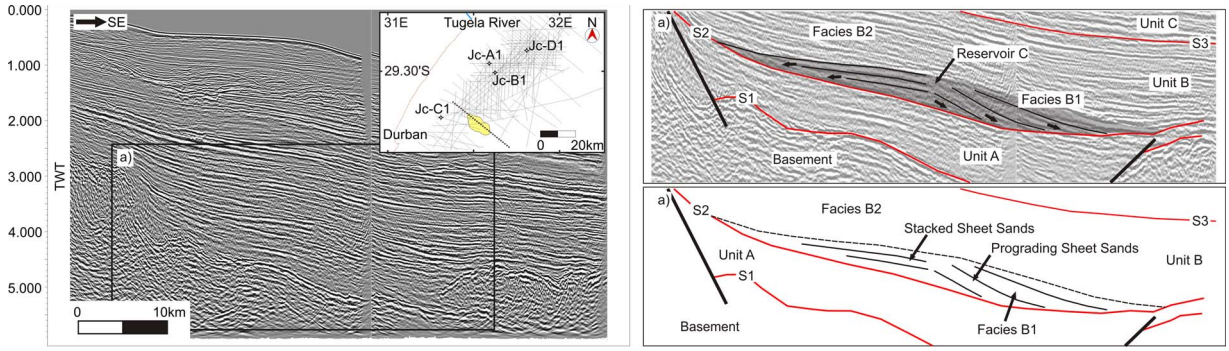

Fig. 5. The seismic architecture of a progradational sheet mound basin floor fan, Reservoir C.

these. Within Reservoir H, the internal architecture of the middle fan along the slope edge, comprises two channel-levee systems with coarse-grained debris flows deposits (Fig. 8) (sensu Shanmugam et al., 1995) and high density turbidite flows similar to those discussed by Bouma (2000). These are separated by an unchannelised HARP unit. The lower fan (Fig. 8) exhibits shingled stacking of sheet sand lobes in keeping with those described by Bouma (2000). Intervening distributary turbidite channels and associated levees (e.g. Mayall et al., 2006) occur within the lower fan. Similar submarine fan lobes of late Cretaceous age have been identified in the distal slope offshore Mozambique (Castelino et al., 2015).

5.1.2.2. Proximal Basin reservoir systems. In the inner shelf, Reservoir I of facies C2 represents a truncated, forced regressive shelf-edge delta (e.g. Hunt and Tucker, 1992). A similar depositional model for sand-rich, multiple source, ramp margins (c.f. Reading and Richards, 1994) is envisaged, whereby the delta front progrades to the shelf edge supplying sediment directly to the upper slope from multiple point sources. These margins commonly exhibit, aggradational, to progradational sequences derived from multiple channel switching (Stow et al., 1996). Coster et al. (1989) and Walford et al. (2005) propose a similar depositional environment for the age-equivalent, hydrocarbon-bearing (Mashaba and Altermann, 2015), lower Grudja Formation in Mozambique, which comprises proximal deltaic and distal basin floor fan sediments (Fig. 10). Coster et al. (1989) suggest that the lower Grudja Formation represents excellent reservoirs, having been deposited as beach and chenier barrier sands. Here depositional cycles occur as a stack of upward coarsening packages with net reservoir thicknesses of 16 m and porosities between 15 and 30% (Coster et al., 1989).

Hicks and Green (2016), following observations of Green (2011b), propose that facies C2 is identified along much of the KwaZulu-Natal margin northwards towards Mozambique. We therefore suggest that the reservoir systems (G-I) within the Durban Basin are coeval with the lower Grudja Formation in Mozambique (Coster et al., 1989) and were deposited through proximal deltaic, and distal submarine fan deposition during relative sea-level fall during the late Campanian and early Maastrichtian.

5.2. Seals

Seals within the Durban Basin occur as prominent marine claystone successions at varying intervals.

5.2.1. Turonian to Coniacian seal systems

Basin floor fan Reservoirs (A–E) and sheet sands of Reservoir F are overlain by thick (> 100 m) successions of deep marine claystones in Jc-A1 and Jc-B1 (Figs. 3 and 4). Hicks and Green (2016) propose that these claystones developed during late lowstand and early transgression within the basin.

5.2.2. Campanian seal systems

The basin floor fan Reservoirs (G-H) and Reservoir I deltaic sandstones of Facies C1 are further overlain by deep marine claystones and siltstone packages of facies C4 (Hicks and Green, 2016). Intersected by boreholes Jc-A1, Jc-B1 and Jc-C1, this succession represents a transgressive systems tract capped by a maximum flooding surface (Hicks and Green, 2016).

5.3. Storage capacity estimate

Initial storage estimates for the offshore basins of the east coast of South Africa (Viljoen et al., 2010) identified a theoretical CO_2 storage capacity of 42,000 Mt (Table 4) based upon a net sandstone thickness of 60 m, over an area of ~81,000 km^2, spanning the Durban and Zululand basins. For their assessment, Viljoen et al. (2010) used a CO_2 density of 580 kg m^{-3}, with an average porosity of 15% and an efficiency factor of 0.1. This was based on calculations adapted from the US Department of Energy (US DOE, 2008). However, Broad et al. (2006) indicated that the Durban Basin has a total extent of only ~10,000 km^2 to the 2500 m isobath, thereby leading Hicks et al. (2014) to propose a theoretical storage capacity of ~5200 Mt within the Durban Basin using Viljoen et al. (2010)'s criteria. Table 4 highlights a review of the identified potential storage reservoirs (this study) and previous data for the basin (Viljoen et al., 2010; Hicks et al., 2014) utilising the 0.1 E-factor of Viljoen et al. (2010). These can be compared with currently accepted E values defined by Goodman et al. (2011) which are now employed for

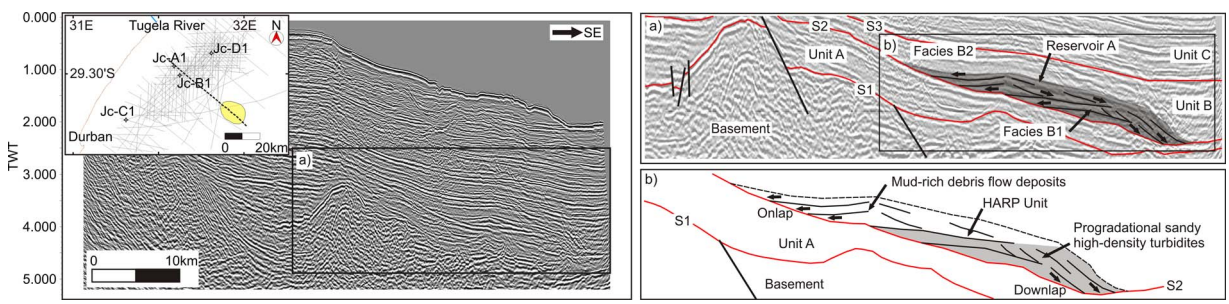

Fig. 6. Seismic architecture of Reservoir A. Note the progradational architecture of the internal reflectors, with individual fan structures separated by laterally extensive HARP's.

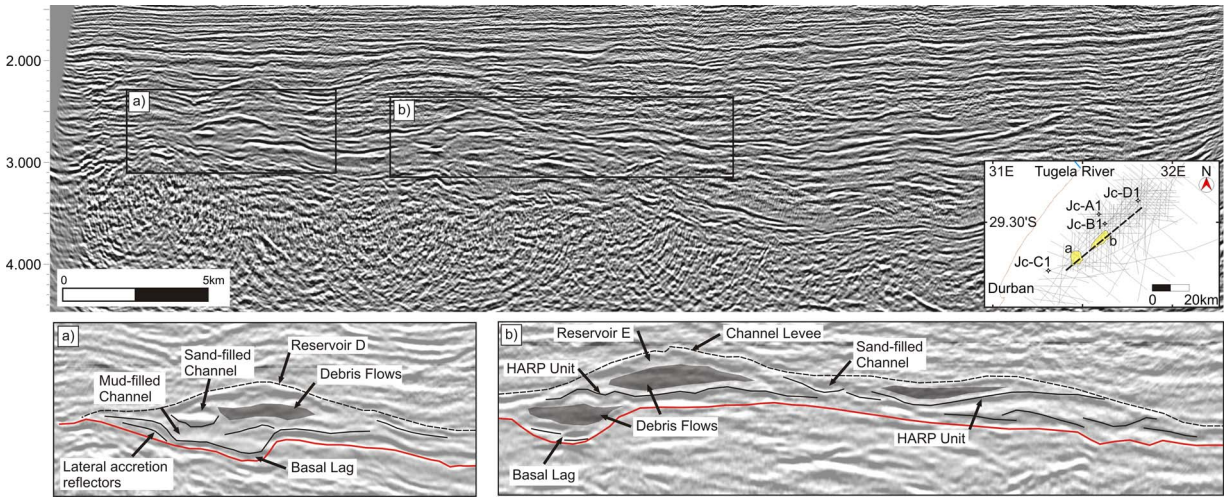

Fig. 7. Coast-parallel seismic profile and associated stratigraphic architecture of Reservoirs D and E. Note the channel and levee structures within individual fans.

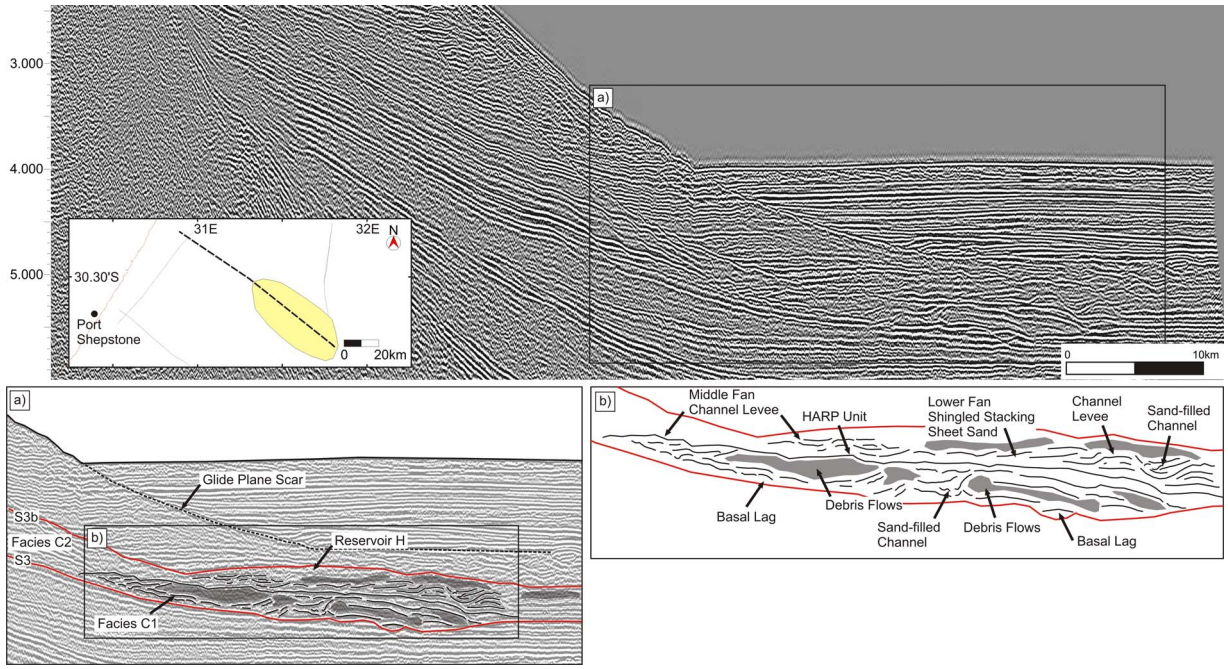

Fig. 8. Seismic architecture of Reservoir H showing the complex internal reflector configurations that comprise channel-levee units in the middle fan and stacked sheet sands in the lower fan. Note how individual fan structures are separated by laterally extensive HARP's.

this study (Table 3).

When using the 0.1 E-factor of Viljoen et al. (2010), a close relationship is observed between the ~5000 Mt theoretical storage capacity for the regional basin evaluation of Hicks et al. (2014) when compared with a combined storage capacity of ~5357 Mt as defined by volumetrics obtained in this study (Table 4). However, the initial estimates of Hicks et al. (2014) defined only laterally extensive, shelf-bound saline aquifers, which here account for ~2727 Mt storage at an E-factor of 0.1 (Table 4).

Although the estimates shown in Table 4 correlate well with the initial estimates of Viljoen et al. (2010) and Hicks et al. (2014), a more cautious approach (Goodman et al., 2011; Li et al., 2015) is deemed necessary for effective CO_2 storage capacity calculations. Therefore, the calculated results of this study, outlined in Table 3, suggest a total CO_2 storage capacity of 643 Mt at a P10 probability level (1286 Mt at P50; 2196 Mt at P90). These P10 estimates can be further subdivided into 327 Mt in deltaic and shelf confined sheet sands in Reservoirs F and I; and 464 Mt in basin floor fan systems.

Although no capacity estimates have been undertaken for analogous basin floor fan deposits along the east African shelf, the potential basin floor fan reservoir systems identified in this study are comparable with storage capacity estimates compiled for fan systems within the Jubilee oilfield, offshore Ghana (Dailly et al., 2013). In the Jubilee field, hydrocarbon plays occur in a 90 m thick, stacked succession of Turonian-age basin floor fan sandstones, with individual play sands up to 35 m thick with porosities of ~20% (Dailly et al., 2013). Field statistics (Dailly et al., 2013) suggest that the play has an area of ~110 km^2 and net thickness of 40–90m, comparable with dimensions defined for the facies B1 reservoirs in the Durban Basin. A determination of the effective CO_2 storage capacity of the Jubilee Field undertaken during this study, at P10 probability (Goodman et al., 2011), suggests a total storage capacity of 16 Mt CO_2, akin to the 10–36 Mt capacities defined for individual basin floor fan reservoirs in the Durban Basin (Table 3). As shown in analogous hydrocarbon-bearing systems within the Jubilee Field, basin floor fan systems characterize well-defined stratigraphic traps. We therefore suggest that, dependent upon their sedimentology

Table 3
CO_2 storage capacity estimates of the Durban Basin (E factors of Goodman et al., 2011).

Reservoir	Facies	Reservoir Description	Areal Extent (km^2)	Areal Extent (m^2)	Nett Thickness (m)	Porosity	CO_2 Density (kg m^{-3})	CO_2 Storage Capacity (Mt CO_2) (P10)	CO_2 Storage Capacity (Mt CO_2) (P50)	CO_2 Storage Capacity (Mt CO_2) (P90)
I	C2	Shelf Sand	1500	1.5E + 09	50	0.30	663	179.01	358.02	611.62
H	C1	Basin-floor Fan	730	730000000	161	0.15	695	147.03	294.06	502.35
G	C1	Basin-floor Fan	10	10000000	123.5	0.15	679	1.51	3.02	5.16
F	B2	Shelf Sand	1500	1.5E + 09	40	0.30	687	148.39	296.78	507.01
E	B1	Basin-floor Fan	280	280000000	180	0.2	681	82.37	164.75	281.44
D	B1	Basin-floor Fan	38	38000000	156	0.2	685	9.75	19.49	33.30
C	B1	Basin-floor Fan	93	93000000	234	0.2	692	36.14	72.28	123.49
B	B1	Basin-floor Fan	50	50000000	125	0.2	686	10.29	20.58	35.16
A	B1	Basin-floor Fan	120	120000000	142.5	0.2	691	28.36	56.72	96.89
Subtotal Shelf Sand Reservoirs								327.40	654.80	1118.62
Subtotal Basin Floor Fans								463.84	927.68	1584.79
Total								642.85	1285.70	2196.41
CO_2 Storage Capacities for analogous systems										
Jubilee Field Ghana		Basin-floor Fan	110	110000000	90	0.2	695	16.51	33.03	56.42

CO_2 Storage Capacity—$MCO_2 = A \times h \times \phi \times \rho CO_2 \times E$.
Efficiency Factor (P10)—0.012 (Goodman et al., 2011).
Efficiency Factor (P50)—0.024 (Goodman et al., 2011).
Efficiency Factor (P90)—0.041 (Goodman et al., 2011).

and net-gross ratios, basin floor fan systems within the Durban Basin represent viable targets for CO_2 storage.

Laterally extensive inner shelf, sheet sands and deltaic sandstones are confined to Reservoirs F and I respectively. Conservative (P10) storage capacity estimates for individual reservoirs (148 Mt Reservoir F; 179 Mt Reservoir I) are comparable with minimum estimates of 170 Mt CO_2 for regions of the Rotliegend sandstone in the North Sea (Wilkinson et al., 2013), as well as effective CO_2 storage capacities (160 Mt CO_2) identified for the Fushan sag within the Beibuwan Basin offshore China (Li et al., 2015).

Within the Mozambique Basin, the base data utilised by Solomon et al. (2014) for their basin-scale assessment, suggested a low-end, theoretical storage of 579 Mt CO_2 for sandstones of the Turonian-age Domo Formation, of which 163 Mt CO_2 of storage potential is available in southern Mozambique. Similar low-end storage capacity estimates (E = 0.04) of 228 Mt CO_2 (Chabangu et al., 2014) were indicated for the Cenomanian-Turonian sandstones of the analogous lower St Lucia Formation in the onshore Zululand Basin in northern KwaZulu-Natal. Estimates defined for the Zululand and southern Mozambique Basins respectively, compare well with the 148 Mt (P10) capacity defined here for the equivalent Turonian-age sandstone Reservoir F in facies B2.

A similar scenario occurs within reservoirs of the Maastrichtian-age, lower Grudja Formation in Mozambique. These occur in the context of the palaeo-Limpopo delta (Fig. 10). Solomon et al. (2014) indicate a low-end capacity of 1129 Mt CO_2 of which 369 Mt occurs within southern Mozambique. These values represent double the capacity when compared with the P10 estimate of 179 Mt CO_2 for Reservoir I in this study. Reservoir I however, is analogous with hydrocarbon-bearing sediments of the lower Grudja Formation in Mozambique, and we therefore suggest that, based upon these correlations, the laterally extensive sandstone Reservoirs F and I represent primary potential targets for CO_2 storage in the Durban Basin.

5.4. Quantifying uncertainties and confidence of analogous data

In the case of the Durban Basin as with similar frontier basins (Green et al., 2014), uncertainties are high due to a dearth of core data. However, the use of analogous data is common practice worldwide with hydrocarbon discoveries in French Guiana utilising only seismic, gravity and magnetic data, coupled with analogous data from equatorial African discoveries (Green et al., 2014). The quantification of risk and uncertainties of reservoir conditions are commonly conducted using simplifications and conservatisms built into reservoir simulation models (Kahnt et al., 2015). In any given project a realistic degree of uncertainty must be accepted. Ringrose and Simone, (2009) suggest that at least 50% uncertainty can be defined in early project stages but this does not commonly reduce below 10% even in a mature project.

Within this study, data from analogous successions give representative estimations of the potential reservoir conditions within the Durban Basin. This can be defined through largely consistent values obtained by various authors for the Domo and Grudja Formations in Mozambique (Table 5). However, the potential for variations in facies between the known analogues and the Durban Basin cannot be discounted. Furthermore core data do not exist for the basin floor fans systems mapped within the Durban Basin, thereby leading to a large uncertainty in the injectivity potential for these reservoirs.

A major risk associated with injecting large quantities of CO_2 into a subsurface reservoir is pressure build-up (Oruganti and Bryant, 2009). Cavanagh and Wildgust (2011) suggest that over-pressurization may lead to poor injectivity, caprock failure, CO_2 leakage, and brine displacement via uncontrolled migration with such impacts having major consequences upon the technical and economic viability of a project. Natural overpressure is commonly associated with thick shale/mudstone sequences in deepwater hydrocarbon systems, and may lead to a reduction in injectivity potential within a specific reservoir (Green et al., 2014). Green et al. (2014) however, suggest that feeder channels associated with basin floor fan systems act as pressure release conduits, allowing depressurization of the fan system to create a mobile aquifer similar to fan systems in the North Sea. Cavanagh and Wildgust (2011) suggest that, in general, concerns regarding pressurization and brine displacement in existing CCS projects are largely model-driven due to a scarcity of data, with pressure prediction models relying on hypothetical ranges and conceptual constraints for likely scenarios. Although reservoir conditions data are lacking for the Durban Basin, a zone of overpressure was noted in Jc-B1 within basement lithologies below the Cretaceous and Cenozoic reservoir plays (GGS, 1983). In all other wells, no overpressure was identified suggesting the possibility of open systems that may allow for good injectivity. This however, will need further modelling for both open and closed systems to define likely scenarios.

We therefore propose that, although data are only at a regional scale in the Durban Basin, volumetric calculations based upon detailed seismo-stratigraphic interpretations coupled with reservoir property data from analogous successions still provide new evidence of

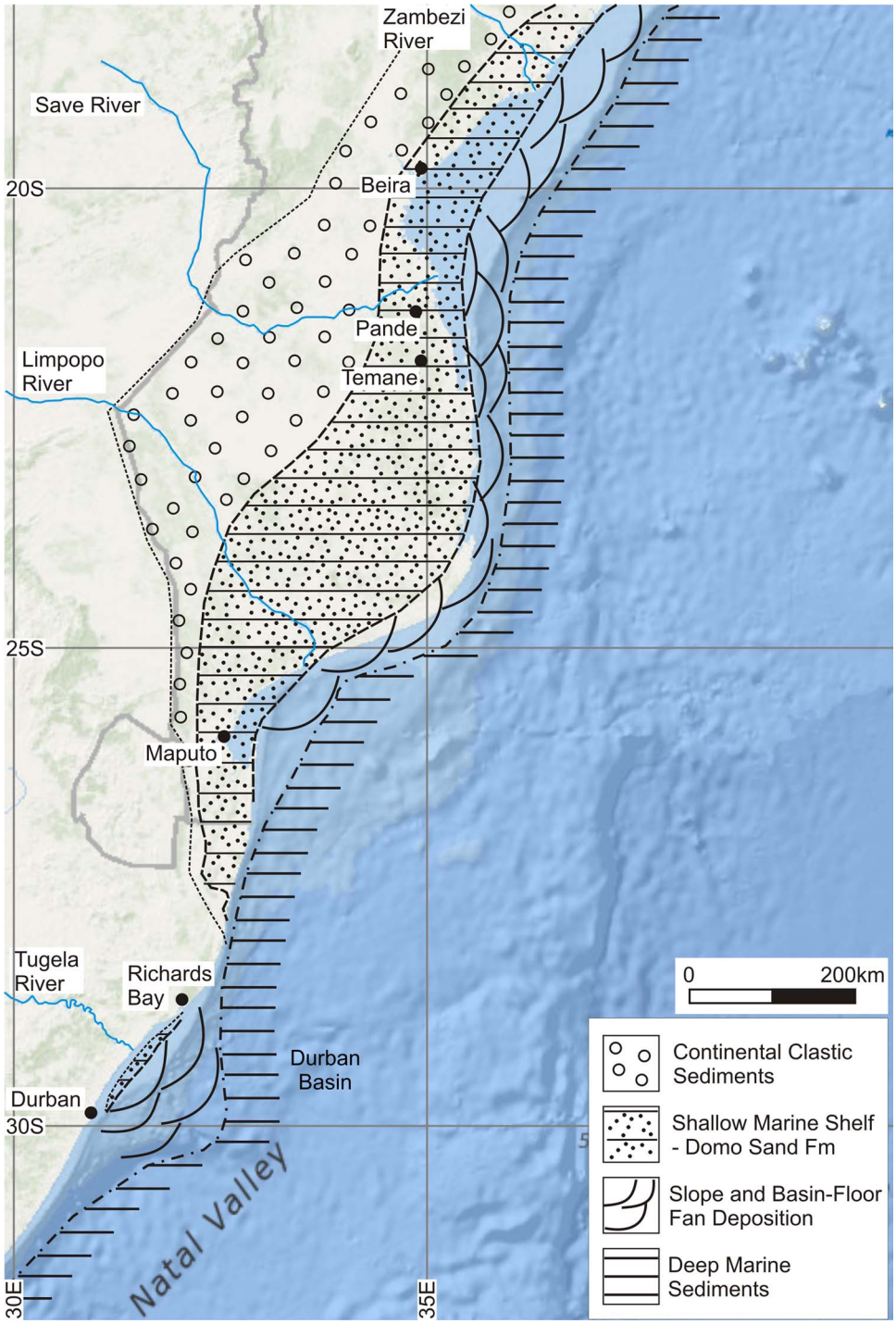

Fig. 9. Turonian (Domo Formation) reservoir development and depositional environment for the Durban, Zululand and Mozambique Basins, modified after Coster et al. (1989).

reservoir/seal pairs in saline aquifers. These may represent potential storage sites for CO_2 injection. The lack of overpressures in the Jc-series wells suggests potential injectivity for CO_2 storage within the mapped basin floor fans systems, as well as laterally extensive shallow marine shelf sands.

6. Conclusions

This study provides a basin-scale, effective CO_2 storage capacity estimation for individual sedimentological units within the Durban Basin, east coast of South Africa. Potential saline aquifer formations deeper than 800 m below seafloor are targeted, with basin floor fan and deltaic to inner shelf sedimentary units identified. Sedimentation occurred predominantly under forced and normal regressive conditions on a shallow ramp margin prior to, and during, the incipient progradation of the Tugela Cone submarine delta.

Storage capacity estimates are undertaken based upon P10, P50, and P90 probability levels, with specific efficiency data obtained from Goodman et al. (2011). The initial assessment suggests a conservative total CO_2 storage capacity of 643 Mt at a P10 probability level (1286 Mt at P50; 2196 Mt at P90). This can be subdivided into 327 Mt in deltaic and shelf confined sheet sands in Reservoirs F and I; and 464 Mt in basin floor fan systems. Estimated capacities for saline formations are comparable with estimates for neighbouring sedimentary basins and others worldwide.

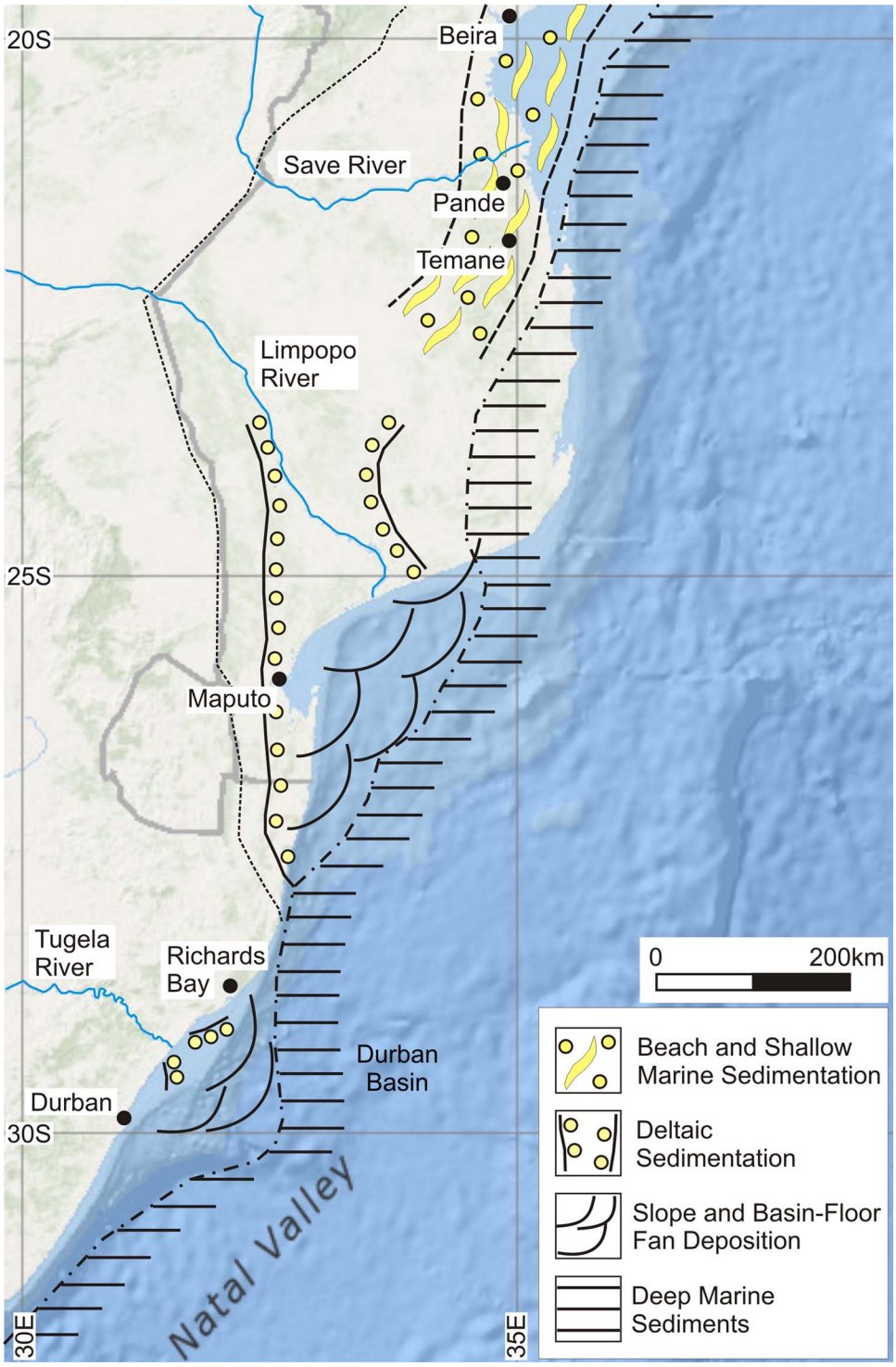

Fig. 10. Maastrichtian (Lower Grudja Formation) reservoir development and depositional environment for the Durban, Zululand and Mozambique Basins, modified after Coster et al. (1989).

Acknowledgements

This research was funded by a PhD bursary from the South African Centre for Carbon Capture and Storage (SACCCS), a division of the South African National Energy Development Institute (SANEDI), and comprises part of a Council for Geoscience (CGS) statutory programme (ST-2013-1183). The financial assistance of the South African Centre for Carbon Capture and Storage towards this research is hereby acknowledged. Opinions expressed and conclusions arrived at, are those of the author and are not necessarily to be attributed to SACCCS. NH thanks the CGS and SANEDI/SACCCS for their financial and technical support towards the project. We acknowledge the Petroleum Agency South Africa for supplying data to the University of KwaZulu-Natal. We would like to acknowledge IHS for the Kingdom Suite academic software grant supplied to the University of KwaZulu-Natal. Dr. Clare Bond is acknowledged for her constructive comments on an early version of the manuscript. We finally thank the two anonymous reviewers for their comments and suggestions, which helped to improve the manuscript.

Table 4
CO_2 storage capacity estimates of the Durban Basin (E factors of Viljoen et al., 2010).

Reservoir	Facies	Reservoir Description	Areal Extent (km^2)	Areal Extent (m^2)	Net Thickness (m)	Porosity	CO_2 Density ($kg\ m^{-3}$)	CO_2 Storage Capacity (Mt) (0.1 E)
I	C2	Shelf Sand	1500	1.5E + 09	50	0.30	663	1491.75
H	C1	Basin-floor Fan	730	730000000	161	0.15	695	1225.25
G	C1	Basin-floor Fan	10	10000000	123.5	0.15	679	12.58
F	B2	Shelf Sand	1500	1.5E + 09	40	0.30	687	1236.60
E	B1	Basin-floor Fan	280	280000000	180	0.2	681	686.45
D	B1	Basin-floor Fan	38	38000000	156	0.2	685	81.21
C	B1	Basin-floor Fan	93	93000000	234	0.2	692	301.19
B	B1	Basin-floor Fan	50	50000000	125	0.2	686	85.75
A	B1	Basin-floor Fan	120	120000000	142.5	0.2	691	236.32
Total								5357.10
DBN/Zululand		Saline Aquifer	81000	8.1E + 10	60	0.15	580	42282.00
Durban Basin		Saline Aquifer	10000	1E + 10	60	0.15	580	5220.00

CO_2 Storage Capacity—$MCO_2 = A \times h \times \phi \times \rho CO_2 \times E$.
Efficiency Factor of Viljoen et al. (2010)—0.1.

Table 5
Average reservoir characteristics from known analogous systems in Mozambique and Zululand with available data shown.

Reservoir	Sand Thickness (m)	Porosity%	Permeability (mD)	Data Source
Grudja	30–45	20–30		Nairn et al. (1991)
Grudja	16	15–30		Coster et al. (1989)
Grudja		15–35		Solomon et al. (2014)
Domo Sand	40–45	20–25		Nairn et al. (1991)
Domo Sand	40	28		Coster et al. (1989)
Domo Sand		7.5–25		Solomon et al. (2014)
Domo Sand		15–35	20–229 mD	Chabangu et al. (2014)

References

Bachu, 2008. Comparison between Methodologies Recommended for Estimation of CO_2 Storage Capacity in Geological Media by the CSLF Task Force on CO_2 Storage Capacity Estimation and the USDOE Capacity and Fairways Subgroup of the Regional Carbon Sequestration Partnerships Program, Phase III Report, 21 pp.

Bachu, S., Bonijoly, D., Bradshaw, J., Burruss, R., Holloway, S., Christensen, N.P., Maathiassen, O.M., 2007. CO_2 storage capacity estimation: methodology and gaps. Int. J. Greenh. Gas Control 1 (4), 430–443.

Bachu, S., 2015. Review of CO_2 storage efficiency in deep saline aquifers. Int. J. Greenh. Gas Control 40, 188–202.

Borissova, I., Kennard, J., Lech, M., Wang, L., Johnston, S., Lewis, C., Southby, C., 2013. Integrated approach to CO_2 storage assessment in the offshore South Perth Basin, Australia. Energy Procedia 37, 4872–4878.

Submarine Fans and Related Turbidite Systems. In: Bouma, A.H., Normark, W.R., Barnes, N.E. (Eds.), Springer- Verlag, New York 351 pp.

Bouma, A.H., 2000. Coarse-grained and fine-grained turbidite systems as end member models: applicability and dangers. Mar. Petrol. Geol. 17, 137–143.

Bradshaw, J., Bachu, S., Bonijoly, D., Burruss, R., Holloway, S., Christensen, N.P., Mathiassen, O.M., 2007. CO_2 storage capacity estimation: issues and development of standards. Int. J. Greenh. Gas Control 1, 62–68.

Broad, D.S., Jungslager, E.H.A., McLachlan, I.R., Roux, J., 2006. Offshore Mesozoic Basins. In: Johnson, M.R., Anhaeusser, C.R., Thomas, R.J. (Eds.), The Geology of South Africa. Geological Society of South Africa, Johannesburg/Council for Geoscience, Pretoria, pp. 553–571.

CSLF (Carbon Sequestration Leadership Forum), 2005. A Taskforce for Review and Development of Standards with Regards to Storage Capacity Measurement; CSLF-T-2005-9 15, 16 p.

Carman, G.J., Young, R., 1981. Reservoir Geology of the Forties Oilfield. Petroleum Geology of the Continental Shelf of North-west Europe. Institute of Petroleum, London, pp. 371–379.

Castelino, J.A., Reichert, C., Klingelhoefer, F., Aslanian, D., Jokat, W., 2015. Mesozoic and Early Cenozoic sediment influx and morphology of the Mozambique Basin. Mar. Petrol. Geol. 66, 890–905.

Catuneanu, O., Abreu, V., Bhattacharya, J.P., Blum, M.D., Dalrymple, R.W., Eriksson, P.G., Fielding, C.R., Fisher, W.L., Galloway, W.E., Gibling, M.R., Giles, K.A., Holbrook, J.M., Jordan, R., Kendall C.G.St.C. Macurda, B., Martinsen, O.J., Miall, A.D., Neal, J.E., Nummedal, D., Pomar, L., Posamentier, H.W., Pratt, B.R., Sarg, J.F., Shanley, K.W., Steel, R.J., Strasser, A., Tucker, M.E., Winker, C., 2009. Towards the standardization of sequence stratigraphy. Earth Sci. Rev. 92, 1–33.

Catuneanu, O., Galloway, W.E., Kendall, C.G.St.C., Miall, A.D., Posamentier, H.W., Strasser, A., Tucker, M.E., 2011. Sequence stratigraphy: methodology and nomenclature. Newsl. Stratigr. 44 (3), 173–245.

Cavanagh, A., Wildgust, N., 2011. Pressurization and brine displacement issues for deep Saline formation CO_2 storage. Energy Procedia 4, 4814–4821.

Chabangu, N., Beck, B., Hicks, N., Botha, G., Viljoen, J., Davids, S., Cloete, M., 2014. The investigation of CO_2 storage potential in the Zululand Basin in South Africa. Energy Procedia 63, 2789–2799.

Cloete, M. 2010 (compiler). Atlas on the geological storage of carbon dioxide in South Africa. Council for Geoscience, South Africa 18 pp.

Cook, P.J., 2012. Clean Energy Climate and Carbon. CO2CRC, CSIRO Publishing, Collingwood, Australia 215 pp.

Coster, P.W., Lawrence, S.R., Fortes, G., 1989. Mozambique: a new geological framework for hydrocarbons exploration. J. Pet. Geol. 12 (2), 205–230.

Dailly, P., Henderson, T., Hudgens, E., Kanschat, K., Lowry, P., 2013. Exploration for Cretaceous stratigraphic traps in the Gulf of Guinea, West Africa and the discovery of the Jubilee Field: a play opening discovery in the Tano Basin, Offshore Ghana. In: Mohriak, W.U., Danforth, A., Post, P.J., Brown, D.E., Tari, G.C., Nemcok, M., Sinha, S.T. (Eds.), Conjugate Divergent Margins. Geological Society London, pp. 235–248 Special Publications, 369.

Dingle, R.V., Goodlad, S.W., Martin, A.K., 1978. Bathymetry and stratigraphy of the Northern Natal Valley (SW Indian Ocean). A preliminary report. Mar. Geol. 28, 89–106.

Dingle, R.V., Siesser, W.G., Newton, A.R., 1983. Mesozoic and Tertiary Geology of Southern Africa. Balkema, Rotterdam 375 pp.

Du Toit, S.R., Leith, M.J., 1974. The J(c)-1 bore-hole on the continental shelf near Stanger, Natal. Trans. Geol. Soc. S. Afr. 77, 247–252.

Engelbrecht, A., Golding, A., Hietkamp, S., Scholes, B., 2004. The potential for sequestration of carbon dioxide in South Africa, Process Technology Centre, CSIR, Report 86DD/HT339, 54 pp.

GGS (Gearhart Geodata Services), 1983. Well completion report Jc-B1. Durban Basin, East Coast R.S.A. Soekor internal report POF 3427. 69pp.

Galloway, W.E., 2002. Paleogeographic setting and depositional architecture of a sand-dominated shelf depositional system, Miocene Utsira Formation, North Sea Basin. J. Sediment. Res. 72 (4), 476–490.

Gerrard, I., 1972. Report on progress on the evaluation of the Zululand Basin. Report, SOEKOR, PSV 1325 (unpubl.).

Gibson-Poole, C.M., 2009. Site Characterisation for Geological Storage of Carbon Dioxide: Examples of Potential Sites from the North West Shelf, Australia. Unpublished PhD Thesis. Australian School of Petroleum, University of Adelaide 422 pp.

Goodlad, S.W., 1986. Tectonic and sedimentary history of the mid-Natal Valley (S.W. Indian Ocean). Bulletin of Joint Geological Survey/University of Cape Town Marine Geoscience Unit, 15, 415 pp.

Goodman, A., Hakala, A., Bromhal, G., Deel, D., Rodosta, T., Frailey, S., Small, M., Allen, D., Romanov, V., Fazio, J., Huerta, N., McIntyre, D., Kutchko, B., Guthrie, G., 2011. U.S. DOE methodology for the development of geologic storage potential for carbon dioxide at the national and regional scale. Int. J. Greenh. Gas Control 5, 952–965.

Green, A.N., 2011a. The late Cretaceous to Holocene sequence stratigraphy of a sheared passive upper continental margin northern KwaZulu-Natal, South Africa. Mar. Geol.

289, 17–28.
Green, A.N., 2011b. Submarine canyons associated with alternating sediment starvation and shelf-edge wedge development: northern KwaZulu-Natal continental margin, South Africa. Mar. Geol. 284, 114–126.
Green, A.N., Garlick, L.G., 2011. A sequence stratigraphic framework for a narrow current-swept continental shelf: the Durban Bight, central KwaZulu-Natal, South Africa. J. Afr. Earth. Sci. 60, 303–314.
Green, S., O'Connor, S.A., Edwards, A.P., Carter, J.E., Cameron, D.E.L., Wright, R., 2014. Understanding potential pressure regimes in undrilled Labrador deep water by use of global analogues. Lead. Edge 33 (4), 414–416.
Haq, B.U., Hardenbol, J., Vail, P.R., 1987. Chronology of fluctuating sea levels since the triassic. Science 235, 1156–1167.
Haq, B.U., Hardenbol, J., Vail, P.R., 1988. Mesozoic and Cenozoic Chronostratigraphy and cycle of sea-level change. In: Wigus, C.K., Hastings, B.S., Posamentier, H., Van Wagoner, J., Ross, C.A., Kendall, C.G.St. C. (Eds.), Sea-level Changes—An Integrated Approach. Society of Economic Paleontologists and Mineralogists Special Publication No 42, 411 pp.
Heller, P.L., Dickinson, W.R., 1985. Submarine ramp facies model for delta-fed, sand-rich turbidite systems. Am. Assoc. Pet. Geol. Bul. 69 (6), 960–976.
Hicks, N., Green, A.N., 2016. Sedimentology and depositional architecture of a submarine delta-fan complex in the Durban Basin, South Africa. Mar. Petrol. Geol. 78, 390–404.
Hicks, N., Davids, S., Beck, B., Green, A.N., 2014. Investigation of CO_2 storage potential of the Durban basin in South Africa. Energy Procedia 63, 5200–5210.
Hunt, D., Tucker, M.E., 1992. Stranded parasequences and the forced regressive wedge systems tract: deposition during baselevel fall. Sediment. Geol. 81, 1–9.
Hutcheon, I., Shevalier, M., Durocher, K., Bloch, J., Johnson, G., Nightingale, M., Mayer, B., 2016. Interactions of CO_2 with formation waters, oil and minerals and CO_2 storage at the Weyburn IEA EOR site Saskatchewan, Canada. Int. J. Greenh. Gas Control 53, 354–370.
IEAGHG, 2009. Development of storage coefficients for carbon dioxide storage in deep saline formations. International Energy Agency Greenhouse Gas R & D Programme Report 2009/13, 118pp.
IPCC, 2005. IPCC Special Report on Carbon Dioxide Capture and Storage. Prepared by Working Group III of the Intergovernmental Panel on Climate Change. In: Metz, B., Davidson, O., de Coninck, H.C., Loos, M., Meyer, L.A. (Eds.), Cambridge University Press, Cambridge, United Kingdom and New York, NY, USA 442 pp.
Kahnt, R., Kutzke, A., Martin, M., Eckart, M., Schlüter, R., Kempa, T., Tillner, E., Hildenbrand, A., Krooss, B.M., Gensterblum, Y., Adams, M., Feinendegen, M., Klebingat, S., Neukum, C., 2015. CO_2RINA—CO_2 storage risk intergrated analysis. In: Liebscher, A., Münch, U. (Eds.), Geological Storage of CO_2-Long Term Security Aspects. Geotechnologien Science Report No. 22. Springer, Switzerland, pp. 139–166.
Leetaru, H.E., Freiburg, J.T., 2014. Perspective: litho-facies and reservoir characterization of the Mt Simon Sandstone at the Illinois Basin—Decatur project. Greenh. Gases Sci. Technol. 4, 580–595.
Leith, M.J., 1971. Jc-A1 geological well completion report. SOEKOR internal report, unpublished, SOE-DRG-WCR-346, 19 pp.
Li, P., Zhou, D., Zhang, C., Chen, G., 2015. Assessment of the effective CO_2 storage capacity in the Beibuwan Basin, offshore of southwestern P. R. China. Int. J. Greenh. Gas Control 37, 325–339.
Lowe, D.R., 1982. Sediment gravity flows; II. Depositional models with special reference to the deposits of high-density turbidity currents. J. Sediment. Petrol. 52, 279–297.
Martin, A.K., Flemming, B.W., 1986. The Holocene shelf sediment wedge off the south and east coast of South Africa. In: Knight, R.J., McLean, J.R. (Eds.), Shelf Sands and Sandstones. Canadian Society of Petroleum Geologists, Memoir II, pp. 27–44.
Martin, A.K., 1984. Plate tectonic status and sedimentary basin in-fill of the Natal Valley (SW Indian Ocean). Bulletin of the Joint Geological Survey/University of Cape Town, Marine Geoscience Unit 14, pp 209.
Mashaba, V., Altermann, W., 2015. Calculation of water saturation in low resistivity gas reservoirs and pay-zones of the Cretaceous Grudja Formation, onshore Mozambique basin. Mar. Petrol. Geol. 67, 249–261.
Mayall, M., Jones, E., Casey, M., 2006. Turbidite channel reservoirs—key elements in facies prediction and effective development. Mar. Petrol. Geol. 23, 821–841.
McMillian, I.K., 2003. Foraminiferally defined biostratigraphic episodes and sedimentation pattern of the Cretaceous drift succession (Early Barremian to Late Maastrichtian) in seven basins on the South African and southern Namibian continental margin. S. Afr. J. Sci. 99, 537–576.
Miller, K.G., Kominz, M.A., Browning, J.V., Wright, J.D., Mountain, G.S., Katz, M.E., Sugarman, P.J., Cramer, B.S., Christie-Blick, N., Pekar, S.F., 2005. The Phanerozoic record of global sea-level change. Science 310, 1293–1298.
Miller, K.G., 2009. Sea level change, last 250 million years. In: Gornitz, V. (Ed.), Encyclopaedia of Paleoclimatology and Ancient Environments, pp. 879–887.
Muntingh, A., 1983. Geological well completion report of borehole Jc-C1. SOEKOR internal report. SOE-DRG-WCR-363. 23 pp.
Normark, W.R., 1970. Growth patterns of deep sea fans. AAPG Bull. 54, 2170–2195.
Noy, D.J., Holloway, S., Chadwick, R.A., Williams, J.D.O., Hannis, S.A., Lahann, R.W., 2012. Modelling large-scale carbon dioxide injection into the Bunter Sandstone in the UK Southern North Sea. Int. J. Greenh. Gas Control 9, 220–233.
Oruganti, Y.D., Bryant, S.L., 2009. Pressure build-up during CO_2 storage in partially confined aquifers. Energy Procedia 1, 3315–3322.
Porebski, S.J., Steel, R.J., 2003. Shelf-margin deltas: their stratigraphic significance and relation to deepwater sands. Earth Sci. Rev. 62, 283–326.
Posamentier, H.W., Allen, G.P., 1999. Siliciclastic sequence stratigraphy: concepts and applications. SEPM Concepts Sedimentol. Paleontol. 7 210 pp.
Reading, H.G., Richards, M., 1994. Turbidite systems in deep-water basin margins classified by grain size and feeder system. Bull. Am. Assoc. Petrol. Geol. 78, 792–822.
Ringrose, P., Simone, A., 2009. Site selection. In: Cooper, C. (Ed.), A Technical Basins for Carbon Dioxide Storage. CO_2 Capture Project. CPL Press, United Kingdom 92 pp.
Salman, G., Abdula, I., 1995. Development of the Mozambique and Ruvuma sedimentary basins: offshore Mozambique. Sediment. Geol. 96, 7–41.
Shanmugam, G., Bloch, R.B., Mitchell, S.M., Beamish, G.W.J., Hodgkinson, R.J., Damuth, J.E., Straume, T., Syvertsen, S.E., Shields, K.E., 1995. Basin-floor fans in the North Sea: sequence stratigraphic models vs. sedimentary facies. Am. Assoc. Pet. Geol. Bul. 79 (4), 477–512.
Shanmugam, G., 2016. Submarine fans: a critical retrospective (1950–2015). J. Palaeogeogr. 5 (2), 110–184.
Singh, V., McLachlan, I., 2003. South Africa's east coast frontier offers untested mid to deepwater potential. Oil Gas J. 101 (22), 40–45.
Solomon, S., Bureau-Cauchois, G., Ahmed, N., Aarnes, J., Holtedahl, P., 2014. CO_2 storage capacity assessment of deep saline aquifers in the Mozambique Basin. Energy Procedia 63, 5266–5283.
Span, R., Wagner, W., 1996. A new equation of state for carbon dioxide covering the fluid region from the triple-point temperature to 1100 K at pressures up to 800 MPa. J. Phys. Chem. Ref. Data 25, 1509–1596.
Stow, D.A.V., Mayall, M., 2000. Deep-water sedimentary systems: new models for the 21st century. Mar. Petrol. Geol. 17, 125–135.
Stow, D.A.V., Reading, H.G., Collinson, J.D., 1996. Deep seas. In: Reading, H.G. (Ed.), Sedimentary Environments: Processes, Facies and Stratigraphy, third edition. Blackwell Publishing, Australia, pp. 395–453.
US DOE, 2008. Carbon Sequestration Atlas of the United States and Canada, Second Edition: Appendix A-Methodology for Development of Carbon Sequestration Capacity Estimates. National Energy Technology Laboratory, United States Department of Energy, Office of Fossil Energy, 37 pp.
Underschultz, J., Boreham, C., Dance, T., Stalker, L., Freifeld, B., Kirste, D., Ennis-King, J., 2011. CO_2 storage in a depleted gas field: an overview of the CO2CRC Otway Project and initial results. Int. J. Greenh. Gas Control 5 (4), 922–932.
Unstead, P.J., Muntingh, A., Mills, S.R., McLachlan, I.R., 1983. Jc-B1 Geological well completion report. SOEKOR internal report, unpublished. 15 pp.
Viljoen, J.H.A., Stapelberg, F.D.J., Cloete, M., 2010. Technical report on the geological storage of carbon dioxide in South Africa. Report, Council for Geoscience, 236 pp.
Würdemann, H., Möller, F., Kühn, M., Heidug, W., Christensen, N.P., Borm, G., Schilling, F.R., the CO2SINK Group, 2010. CO_2SINK—from site characterisation and risk assessment to monitoring and verification: one year of operational experience with the field laboratory for CO_2 storage at Ketzin, Germany. Int. J. Greenh. Gas Control 4 (6), 938–951.
Walford, H.L., White, N.J., Sydow, J.C., 2005. Solid sediment load history of the Zambezi Delta. Earth Planet. Sci. Lett. 238, 49–63.
Wilkinson, M., Haszeldine, R.S., Mackay, E., Smith, K., Sargeant, S., 2013. A new stratigraphic trap for CO_2 in the UK North Sea: appraisal using legacy information. Int. J. Greenh. Gas Control 12, 310–322.